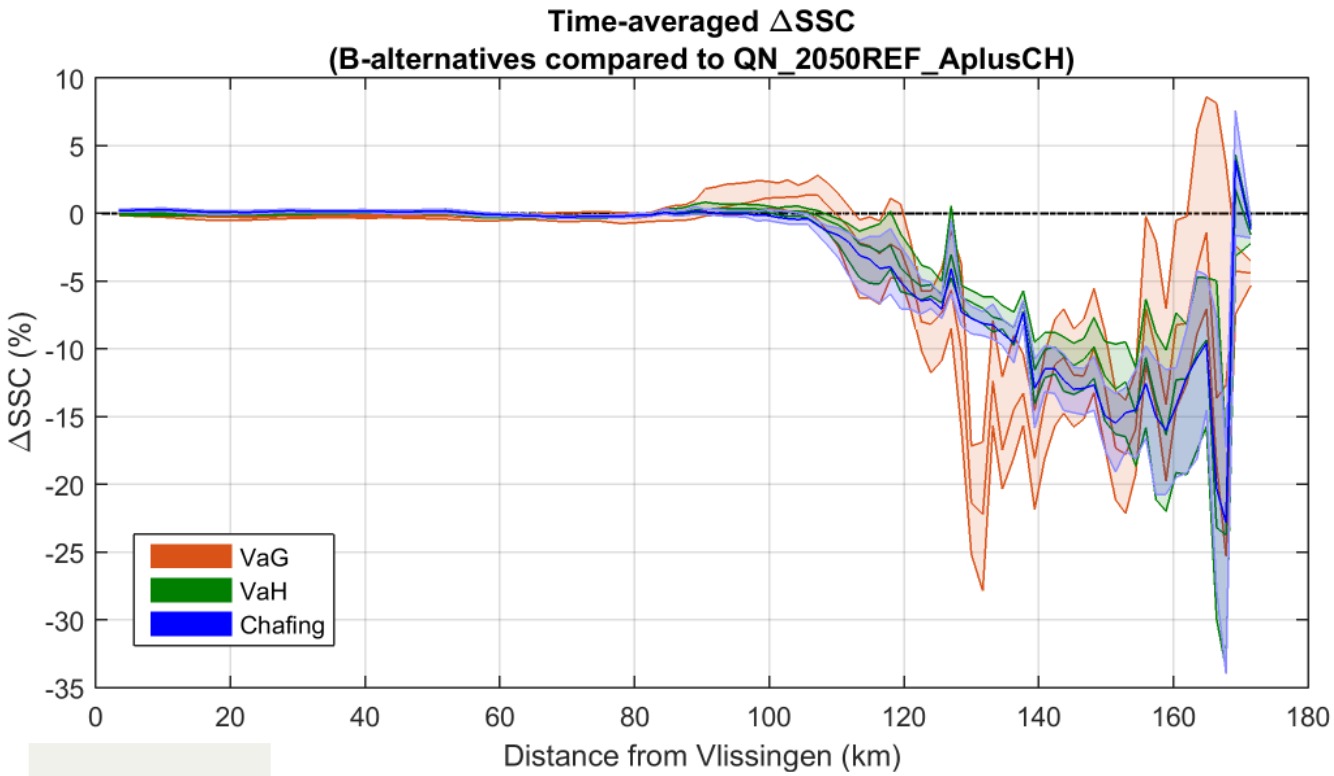

Flanders
State of
the Art

13_131_9
FHR reports

Integraal Plan Boven-Zeeschelde

Sub report 9
Effect of B-alternatives on Mud Transport

DEPARTMENT
MOBILITY &
PUBLIC
WORKS

www.flandershydraulicsresearch.be

Integraal Plan Bovenzeeschelde

Sub report 9 – Effect of B-alternatives on Mud Transport

Bi, Q.; Smolders, S.; De Maerschalck, B.; Vanlede, J.

Flanders Hydraulics Research
Flanders State of the Art

Cover figure © The Government of Flanders, Department of Mobility and Public Works, Flanders Hydraulics Research

Legal notice

Copyright and citation

This publication should be cited as follows:

Bi, Q.; Smolders, S.; De Maerschalck, B.; Vanlede, J. (2021). Integraal Plan Bovenzeeschelde: Sub report 9 – Effect of B-alternatives on Mud Transport. Version 2.0. FHR Reports, 13_131_9. Flanders Hydraulics Research: Antwerp

Document identification

Customer:	Flanders Hydraulics Research	Ref.:	WL2021R13_131_9
Keywords (3-5):	Scaldis Mud Transport		
Knowledge domains:	Hydraulics and sediment > Sediment > Cohesive sediment > Numerical modelling		
Text (p.):	156	Appendices (p.):	/
Confidential:	☒ No	☒ Available online	

Author(s):	Bi, Q.; Smolders, S.; Vanlede, J.

Control

	Name	Signature
Reviser(s):	De Maerschalck B.	Getekend door:Bart De Maerschalck (Sig Getekend op:2021-12-20 11:13:43 +01:0 Reden:Ik keur dit document goed Bart De Maerschalck
Project leader:	Vanlede J.	Getekend door:Joris Vanlede (Signature) Getekend op:2022-01-19 15:18:18 +01:0 Reden:Ik keur dit document goed Joris Vanlede

Approval

Head of Division:	Bellafkih, K.	Getekend door:Abdelkarim Bellafkih (Sign Getekend op:2021-12-20 10:37:38 +01:0 Reden:Ik keur dit document goed Abdelkarim Bellafkih

Abstract

A new mud transport model was developed based on the SCALDIS- hydrodynamic model for the (tidal) Scheldt estuary and Upper Sea Scheldt. Calibration of the mud transport model is described in Smolders et al. (2018).

The calibrated mud transport model is used to analyse the effects of three potential alternative bathymetries that allow accessibility for CEMT[1] class Va ships: Chafing (Schaaf), Va “Geul” (VaG) and Va “Hybrid” (VaH).

This report describes the effects against a future reference situation (2050). The focus is on expected effects on mud transport and suspended sediment concentrations in the Upper Sea Scheldt. The model results are described in terms of suspended sediment concentration (SSC), the residual transport of sediment due to tidal asymmetry and sediment flux through transects in the area of interest.

[1] CEMT - Conférence Européenne des Ministres de Transport 1992

Contents

List of tables

List of figures

1 Introduction

In the framework of the project 'Agenda for the Future', it is aimed to develop a well validated hydrodynamics and sediment transport model that covers the entire tidally influenced zone of the Scheldt estuary and the mouth area with a sufficient resolution in the upstream part. Previous models lack a high resolution in the Upper Sea Scheldt, Durme, Rupel and Nete. For this reason a new unstructured high resolution model (SCALDIS-model) of the (tidal) Scheldt estuary is developed in TELEMAC-3D for the entire estuary (Smolders et al., 2017).

Based on the SCALDIS model, a mud transport model, as a part of high-resolution sediment transport model for the whole Scheldt estuary is developed and calibrated. The details of the mud model is reported in Smolders et al. (2018).

The main objectives of this mud transport model is to study future (2050) scenarios/alternatives of the Scheldt estuary by quantifying the effects compared to the reference case, e.g. the effects on suspended sediment concentration (SSC), sediment flux through zones of interest and erosion/deposition on intertidal flats and subtidal channels.

The present report describes the model results with new future bathymetry alternatives in the intertidal zones of the estuary. These alternatives are called B-alternatives within this project and summarized below:

- Chafing (Schaaf): accessibility for CEMT[2] class Va ships: 110 m long and 11.4 m wide, with designed draught 1.80 m (empty) - 3.50 m (loaded), *Groot Rijnvaartschip*. For these scenarios the design of the fairway is not based on standard design rules but consists of fairway envelopes based on real time shipping simulations;
- VaG: Class Va standard design rules applied, mostly in the current channel ("G" for "Geul" or channel) leading to a single lane Va functionality upwards Wichelen (between Ghent and Dendermonde, uppermost part of Upper Sea Scheldt);
- VaH: Class Va standard design rules applied with Hybrid ("H") properties, specifically the "Chafing" alternative downstream Wichelen, and "VaG" upstream Wichelen.

The comparison of modelled results from different scenarios/alternatives are analysed with a focus in the Upper Sea Scheldt, where most of these future scenarios/alternatives are located.

More information about the alternatives and scenarios, model sequence and an overview of the data flow are given in the memo 'Afstemming Modelinstrumentarium' (IMDC, INBO, UA, WL, 2015).

[2] CEMT - Conférence Européenne des Ministres de Transport 1992

2 Units and reference plane

Time is expressed in CET (Central European Time).

Depth, height and water levels are expressed in meter TAW (Tweede Algemene Waterpassing).

Bathymetry and water levels are positive above the reference plane.

The horizontal coordinate system is RD Paris.

3 The Calibrated Mud Model and Scenarios

3.1 Model set-up

The calibrated mud model (CAL_007) is described in Smolders et al., (2018). An overview of the physical parameters is summarized in Table 1.

Table 1 – Physical parameters used in the calibrated model (CAL_007)

Physical parameters	**CAL_007**
INITIAL MUD CONCENTRATION (g/L)	0.5
MEAN DIAMETER OF THE SEDIMENT (m)	5.0E-05
DENSITY OF THE SEDIMENT (kg/m^3)	2650
CONSTANT SEDIMENT SETTLING VELOCITY (m/s)	5.0E-04
HINDERED SETTLING	NO
NUMBER OF SEDIMENT BED LAYERS	1
INITIAL THICKNESS OF SEDIMENT LAYERS (m)	0.0
MUD CONCENTRATIONS PER LAYER (kg/m^3)	500
EROSION COEFFICIENT (kg/m^2/s)	1.0E-04
CRITICAL EROSION SHEAR STRESS OF THE MUD LAYERS (Pa)	0.05
CRITICAL SHEAR STRESS FOR DEPOSITION (Pa)	1.0E06

3.1.1 Parametrisation of dredging and disposal

As mentioned in the report of calibrated mud model (Smolders et al., 2018), a point source is placed in the model near the Oosterweel, releasing disposed material into water column. This is used to simulate the sediment disposal process in our 3D sediment transport model. The yearly averaged amount of sediment deposited back in the estuary is 4.545.995 Tons (averaged over period 2007 – 2015). This number is converted into a constant sediment releasing rate at the point source to make sure the same amount of material is put back into the system.

This point source remains the same in all the reference cases and scenarios.

3.1.2 On roughness parametrisation

Instead of using spatial varying bottom roughness (Manning coefficients) as in the hydrodynamic model, a constant and uniform Manning coefficient (0.02) is used in the mud model (Smolders et al., 2018). Therefore, only flow velocity and water level are used from the hydrodynamics in the mud model, while the bed shear stress for erosion-deposition is computed separately instead of borrowing from the hydrodynamic model.

3.2 Boundary conditions

3.2.1 Upstream Boundary Conditions in the Mud Model

Upstream tributaries feed the model with a discharge. There are 8 upstream boundaries with prescribed discharge and free tracer. Discharges are defined as upstream boundary conditions at the Upper Sea Scheldt for Merelbeke, Dender, Zenne, Dijle, Kleine Nete, Grote Nete, channel Ghent – Terneuzen (Smolders et al., 2016).

The discharges are representative discharges for a summer period and remain constant until an event lasting five days starting 34 days into the simulation. This discharge event is synthetic and is representative for an event with return period 1/6 year (synthetic boundary discharge values determined in IMDC, 2015). This boundary condition is called the Normal Discharge scenario (QN).

Table 2 – Imposed mud concentrations at upstream tributaries

Tributaries	Imposed concentration (g/L)
Dender	0.098
Zenne	0.062
Kleine Nete	0.041
Dijle	0.074
Grote Nete	0.045
Merelbeke	0.094

Beside of the discharges, in the mud model, sediment concentration is imposed to each upstream tributaries. The imposed sediment concentration is calculated based on the yearly averaged redistributed sediment loads as shown in Table 2 (taken from Smolders et al., 2018). These imposed concentrations stay the same in all the reference cases and scenarios.

3.2.2 Downstream Boundary Conditions in the Mud Model

A model chain is used to generate downstream boundary conditions for the mud model. There are two levels of nesting involved in this procedure, from CSM (Continental Shelf Model) to ZUNO (Zuidelijke Noordzee), and from ZUNO to SCALDIS. Sea level rise (SLR) is implemented in the boundary of CSM model. The effect of SLR is calculated throughout the model chain.

Both water level and velocities are used as downstream boundary conditions in the SCALDIS mud model. This resolves instability issues near the North Sea boundary when there was only water level imposed in earlier versions of SCALDIS.

The detailed workflow for generating new downstream boundary conditions for the mud model with additional velocity components is described below.

(1). 2013 Normal Scenarios (CN)

For the 2013 Normal Scenarios (CN), since there is no sea level rise involved, the ZUNO model (ZUNO_2013_harmonic) is used for obtaining water levels, velocity and salinity at the downstream boundary.

(2). 2050 Sea Level Rise Scenarios (CL and CH)

The downstream boundary conditions in the mud model are inherited sea level rise scenarios from the CSM-ZUNO model chain, in which the sea level rise is added into the boundary conditions of the CSM model. To be more specific, the CSM models with sea level rise scenarios ("CSM_2050_noWind_plus15cm" and "CSM_2050_noWind_plus40cm") are used. In this case, the nested ZUNO model will naturally have sea level rise when it uses the water levels generated by CSM models as its boundary conditions. The mud model is then nested in ZUNO model, and will therefore "inherit" the sea level rise by using water levels, velocity and salinity from the ZUNO model at its downstream boundary nodes.

(3). Sediment concentration at downstream boundary

The downstream boundary also has a prescribed sediment concentration, which is derived from satellite images in the study of Fettweis et al. (2007). An average value of 12 mg/L is taken to represent SSC values at the North Sea. This value is kept constant over space and time for the downstream boundary, and remains the same for all alternatives and scenarios described in this report

3.3 Initialization of the model

The mud transport model is initialized with an empty bed and uniform suspension concentration of 500 mg/L as described in Smolders et al. (2018). For the hydrodynamics, the mud model is initialized with the flow field from the last time step of a 2-day pure-hydrodynamic hotstart run.

3.4 Simulation period

All the runs have a simulation period of 42 days, including a pure hydrodynamic spin up period of 2 days. For the run 2013_REF_A0CN and 2050_REF_A0CN, the simulation period is from 2013/07/29 22:20:00 to 2013/09/09 22:20:00. For the rest of the runs, the 2050 future scenarios are applied, with the simulation period from 2050/08/09 22:00:00 to 2050/09/20 22:00:00.

3.5 Alternatives and scenarios for the mud model

The calibrated mud transport model is used to evaluate the effects of different B-alternatives (specified geometry of the Scheldt estuary), under different climate scenarios (a range of boundary conditions to take into account climate change, sea level rise, increasing or decreasing tidal amplitude, high or low river discharge). The list of the scenario runs is presented in Table 4.

More information about the SCALDIS model can be found in (Smolders et al., 2016).

3.5.1 Representative discharges for 2013 and 2050

There are two different sets of synthetic discharges used as the upstream boundary conditions in the mud model scenarios. One is based on the current situations of 2013 (Q2013), and the other one is made for the future scenarios in 2050 (Q2050). Each of these synthetic time series of discharge contains one event with a peak discharge.

As shown in Figure 1, the discharges at Melle, Dender and Rupel (the sum of Zenne, Dijle, Grote Nete and Kleine Nete) for the current situation and for the 2050 scenarios are plotted together. It can be seen that the discharge becomes larger for Melle and Dender in 2050, and smaller for Rupel. The Rupel basin also has a smaller average discharge in 2050 compared to the current situation.

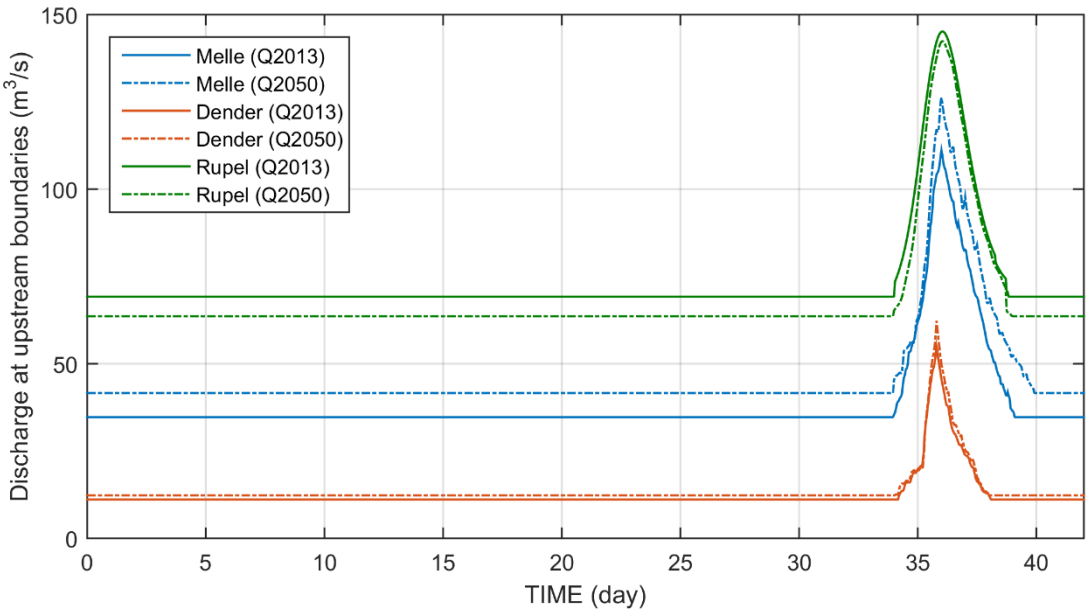

Figure 1 – Upstream discharges used in mud model scenarios

These two sets of upstream discharges are provided by IMDC, based on statistical analysis for the current and future scenarios (IMDC, 2015). The original set of synthetic boundary conditions had a period of 3 months, from May to August, in 2013 and 2050, respectively.

For the scenario runs of the mud model, only a part of this is used (Figure 2). To be more specific, one peak event is selected and placed near the end of simulation, and the constant discharges are extended to the rest of the simulation period in the mud model runs.

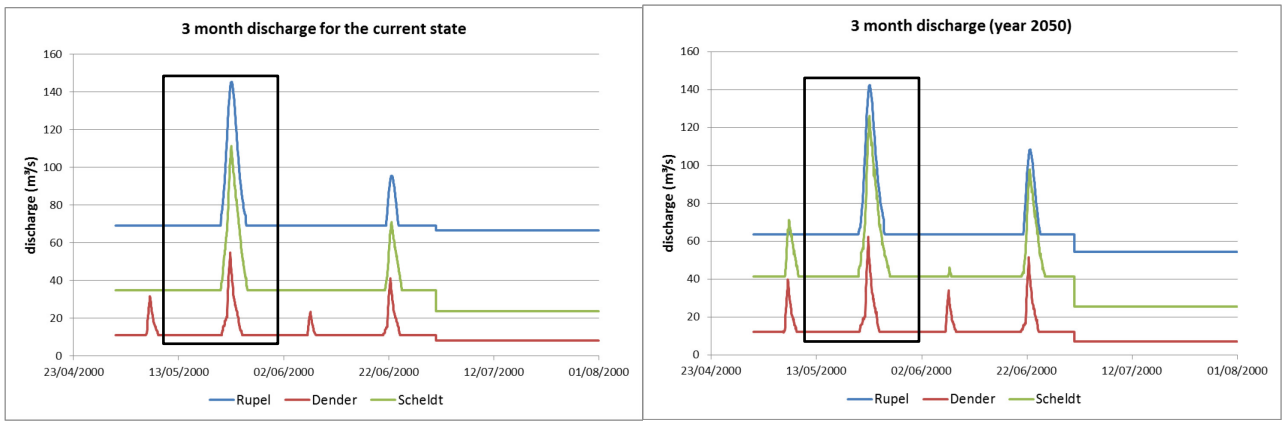

Figure 2 – Original data of upstream discharge provided by IMDC (2015) for the current state and year 2050

The discharge for the current situation (Q2013) is applied in the run 2013_REF_A0CN and 2050_REF_A0CN, which are used as reference in the comparison. The discharge for the 2050 is used in the rest of the scenarios. The details is summarized in § 3.5.5.

3.5.2 Tidal range scenarios

The SCALDIS model is used to evaluate the effect of increased and reduced tidal range near Schelle and further upstream in the Upper Sea Scheldt. In this study, tidal range scenarios **A+**, **A0** and **A-** have been implemented in both the hydrodynamic model and the mud model. In these three scenarios, the tidal amplitude at Schelle is equal to 5.70, 5.40 and 5.00 m, respectively (Table 3).

Table 3 – Tidal range scenarios

Scenario	Bottom friction	Tidal amplitude at Schelle (m)
A+	The bottom friction for hydrodynamics in the Western Scheldt is lowered.	5.70
A0	The bottom friction for hydrodynamics in the Western Scheldt remains as in the SCALDIS hydrodynamic model.	5.40 (current tidal range)
A-	The bottom friction for hydrodynamics in the Western Scheldt is increased.	5.00

The increase and decrease of the tidal range is realised in the model by changing the roughness (Manning coefficient) in the Western Scheldt. The zone with altered bottom roughness is indicated in Figure 3. By changing the roughness, the tidal propagation is influenced.

For the scenario “A+”, the Manning coefficient at each point in the red zone is decreased by 0.00426; for the scenario “A-”, the Manning coefficient at each point in the red zone is increased by 0.00554.

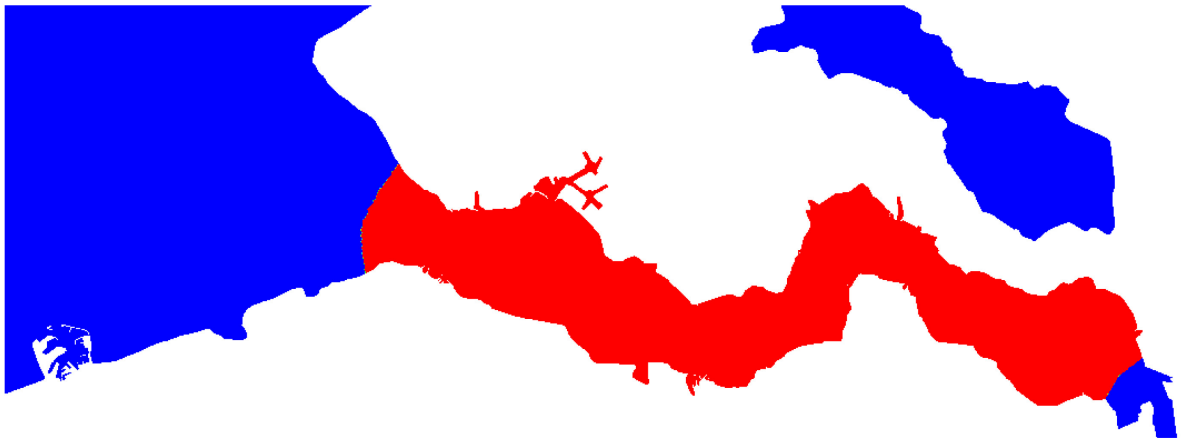

Figure 3 – The zone with changed bottom friction in the tidal range scenarios (red indicates the area with changes).

3.5.3 Sea level rise scenarios

The following sea level rise scenarios are modelled in different runs for 2050:

- The “current” situation (**CN**, +0 cm in 2050);
- The “low” scenario (**CL**, +15 cm in 2050);
- The “high” scenario (**CH**, +40 cm in 2050).

The downstream boundary conditions for “CL” and “CH” scenarios are generated from CSM-ZUNO model, instead of adding the values directly on the water levels at the boundary.

The “current” situation CN is always used in the reference cases for comparison, and never combined with the change of tidal range. The tidal range scenario A+ is combined with the sea level rise CH. The tidal range scenario A- is combined with the sea level rise CL. More information about the scenarios is given in IMDC/INBO/UA/WL (2015).

3.5.4 Sustainable Bathymetry and B-alternatives

The main purpose of the SCALDIS mud model is to study the influence of future (2050) scenarios/alternatives of the Scheldt estuary on suspended sediment transport. Hence, different bathymetry datasets are used as input in the mud model for different comparisons. Bathymetry of the deeper part of the river channel for the B-alternatives is defined based on the data provided by IMDC in the end of May 2016.

(1). The Sustainable Bathymetry (2050 REF)

The Sustainable Management Plan was developed for a sustainable management of the Upper Sea Scheldt and the Ringvaart. This plan focusses on maintaining the fairway with respect for the tidal nature. The designed bathymetry takes into account the needs for navigation and the characteristics of the river. The impact on the tidal nature is limited to specific areas. The hydrodynamic and morphological processes can develop to the extent that the safety and tidal nature are not endangered. The Management Plan aims to optimize the existing management efforts for navigation and protection of the riverbanks (IMDC, 2015). The difference between the 2050 bathymetry and the current bathymetry is shown in Figure 4 to Figure 6.

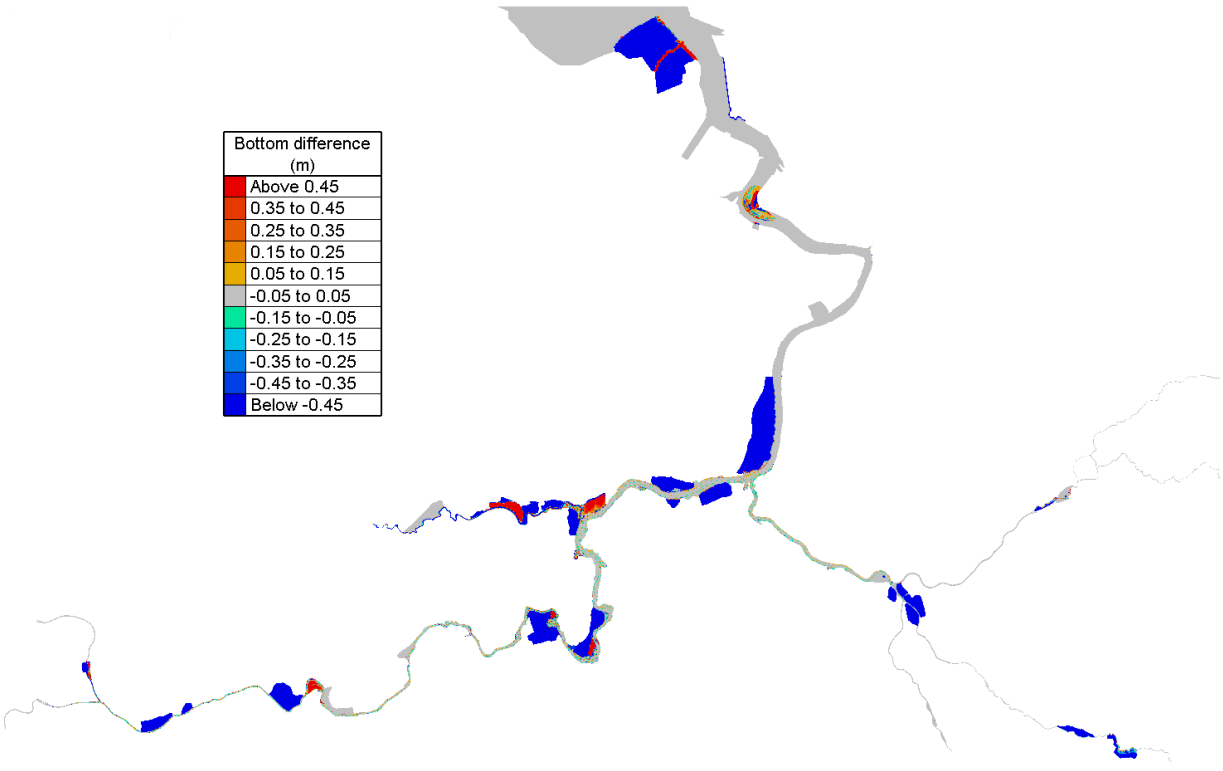

Figure 4 – Difference of bottom elevation in the Sea Scheldt (2050_REF_A0CN - 2013_REF_A0CN) – overview

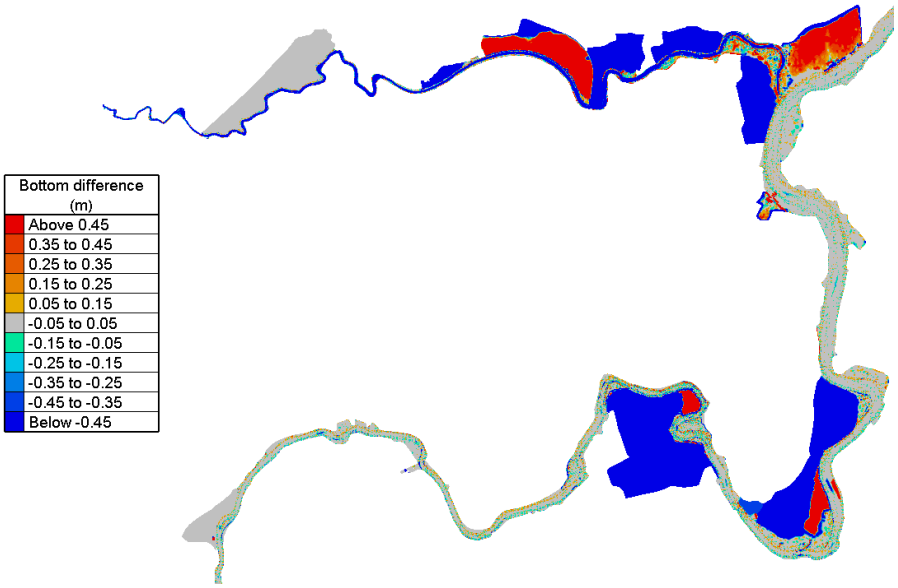

Figure 5 – Difference of bottom elevation in Upper Sea Scheldt (2050_REF_A0CN - 2013_REF_A0CN) – Upper Sea Scheldt (part 1)

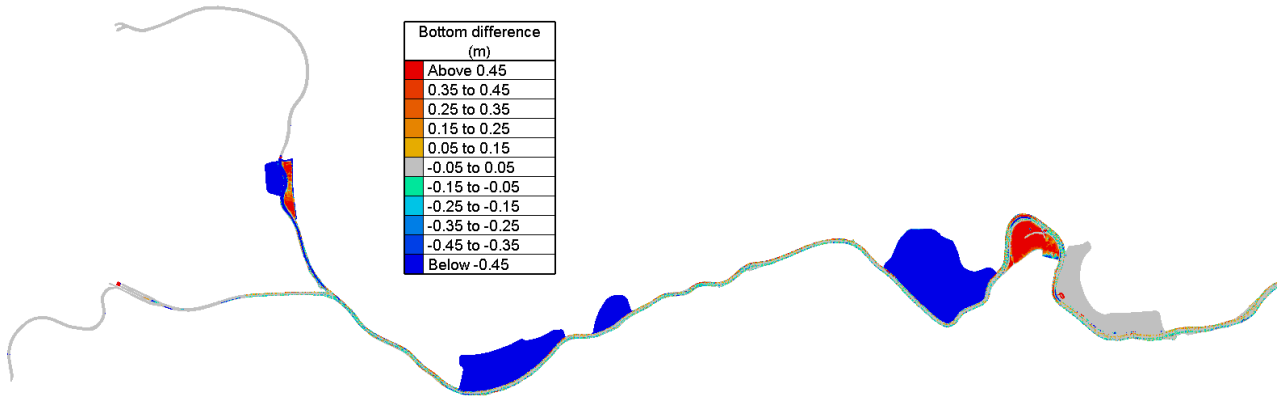

Figure 6 – Difference of bottom elevation in Upper Sea Scheldt (2050_REF_A0CN - 2013_REF_A0CN) – Upper Sea Scheldt (part 2)

The bathymetry change near the upstream boundary is shown in detail in Figure 7. A de-embankment is added in the sustainable bathymetry in 2050 in the tributary near Heusden. Moreover, there is a new sluice installed at the North end of the de-embankment. The new sluice will prevent the tide from attenuating further upstream in this tidal arm. It is modelled as a culvert, which means water can flow through this sluice further upstream or downstream depending on the relative water depth between the two sides, but the discharge through the sluice is limited and it makes the time averaged velocity become less downstream in this tributary. Note that upstream the tidal arm at Gentbrugge, no discharge is imposed in the model.

The elevation of the batymetry at upstream end of the Ringvaart is due to model-technical reasons. In the HD model, the model was articially deepened for stability reasons. This problem is fixed in the Mud model, so now the actual bathymetry is implemented in the Ringvaart.

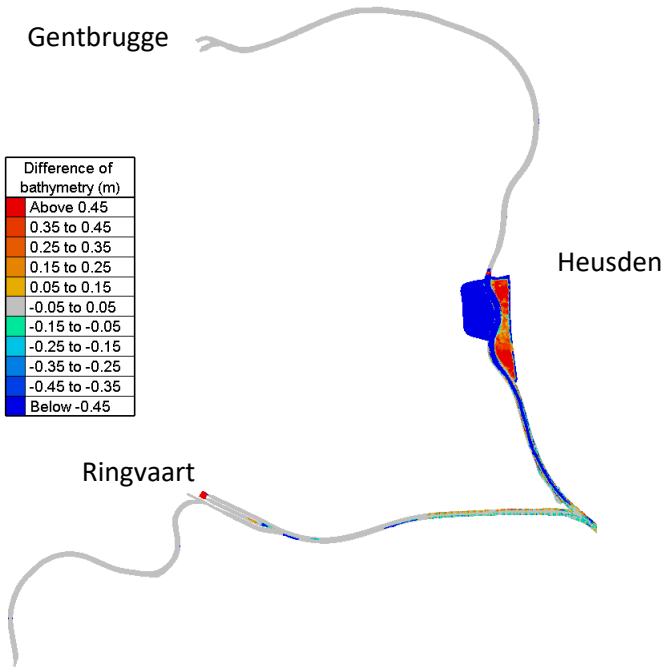

Figure 7 – Difference of bathymetry in the tributaries near the upstream boundary

(2). The B alternatives (Chafing)

Chafing (Schaaf): accessibility for class Va ships of 110 m long and 11.4 m wide with designed draught 1.80 m (empty) – 3.50 m (loaded), not following standard design rules but using fairway envelopes based on real time shipping simulations. The differences in bathymetry from REF to Chafing are shown in Figure 8 to Figure 13.

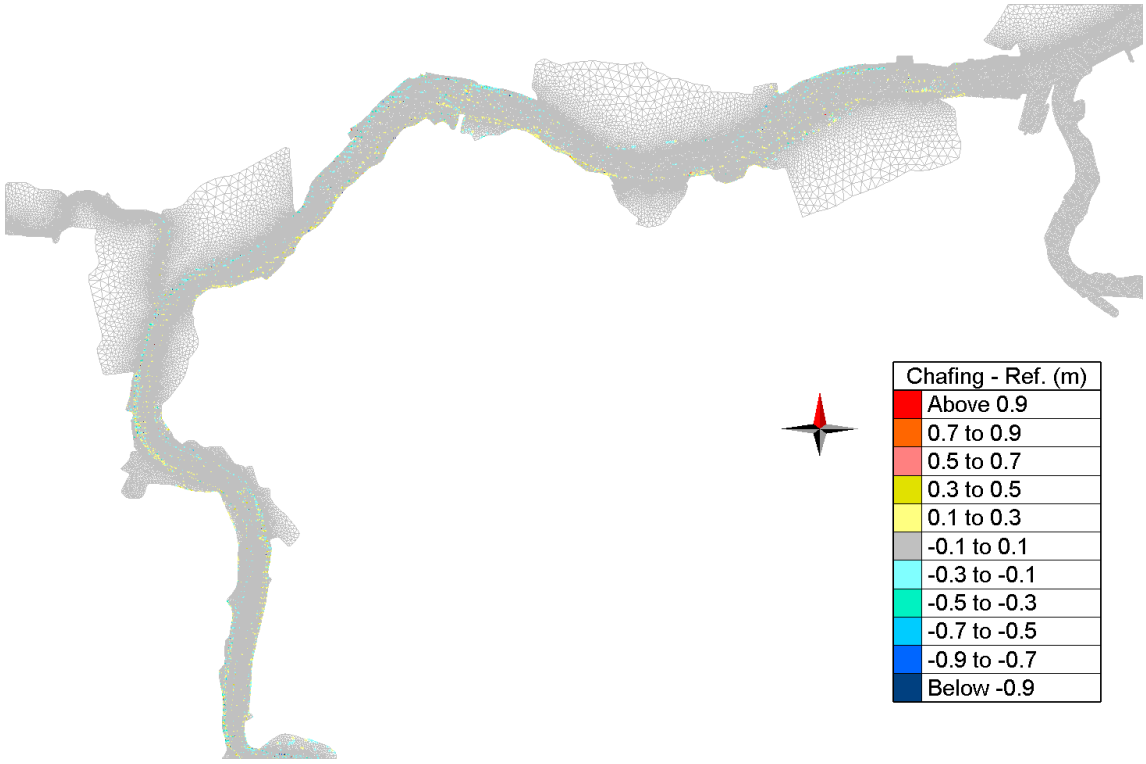

Figure 8 – Difference in bathymetry (Chafing – Reference 2050) in zone 1

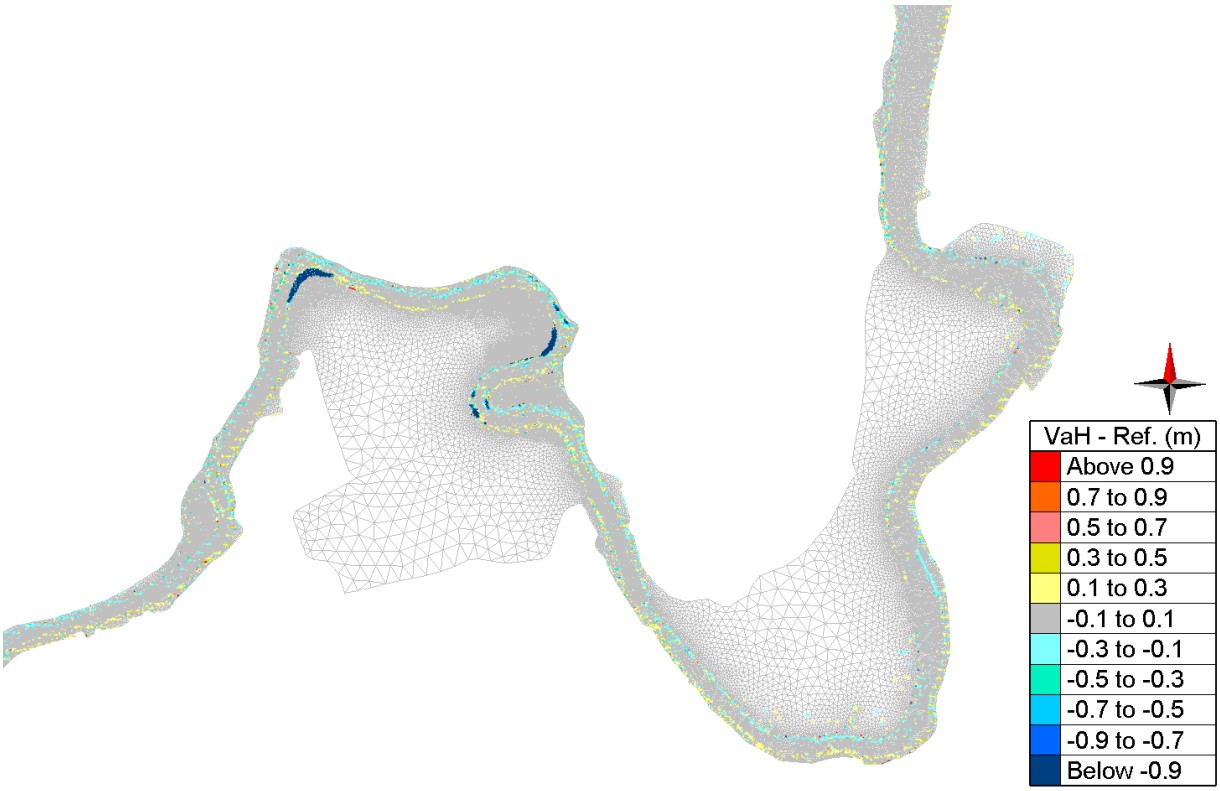

Figure 9 – Difference in bathymetry (Chafing – Reference 2050) in zone 2

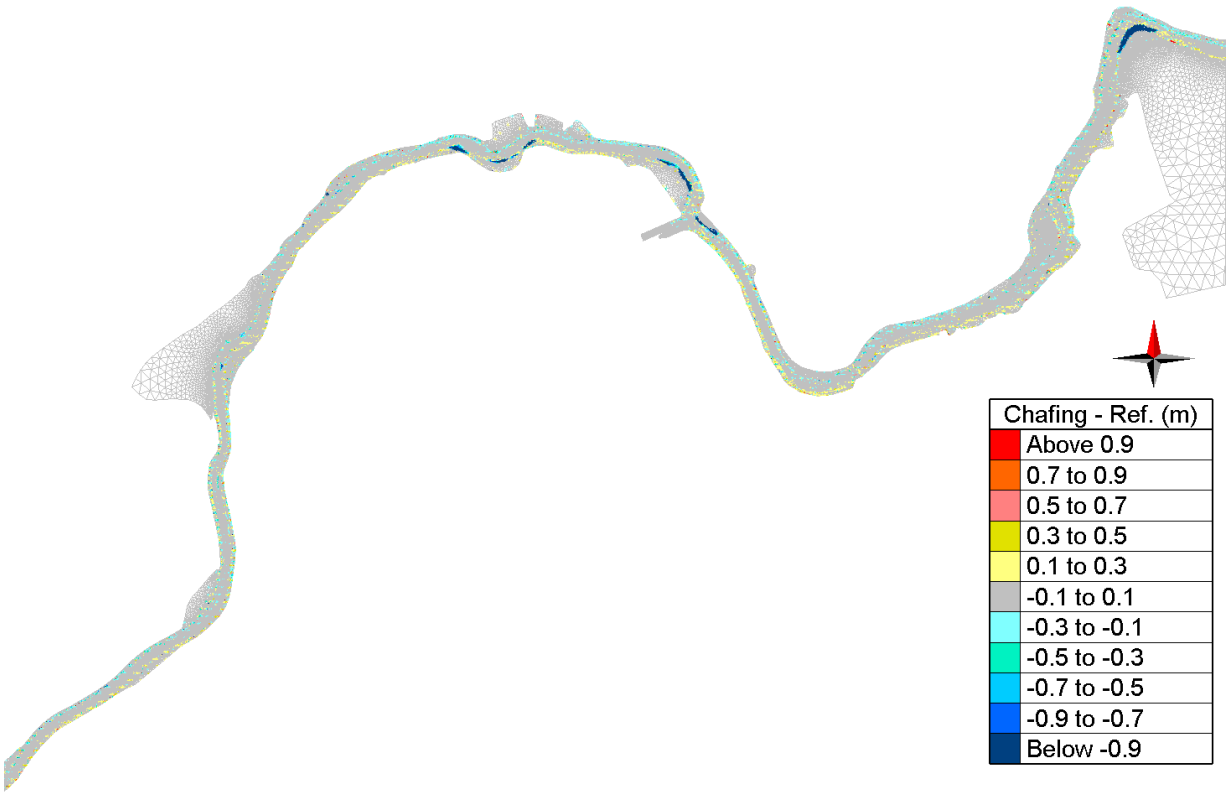

Figure 10 – Difference in bathymetry (Chafing – Reference 2050) in zone 3

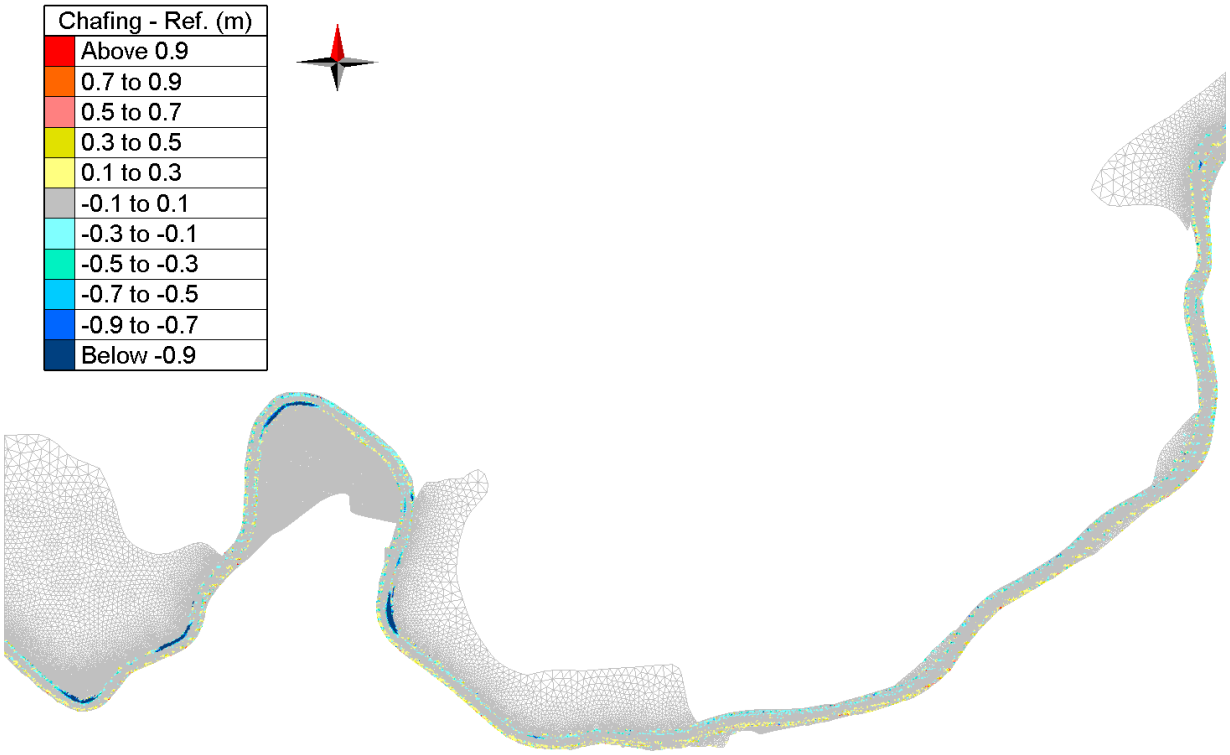

Figure 11 – Difference in bathymetry (Chafing – Reference 2050) in zone 4

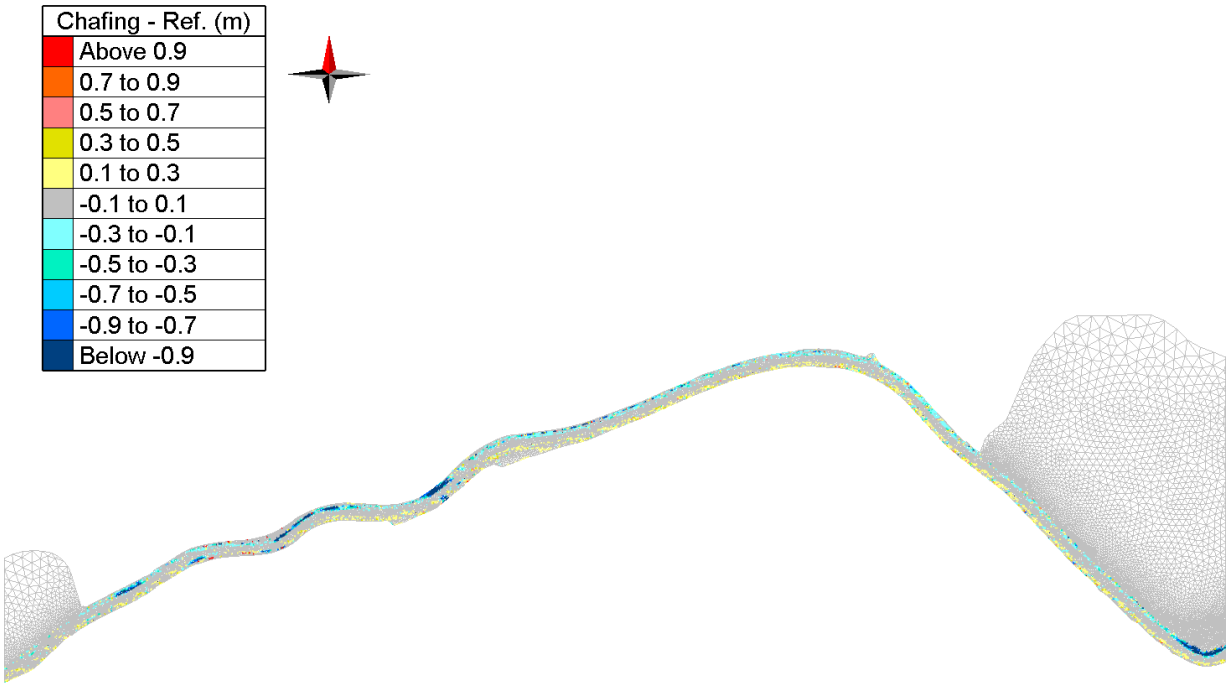

Figure 12 – Difference in bathymetry (Chafing – Reference 2050) in zone 5

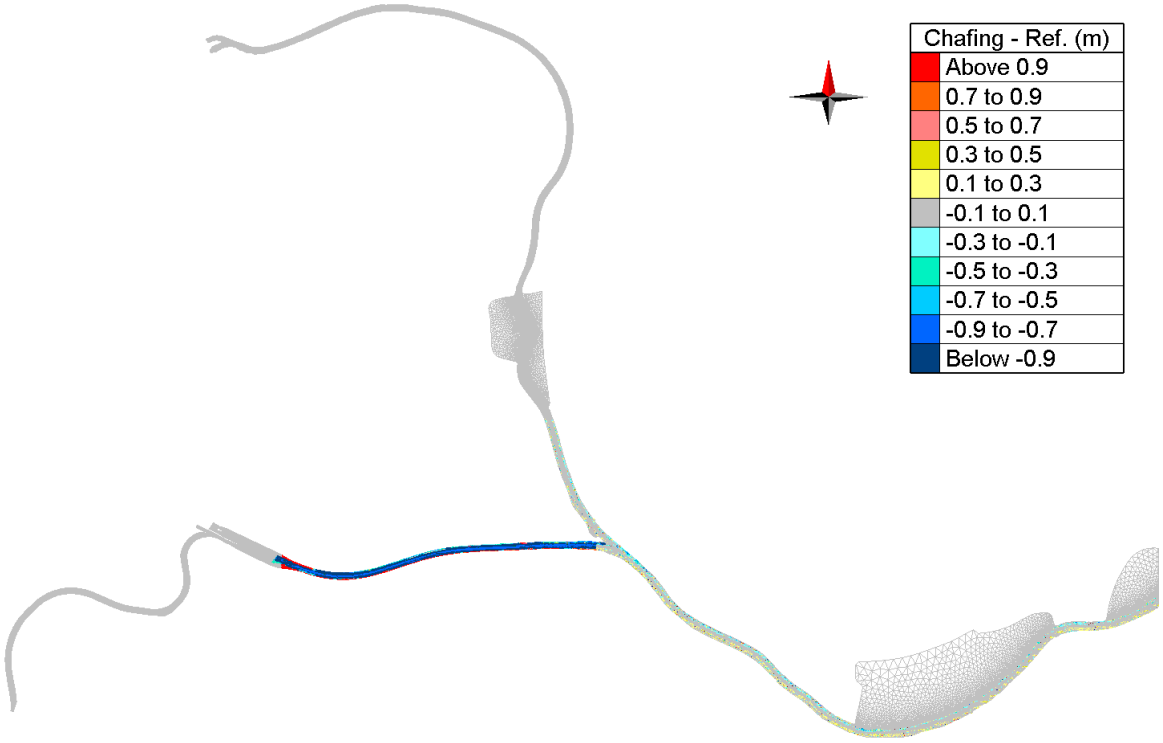

Figure 13 – Difference in bathymetry (Chafing – Reference 2050) in zone 6

(3). The B alternatives (VaG)

VaG: Class Va standard design rules are applied, stretching the narrow bends (“G” for “Geul” or channel) leading to a single lane Va functionality upwards Wichelen (between Ghent and Dendermonde, uppermost part of Upper Sea Scheldt). The differences in bathymetry are shown from Figure 14 to Figure 19.

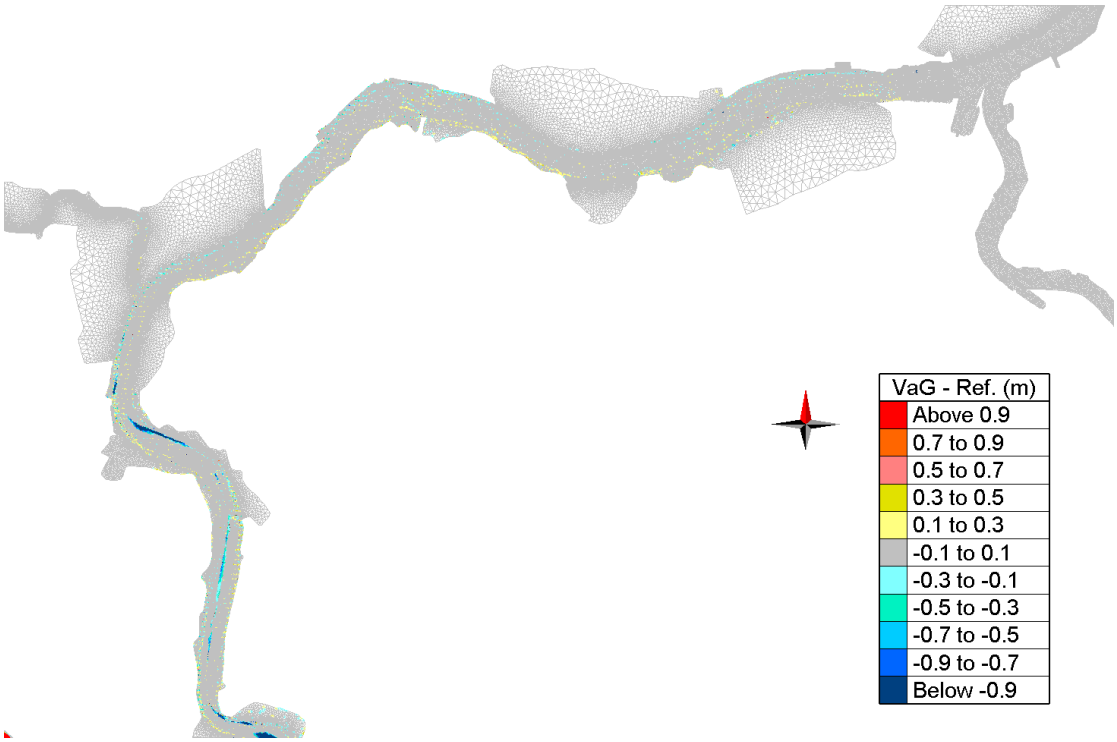

Figure 14 – Difference in bathymetry (VaG – Reference 2050) in zone 1

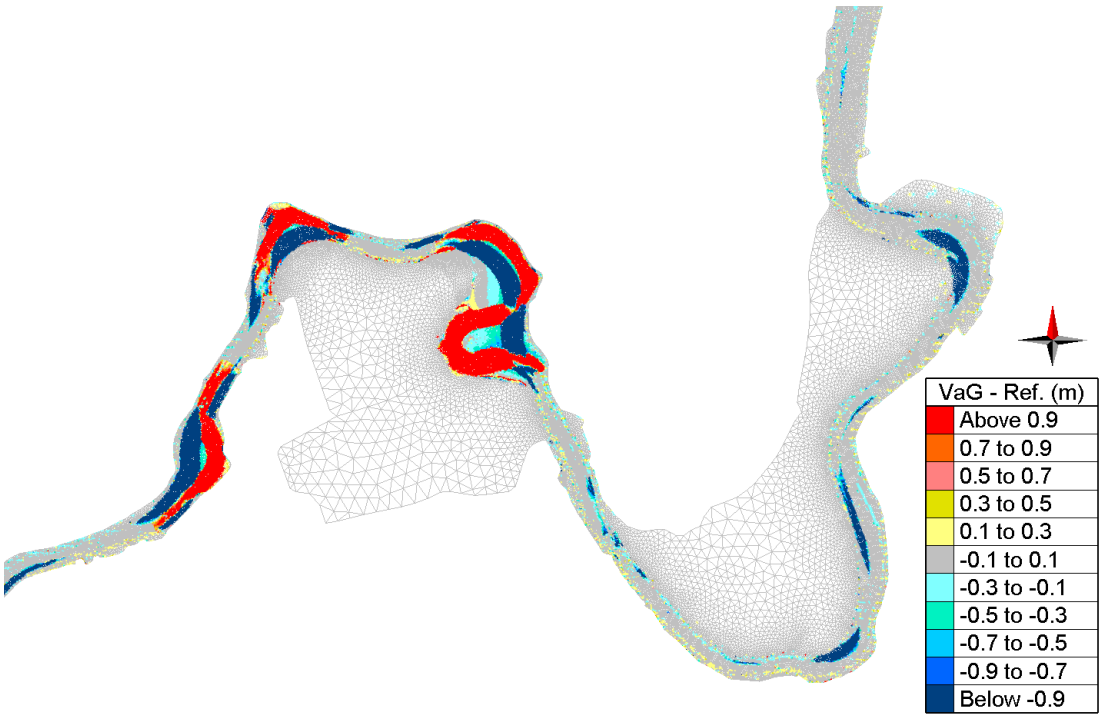

Figure 15 – Difference in bathymetry (VaG – Reference 2050) in zone 2

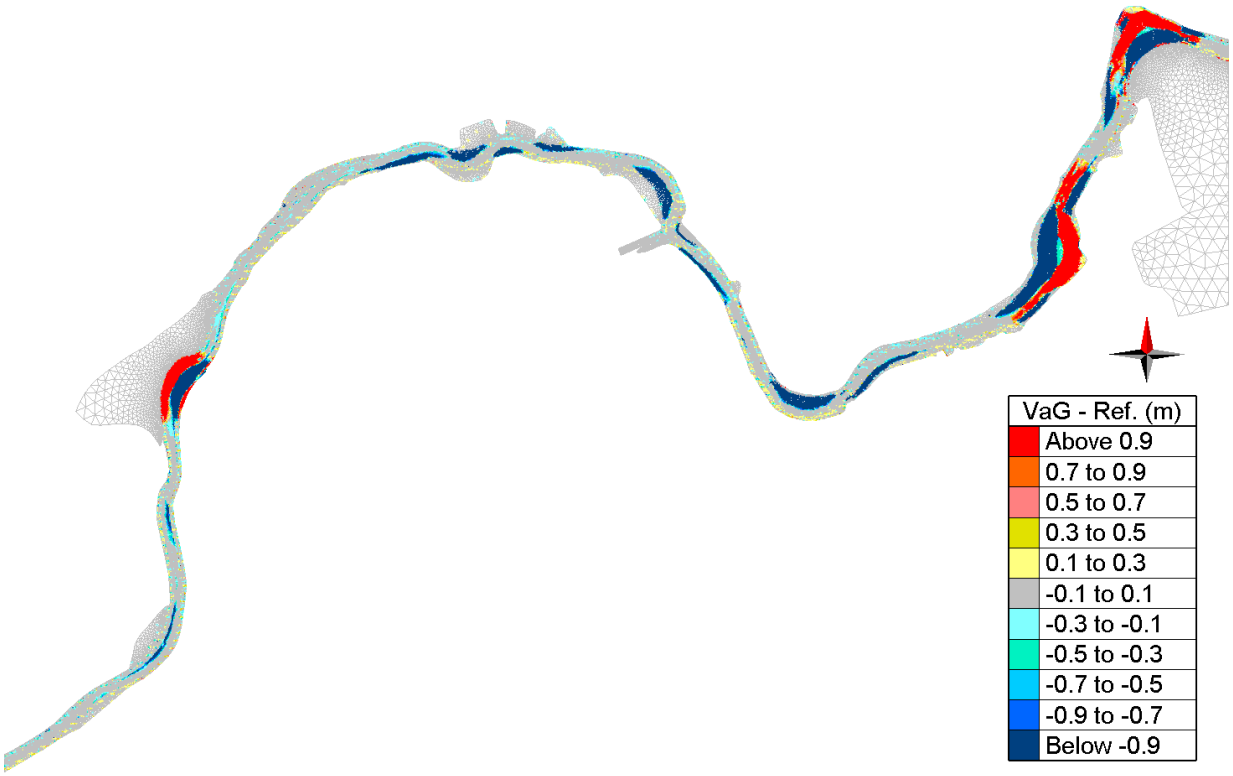

Figure 16 – Difference in bathymetry (VaG – Reference 2050) in zone 3

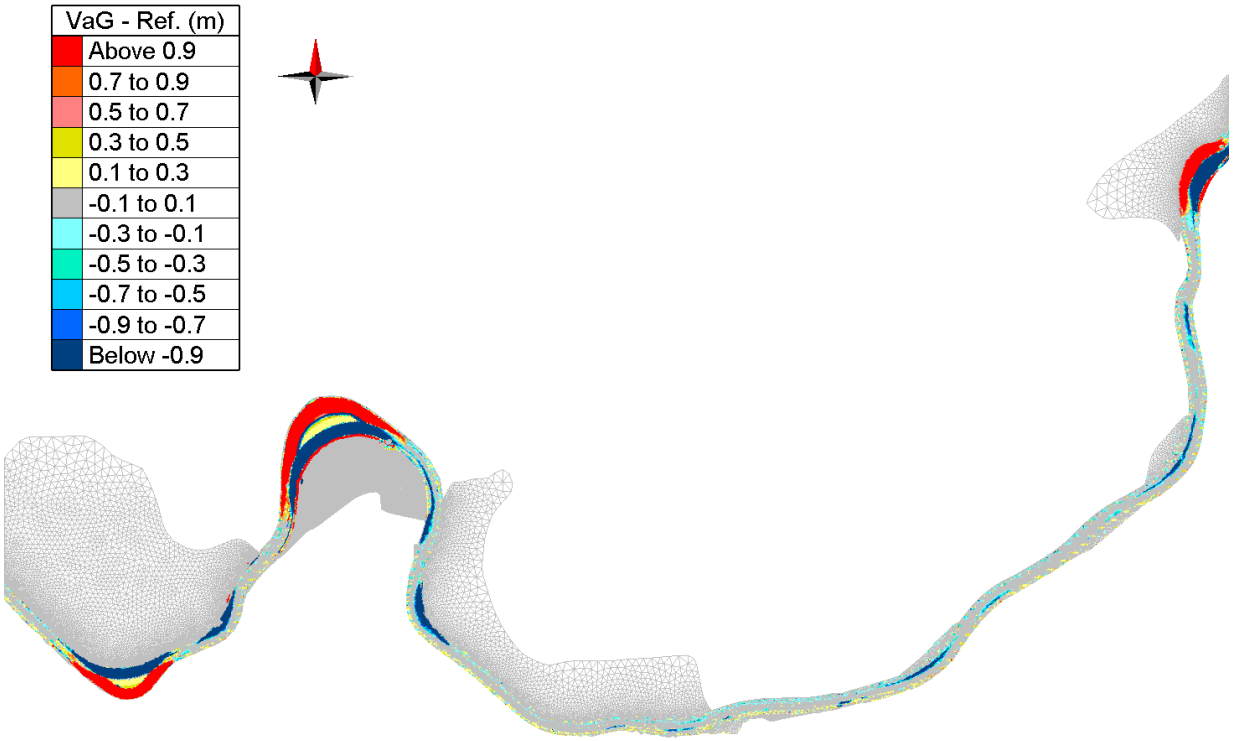

Figure 17 – Difference in bathymetry (VaG – Reference 2050) in zone 4

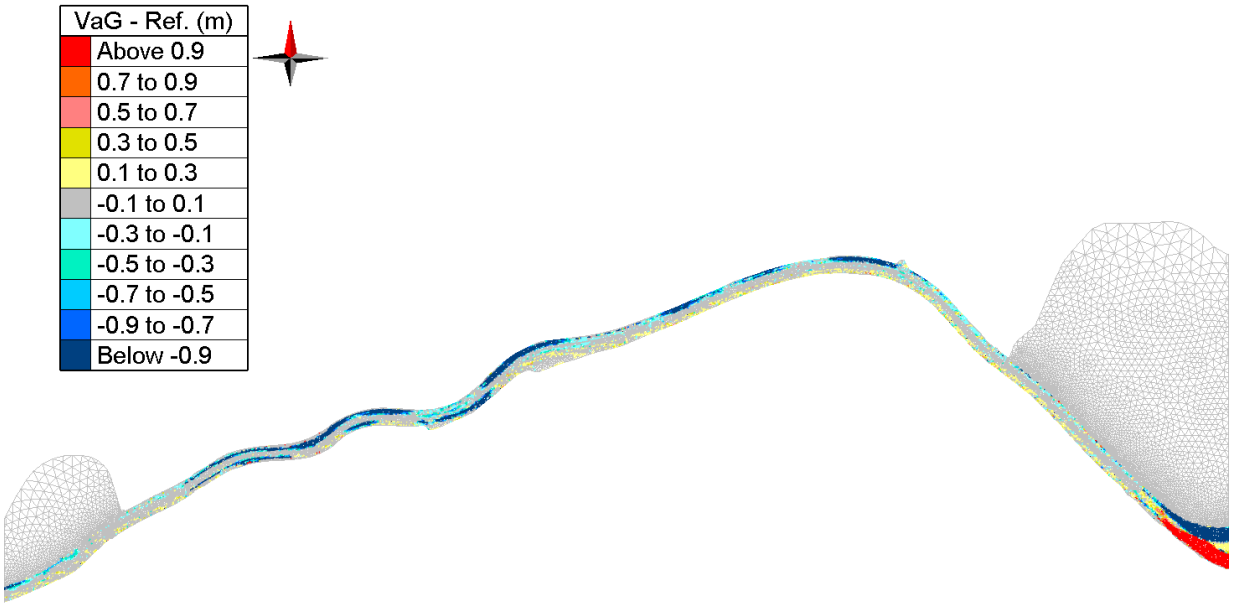

Figure 18 – Difference in bathymetry (VaG – Reference 2050) in zone 5

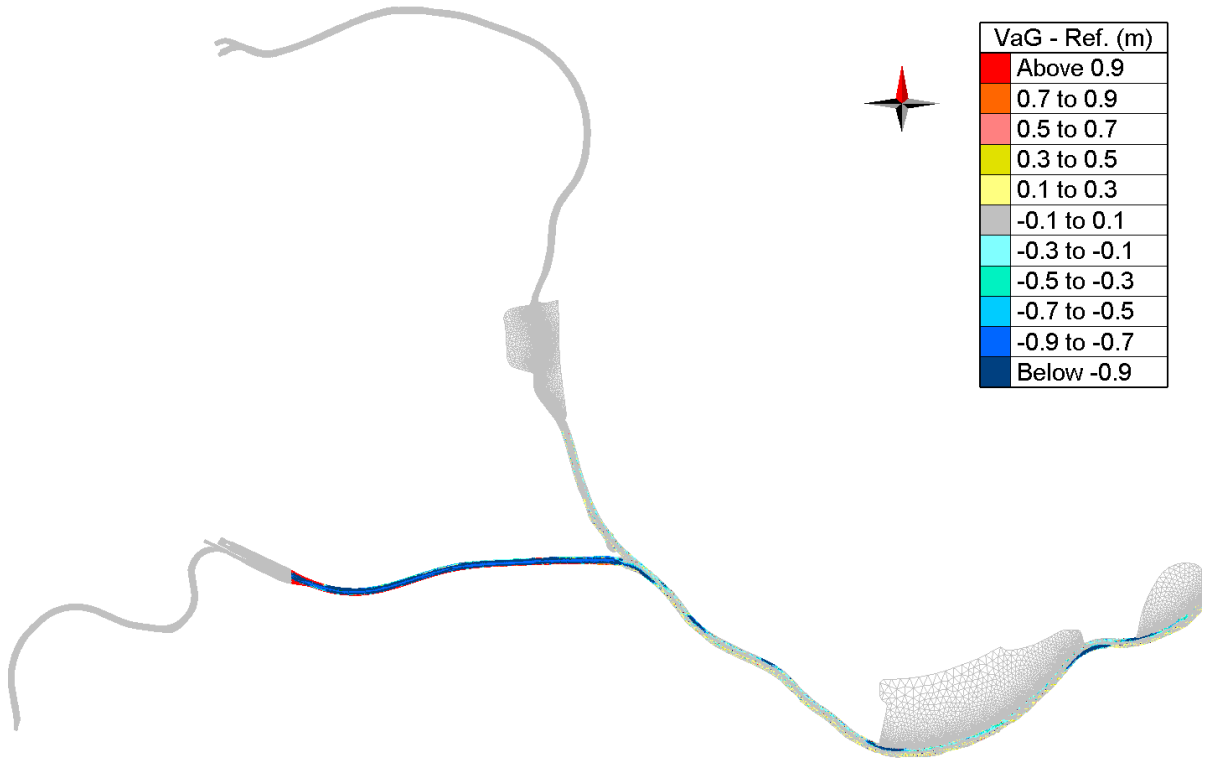

Figure 19 – Difference in bathymetry (VaG – Reference 2050) in zone 6

(4). The B alternatives (VaH)

VaH: Class Va standard design rules applied with Hybrid ("H") properties, specifically the "Chafing" alternative downstream Wichelen, and "VaG" upstream Wichelen. The differences in bathymetry from REF to VaH are shown in Figure 20 to Figure 25.

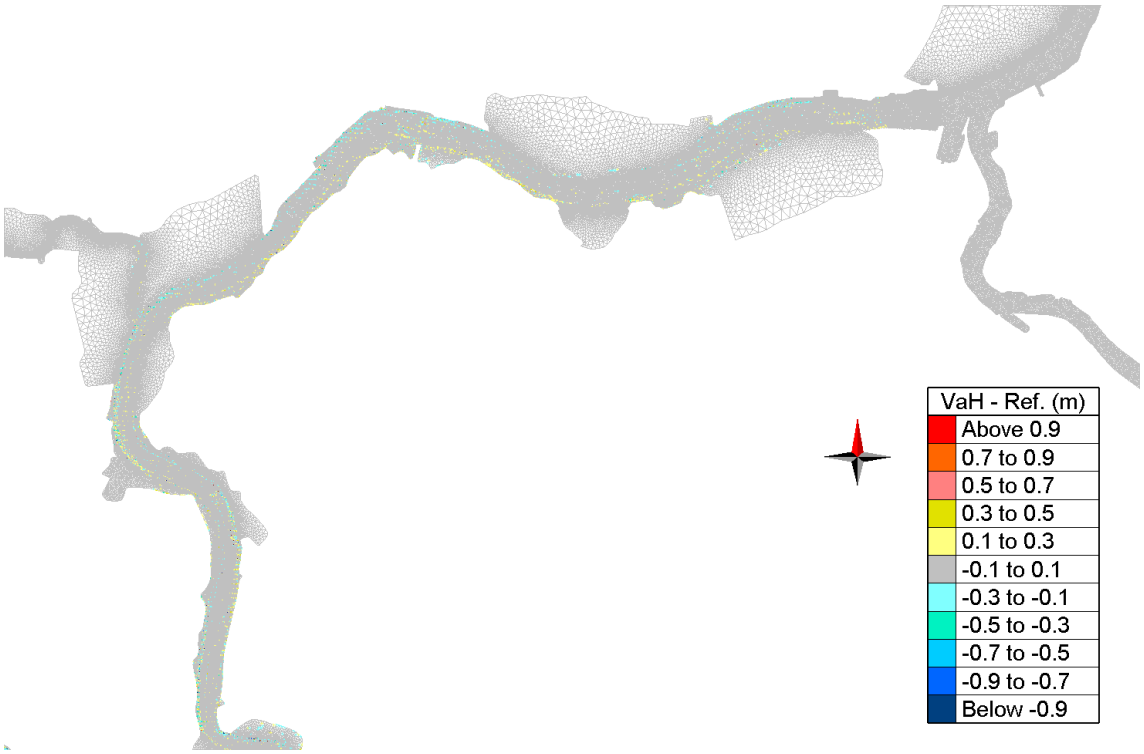

Figure 20 – Difference in bathymetry (VaH – Reference 2050) in zone 1

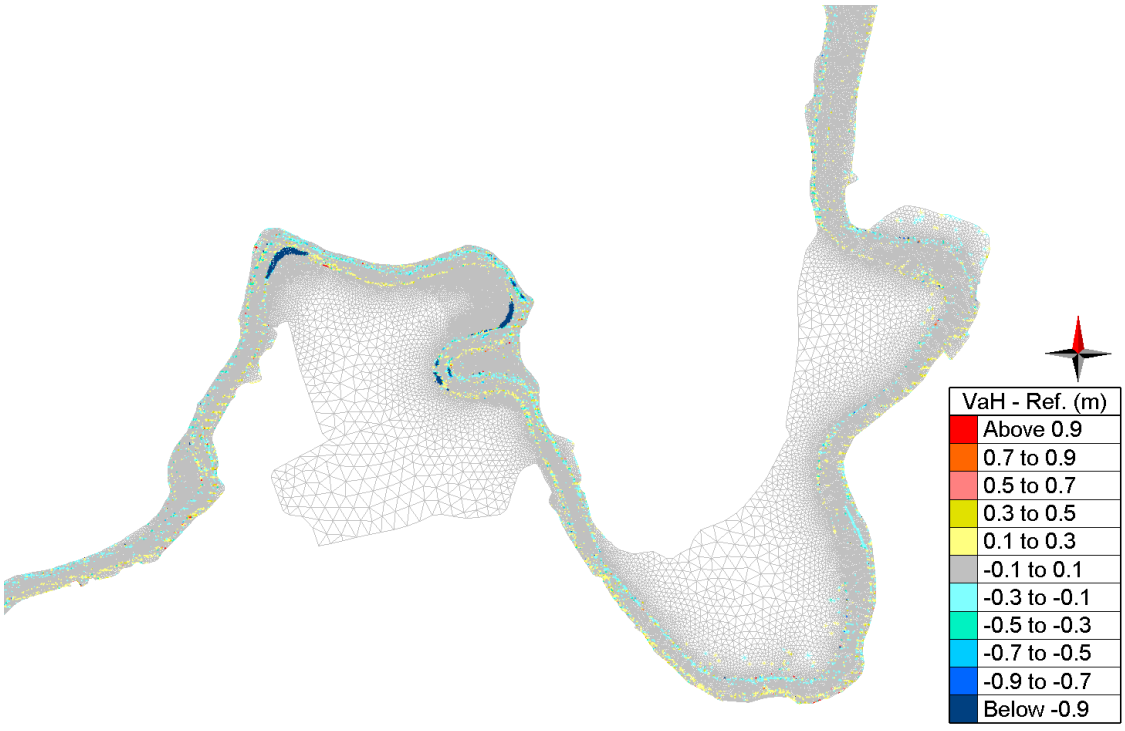

Figure 21 – Difference in bathymetry (VaH – Reference 2050) in zone 2

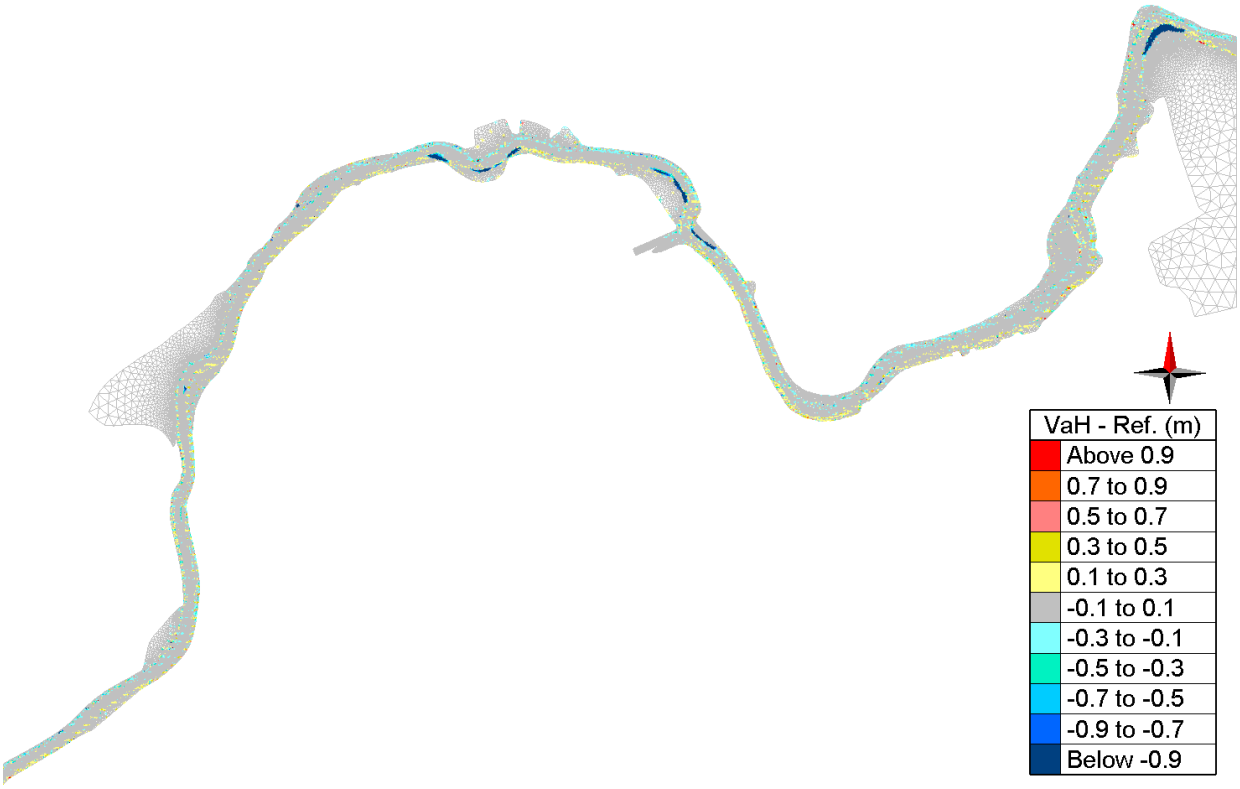

Figure 22 – Difference in bathymetry (VaH – Reference 2050) in zone 3

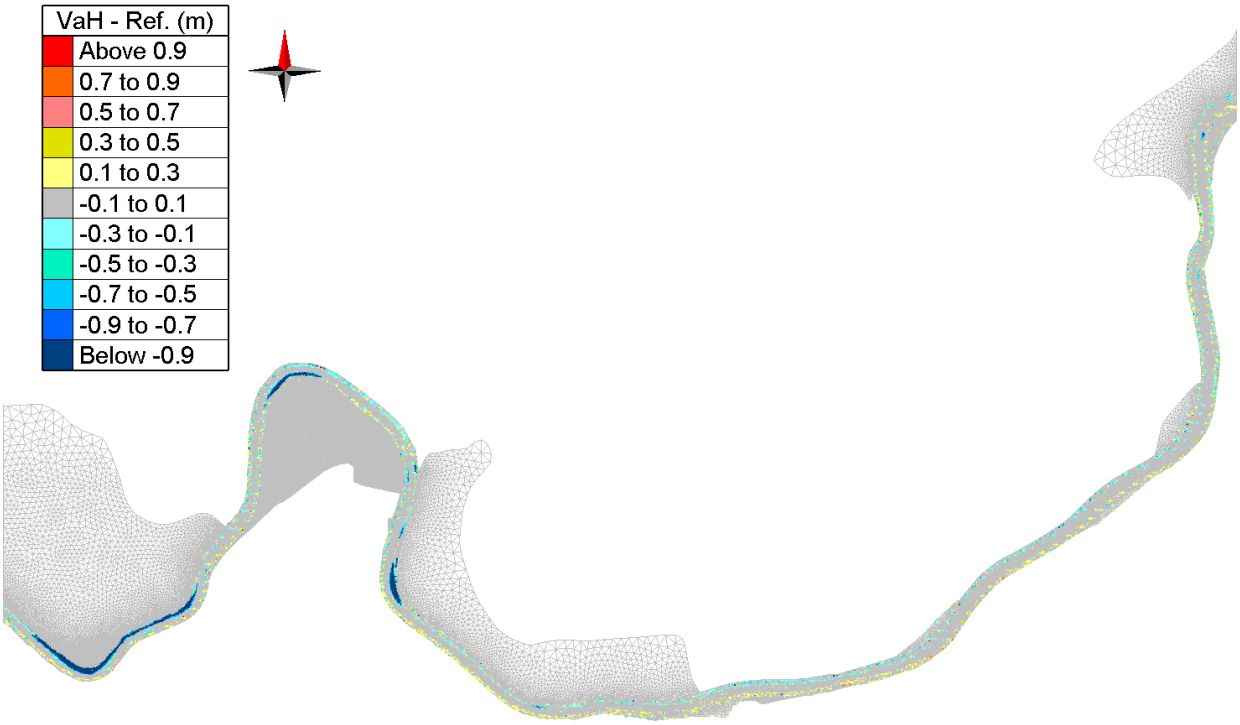

Figure 23 – Difference in bathymetry (VaH – Reference 2050) in zone 4

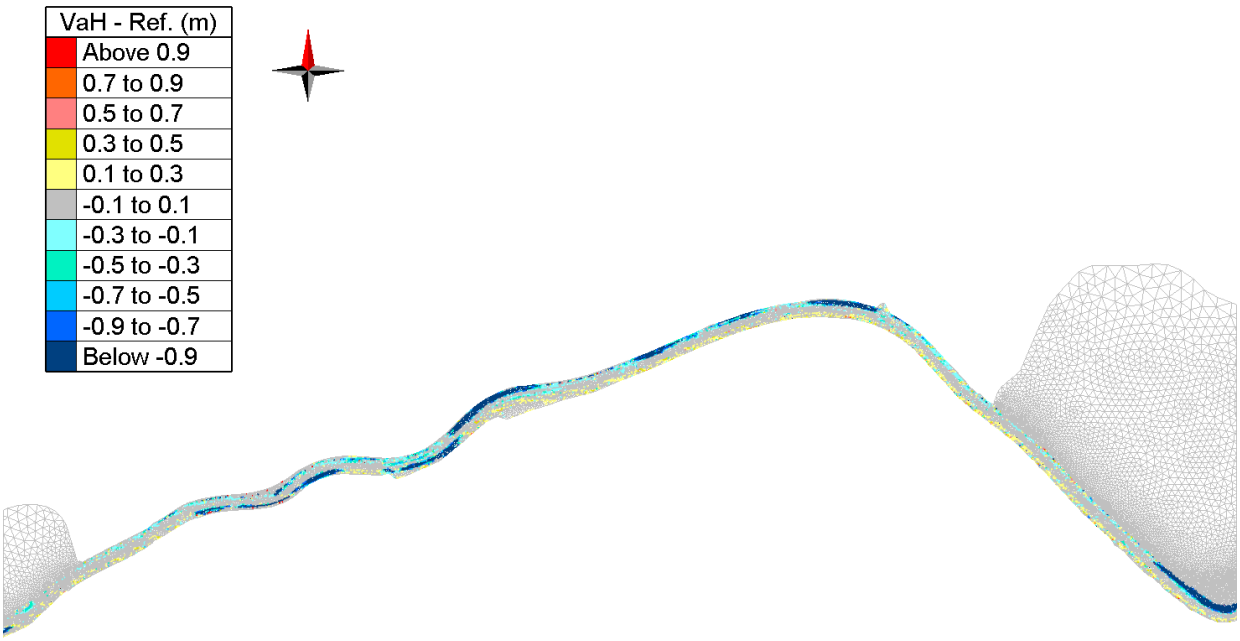

Figure 24 – Difference in bathymetry (VaH – Reference 2050) in zone 5

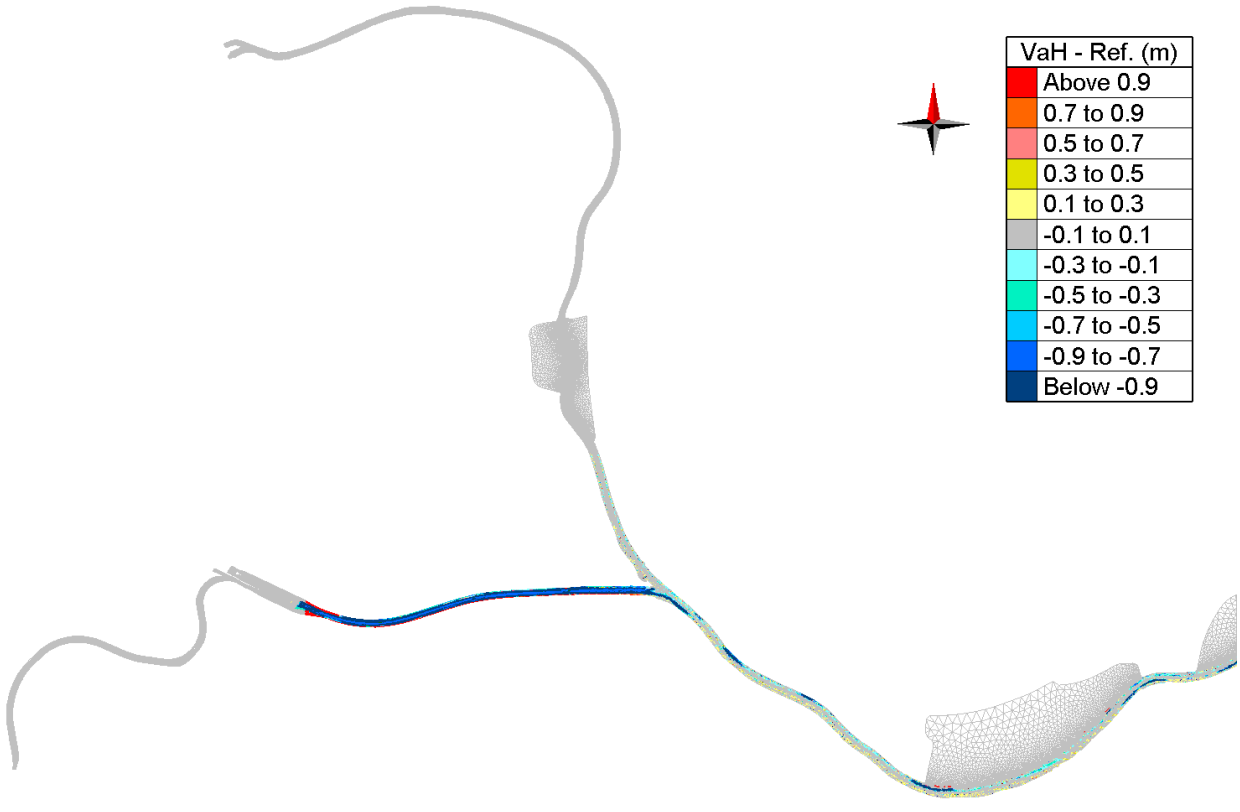

Figure 25 – Difference in bathymetry (VaH – Reference 2050) in zone 6

3.5.5 Overview of Model Runs

Eight model runs are devised to study the changes in sediment transport. The overview of model runs is listed in Table 4.

Table 4 – List of the different scenarios/alternatives runs

Code	Bathymetry (alternatives)	Discharge Type	Amplitude correction	Climate Scenario
2013_REF_A0CN (CAL_007)	2013	Q2013	A0	CN (2013)
2050_REF_A0CN	Reference	Q2013	A0	CN (2013)
2050_REF_AminCL	Reference	Q2050	A-	CL (2050)
2050_REF_AplusCH	Reference	Q2050	A+	CH (2050)
2050_Chafing_AplusCH	Chafing	Q2050	A+	CH (2050)
2050_VaG_AminCL	VaG	Q2050	A-	CL (2050)
2050_VaG_AplusCH	VaG	Q2050	A+	CH (2050)
2050_VaH_AplusCH	VaH	Q2050	A+	CH (2050)

(**A0**, **A+**, **A-**): Different tidal range scenarios.

(**CL**, **CH**): Sea level rise scenarios.

4 Methodology of Determining the Effects

4.1 Evaluation Framework

The evaluation of alternatives is based on the evaluation framework for the Integrated Plan Upper Seascheldt (IMDC, 2018). This partial evaluation framework addresses elements of the EIA disciplines Water and Fauna&Flora. The partial framework is based on the well-established Evaluation Method for the Scheldt Estuary (EMSE) (Holzhauer et al., 2011; Maris et al., 2014). The EMSE is a mostly quantitative and multidisciplinary approach to evaluating the state of the estuarine system of the Scheldt. The method is divided in themes but many links and relations between those themes are included in the method. The EMSE has a hierarchical structure that we also take over in our evaluation framework.

A difference is made between explanatory and evaluation parameters. These are grouped under indicators and themes. Note that an explanatory parameter can come back under different indicators.

The different explanatory and evaluation parameters that are described in this report are indicated in green in the table below.

Table 5 – Selected explanatory and evaluation parameters from the evaluation framework

Theme	Indicator	Evaluation Parameter	Explanatory Parameter
Water Quality			SPM concentration
Sediment and morphology	Sediment management	Maintenance dredging volumes	Sedimentation/erosion (maps)
			Bottom shear stress
			Suspended sediment fluxes
Hydrodynamics			Tidal asymmetry

The evaluation framework will be applied to the B- and C-alternatives in the Integrated Plan, as well as to the “Current” and “Reference” situation.

It is worth pointing out that, Delta SSC used in this study is calculated from surface SSC as requested, since the surface SSC is more important for ecological models used by other project partners. But the suspended sediment flux and its decomposed products (see §4.7) is based on cross-sectionally averaged quantities.

4.2 Delta SSC

The model is calibrated against measurements as described in Smolders et al. (2018).

Three models that are downstream in the modelling chain (ecosystem, fish and bird model) take surface SSC as an input. The modelling chain is explained in more detail in Smolders et al. (2018). These models are termed ‘subsequent models’ further in the text.

The methodology of working with Delta’s as shown in Figure 26 comes down to the simple notion that we don’t pass the modelled concentrations in the different scenario’s on to the subsequent models, but that

we rather calculate the relative effect of a change in bathymetry and/or boundary conditions in a dimensionless measure Δ. This dimensionless measure is then used to perturb the measured data that was used in setting up a subsequent model to take into account the expected effect in change of SSC.

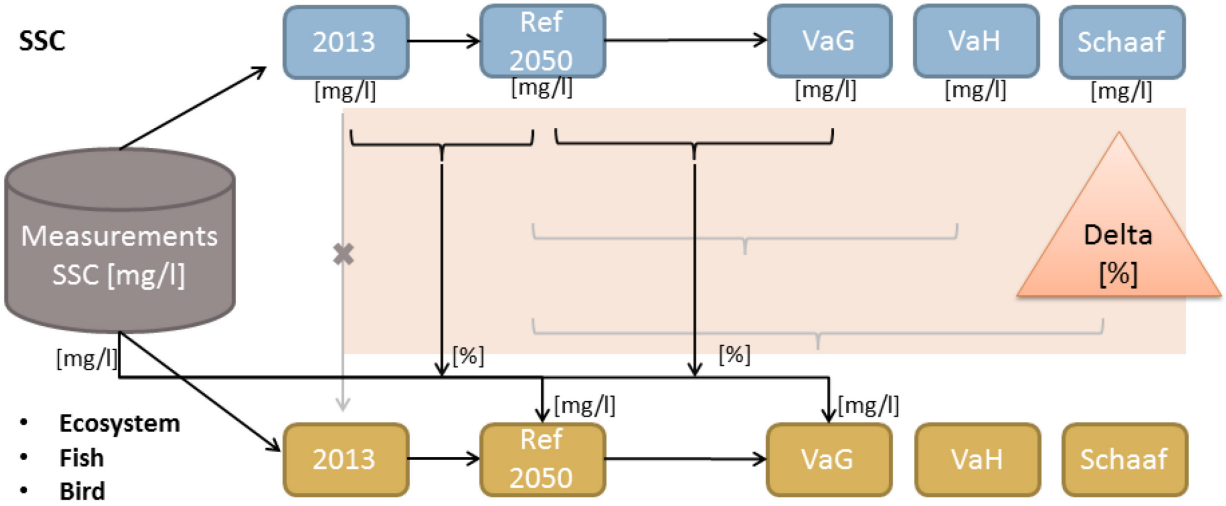

Figure 26 – Methodology of working with Delta's

We choose to calculate the delta's over the spatial extent of the boxes in the ecosystem model.

There are 87 boxes of the ecosystem model in total. The locations and its numbering are shown in detail in Figure 27 to Figure 30.

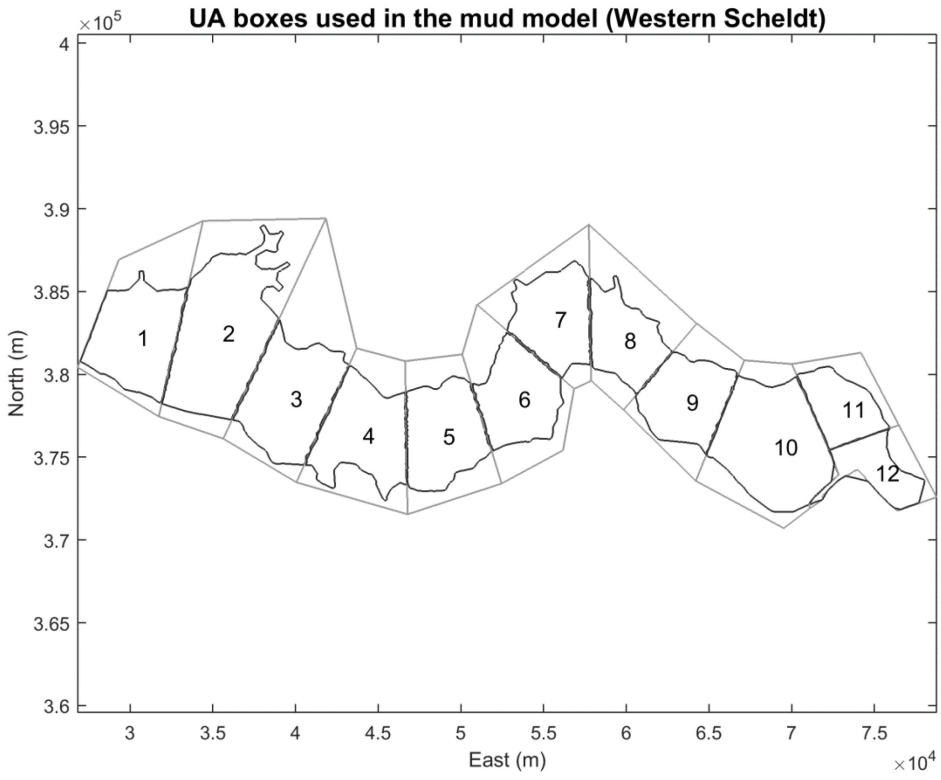

Figure 27 – boxes of the ecosystem model used in the calculation of the deltas (Western Scheldt)

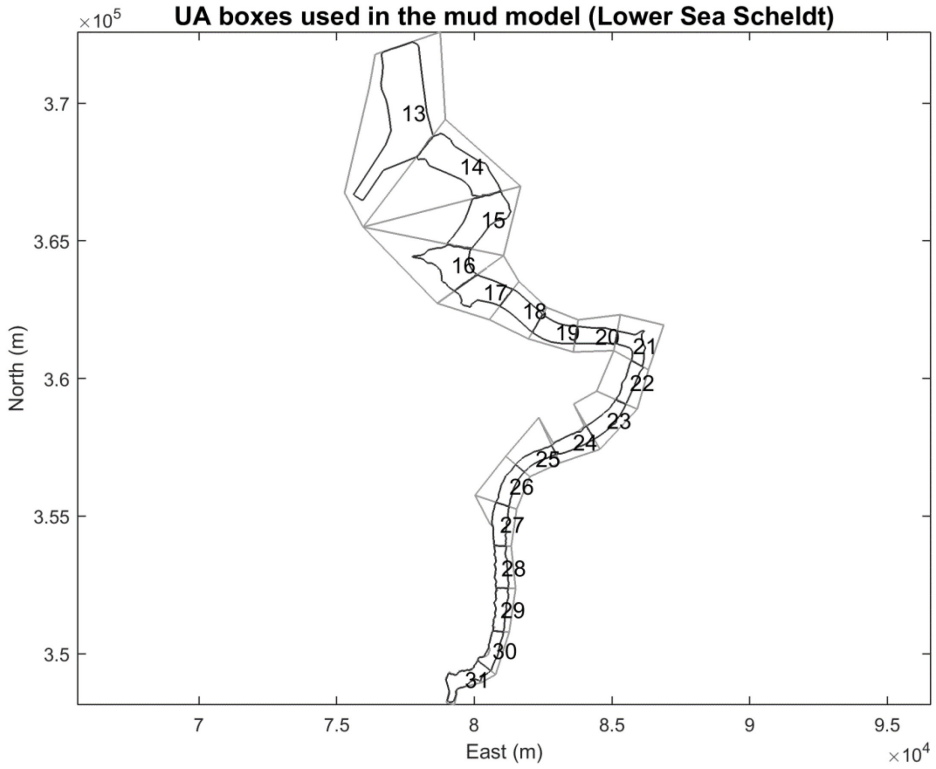

Figure 28 – boxes of the ecosystem model used in the calculation of the deltas (Lower Sea Scheldt)

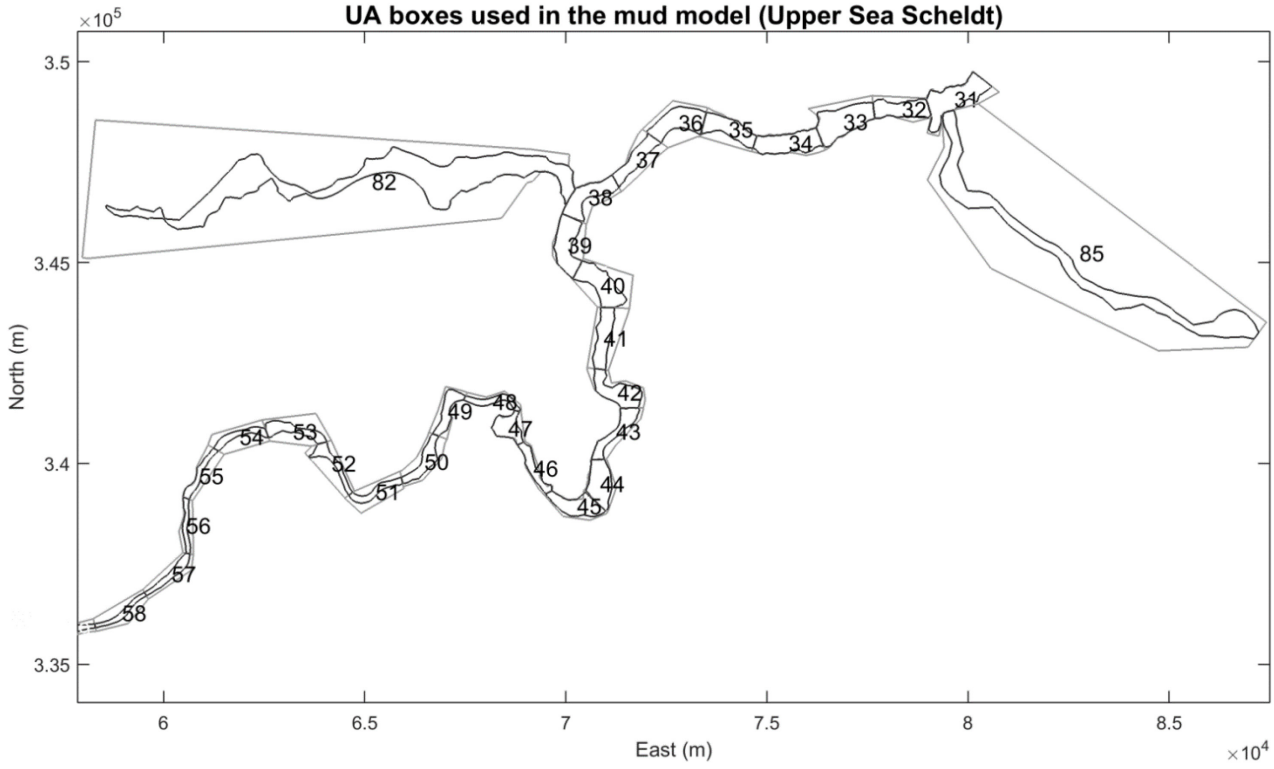

Figure 29 – boxes of the ecosystem model used in the calculation of the deltas (Upper Sea Scheldt Part 1)

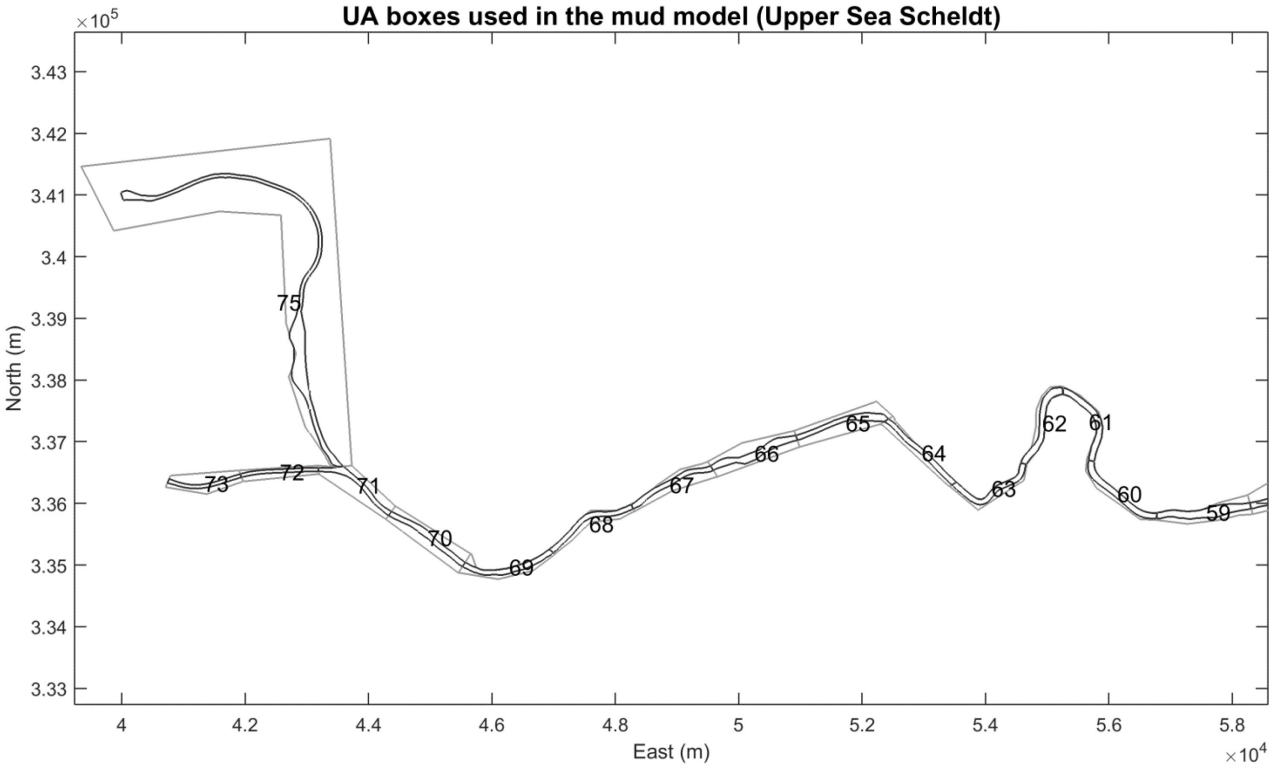

Figure 30 – boxes of the ecosystem model used in the calculation of the deltas (Upper Sea Scheldt Part 2)

The delta of SSC at time step *t* is computed in each box of the ecosystem model and it is defined as:

$$\Delta_{SSC}(t) = \frac{C_{sce} - C_{ref}}{C_{ref}} \quad (1)$$

in which C_{sce} and C_{ref} are the area-weighted mud concentration (surface concentration or depth averaged concentration depending on the purpose) from the scenario and the reference, respectively.

$$C_{sce} = \frac{1}{A}\int_A c_{sce} dA \quad (2)$$

$$C_{ref} = \frac{1}{A}\int_A c_{ref} dA \quad (3)$$

where, c_{sce} and c_{ref} are mud concentration at each node in that Box of the ecosystem model from the scenario and the reference, respectively, and A is nodal area. The nodal area is calculated based on the algorithm in Telemac-3D, which is used in the finite element method for spatial discretization. To be more specific, if a node is shared by *n* triangular elements, its nodal area can be found

$$A_{nodal} = \frac{1}{3}\sum_{i=1}^{n} A_i \quad (4)$$

where A is the area of an element, and 1/3 means the area of the triangular element is equally shared by its 3 vertices.

After that, the time series of Δ_{SSC} in each Box of the ecosystem model is averaged out over time in order to get the overall changes of SSC across the estuary.

$$\langle \Delta_{SSC} \rangle = \frac{\sum_t \Delta_{SSC}(t)}{T} \quad (5)$$

in which, t is time step, T is the period used for temporal averaging. The percentile p25 and p75 of the box-averaged Δ_{SSC} are also calculated over the averaging period, thus it can give an indication about how Δ_{SSC}varying in time.

In order to get rid of the unrealistic mud concentration given by the model on the drying/wetting points, only the subtidal channel points are used in the calculation of delta SSC. Note that the subtidal points can be different between two runs (e.g. when a bend is shortened). The subtidal channel points in the domain are found by calculating the minimum water depth at each node over the 40-day simulation period. Because the model is always initialized with hydrodynamic results from a 2-day spin-up run, the points that have minimum water depth above zero are always in the subtidal channels (wet points). The point list for each polygon is built from the wet points. Delta SSC for each polygon is calculated based on these points.

4.3 Thalweg plots

Although delta SSC is computed in each box of the ecosystem model, other indicators that are used to explain the changes in hydrodynamics and sediment flux are usually found at transects between polygons or thalweg points along the estuary. Therefore, a transformation is made to convert the polygon number to the distance from Vlissingen (Figure 31), by using the location of the point in the middle of each box to calculate the distance from Vlissingen.

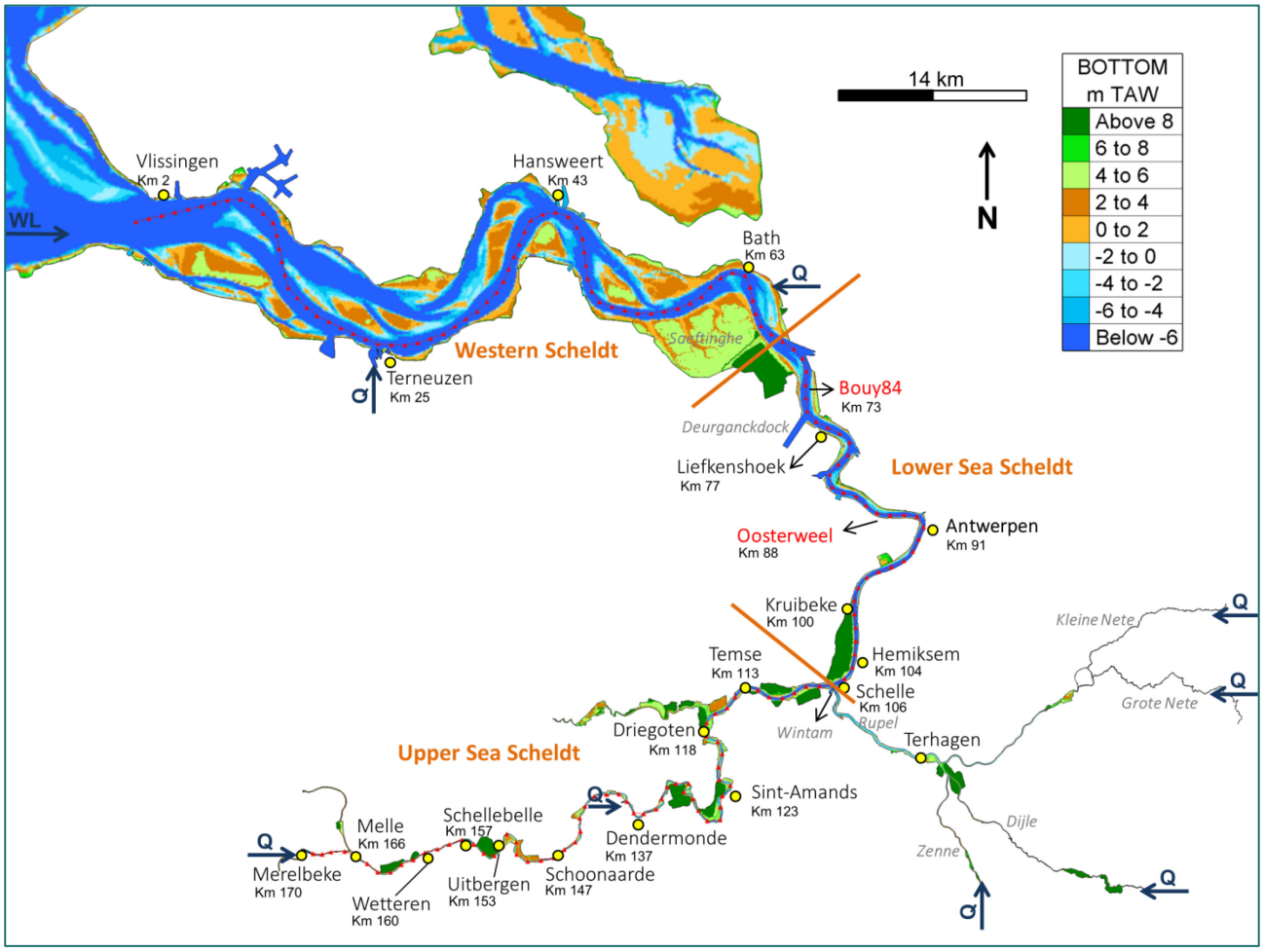

Figure 31 – Map of the Scheldt estuary with main tributaries and most important locations

4.4 Sedimentation rate

The sedimentation rate is computed from the model results for all the references and scenarios. Based on sedimentation rate, erosion-deposition maps could be generated to show the spatial influence of the scenarios during each comparison.

The last 20 days of the results are used for computing the sedimentation rate. In the following formula, B_0 (cm) is the bed thickness at the beginning of the last 20 days, and B_t (cm) is the bed layer thickness at the end of the same period. This gives the sedimentation rate in cm/yr

$$Sedimentation\ rate = (B_t - B_0) \times \frac{365}{20} \tag{6}$$

4.5 Maintenance dredging volumes

The maintenance dredging volumes are estimated based on the sedimentation observed in the mud model results. The computation is performed at two groups of dredging locations, one is located in the Lower Sea Scheldt and the other one is location in the Upper Sea Scheldt.

The sedimentation in polygons is computed based on nodal result of bed thickness.

$$Sedimentation\ in\ polygons = \int_A \rho_B (B_t - B_0) dA \approx \sum_{i=1}^{n} \rho_B (B_{ti} - B_{0i}) A_i \tag{7}$$

The final form of the formula uses nodal area and nodal values of bed layer thickness to approximate the total sedimentation mass in polygons. Here, B_{0i} (m) is the bed thickness at node i at the beginning of the last 20 days, and B_t (m) is the bed layer thickness at node i at the end of the same period, A_i is the nodal area computed in Telemac-3D, ρ_B is the bed layer density (500 kg/m^3 used in the mud model to simulate the freshly deposited layer), and n is the total number of the nodes in the polygons.

For the Lower Sea Scheldt, the sedimentation in the access channels, on the main sill and inside Deurganckdock (DGD) is investigated. There are 6 locations included in the calculation: 1.Deurganckdock, 2.Entrance Zandvliet, 3.Entrance Kallo lock, 4.Kruisschans, 5.Punt van Melsele and 6.Drempel van Frederik. These access channels and docks are within the area between 70 km to 84 km from Vlissingen. Their locations and the polygons used for calculation are plotted in Figure 32.

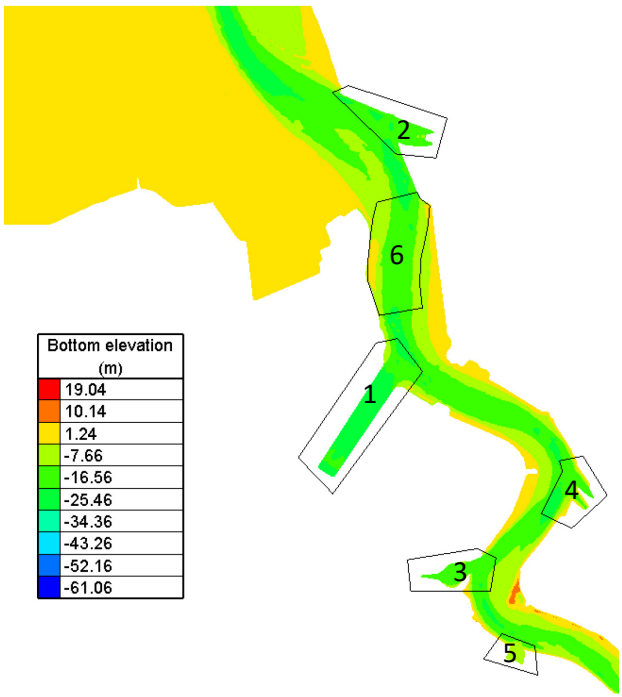

Figure 32 – Dredging locations in the Lower Sea Scheldt (access channels and DGD)

For the Upper Sea Scheldt, five locations are included for the calculation of sedimentation: 1.Durme, 2.Wintam, 3.Gentbrugge, 4.Ringvaart and 5.Zwijnaarde. These locations are indicated in Figure 33.

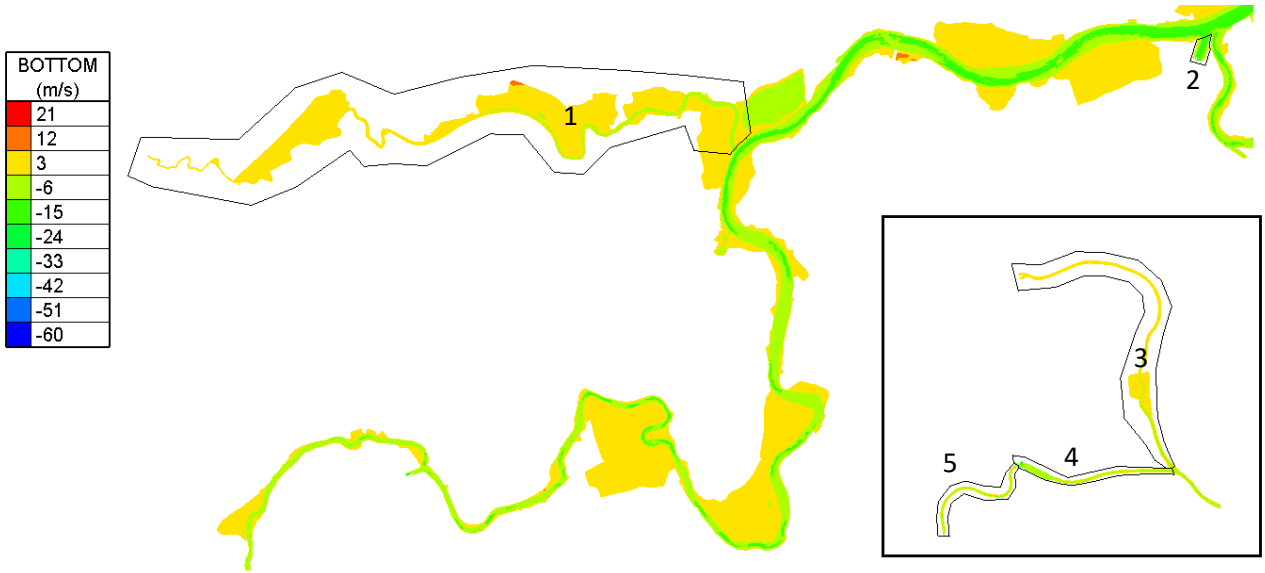

Figure 33 – Dredging locations in the Upper Sea Scheldt (Durme, Wintam, Gentbrugge, Ringvaart and Zwijnaarde)

4.6 Bed shear stress and its exceedance time

As mentioned in the evaluation framework for the model scenarios, Changes in bottom shear stress lead to changes in sedimentation/erosion patterns and habitat suitability. Therefore maps are made in the study area of maximum occurring bottom shear stress during a spring-neap cycle, and exceedance time of a threshold value of 1 Pa.

For getting the maximum bed shear stress, it is worth mentioning that, in the mud model, a uniform and constant bottom friction is used separately while computing the bed shear stress for sediment transport, and this bed stress is not exported in the model results . Therefore, the same computation is done again during post-processing, using the velocity and water depth at each node for every time step, using the quadratic friction law:

$$\tau_b = \frac{1}{2}\rho_w C_D \overline{U}\left|\overline{U}\right| \tag{8}$$

$$C_D = 2n^2 \frac{g}{h^{1/3}} \tag{9}$$

where, τ_b is bed shear stress, C_D is drag coefficient, $\overline{U}$ is the depth-averaged velocity (which is also calculated in SEDI-3D), *n* is the Manning coefficient (0.02 in the mud model), *g* is gravitational constant and *h* is the water depth. Then the maximum value at each node is recorded during a spring-neap cycle.

The exceedance time of bed shear stress > 1Pa is computed at each node based on the above bed shear stress as well. The exceedance time is presented as a ratio (%) between the number of time steps at which the bed shear stress exceeds 1Pa, and the total number of time steps.

4.7 Decomposition of Sediment Transport and Flux

Sediment transport rate and sediment flux is calculated on the transects that separate the different boxes in the ecosystem model.

We distinguish between **sediment transport** (kg/s) and **sediment flux** (kg/s/m²). The ratio between the two is the cross-sectional area at that particular transect.

The total sediment transport (Q_T) is decomposed into three parts, which link to different driving mechanisms:

- Sediment transport related to discharge (Q_A);
- Sediment transport due to tidal pumping (Q_P);
- Residual term (Q_R). This term is not to be confounded with residual transport which is sometimes used to denote the net transport over a spring-neap cycle. The residual term here is simply the closing term in equation (17).

Let *U* be the cross-sectionally averaged along-channel velocity (positive sign means downstream and negative sign means upstream), calculated as

$$U = \frac{\int_A udA}{A} \tag{10}$$

with u the along channel component of velocity. U and A vary over time. U can be decomposed in a tidal average $\langle U \rangle$ and a deviation from the tidal average U'. By definition, $\langle U' \rangle = 0$.

$$U = \langle U \rangle + U' \tag{11}$$

A Godin filter is applied to obtain tidally-averaged quantities $\langle \cdot \rangle$. It is a set of cascaded running-mean filters introduced by Godin (1966), which is commonly used as a low-pass filter to remove diurnal, semidiurnal, and shorter-period components (Emery & Thomson, 2001). The filter consists of successive uses of three running averages of 24h, again 24h and 25h lengths.

Similarly, the transect area A changes due to varying water depth and submerged area and it can be decomposed into a tidal average $\langle A \rangle$ and a deviation from the tidal average A'.

The cross-sectionally averaged suspended sediment concentration C is derived in the same way from suspension concentration c.

$$C = \frac{\int_A c \, dA}{A} \tag{12}$$

And C is decomposed into a tidal average part and its fluctuations:

$$C = \langle C \rangle + C' \tag{13}$$

The instantaneous sediment transport Q (kg/s), using cross-sectionally averaged quantities is

$$Q = UCA \tag{14}$$

Note that this analysis uses cross-sectionally averaged quantities. Therefore, it is a 1D analysis for simplicity, in which variations over the cross section are omitted. It captures the more general driving mechanisms, such as advective transport due to mean flow, and transport due to tidal motion, but will not catch the more complex contributions related to vertical variations or variations over the cross section. This method will not pick up on net transport due to the spatial distribution of u and c (e.g. lock exchange flow).

The tidally averaged sediment transport is

$$\langle Q \rangle = \langle UCA \rangle \tag{15}$$

This can be written out as

$$\langle Q \rangle = \langle U \rangle \langle C \rangle \langle A \rangle + \langle U \rangle \langle C'A' \rangle + \langle C \rangle \langle U'A' \rangle + \langle A \rangle \langle U'C' \rangle + \langle U'C'A' \rangle \tag{16}$$

Following similar procedures in Scully et al. (2007), this is decomposed into advective transport, tidal-pumping and a residual part.

$$\langle Q \rangle = Q_A + Q_P + Q_R \tag{17}$$

The term of advective transport consists of two parts , given as:

$$Q_A = \langle C \rangle (\langle U \rangle \langle A \rangle + \langle U'A' \rangle) \tag{18}$$

Q_A is directly scaled to the water discharge due to the fact that, the water discharge can be expressed as $\langle UA \rangle = \langle U \rangle \langle A \rangle + \langle U'A' \rangle$. It is worth mentioning that Q_A could also include the influence of return flow. But generally discharge is dominant.

The transport due to tidal pumping is then given as:

$$Q_P = \langle U'C' \rangle \langle A \rangle \tag{19}$$

where the primes indicate the deviations from the tidally averaged values. Burchard et al. (2018) denote this flux as “Tidal Covariance Transport” in general, and give tidal pumping as an example of this flux.

The terms left from the decomposition are grouped together in a residual term Q_R.

$$Q_R = \langle U \rangle \langle C'A' \rangle + \langle U'C'A' \rangle \quad (20)$$

Q_R is relatively small and negligible since the correlation between *C'* and *A'* is small.

This way of decomposition of sediment transport enables us to more closely examine the processes driving sediment flux.

In general, the sediment transport is larger in the downstream and smaller in the upstream. This is due to the differences of transect areas. In order to reveal more transport patterns, the transport rate can be divided by their transect areas, which is varying over time.

4.8 Tidal Asymmetry

An important factor that could cause residual sediment transport in estuaries is tidal asymmetry. In the Western Scheldt it is a principal factor influencing the sediment exchange between the ebb tidal delta and the estuary, as well as between the various part of the estuary (Wang et al., 1999).

Eulerian asymmetries (Friedrichs, 2011) are determined based on local (point) variations of velocity and water level.

4.8.1 Duration asymmetry

Based on the different tidal duration, three asymmetry parameters are used to analyse and to evaluate the effects of each bathymetry alternative. These parameters are described as follows:

Ratios bigger than one are interpreted as ebb dominance.

1. The tidal asymmetry of *the duration (time) of rising and falling tide*:

$$\frac{T_{\text{falling}}}{T_{\text{rising}}}$$

   $T_{falling}$ = time required within the tidal cycle to change water level from HW to LW.

   T_{rising} = time required within the tidal cycle to change water level from LW to HW;

2. The tidal asymmetry based on duration of *ebb-period and flood-period*:

$$\frac{T_{\text{ebb}}}{T_{\text{flood}}}$$

   T_{ebb} = duration of ebb flow during the tidal cycle.

   T_{flood} = duration of flood flow during the tidal cycle;

3. The tidal asymmetry based on slack water duration of *ebb-period and flood-period*:

$$\frac{T_{\text{LW slack}}}{T_{\text{HW slack}}}$$

   $T_{LW\ slack}$ = duration of slack water (when velocity magnitude <0.3 m/s) around LW.

   $T_{HW\ slack}$ = duration of slack water (when velocity magnitude <0.3 m/s) around HW;

   This type of asymmetry generally affects finer sediment transport through differential settling times and resuspension lags around high/low slack water (Van Straaten and Kuenen, 1958; Postma, 1961; Pritchard, 2005). If the duration of LW slack water exceeds the duration of the duration of HW slack, the residual sediment transport is more likely to be in ebb direction.

4.8.2 Velocity asymmetry

A difference between maximum ebb and flood velocity induces an asymmetry in sediment transport. The residual transport takes the direction of the highest peak velocity. This mechanism has been mainly investigated for bed-load transport (Van de Kreeke and Robeczewska, 1993; Dronkers, 1986; Friedrichs and Aubrey, 1988). However, also in the case of suspended transport, the concentration is proportional to the erosion flux, which is proportional to the squared velocity via the bed shear stress. Therefore, the sediment flux is proportional to V^3 for non-cohesive fractions, and to V^4 for the cohesive fractions (Gatto, 2017).

Ratios bigger than one are interpreted as ebb dominance.

1. The tidal asymmetry of the *maximum current flow velocities during ebb and flood phases*:

   This tidal asymmetry parameter is based on maximum velocity during flood and maximum velocity during ebb within the tidal cycle. Averaged cross sectional velocities are computed by dividing the discharge at a certain cross-section by the wet area of this cross-section (V= Discharge (Q) / wet area (A)).

$$\frac{V_{\max ebb}}{V_{\max flood}}$$

   V_{maxebb} = maximum current velocity during ebb phase.

   $V_{maxflood}$ = maximum current velocity during flood phase;

2. The tidal asymmetry of the *mean current flow velocities during ebb and flood phases*:

$$\frac{V_{\text{mean } ebb}}{V_{\text{mean } flood}}$$

   $V_{meanebb}$ = mean current velocity during ebb phase.

   $V_{meanflood}$ = mean current velocity during flood phase;

3. The asymmetry calculated based on the velocity as proxy for *the transport of fine sediments (~V^4)*:

$$\frac{\frac{1}{T_{\text{ebb}}}\int^{\text{ebb duration}} V^4 dt}{\frac{1}{T_{\text{flood}}}\int^{\text{flood duration}} V^4 dt}$$

   T_{ebb} = duration of ebb flow during the tidal cycle.

   T_{flood} = duration of flood flow during the tidal cycle;

   Capacity, or near-capacity conditions occur when sediment availability is abundant. Such conditions are encountered in the turbidity maximum of estuaries and coastal areas, above mud banks and in very turbid systems like the Severn estuary. It can be shown that the capacity (or saturation) concentration is proportional to V^3, hence the sediment transport is proportional to V^4. The above reasoning is based on the paper of Winterwerp (2001).

4.8.3 Skewness as a measure of tidal asymmetry

Nidzieko and Ralston (2012) argued that using harmonic constituents to quantify tidal asymmetry is sensitive to record length. Neighbouring constituent pairs, such as M_2 and N_2, cannot be resolved from records that are too short, and phenomena due to spring-neap cycles or weather events are not resolved. Additionally, nonlinearities in velocity can be broad-banded and therefore not properly quantified with harmonic methods alone (Godin, 1991). Therefore, they calculate the third moment about zero, normalized by the second moment about zero to the 3/2 power as a skewness-like indicator for the tidal asymmetry.

$$\gamma_0 = \frac{\mu_3}{\mu_2^{3/2}} \tag{21}$$

where μ_m is the *m*-th moment *about zero* and it is defined as

$$\mu_m = \frac{1}{N-1}\sum_{i=1}^{N}(n_i)^m \tag{22}$$

and *N* is the number of samples n_i.

These samples can be both cross-sectionally averaged velocities (for quantifying the ebb/flood velocity asymmetry), i.e. $n_i = u_i$, or the time derivative of water elevation (for quantifying the duration asymmetry), i.e. $n_i = \frac{d\zeta_i}{dt}$.

The coefficient γ_0 is clearly inspired on the coefficient of skewness γ_1, which is a measure for the degree of symmetry in a distribution (Sheskin, 2011). For comparison, the skewness of a random variable is defined as:

$$\gamma_1 = \frac{\kappa_3}{\kappa_2^{3/2}} \tag{23}$$

with κ_m the m-th *central* moment around the mean

$$\kappa_m = \frac{1}{N-1}\sum_{i=1}^{N}(n_i - \bar{n})^m \tag{24}$$

with $\bar{n}$ the average over the samples.

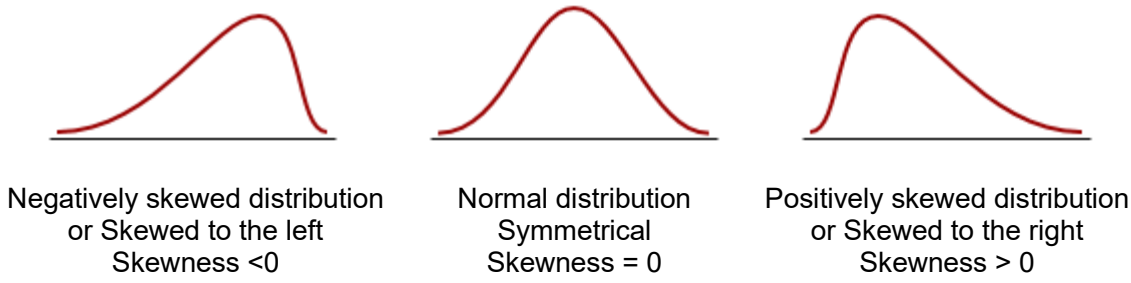

Figure 34 – Skewness and the meaning of being negative and positive.

The difference between the "skewness-like" indicator γ_0 and the "normal" skewness γ_1 is that, instead of using the central moment (moment about the variable's mean), it uses the moment about zero.

Cross-sectionally averaged velocity is already centred at zero, with negative pointing upstream and positive pointing downstream (in current study). Because it can reveal the skewness between upstream and downstream peak-velocities, it can be used to indicate the net transport direction when the peak-velocity asymmetry is most relevant. For instance, positive velocity skewness means larger peak ebb flow velocities, hence, seaward transport; negative velocity skewness means larger peak flood flow velocities, hence, landward transport.

When the indicators $V_{max\,ebb}/V_{max\,flood}$ and $V_{mean\,ebb}/V_{mean\,flood}$ show different behaviour, the velocity skewness can provide additional insight, because it is sensitive to the changes in the entire stochastic distribution, including maximum and mean velocities and its direction.

For quantifying the duration asymmetry, the time derivative of water level is taken as samples in the skewness calculation. A positive value of duration skewness means duration of LW to HW (rising tide) is shorter than the duration of HW to LW (falling tide). This is similar to the ratio $T_{\mathrm{falling}}/T_{\mathrm{rising}}$ being larger than one.

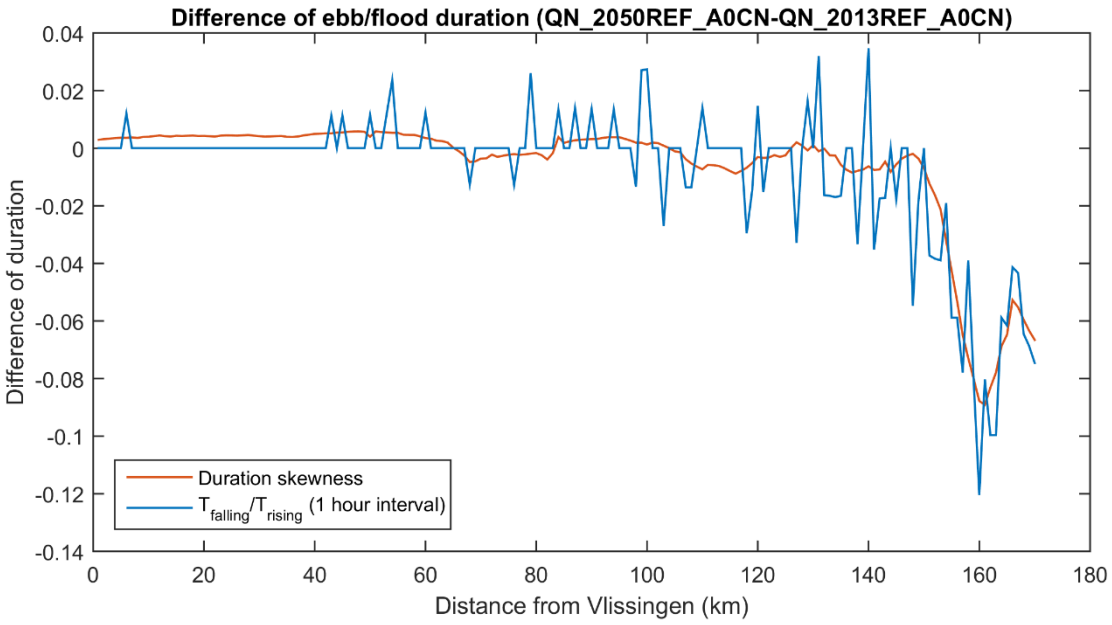

Figure 35 – Comparison of Tfalling/Trising and the duration skewness

An important advantage of using duration skewness is that it is less sensitive to the time interval of the output. To calculate $T_{\mathrm{falling}}/T_{\mathrm{rising}}$ based on its definition usually requires the output of minimum every 10 min since it is sensitive to the number of the data points. This can increase the size of the result file. Skewness appears to be less sensitive to the number of data points, although more data points will also increase its accuracy. An example is illustrated in Figure 35. It can be seen that there are more wiggles in the difference of $T_{\mathrm{falling}}/T_{\mathrm{rising}}$ between scenario and reference. This is due to the coarse time interval (1 hour) in the output file. Duration skewness is apparently less sensitive to the coarse time interval and gives a smoother result.

5 Evaluation of Alternatives

5.1 From 2013 to 2050

The shift from 2013 to 2050 is done in two steps. First, only the bathymetry is changed. The effects of this change is investigated in the 2013 boundary conditions (A0CN) and are described in §5.1.1.

Then the boundary conditions are changed to 2050. Two different downstream boundary conditions are considered: AminCL (in §5.1.2) and AplusCH (in §5.1.3). For the definition of these boundary conditions, reader is referred to chapter 3.5.

5.1.1 From 2013 bathymetry to 2050 sustainable bathymetry

The Sustainable Bathymetry is used in the 2050 scenarios, which is different from the 2013 bathymetry (Figure 4). The Sustainable Bathymetry takes into account the needs for navigation and the characteristics of the river. Furthermore, in 2050_REF_A0CN, there are more culverts activated in the domain, meaning more flood control areas are available along the Scheldt, allowing water flow into and out of the area during ebb and flood.

The two model runs, 2050_REF_A0CN and 2013_REF_A0CN, use the same downstream and upstream boundary conditions (water levels and velocity components for downstream and discharges for upstream) as mentioned in §3.2.2. Sea level rise is not included in these runs. The model settings, including physical parameters are the same.

(1). The difference in hydrodynamics

As can be seen in Figure 36, the difference of flow velocity in the North Sea and the Western Scheldt is negligible due to the fact that the downstream boundary and the bathymetry in these areas remain the same from 2013_REF_A0CN to 2050_REF_A0CN.

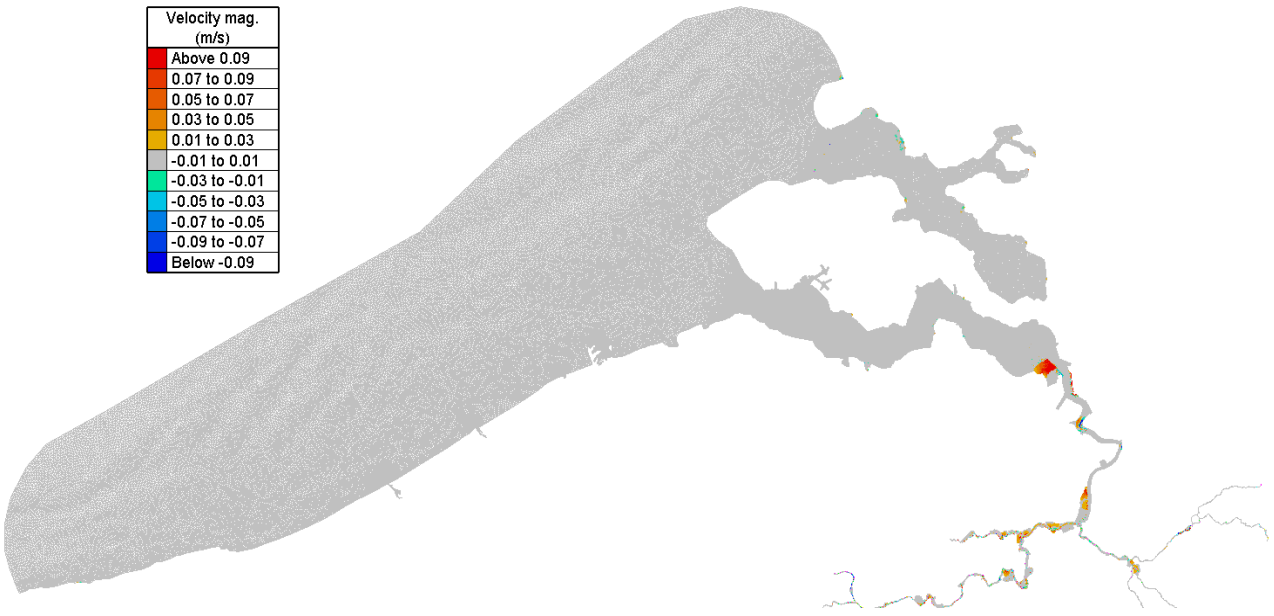

Figure 36 – Time averaged velocity difference between two runs (2050_REF_A0CN - 2013_REF_A0CN)

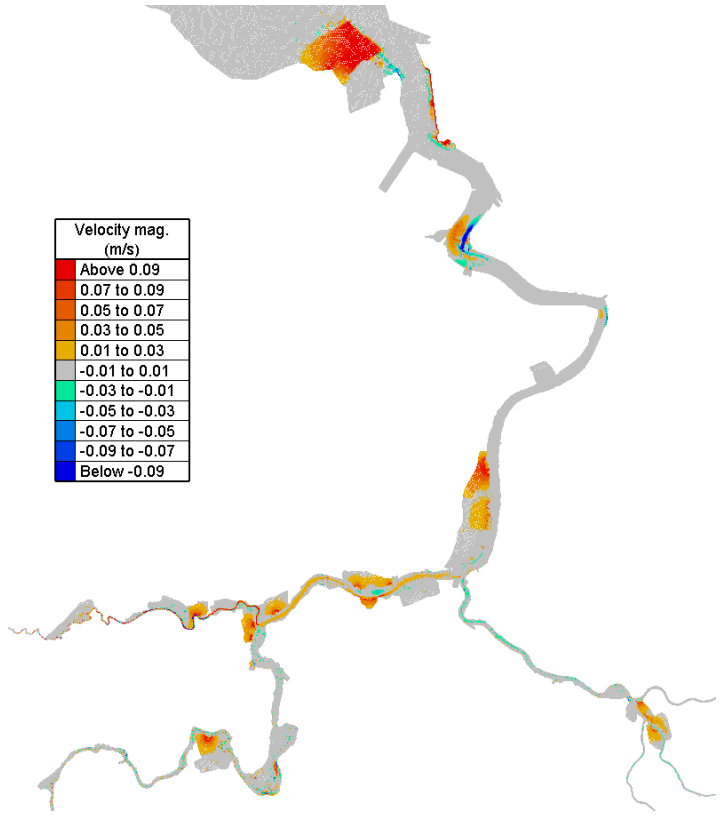

Figure 37 – Time averaged velocity difference in Upper Sea Scheldt (2050_REF_A0CN - 2013_REF_A0CN) – part 1

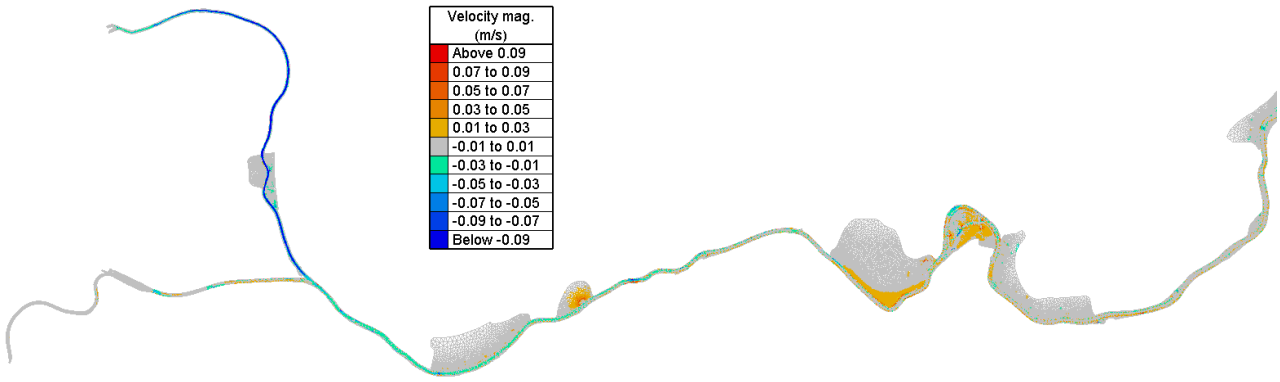

Figure 38 – Time averaged velocity difference in Upper Sea Scheldt (2050_REF_A0CN - 2013_REF_A0CN) – part 2

In 2050_REF_A0CN, there are more culverts and flood control areas activated, all the way up to the Upper Sea Scheldt. In the 2013 reference bathymetry, some of the dikes along the Scheldt prevent water from moving out of the channel and flowing on tidal flats, but for the sustainable bathymetry in 2050, water is allowed to pass the culverts or flow over nearby tidal flats periodically. This is the main reason for the higher velocity on the tidal flats and flood control areas as shown in Figure 37. However, in the navigations channels, especially near the upstream boundary (Figure 38), lower velocity magnitudes are found in 2050_REF_A0CN case, due to the influence of difference bathymetry and more activated culverts and flooding control areas.

In order to have a clear view of the change of hydrodynamics from 2013_REF_A0CN to 2050_REF_A0CN, the time series of water levels are extracted at 170 points along the thalweg of Scheldt estuary, starting from Vlissingen with distance interval of 1 km. Afterwards, the harmonic analysis of water levels is

performed. Figure 39 and Figure 40 show the M_2 and M_4 amplitude for 2013_REF_A0CN and 2050_REF_A0CN respectively, and their differences.

The most important constituent is the semi-diurnal M_2 component. The first overtide of this constituent is M_4. Generally, the M_4 component is small offshore, but rapidly increases within estuaries due to bottom friction and channel geometry (see Speer and Aubrey, 1985; Parker, 1991). The M_2 component and its first harmonic M_4 dominate the non-linear processes within estuaries.

It can be seen that 2050_REF_A0CN gives lower M_2 amplitude compared to 2013_REF_A0CN. This is partly because of more activated culverts along the channel. These culverts could lead to more energy loss during tidal wave propagation, which explains the decrease of M_2 and M_4 amplitude.

M_2 amplitude increases between 150 km to 170 km. This could be due to a new sluice installed in the north of the de-embankment of Heusden in 2050, preventing the tide from attenuating further upstream in this tidal arm. There is also influence of the alternation of the river bathymetry in this area. The sharp changes happening between 130 km to 170 km in the M_4 amplitude is likely to be caused by the same reasons.

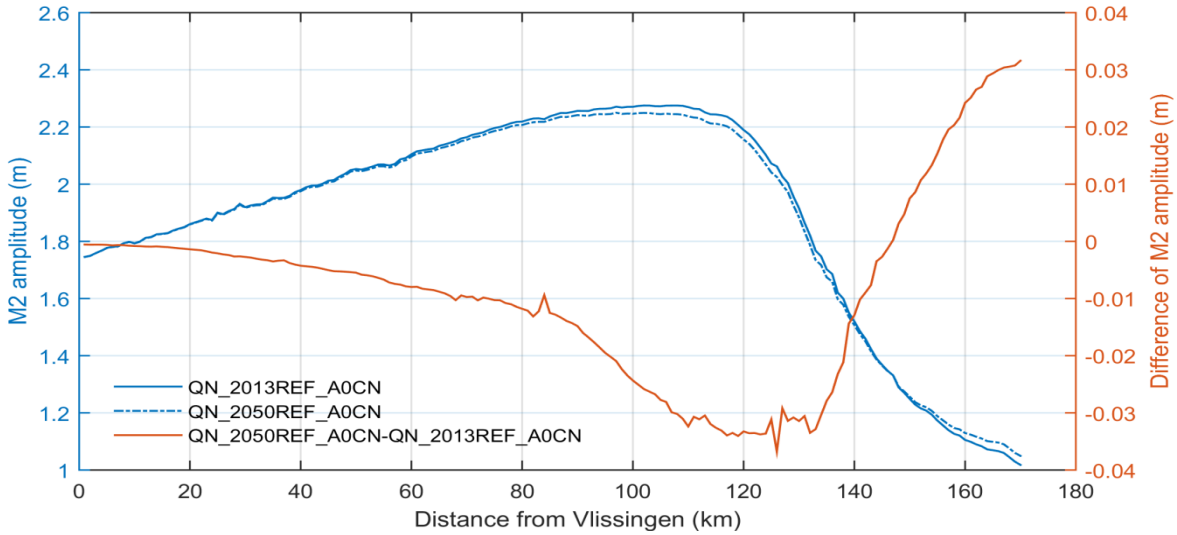

Figure 39 – Comparison of M2 amplitude between 2013_REF_A0CN and 2050_REF_A0CN

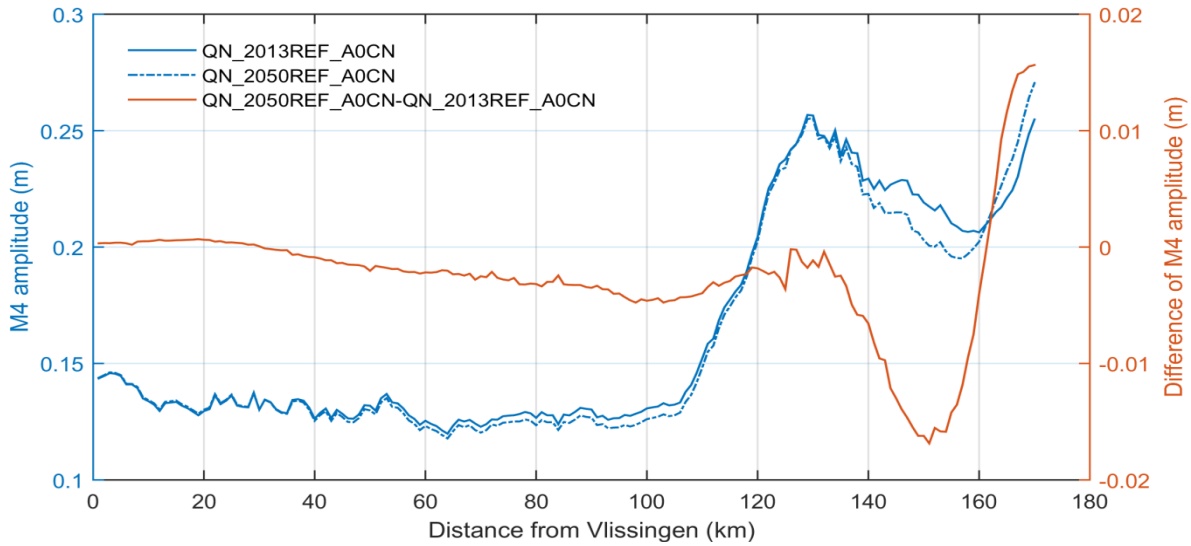

Figure 40 - Comparison of M4 amplitude between 2013_REF_A0CN and 2050_REF_A0CN

The harmonic analysis is performed with cross-sectionally averaged velocity as well (Figure 41). The velocity changes between two runs are generally small, with more frequent fluctuations from 110 km to 170 km under the combination of bathymetric changes, more activated flood controlled areas and sluice installed close to the upstream boundary.

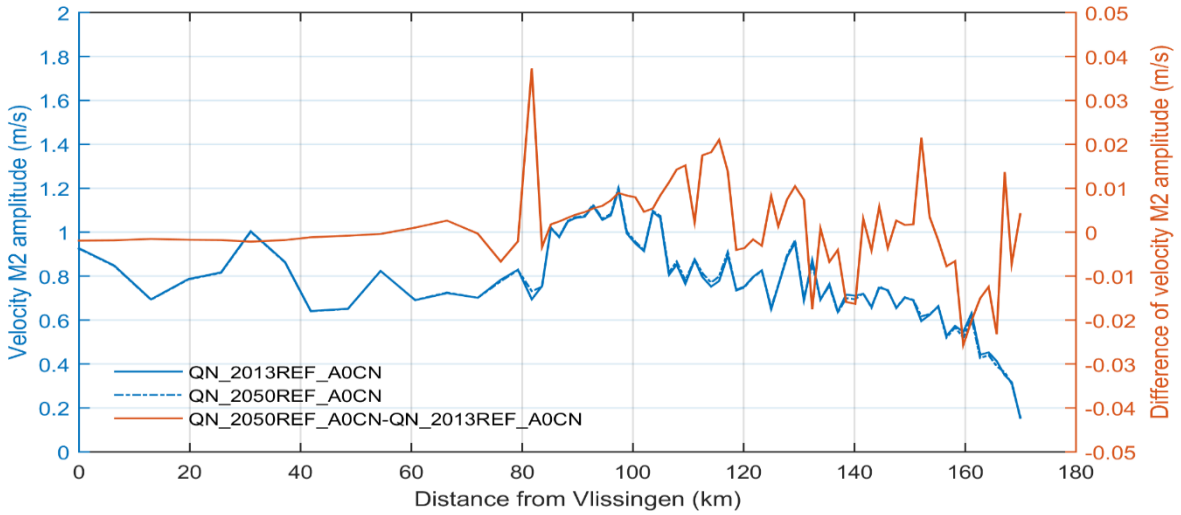

Figure 41 - Comparison of M2 amplitude of cross-sectionally averaged velocity between 2013_REF_A0CN and 2050_REF_A0CN

(2). The change of tidal asymmetry

All the tidal asymmetry indicators as mentioned in §4.8, are calculated in this section. These indicators, 8 in total, are organized in 3 groups, based on time duration, velocity magnitude and skewness, respectively.

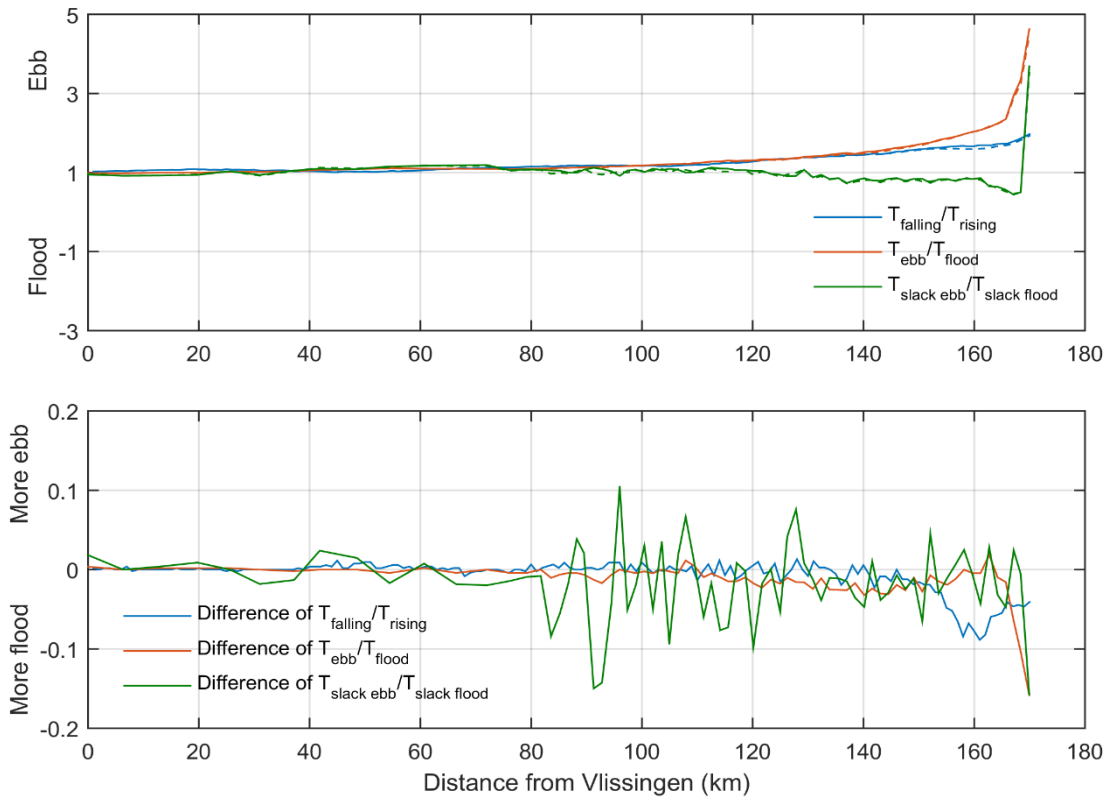

Figure 42 – Indicators of tidal asymmetry (durations).
Solid lines represent the reference 2013_REF_A0CN, dashed lines represent the scenario 2050_REF_A0CN.

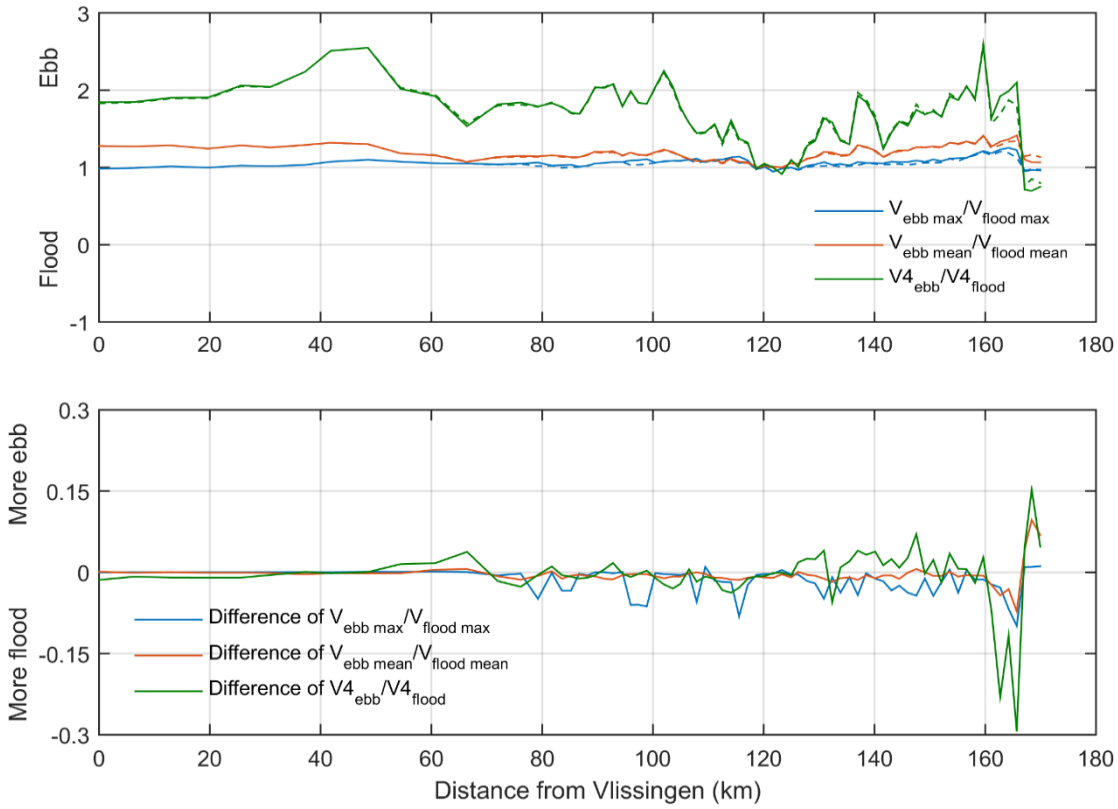

Figure 43 - Indicators of tidal asymmetry (velocities).
Solid lines represent the reference 2013_REF_A0CN, dashed lines represent the scenario 2050_REF_A0CN.

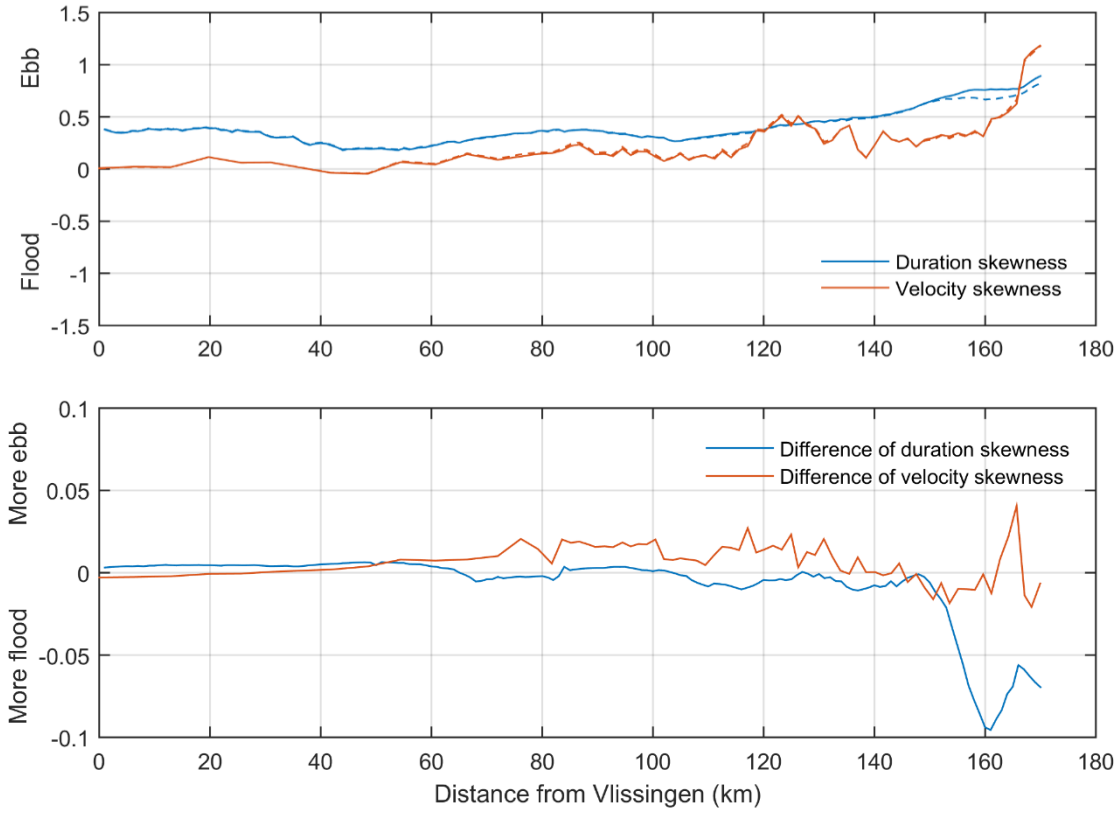

Figure 44 - Indicators of tidal asymmetry (skewness).
Solid lines represent the reference 2013_REF_A0CN, dashed lines represent the scenario 2050_REF_A0CN.

(3). Sediment Transport Decomposition

Figure 45 shows the sediment transport decomposed according to §4.7. Note the overall exporting behaviour of the model.

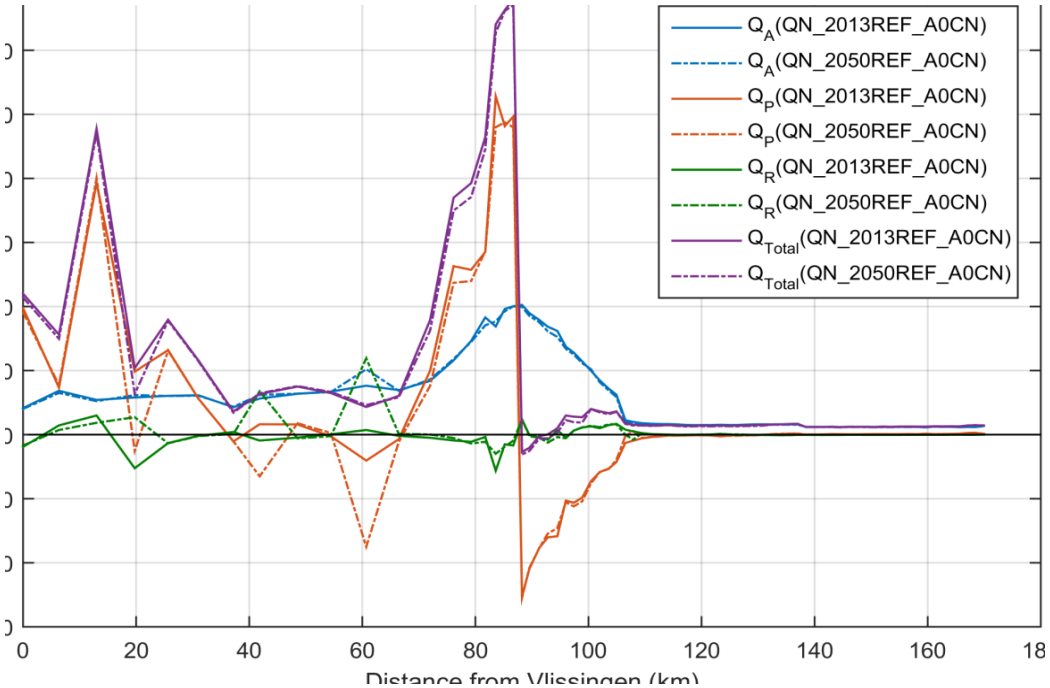

Figure 45 – Decomposed time-averaged sediment transport QA, QP and QR.
Positive sign means downstream direction and negative means upstream direction.

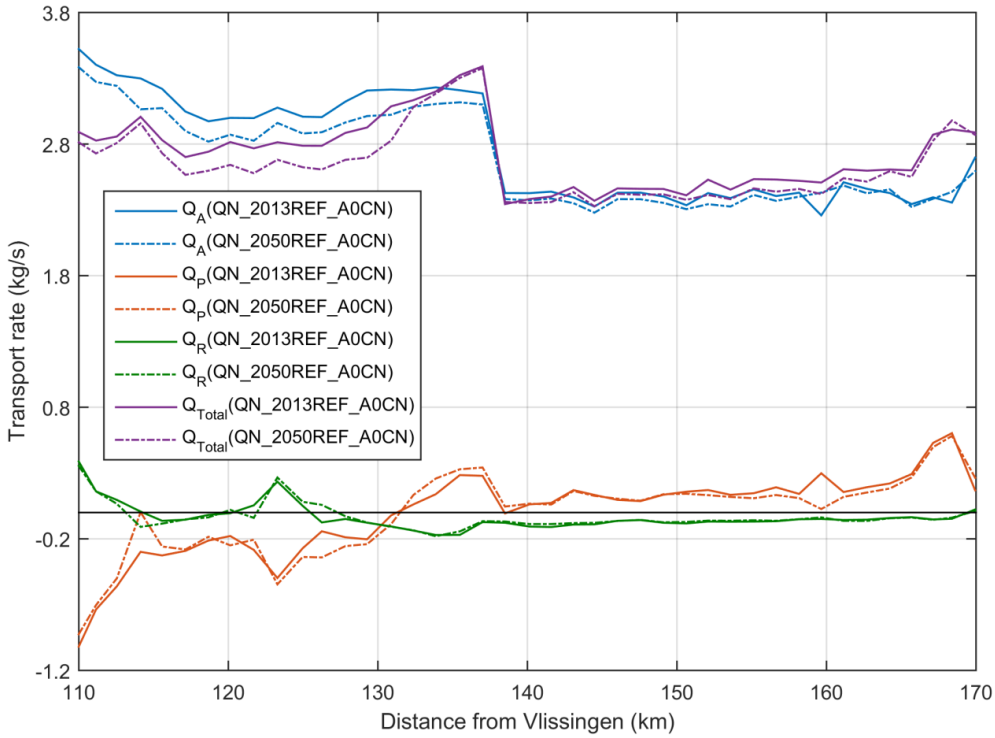

Figure 46 – Decomposed time-averaged sediment transport QA, QP and QR for the Upper Sea Scheldt.
Positive sign means downstream direction and negative means upstream direction.

In the above figures, positive sign means downstream direction and negative means upstream direction. Figure 46 indicates that, for the domain in the Upper Sea Scheldt (from 110 – 170 km from Vlissingen), the most important contribution to the total sediment transport is caused by the discharge (Q_A). Tidal pumping (Q_P) is negligible except in a small channel section near Merelbeke. But even in that area, tidal pumping flux is about 17-20% of the total sediment flux, and it is likely caused by the tidal asymmetry near the upstream boundary.

(4). Erosion-deposition map

The difference of sedimentation rate is calculated between the run 2050_REF_A0CN and 2013_REF_A0CN using the bed layer thickness given in the result files. The sedimentation rate is based on the production period of the last 20 days and it is converted to cm/yr.

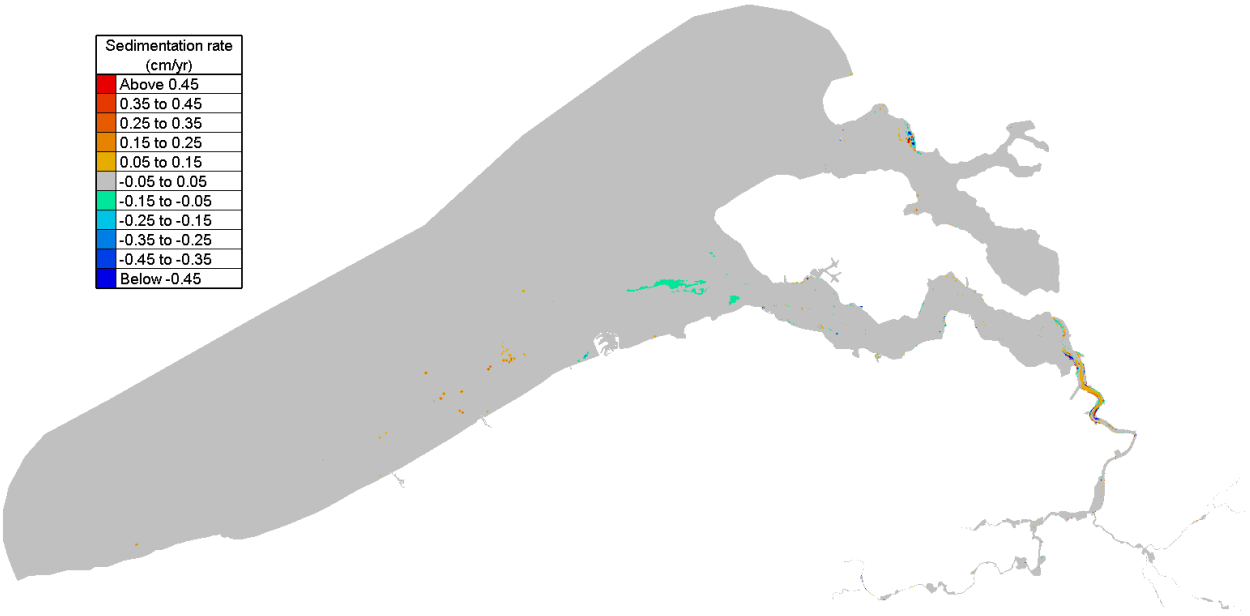

Figure 47 – Difference of sedimentation rate (2050_REF_A0CN-2013_REF_A0CN) – overview

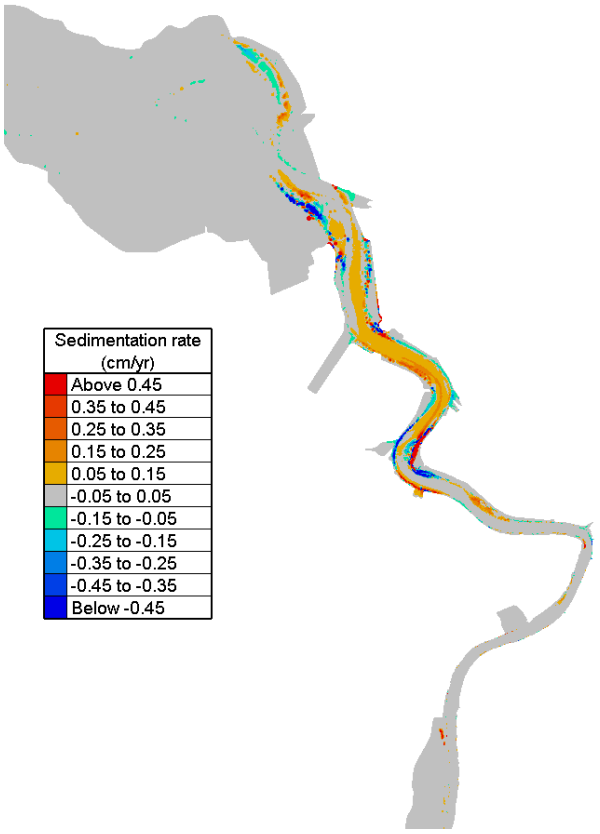

Figure 48 – Difference of sedimentation rate (2050_REF_A0CN-2013_REF_A0CN) – Lower Sea Scheldt

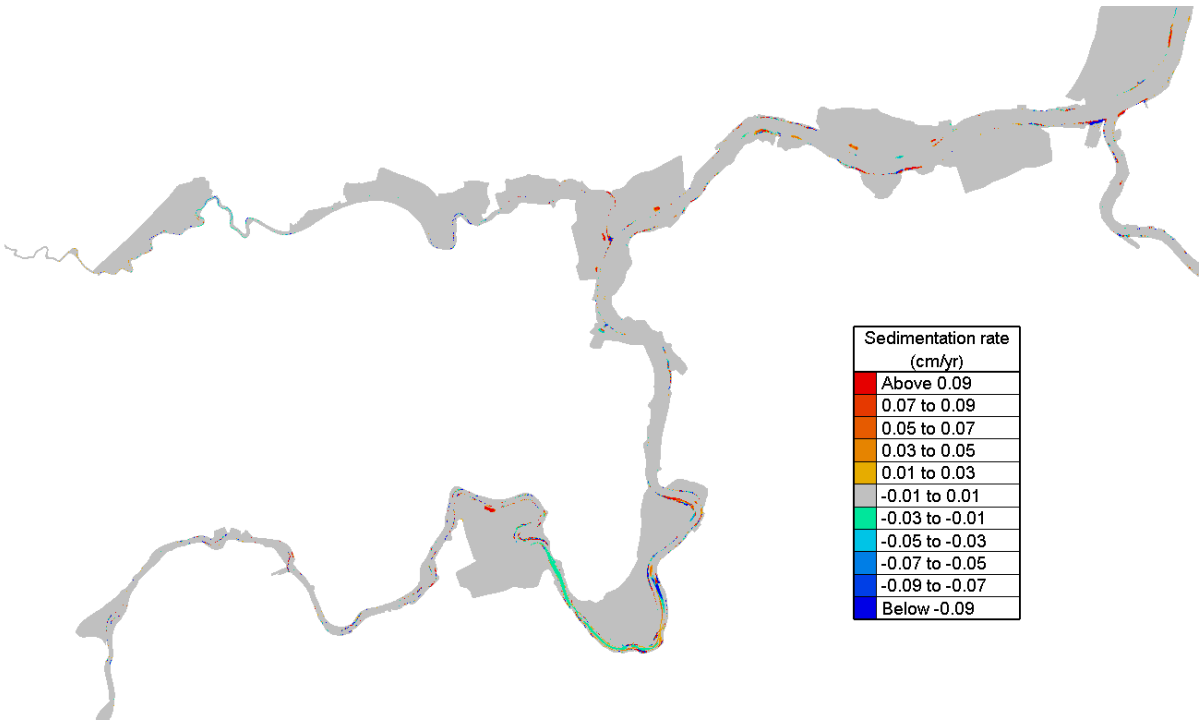

Figure 49 – Difference of sedimentation rate (2050_REF_A0CN-2013_REF_A0CN) – Upper Sea Scheldt (part 1)

Figure 50 – Difference of sedimentation rate (2050_REF_A0CN-2013_REF_A0CN) – Upper Sea Scheldt (part 2)

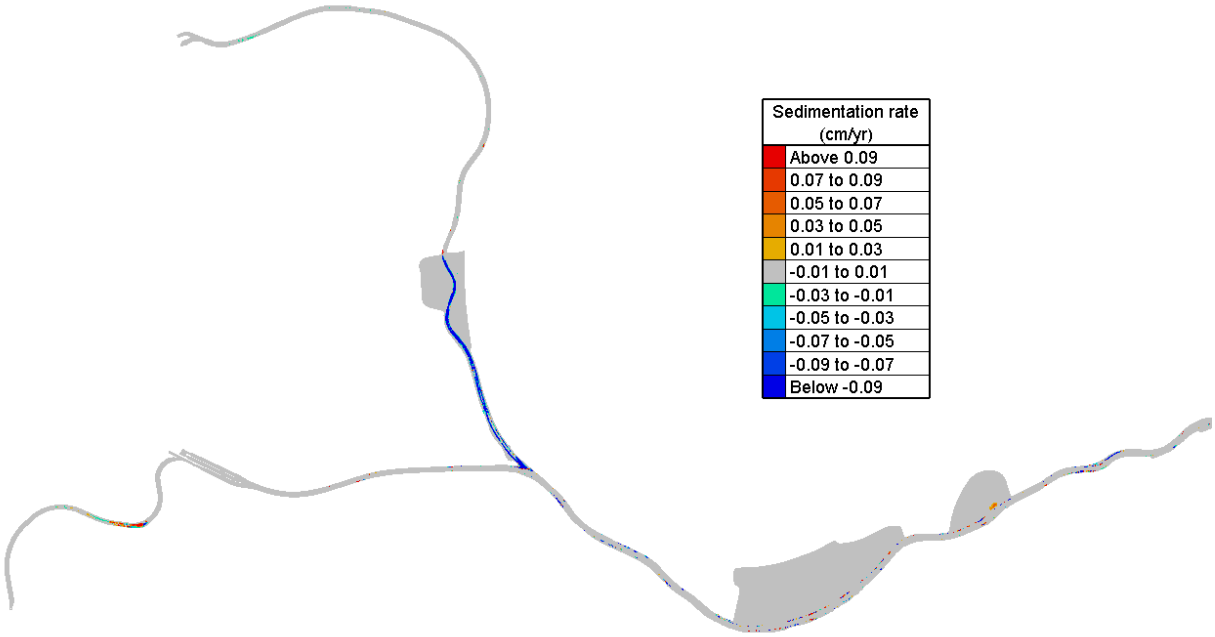

Figure 51 – Difference of sedimentation rate (2050_REF_A0CN-2013_REF_A0CN) – Upper Sea Scheldt (part 3)

As seen in the above figures, the largest difference is found in the area near Deurganck, where more sedimentation happens due to the local bathymetric changes shown in Figure 4. Another noticeable difference is in the upstream tributary near Heusden. The sedimentation rate becomes smaller there, which means the SSC also becomes smaller.

(5). Bed shear stress

Changes in bottom shear stress lead to changes in sedimentation/erosion patterns and habitat suitability. Therefore maps are made in the study area of exceedance time (%) of a threshold value of 1 Pa during a spring-neap cycle. A difference map (in %-points) shows the spatial changes.

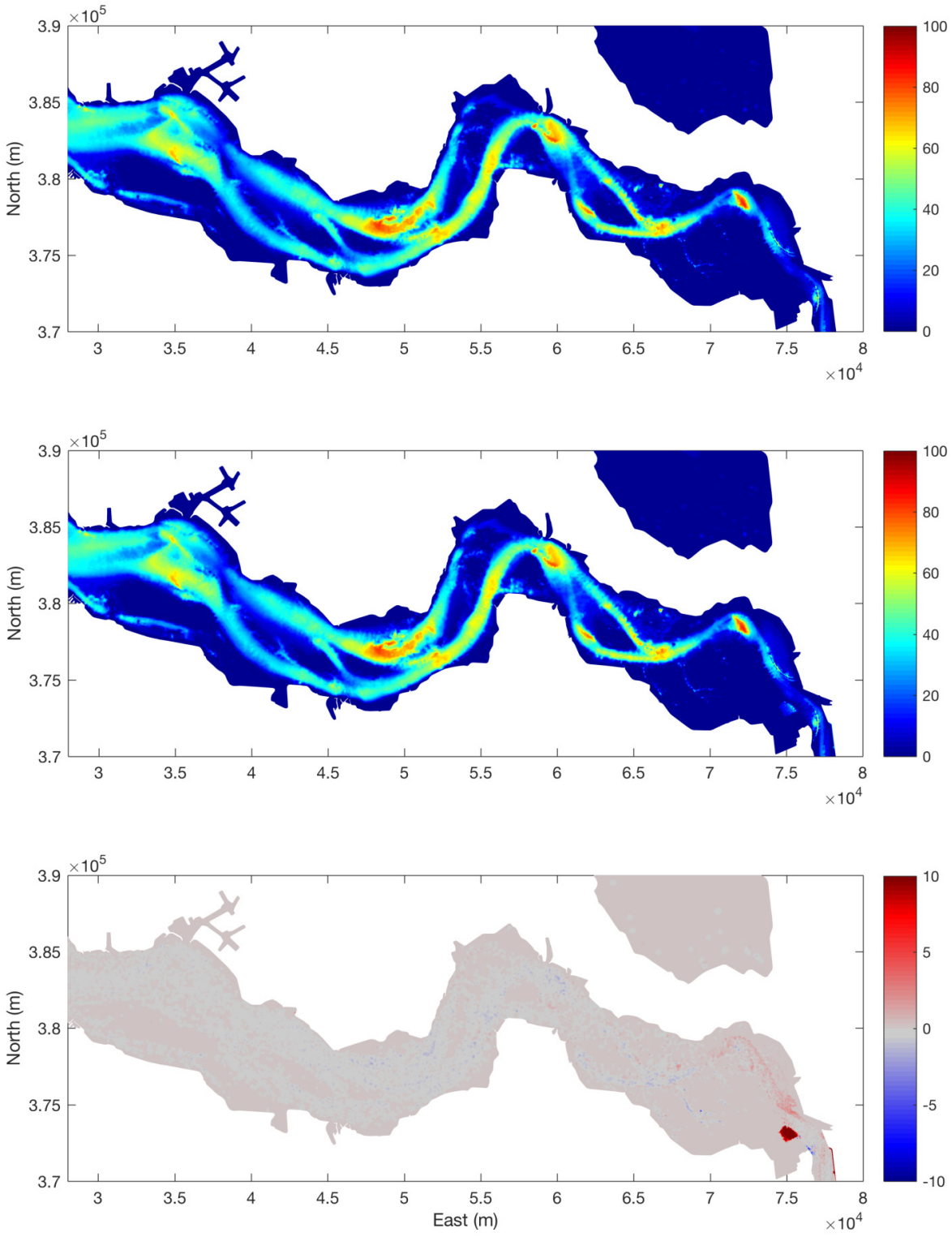

Figure 52 – Exceedance time of bed shear stress >1Pa (%) during a spring-neap cycle in Western Scheldt.
From top to bottom: the reference 2013_REF_A0CN; the scenario 2050_REF_A0CN;
the difference 2050_REF_A0CN - 2013_REF_A0CN.

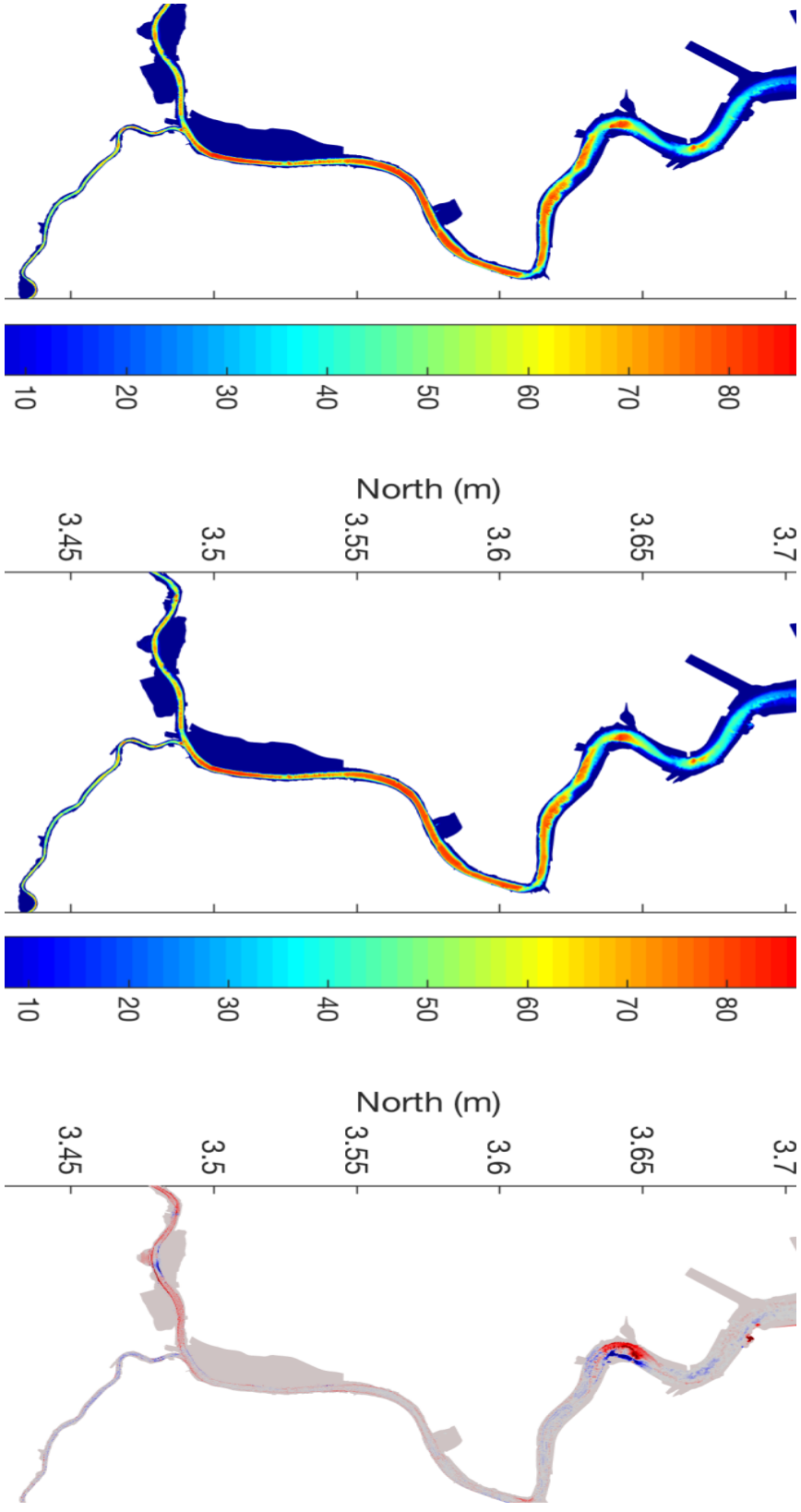

Figure 53 – Exceedance time of bed shear stress >1Pa (%) during a spring-neap cycle in Lower Sea Scheldt.
From top to bottom: the reference 2013_REF_A0CN; the scenario 2050_REF_A0CN;
the difference 2050_REF_A0CN - 2013_REF_A0CN.

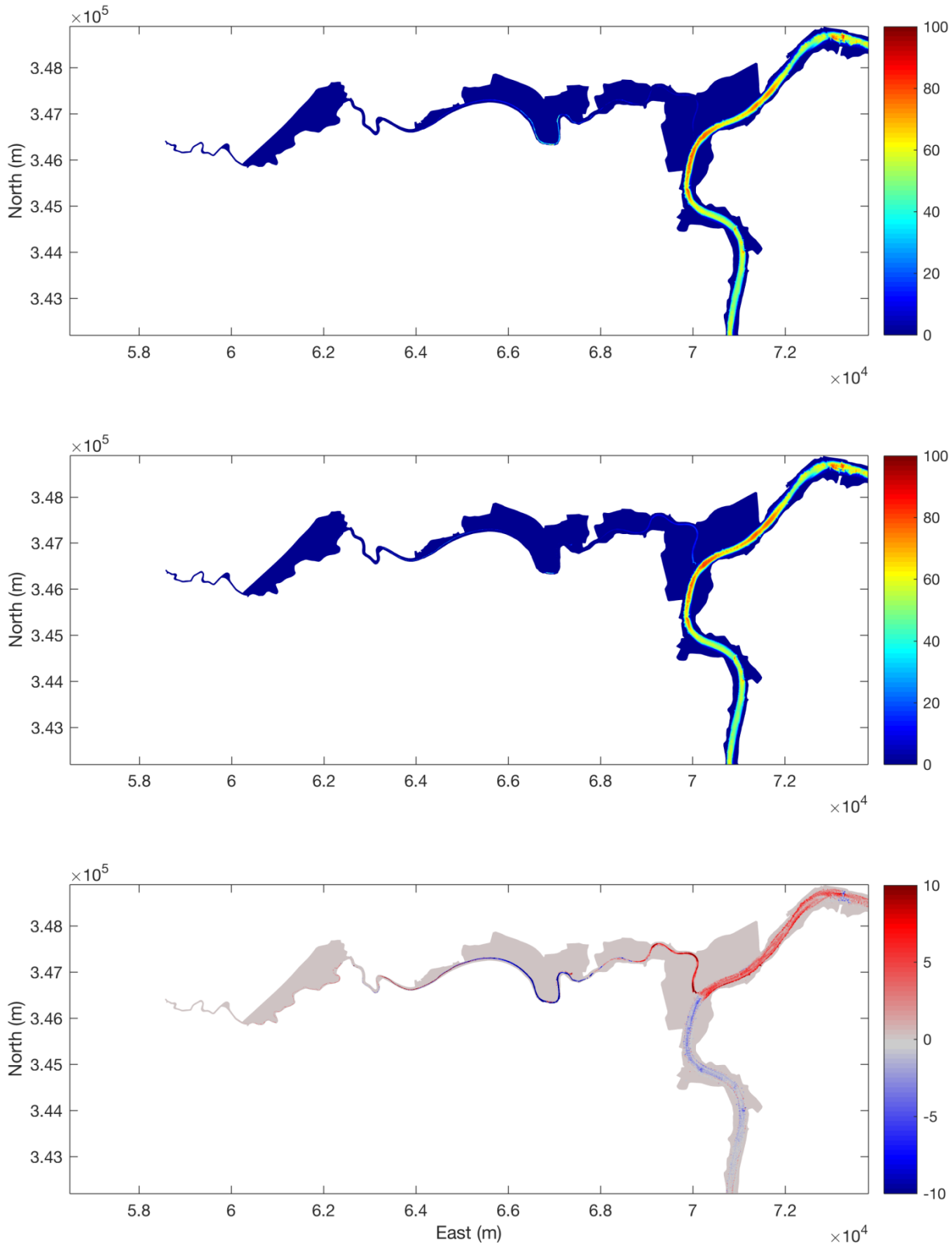

Figure 54 – Exceedance time of bed shear stress >1Pa (%) during a spring-neap cycle in Upper Sea Scheldt.
From top to bottom: the reference 2013_REF_A0CN; the scenario 2050_REF_A0CN;
the difference 2050_REF_A0CN - 2013_REF_A0CN.

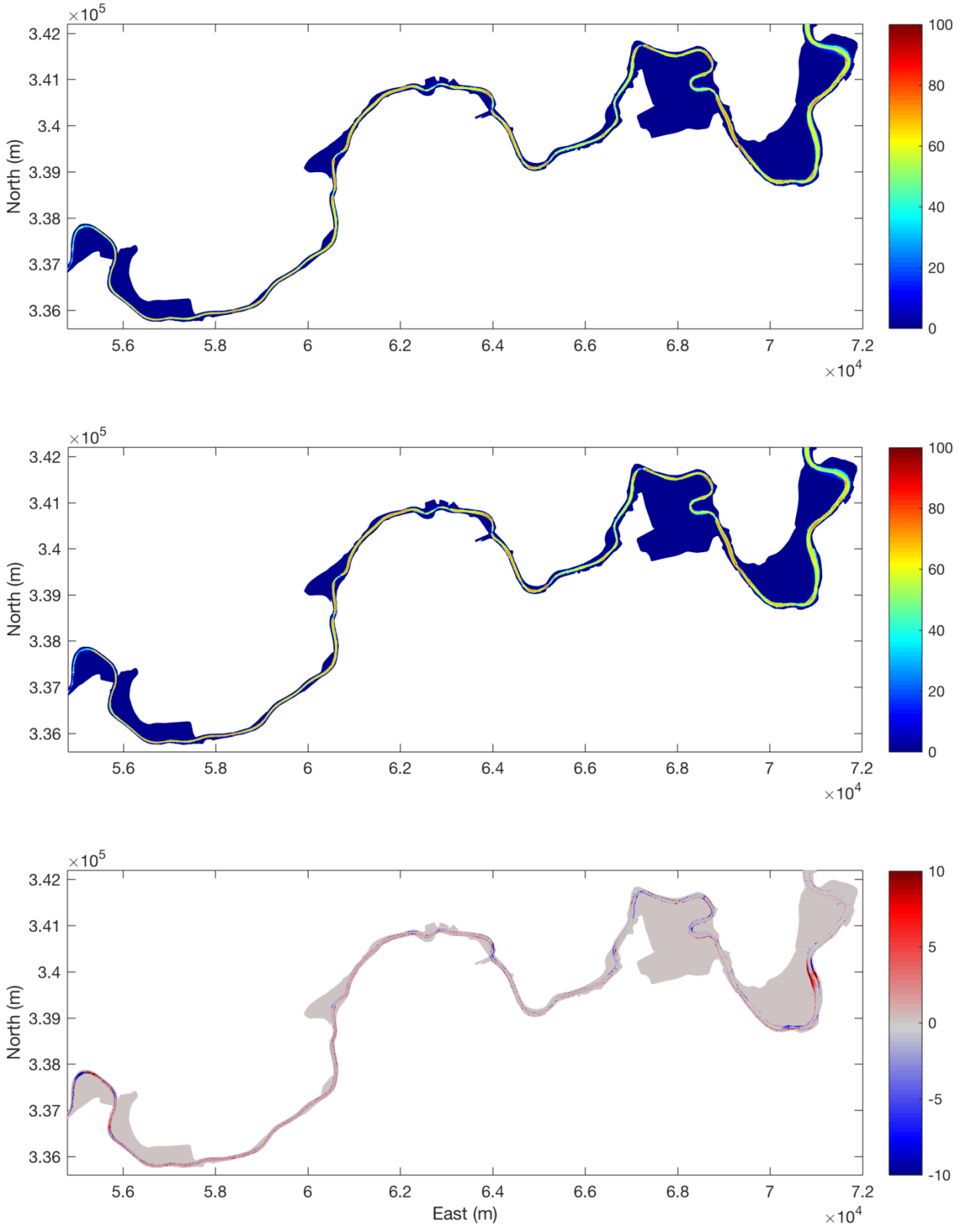

Figure 55 – Exceedance time of bed shear stress >1Pa (%) during a spring-neap cycle in Upper Sea Scheldt.
From top to bottom: the reference 2013_REF_A0CN; the scenario 2050_REF_A0CN;
the difference 2050_REF_A0CN - 2013_REF_A0CN.

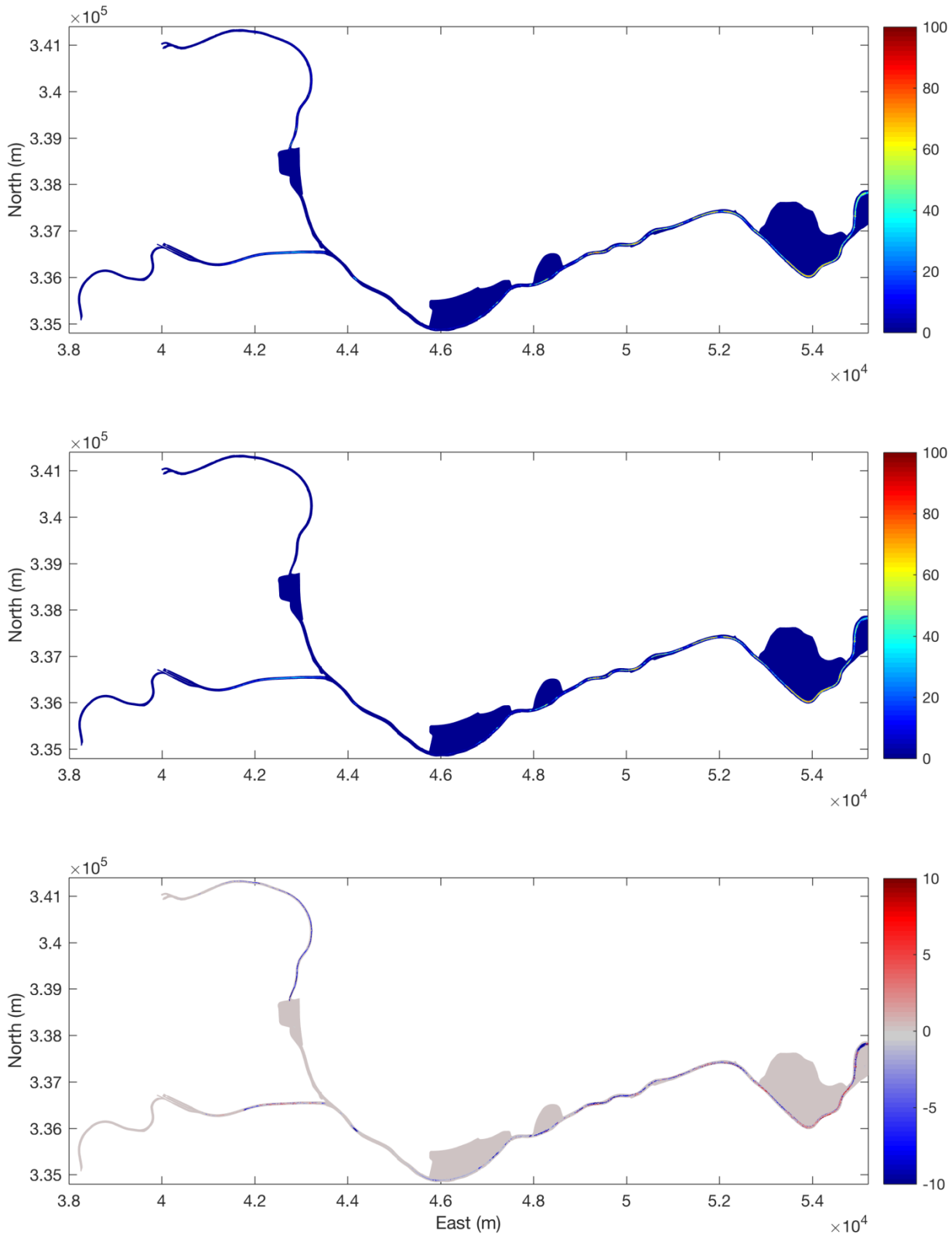

Figure 56 – Exceedance time of bed shear stress >1Pa (%) during a spring-neap cycle in Upper Sea Scheldt.
From top to bottom: the reference 2013_REF_A0CN; the scenario 2050_REF_A0CN;
the difference 2050_REF_A0CN - 2013_REF_A0CN.

(6). Delta SSC

The Delta SSC is calculated based on equation described in §4.1 and the time averaged Delta SSC is given for each box of the ecosystem model in Figure 57. For better comparison, the time averaged Delta SSC in each box of the ecosystem model is plotted using the same X-axis, the distance from Vlissingen.

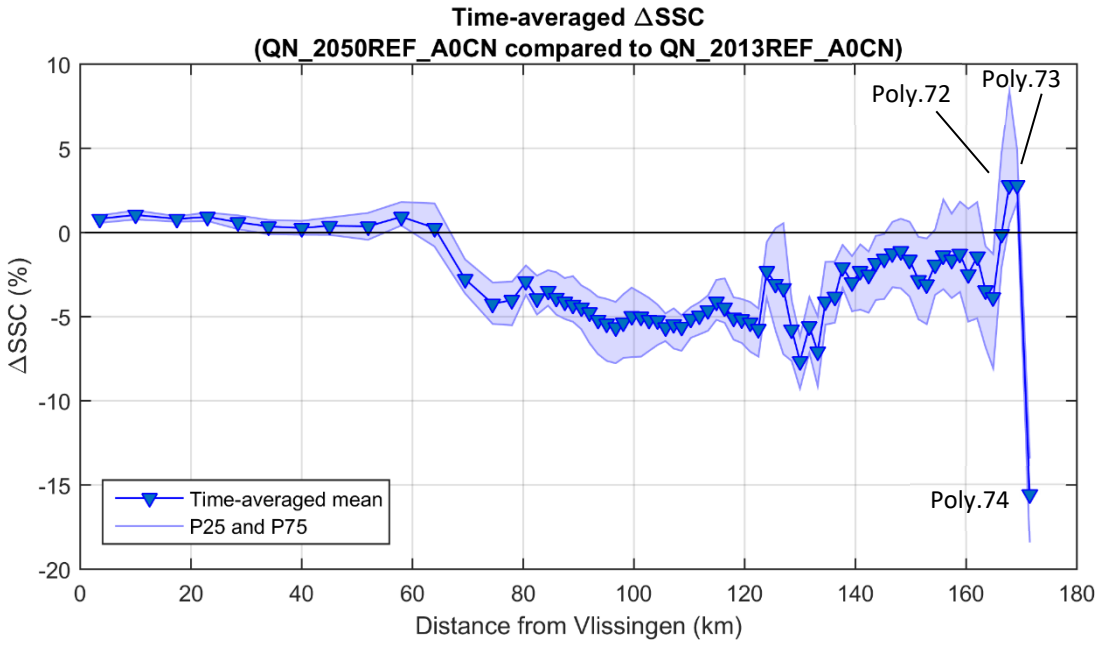

Figure 57 – Time averaged Delta SSC in each box of the ecosystem model (2050_REF_A0CN compared to 2013_REF_A0CN)

As shown in above figure, the mean delta SSC remains around 0% - 1% in the Western Scheldt, which is because the downstream boundary conditions and bathymetry in this part of the domain does not change in both runs. The delta SSC is negative further upstream.

(7). Discussion

The delta SSC at 171.5 km (Polygon 74), which is the first data point from the right side of Figure 57, shows lower SSC in the scenario. This is mostly due to the influence of the bottom changes at the end of Ringvaart. As shown in Figure 58, the time averaged difference of SSC is indeed lower in that area.

The de-embankment and the newly-installed sluice near Heusden also affect the SSC significantly. In the scenario, SSC becomes lower in this tributary, which is consistent with the lower bed shear stress in the same region (Figure 56), meaning the suspension capacity and the erosion become lower. Figure 58 shows that both SSC and sedimentation rate become less downstream of the sluice. Considering there is no sediment input at the upstream of this tributary, these differences can only imply that there is less sediment trapped in this region, hence, more remains in the main channel. This also explains the slightly higher delta SSC in Polygon 72 and 73.

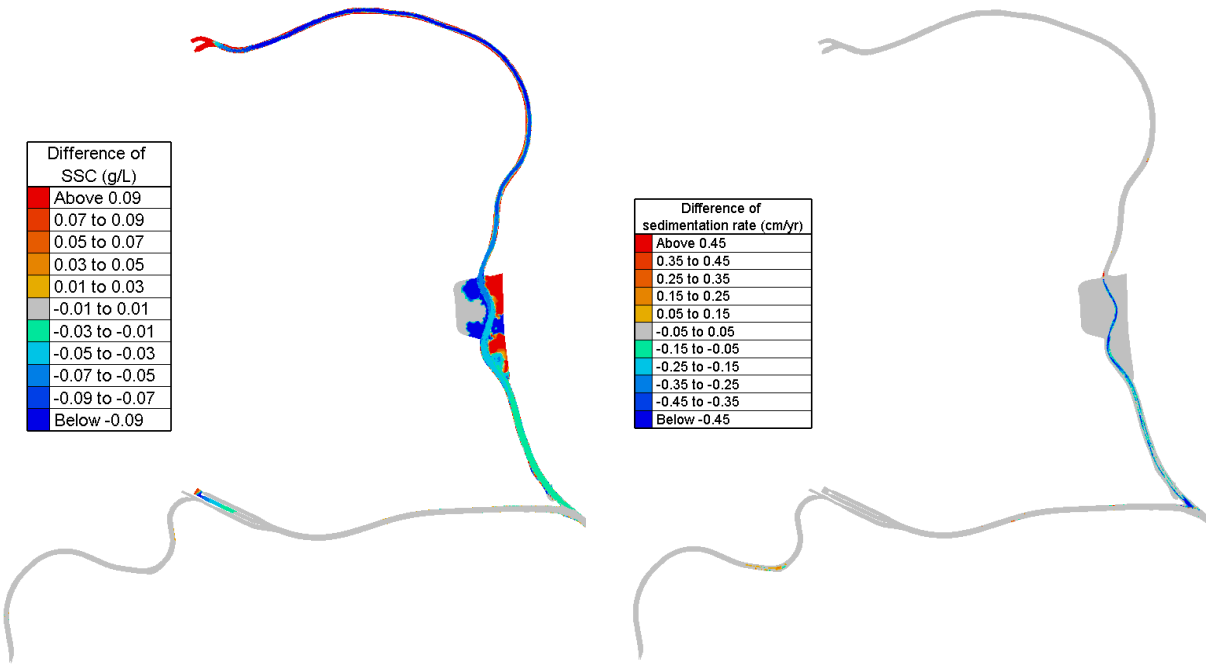

Figure 58 – The time-averaged difference of SSC (left) and the difference of sedimentation rate (right) (2050_REF_A0CN-2013_REF_A0CN).

Between 110 km and 170 km, delta SSC is generally negative. One of the influential factors on the general trend of delta SSC being negative is that the bed shear stress (shown as the change of exceedance time > 1Pa from Figure 54 to Figure 56) becomes lower near the upstream boundary in the region between 170 and 140 km due to the changes in hydrodynamics. The change of bed shear stress is consistent with the difference of time-averaged velocity magnitude and the velocity M_2 amplitude. This suggests less sediment is transported by the flow going downstream. As shown in Figure 46, the total sediment transport indeed becomes slightly lower in 2050_REF_A0CN. Another important reason is that, in the area between 140 km and 110 km, many flood control areas and culverts are activated in 2050_REF_A0CN. The consequence is that water will flow through those areas and the sediment will also be spread into a larger domain. Given less sediment input from upstream due to smaller bed shear stress, it is no surprise the SSC will decrease further in this region.

5.1.2 From 2050 REF A0CN to 2050 REF AminCL

The scenario 2050_REF_AminCL uses the same bathymetry as in the reference 2050_REF_A0CN. There are three main differences:

- A sea level rise of 15 cm is added in the downstream boundary conditions (described in §3.2.2);
- Furthermore, the roughness is increased in the Western Scheldt (from 0 – 68 km from Vlissingen) in order to reduce the tidal amplitude. This has influence on both hydrodynamics and sediment transport. To be more specific, the increased bottom friction will affect the flow field and result in lower velocity magnitude in this region. Because the sediment transport uses a separate (uniform) bottom roughness, the reduced local velocity leads to lower erosion;
- Finally, the upstream discharge is increased based on statistical analysis for year 2050 (see §3.5.1).

(1). The difference in hydrodynamics

The time-averaged difference of depth-averaged velocity magnitude is shown in Figure 59 and Figure 61. Under the influence of sea level rise (+15cm), increase of bottom friction and increase of upstream discharge, higher velocity magnitude can be observed locally in the North Sea and near the upstream boundary at Melle, which are sue to the sea level rise imposed at downstream boundary and increases discharge imposed at upstream, respectively. Foe the rest of the domain, it can be seen that velocity magnitudes become lower in 2050_REF_AminCL comparing to the reference case.

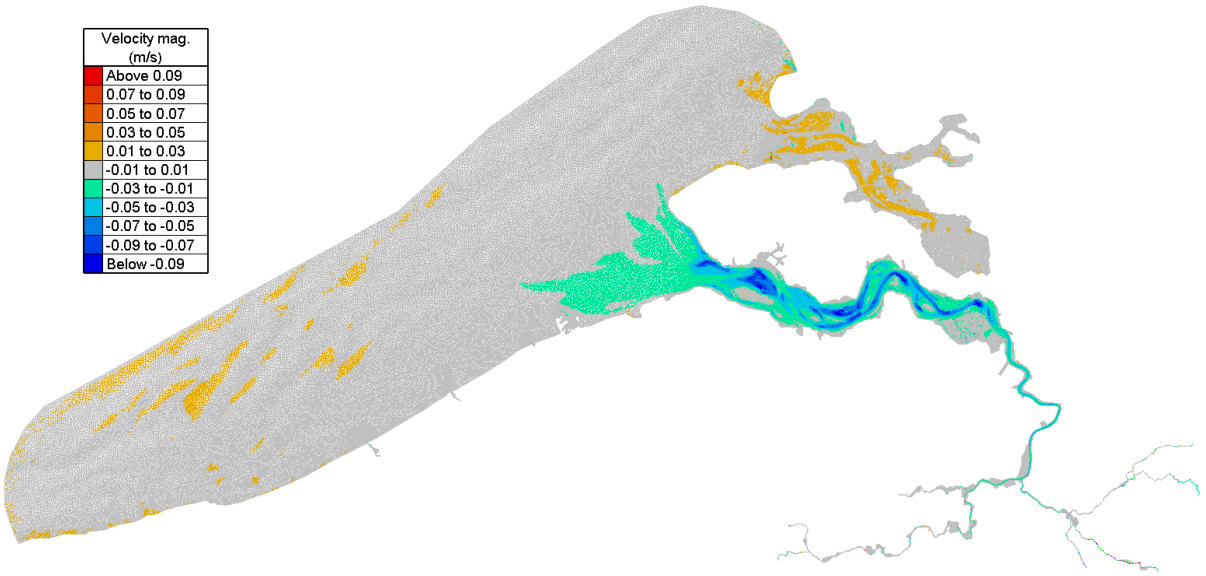

Figure 59– Time averaged velocity difference between two runs (2050_REF_AminCL – 2050_REF_A0CN)

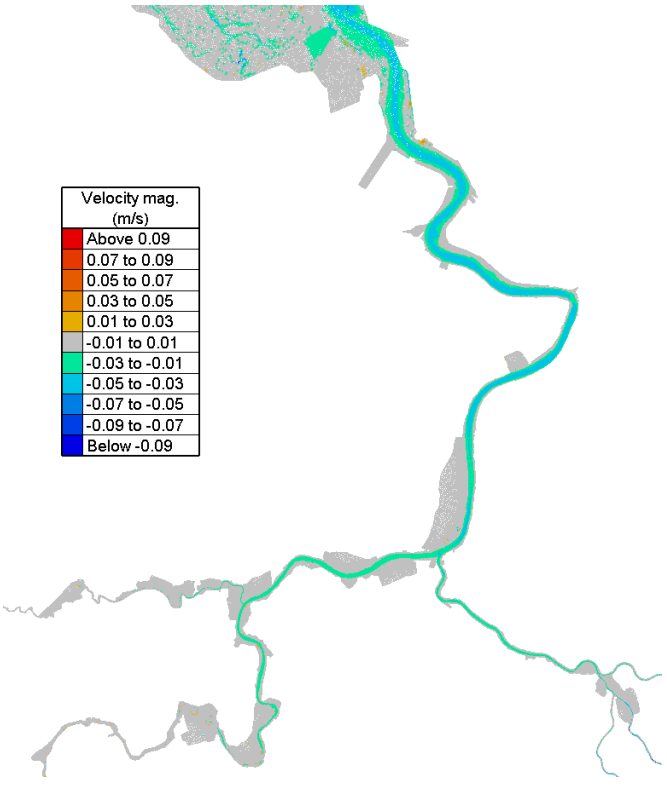

Figure 60 – Time averaged velocity difference in Upper Sea Scheldt (2050_REF_A0CN - 2013_REF_A0CN) – part 1

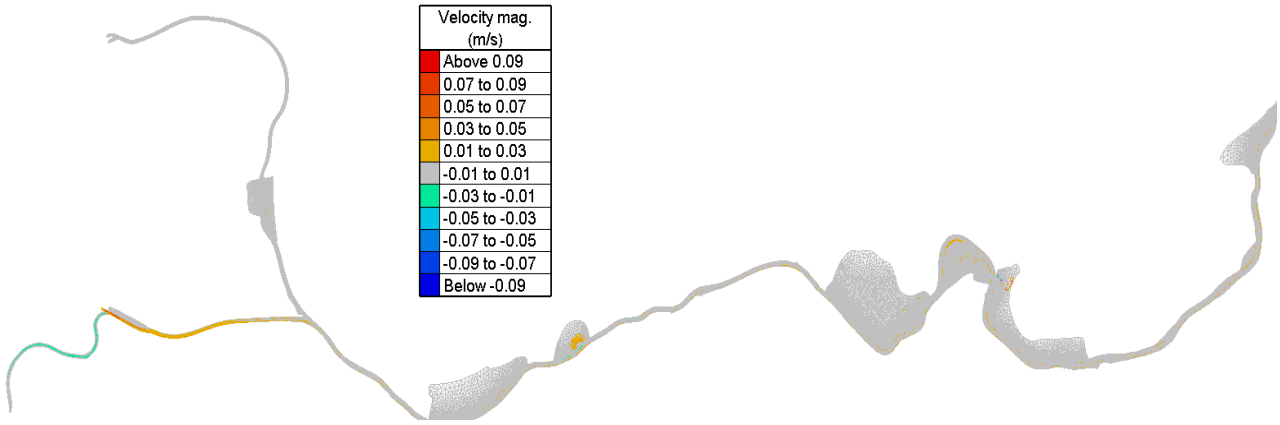

Figure 61 – Time averaged velocity difference in Upper Sea Scheldt (2050_REF_A0CN - 2013_REF_A0CN) – part 2

Time series of water levels along the thalweg points and cross-sectionally averaged velocity at different transects are used in the harmonic analysis, in order to get their M_2 and M_4 constituents (Figure 63 to Figure 65). As can be seen, due to the sea level rise scenario (+15 cm), the water level along the Scheldt increases from 12 cm to 17 cm, depending on the locations.

The increased bottom friction (the reduction in tidal amplitude is implemented by increasing bottom friction in the Western Scheldt) indeed causes tidal attenuation, reducing tidal amplitude, as shown in the difference of M_2 amplitude in Figure 63, by up to 13.4 cm. The influence of the increased bottom friction extends further upstream.

It is worth pointing out that the water level M_4 amplitude decreases in 2050_REF_AminCL. The change of water level M_4 amplitude can be associated with change of bottom friction and water depth in shallow water. The increased water depth due to sea level rise leads to a decreased bottom friction, whereas roughness in the Western Scheldt is increased to attain tidal attenuation. The tidal wave is therefore less distorted and the duration skewness moves closer to zero (Figure 68).

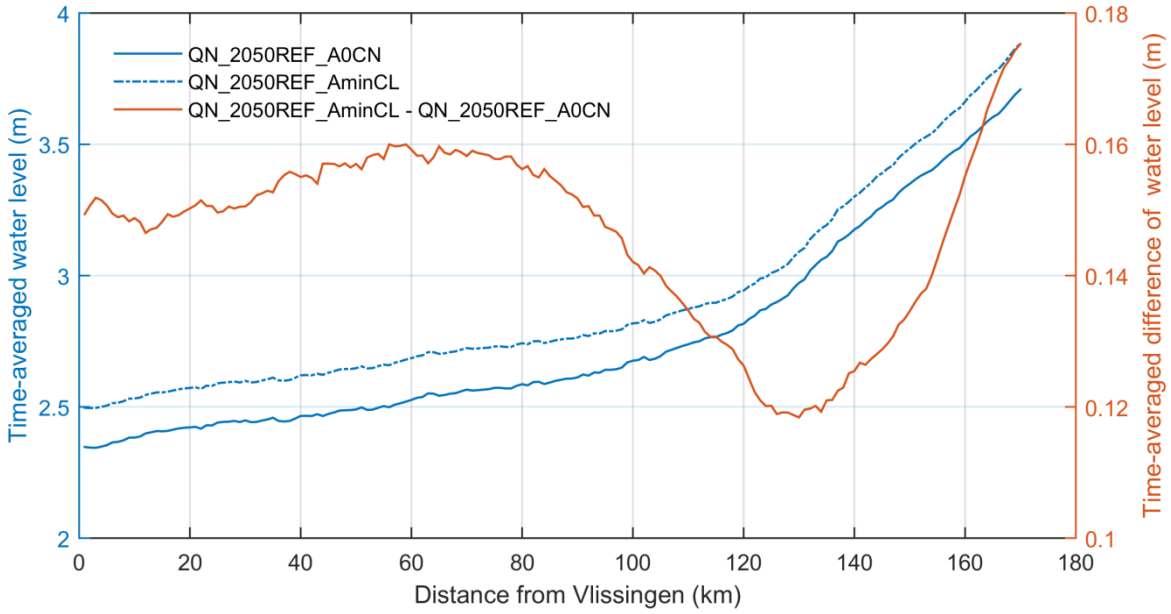

Figure 62 – Comparison of time-averaged water level between 2050_REF_A0CN and 2050_REF_AminCL

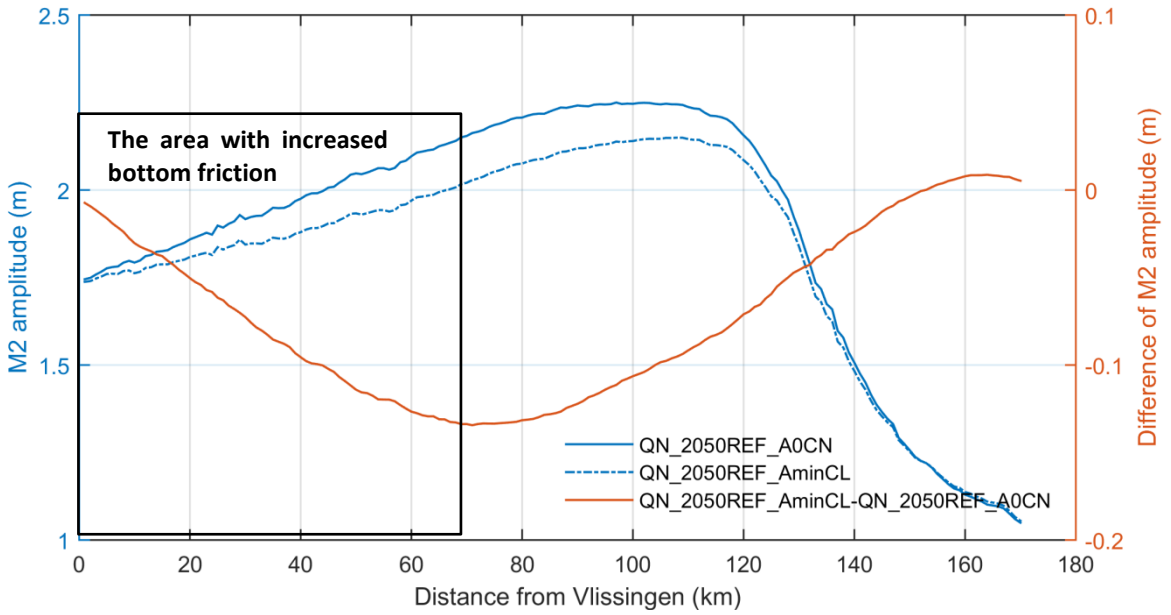

Figure 63 – Comparison of M2 amplitude between 2050_REF_A0CN and 2050_REF_AminCL

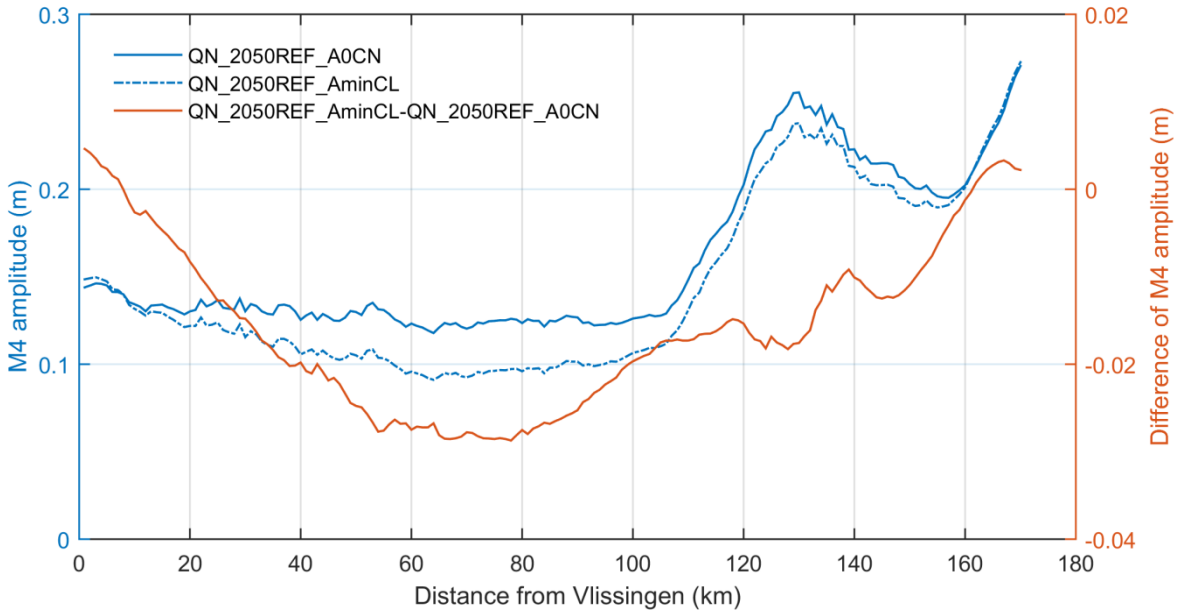

Figure 64 – Comparison of M4 amplitude between 2050_REF_A0CN and 2050_REF_AminCL

Harmonic analysis is performed on the cross-sectionally averaged velocity. Figure 65 suggests that the cross-sectionally averaged velocity in 2050_REF_AminCL has lower M_2 amplitude compared to 2050_REF_A0CN, which implies that the peak velocities, both seaward and landward, become smaller due to loss of energy in the Western Scheldt. The effect on velocities in the Upper Sea Scheldt is smaller, however.

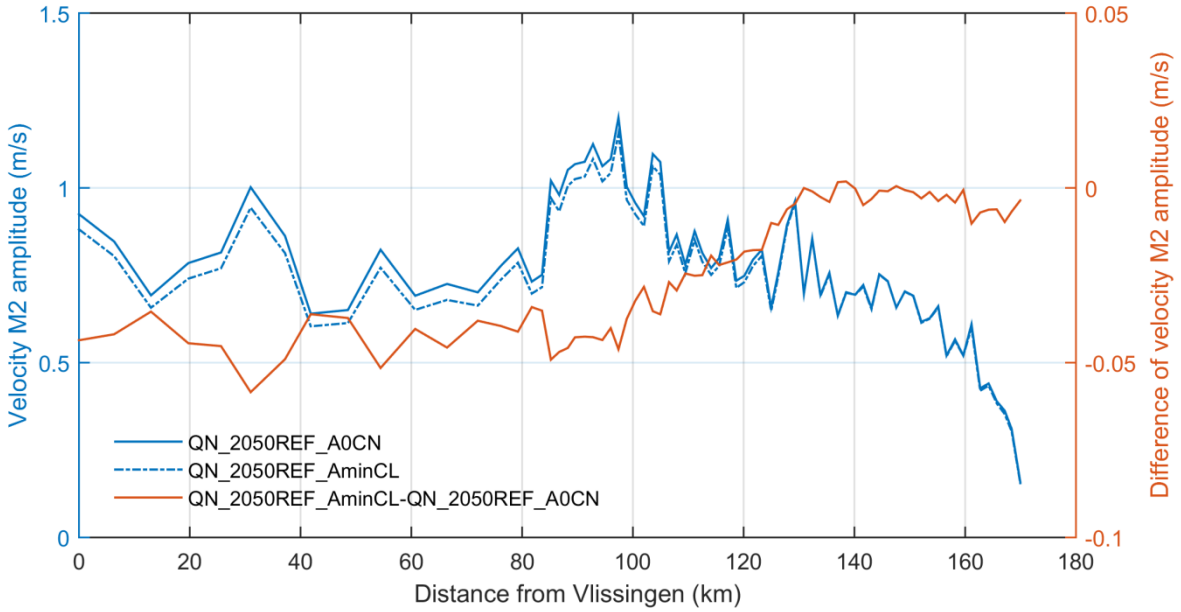

Figure 65 – Comparison of M2 amplitude of cross-sectionally averaged velocity between 2050_REF_A0CN and 2050_REF_AminCL

(2). The change of tidal asymmetry

All the tidal asymmetry indicators as mentioned in §4.8, are calculated in this section. These indicators, 8 in total, are organized in 3 groups, based on time duration, velocity magnitude and skewness, respectively.

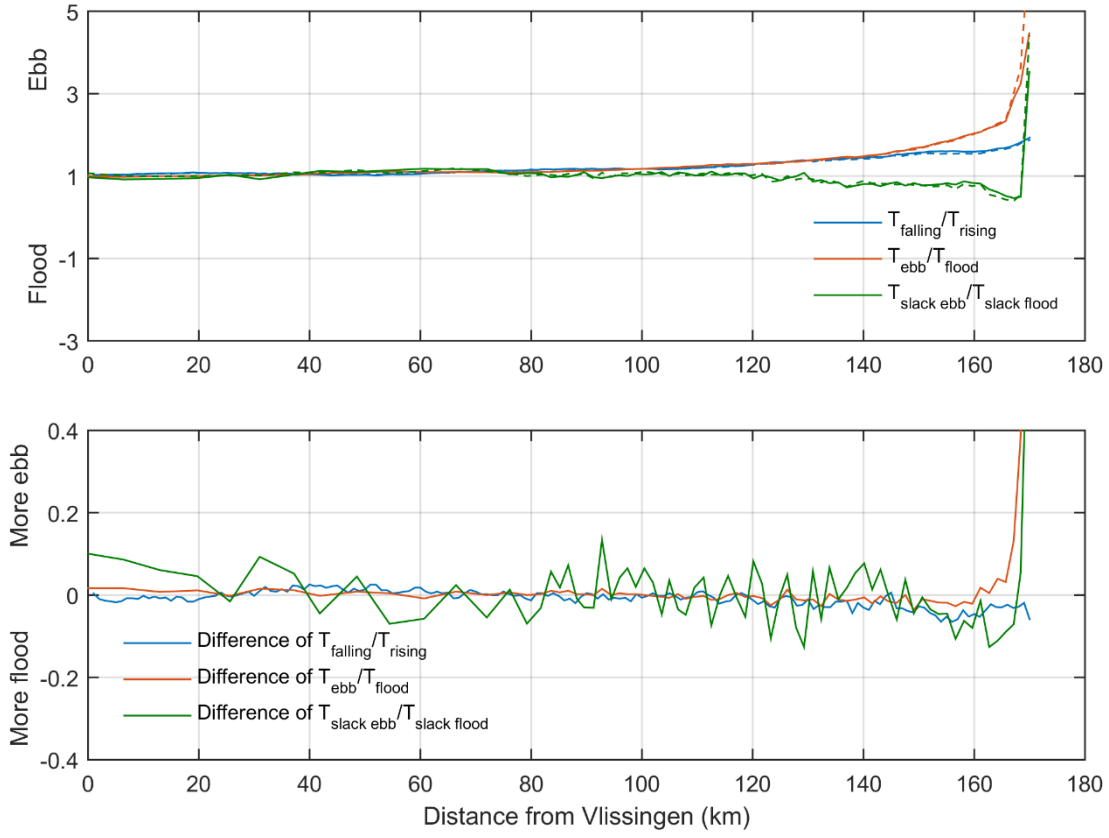

Figure 66 – Indicators of tidal asymmetry (durations).
Solid lines represent the reference 2050_REF_A0CN, dashed lines represent the scenario 2050_REF_AminCL.

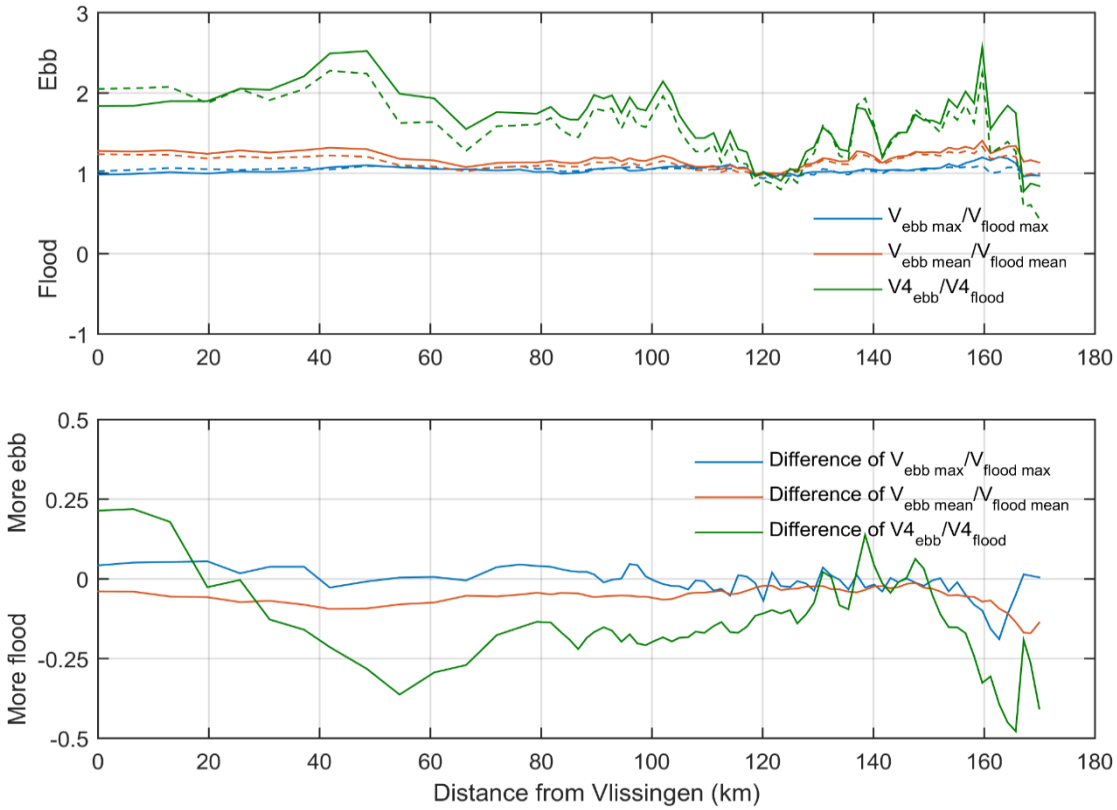

Figure 67 – Indicators of tidal asymmetry (velocities).
Solid lines represent the reference 2050_REF_A0CN, dashed lines represent the scenario 2050_REF_AminCL.

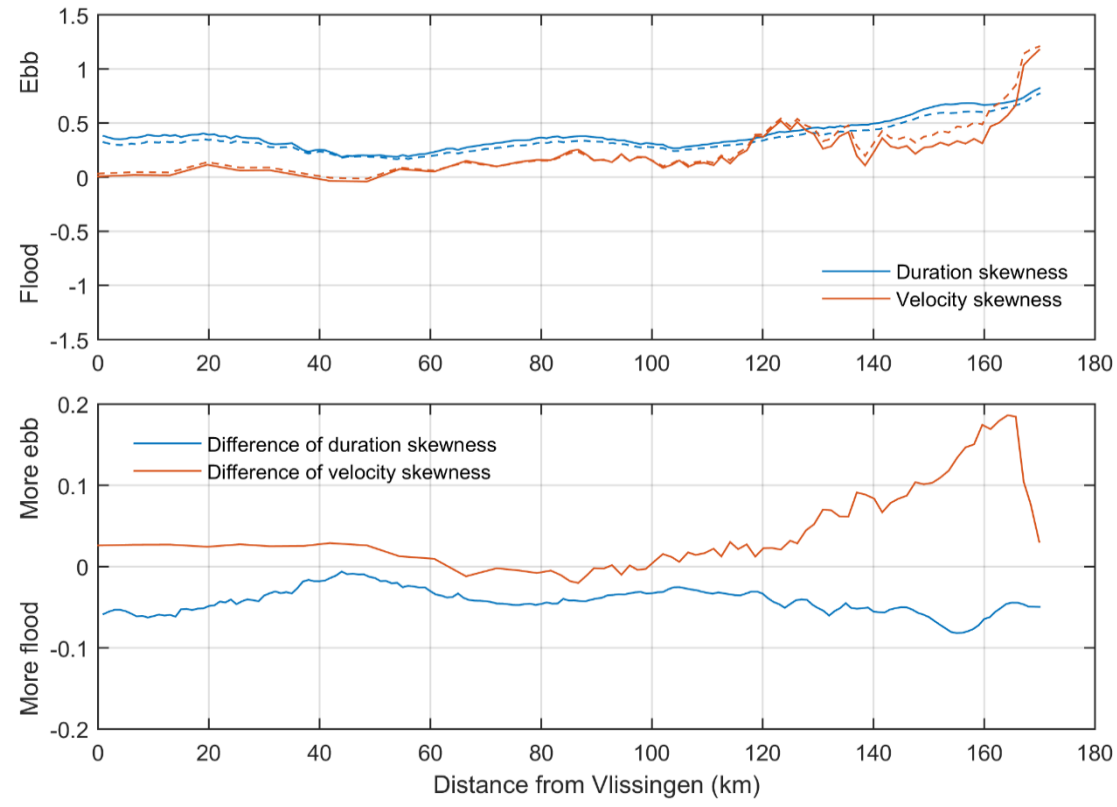

Figure 68 – Indicators of tidal asymmetry (skewness).
Solid lines represent the reference 2050_REF_A0CN, dashed lines represent the scenario 2050_REF_AminCL.

(3). Sediment Transport Decomposition

Figure 69 shows the sediment transport decomposed according to §4.7 and a zoom-in for the Upper Sea Scheldt is shown in Figure 70.

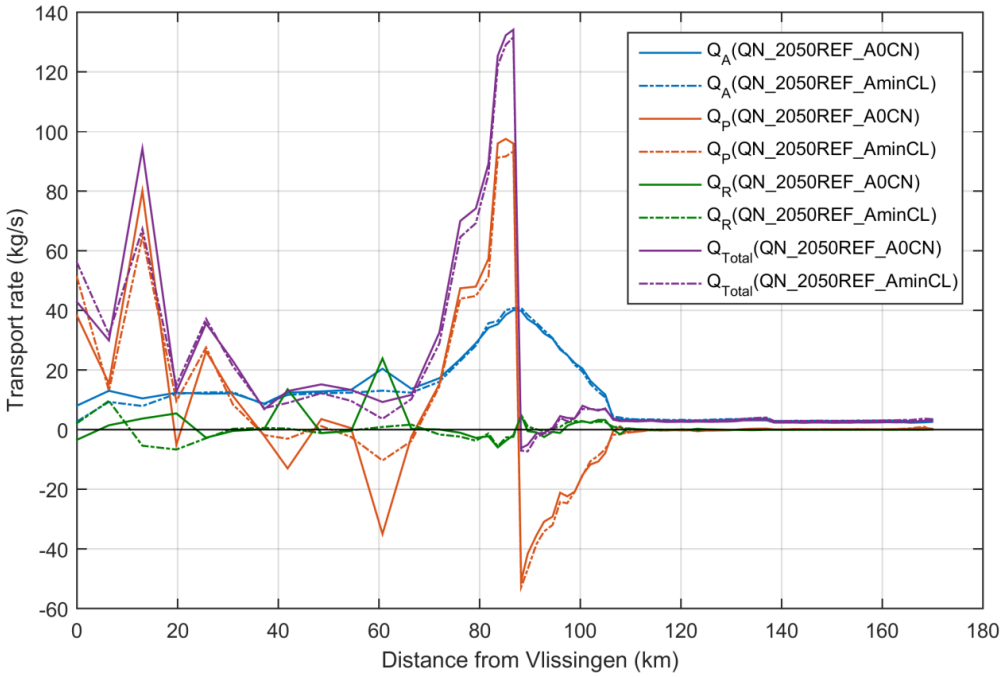

Figure 69 – Time-averaged decomposed sediment transport rate QA, QP and QR.
Positive sign means downstream direction and negative means upstream direction.

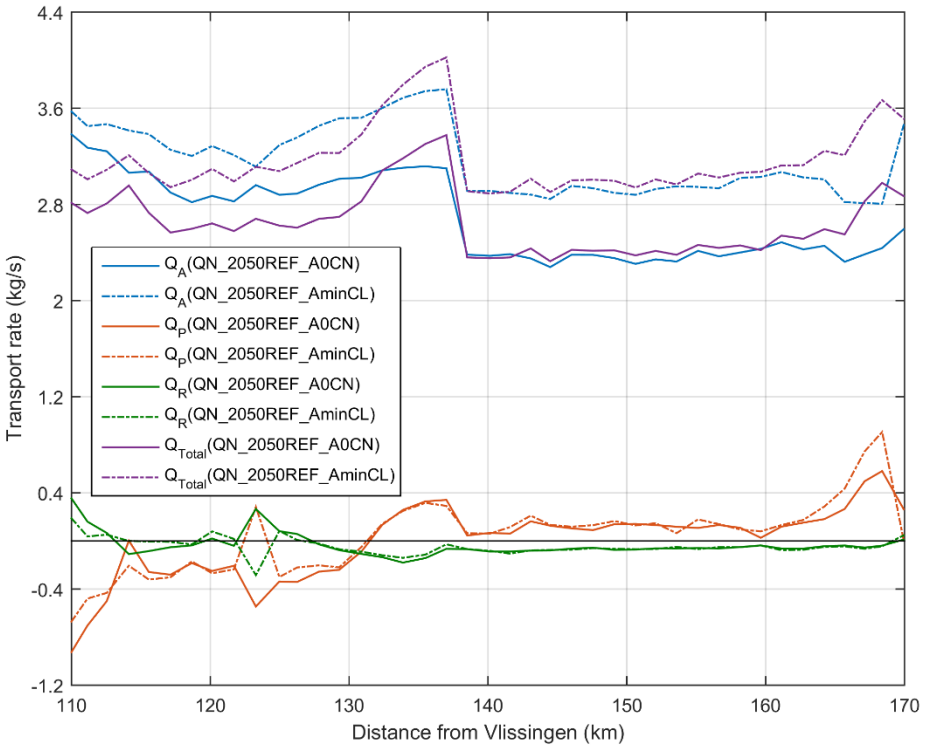

Figure 70 – Decomposed time-averaged sediment transport QA, QP and QR for the Upper Sea Scheldt.
Positive sign means downstream direction and negative means upstream direction

(4). Erosion-deposition map

The difference of sedimentation rate is calculated between the run 2050_REF_AminCL and 2050_REF_A0CN using the bed layer thickness given in the result files. The sedimentation rate is based on the production period of the last 20 days and it is converted to cm/yr.

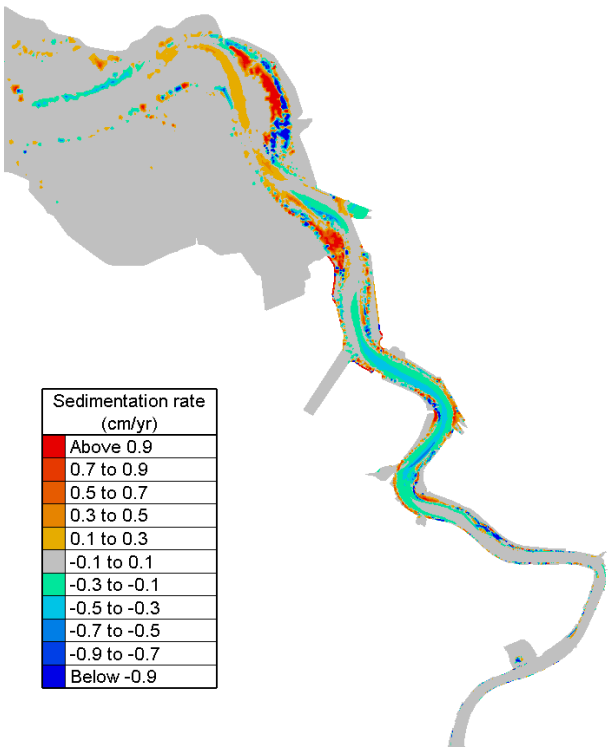

Figure 71 – Difference of sedimentation rate (2050_REF_AminCL-2050_REF_A0CN) – Lower Sea Scheldt

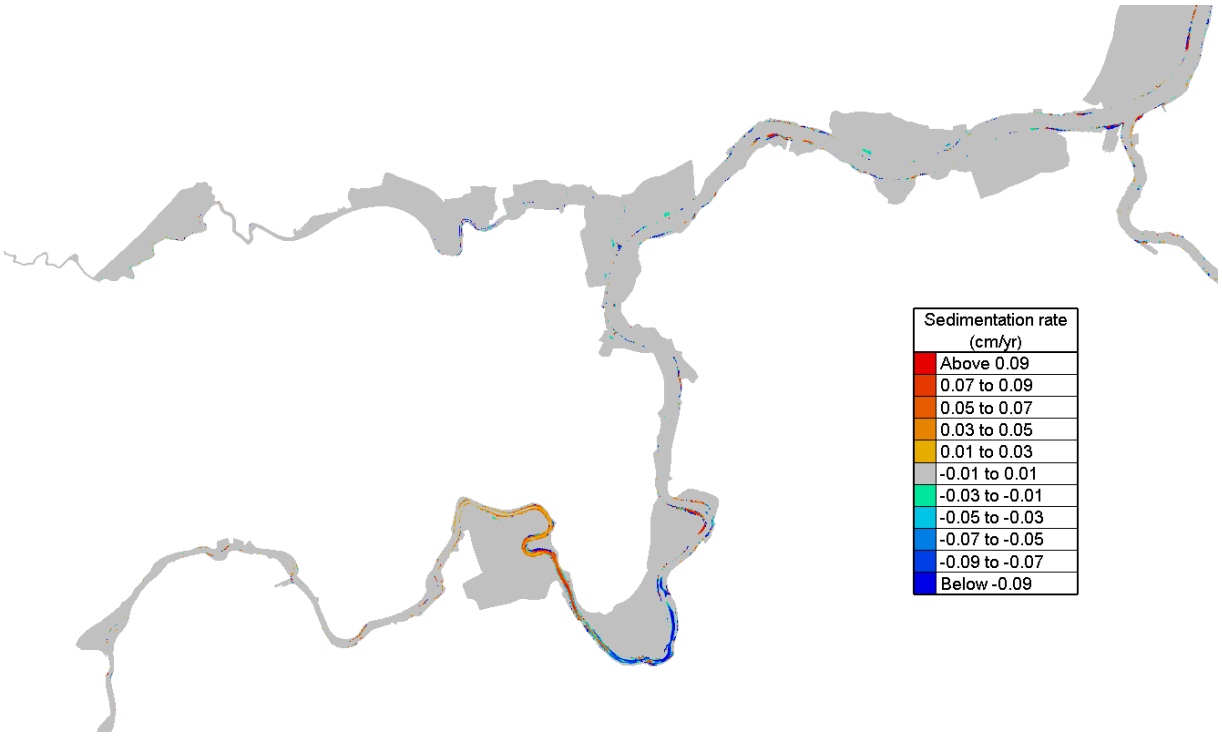

Figure 72 – Difference of sedimentation rate (2050_REF_AminCL-2050_REF_A0CN) – Upper Sea Scheldt (part 1)

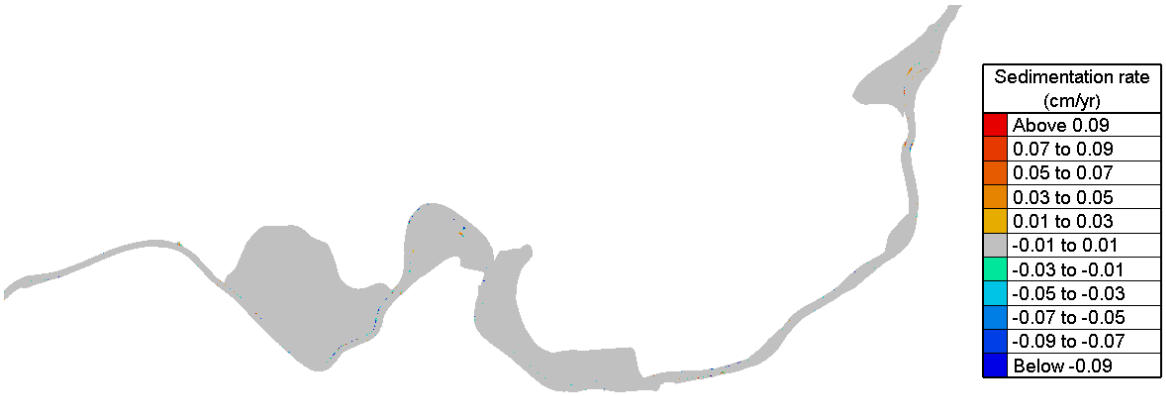

Figure 73 – Difference of sedimentation rate (2050_REF_AminCL-2050_REF_A0CN) – Upper Sea Scheldt (part 2)

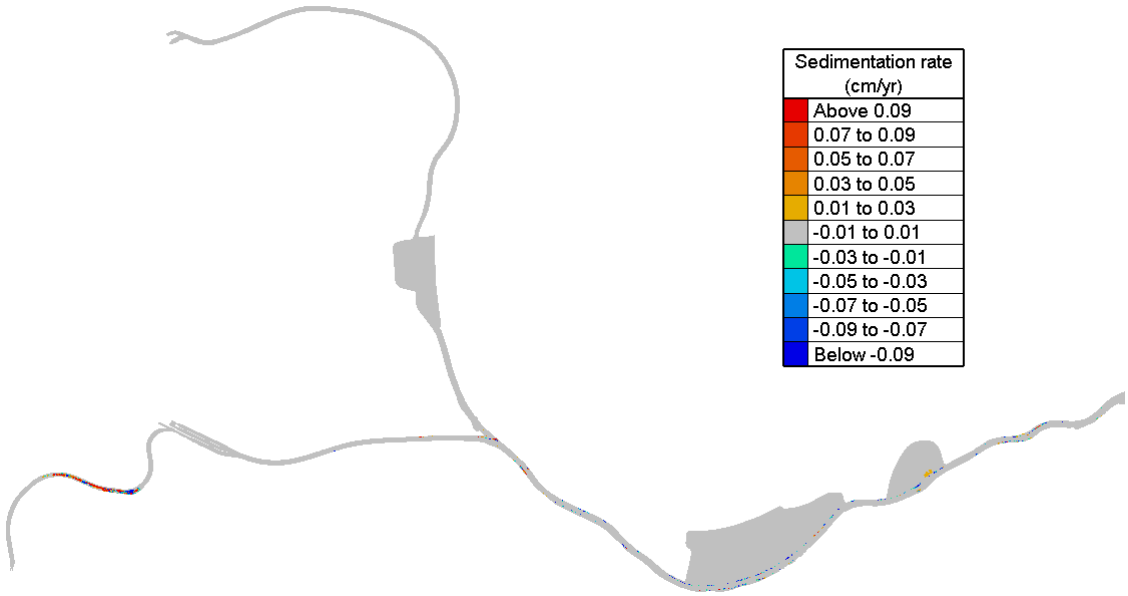

Figure 74 – Difference of sedimentation rate (2050_REF_AminCL-2050_REF_A0CN) – Upper Sea Scheldt (part 3)

In the Western Scheldt and Lower Sea Scheldt, the general trend shows a larger sedimentation rate on the intertidal flats and a smaller sedimentation rate in the channel. In the Upper Sea Scheldt, the difference seems much smaller, with a spatial shift in sedimentation rates near Baasrode.

(5). Bed shear stress

Changes in bottom shear stress lead to changes in sedimentation/erosion patterns and habitat suitability. Therefore maps are made in the study area of exceedance time (%) of a threshold value of 1 Pa during a spring-neap cycle. A difference map (in %-points) shows the spatial changes.

Note that changes in shear stress in the Western Scheldt are an artefact and related to the way the Amin amplitude reduction is implemented.

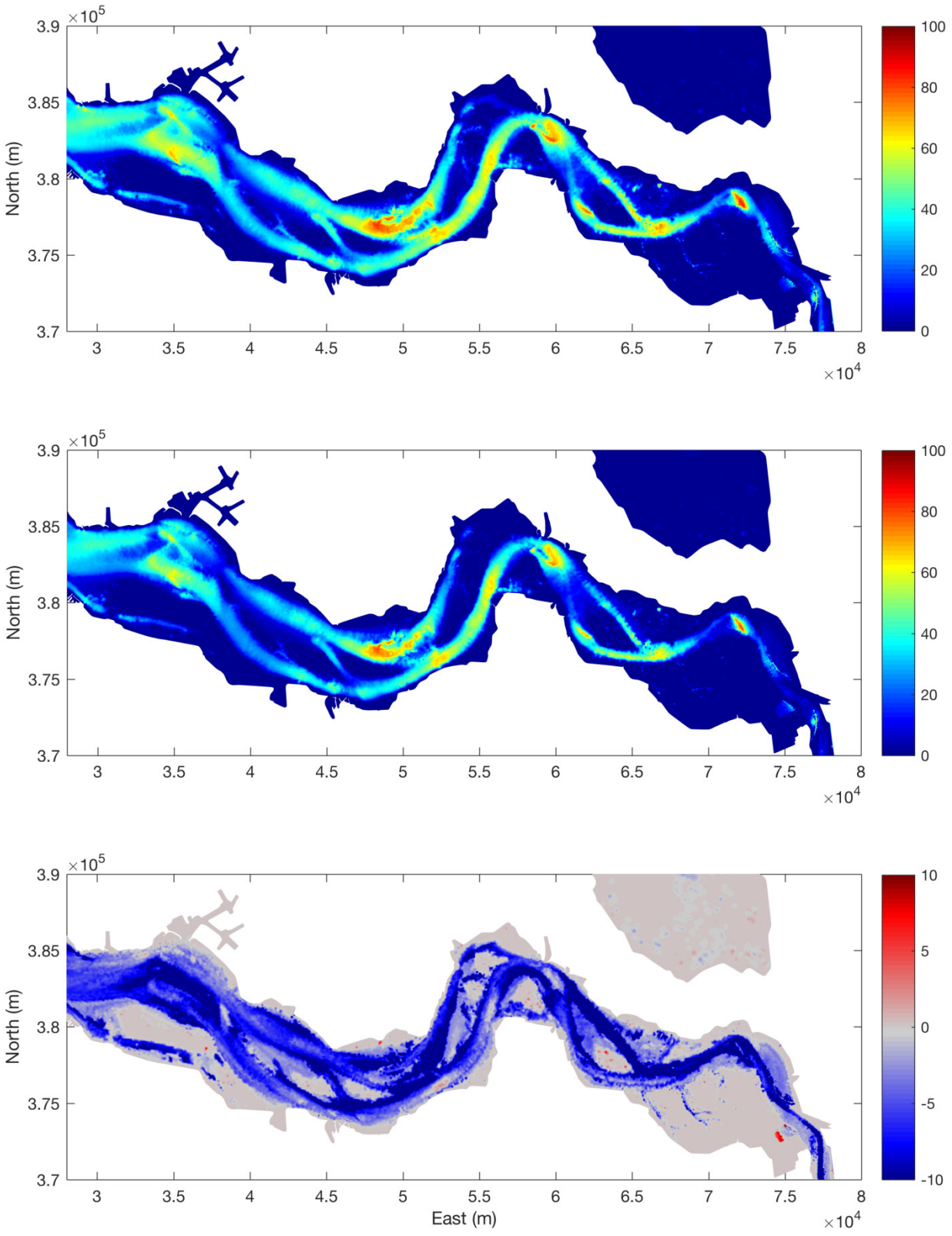

Figure 75 – Exceedance time of bed shear stress >1Pa (%) during a spring-neap cycle in Western Scheldt.
From top to bottom: the reference 2050_REF_A0CN; the scenario 2050_REF_AminCL;
the difference 2050_REF_AminCL – 2050_REF_A0CN.

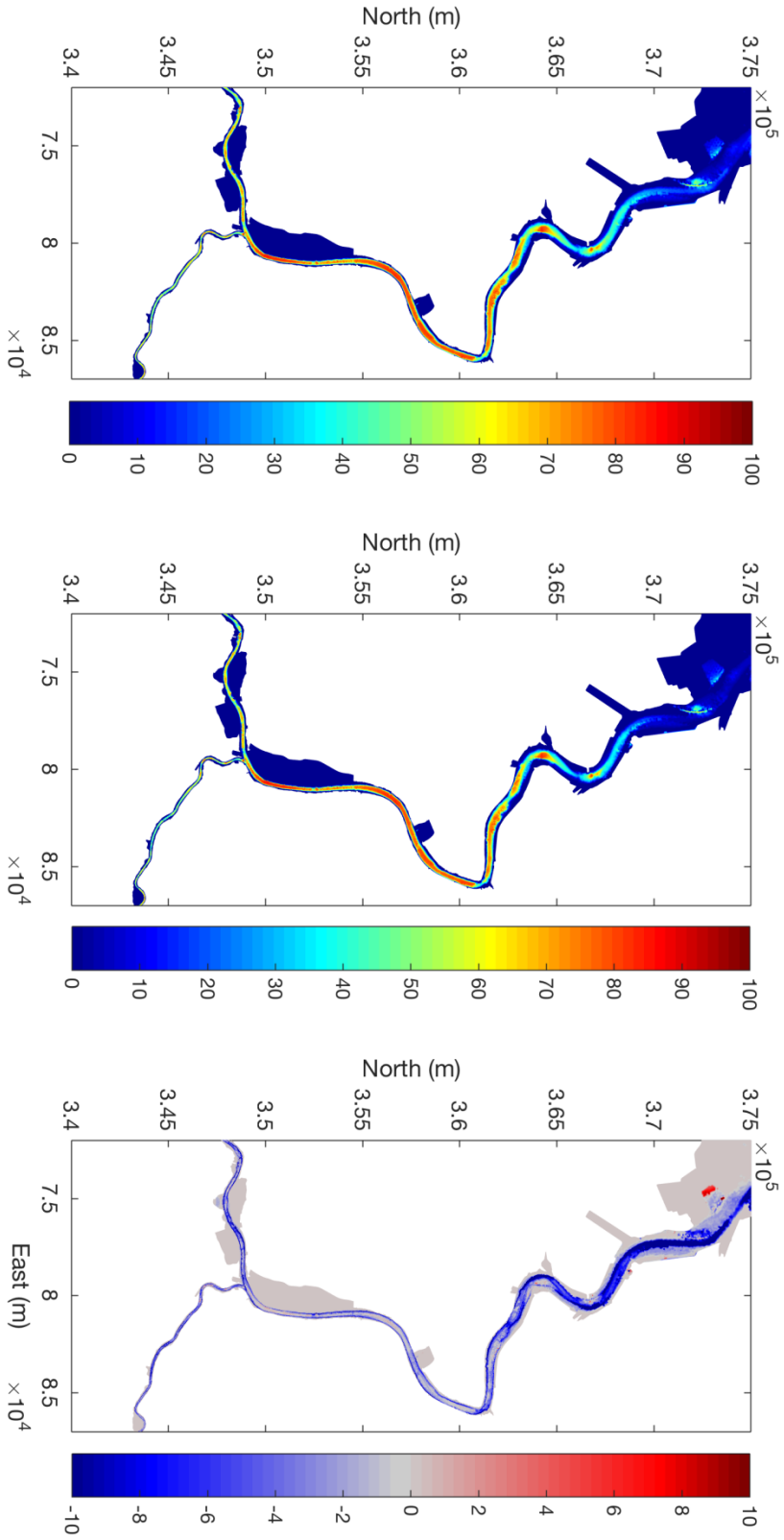

Figure 76 – Exceedance time of bed shear stress >1Pa (%) during a spring-neap cycle in Lower Sea Scheldt.
From top to bottom: the reference 2050_REF_A0CN; the scenario 2050_REF_AminCL;
the difference 2050_REF_AminCL - 2050_REF_A0CN.

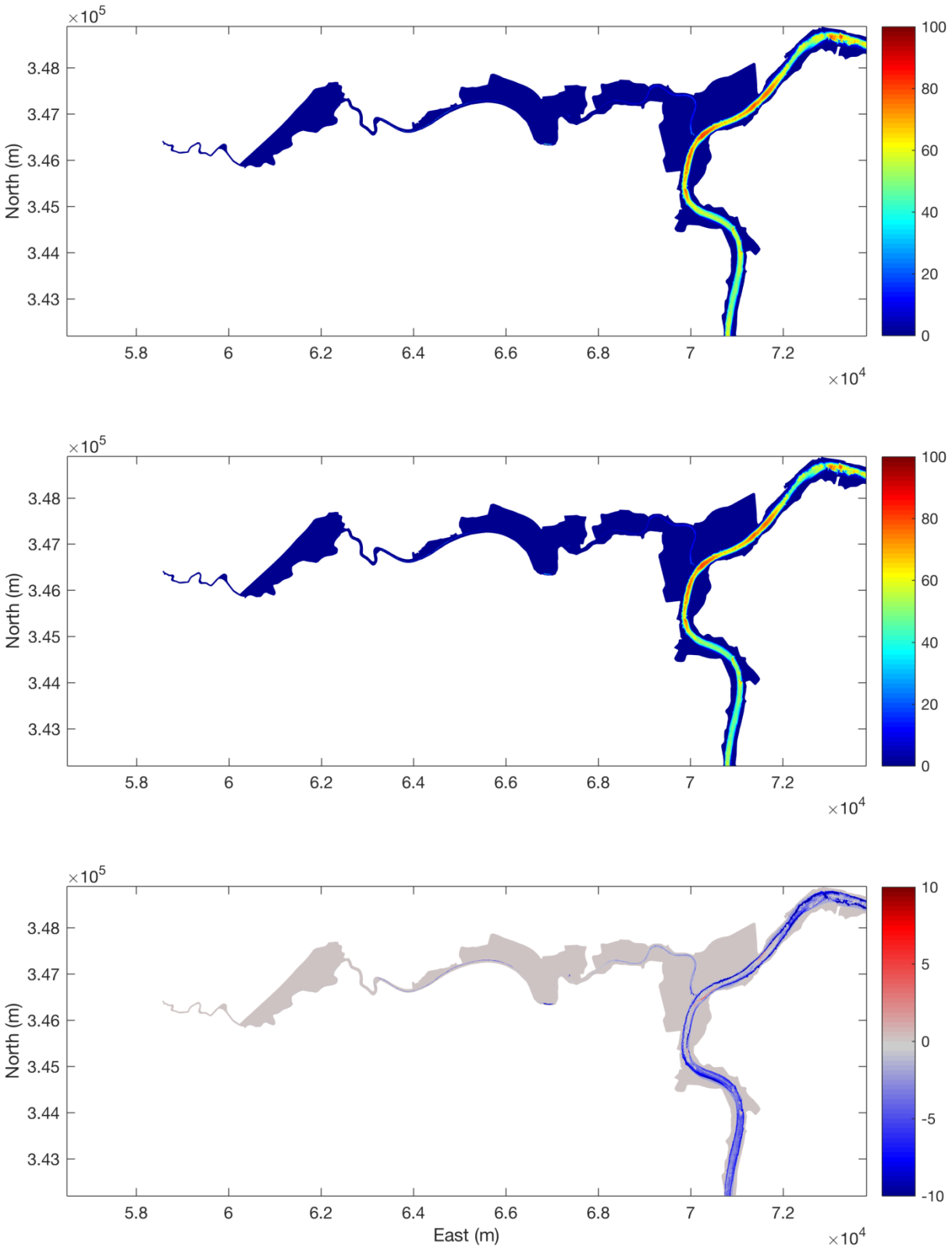

Figure 77 – Exceedance time of bed shear stress >1Pa (%) during a spring-neap cycle in Upper Sea Scheldt.
From top to bottom: the reference 2050_REF_A0CN; the scenario 2050_REF_AminCL;
the difference 2050_REF_AminCL - 2050_REF_A0CN.

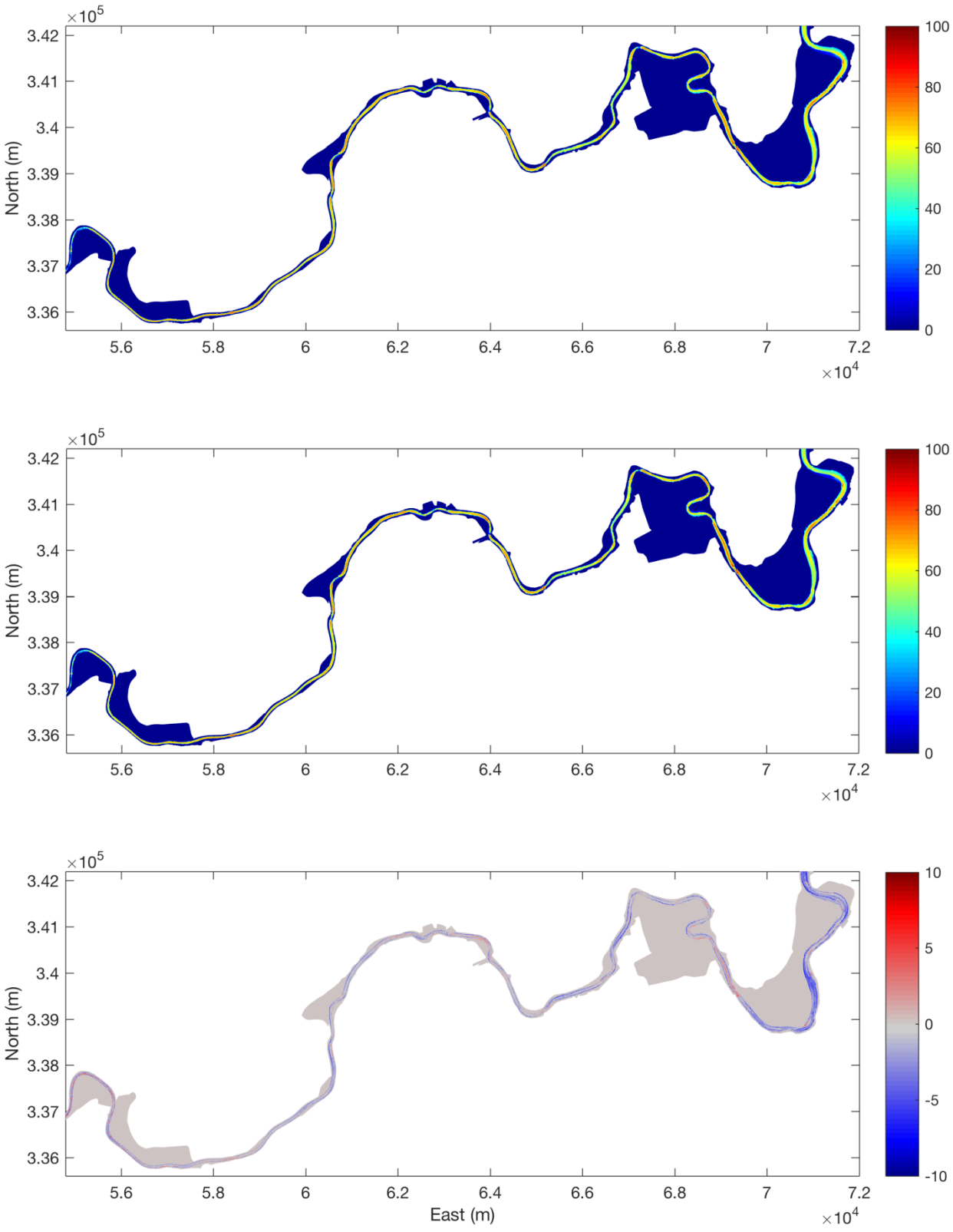

Figure 78 – Exceedance time of bed shear stress >1Pa (%) during a spring-neap cycle in Upper Sea Scheldt.
From top to bottom: the reference 2050_REF_A0CN; the scenario 2050_REF_AminCL;
the difference 2050_REF_AminCL - 2050_REF_A0CN.

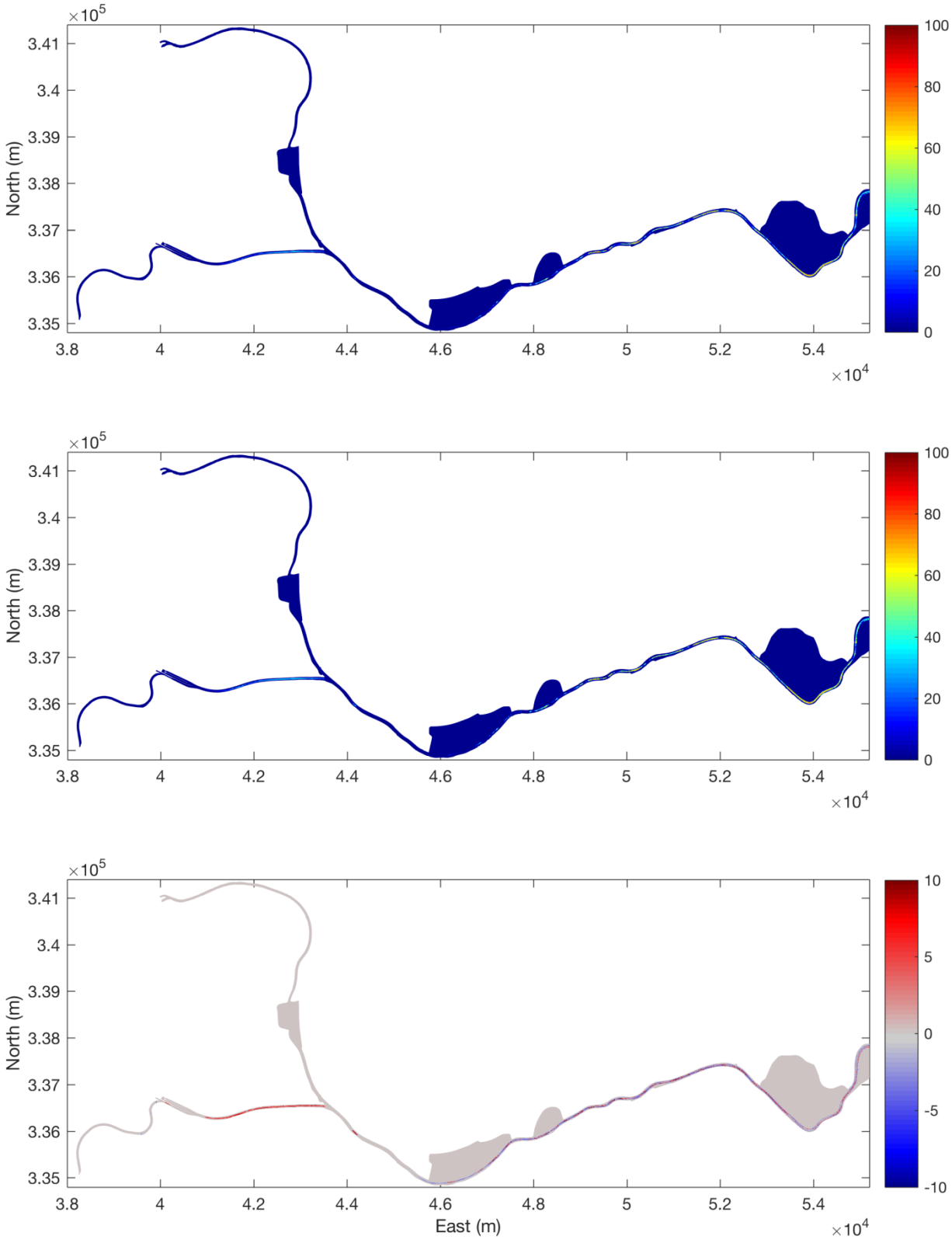

Figure 79 – Exceedance time of bed shear stress >1Pa (%) during a spring-neap cycle in Upper Sea Scheldt.
From top to bottom: the reference 2050_REF_A0CN; the scenario 2050_REF_AminCL;
the difference 2050_REF_AminCL - 2050_REF_A0CN.

(6). Delta SSC

The Delta SSC is calculated based on equation described in §5.1 and the time averaged Delta SSC is given for each box of the ecosystem model in Figure 80.

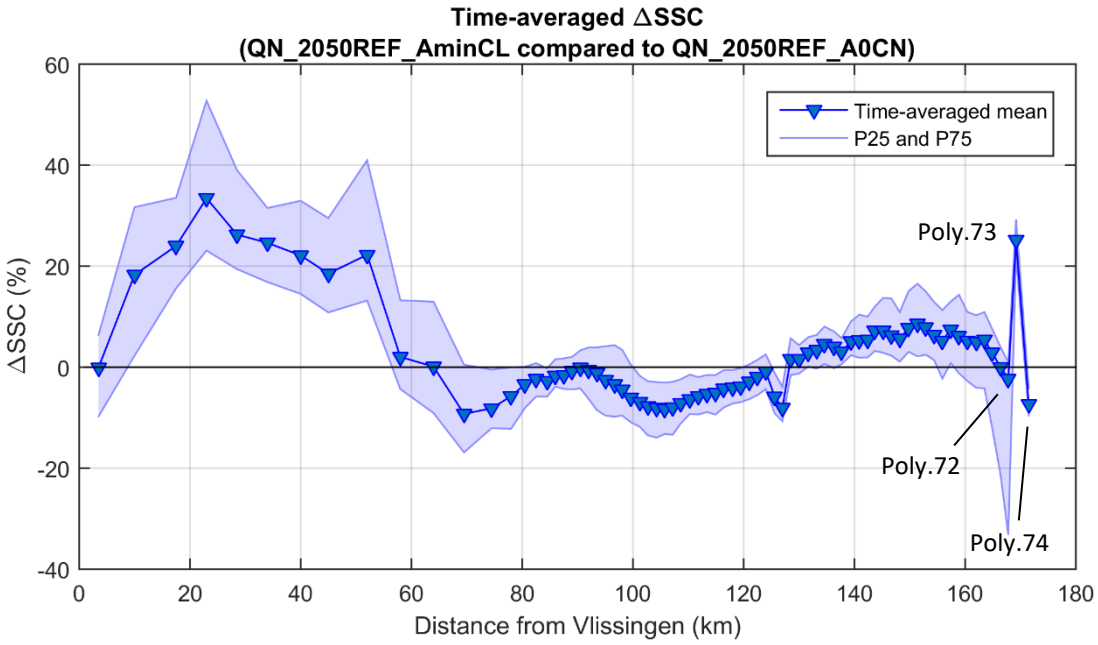

Figure 80 – 2050_REF_AminCL compared to 2050_REF_A0CN

The delta SSC stays in a relatively high level in the Western Scheldt, where the mean values are around 20% - 30%. But it decreases when it is further upstream, staying negative from 60 km to 130 km. From 130 km and upwards, delta SSC increases again and becomes positive.

In the delta SSC result, as shown in Figure 80, there is a peak appearing at the location 169.2 km from Vlissingen (Polygon 73). Comparing to it, the nearby locations, e.g. at 171.5 km (Polygon 74) and 167.8 km (Polygon 72), have much lower delta SSC. In order to understand the discontinuity in the trend of delta SSC in this region, SSC maps during flood phase and ebb phase from the reference and scenario respectively are plotted (Figure 81). Because of the higher discharge (Q2050), the downstream flow becomes stronger and sediment input from the boundary is increased. The consequence is that, in the scenario, larger amount of sediment is pushed further downstream during flood phase, extending the higher SSC zone into Polygon 73. Due to stronger downstream flow, the low SSC zone is extended as well, and shifted towards downstream. This is the main reason why delta SSC reaches the peak in Polygon 73 and then suddenly drops in Polygon 72. For Polygon 74, because of the stronger flow imposed at the upstream boundary, the flood phase becomes shorter, thus sediment coming to this polygon becomes less frequent, which leads to lower time-averaged delta SSC.

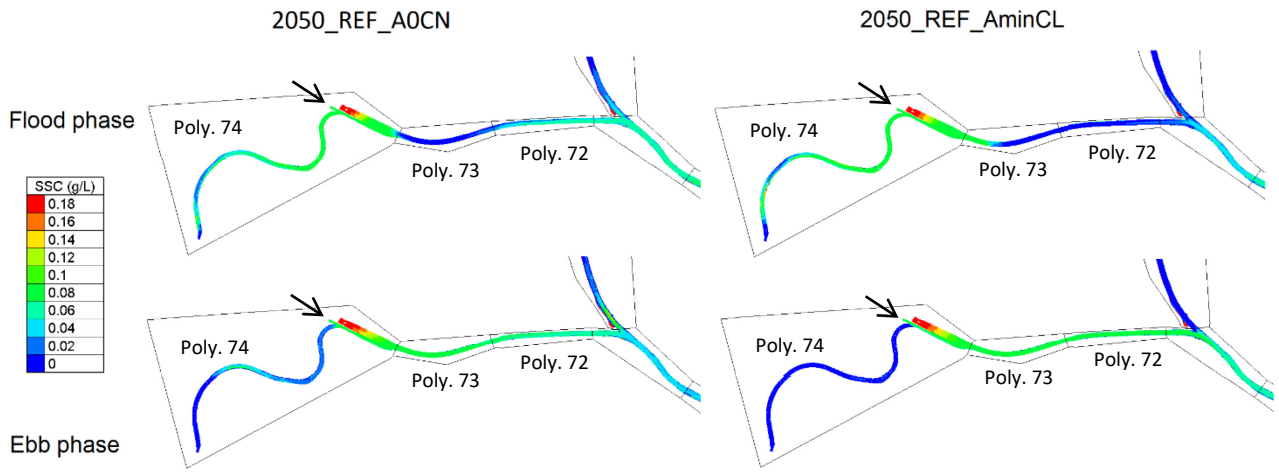

Figure 81 – Comparison of SSC near the upstream boundary during ebb and flood phases

(7). Discussion

It is difficult to separate different contributions to the delta SSC from different influential factors in 2050_REF_AminCL. In general, they all have effects throughout the entire domain, but their relative importance depends on the regions.

The change of tidal asymmetry has influence on delta SSC, especially its spatial variations. As seen in Figure 66 to Figure 68, although the system is not fundamentally different, the system becomes slightly less ebb dominant from km140 to km160.

The transport rate (Figure 70) shows more advection-driven downstream sediment transport, which is consistent with the increase in fresh water discharge upstream. Because the imposed concentrations do not change between reference case and scenario's, this means that the sediment transport rate (kg/s) at the upstream boundary of the Upper Sea Scheldt (Melle) increases.

Delta SSC starts to decrease after reaching the peak at 151.4 km. The delta SSC decreasing is consistent with the lower bed shear stress found in this area (Figure 79). The decrease of maximum bed shear stress is also confirmed in the difference of velocity M_2 amplitude, which is correlated with the change of bed shear stress. As shown in Figure 82, the effect on velocity M_2 amplitude starts downstream of 140 km, which suggests the flow has less energy compared to the reference case, thus, less suspension capacity in the water column. This is consistent with the decrease of delta SSC and total sediment flux in this region.

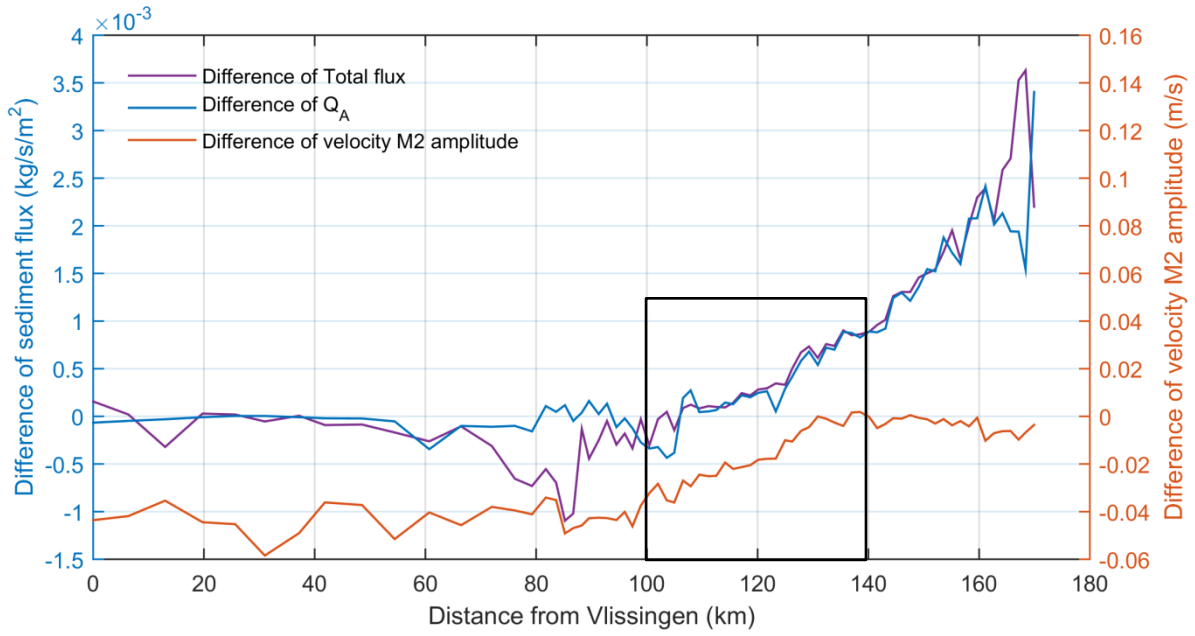

Figure 82 – Velocity M2 amplitude and its influence on decomposed sediment flux

Around km88, the effect is zero, because the local SSC solution is determined there by the disposal flux, which is kept constant between the scenario's. It is worth mentioning that, the delta SSC does not reach zero at about 88 km, where the point source is placed. Instead, it reaches about zero in the polygon upstream next to it. The reason is that the "AminCL" scenario (sea level rise + reduced tidal range) tends to push sediment further upstream (the system becomes slightly less ebb-dominant). This is confirmed in the decomposed sediment flux in Figure 69, in which total sediment flux becomes less on the downstream side of the point source, suggesting less downstream sediment flux. On the upstream side, it becomes larger towards upstream, meaning more sediment is transported towards upstream. Also it can be seen that, the convergence point of total sediment flux, where the flux cross the zero axis, shifts further upstream, from about 93.8 km to 94.6 km.

Downstream of 70 km, the results in terms of concentration become unreliable. The bottom friction is increased in the hydrodynamic model but the mud model uses a separate bottom friction for calculating bed shear stress. This makes the results difficult to interpret. The bed shear stress becomes smaller in this region (Figure 75), but the SSC increases instead of decreasing.

5.1.3 From 2050 REF A0CN to 2050 REF AplusCH

The scenario 2050_REF_AplusCH uses the same bathymetry as in the reference 2050_REF_A0CN. As indicated in the name of the run, the sea level rise of 40 cm is added in the downstream boundary conditions (details is described in §3.2.5). Moreover, the roughness is decreased in the Western Scheldt (from 0 – 68 km from Vlissingen) in order to have higher tidal amplitude. And finally, the upstream discharge is increased based on statistical analysis for year 2050. There is no difference in rest of model settings and in the input data.

(1). The difference in hydrodynamics

The time-averaged difference of depth-averaged velocity magnitude is shown in Figure 83 and Figure 84.

With the combination effects from sea level rise (+40cm), decreased bottom friction and increased upstream discharge, higher velocity magnitude can be observed in the North Sea, Western Scheldt and almost the entire Upper Sea Scheldt, except a small section near the upstream boundary at Melle.

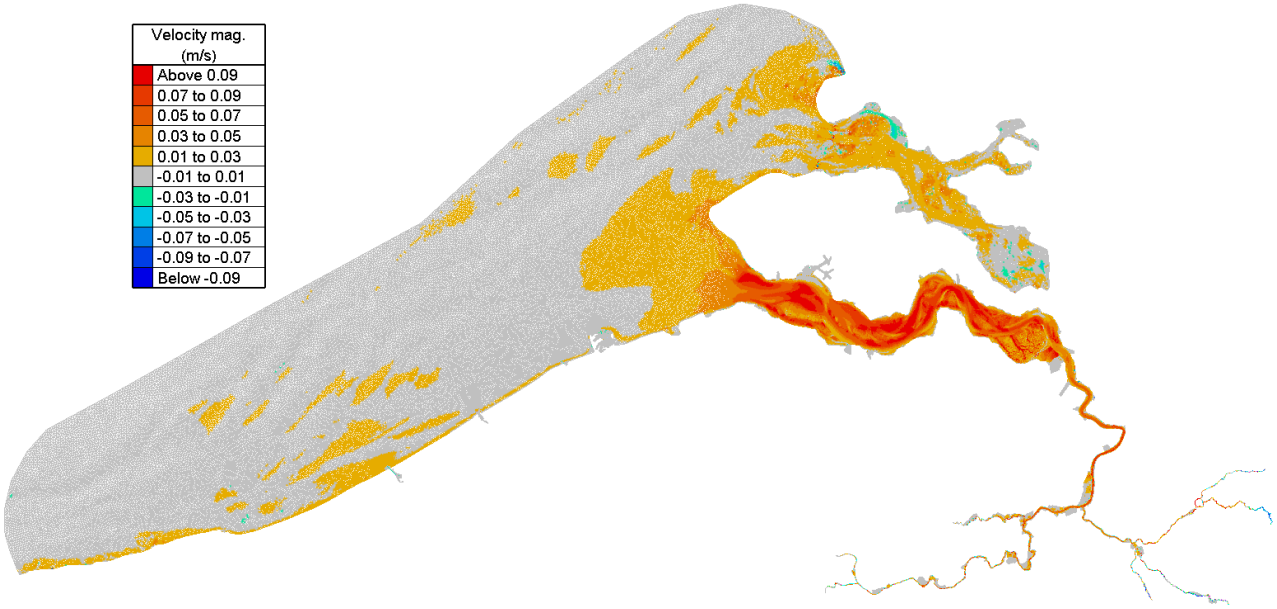

Figure 83 – Time averaged velocity difference between two runs (2050_REF_AplusCH – 2050_REF_A0CN)

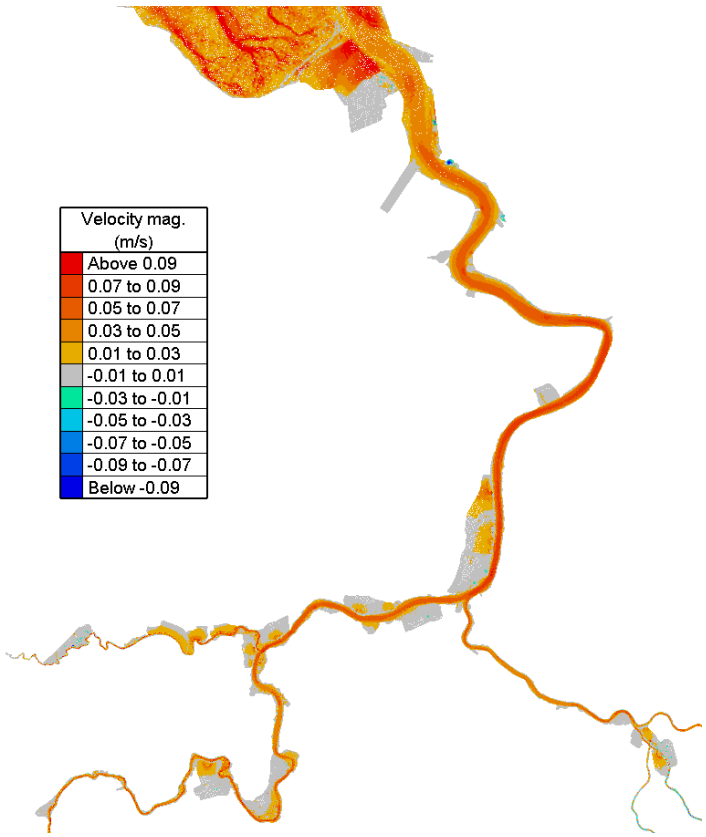

Figure 84 – Time averaged velocity difference in Upper Sea Scheldt (2050_REF_AplusCH – 2050_REF_A0CN) – part 1

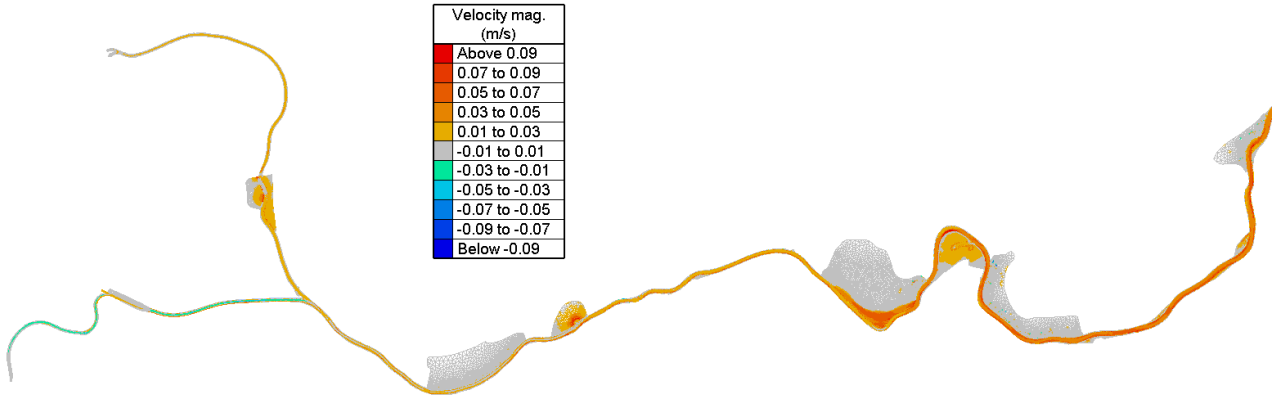

Figure 85 – Time averaged velocity difference in Upper Sea Scheldt (2050_REF_AplusCH – 2050_REF_A0CN) – part 2

Because the sea level rise (+40cm) is added at downstream boundary, and decrease of bottom friction in the Western Scheldt, the scenario 2050_REF_AplusCH gives different time-averaged water level along the thalweg (Figure 86). The increased water level in the scenario is from 38cm to 54cm, depending on the location.

The tidal range is amplified due to the reduced bottom friction (Figure 87). The most amplified region is in the Western Scheldt, where the water level M_2 amplitude increases by 15 - 20cm. The water level M_4 amplitude increases in the Western Scheldt whereas it decreases in the rest of the domain. As mentioned in §5.1.2, the change of water level M_4 amplitude can be associated with change of tidal wave distortion or tidal asymmetry.

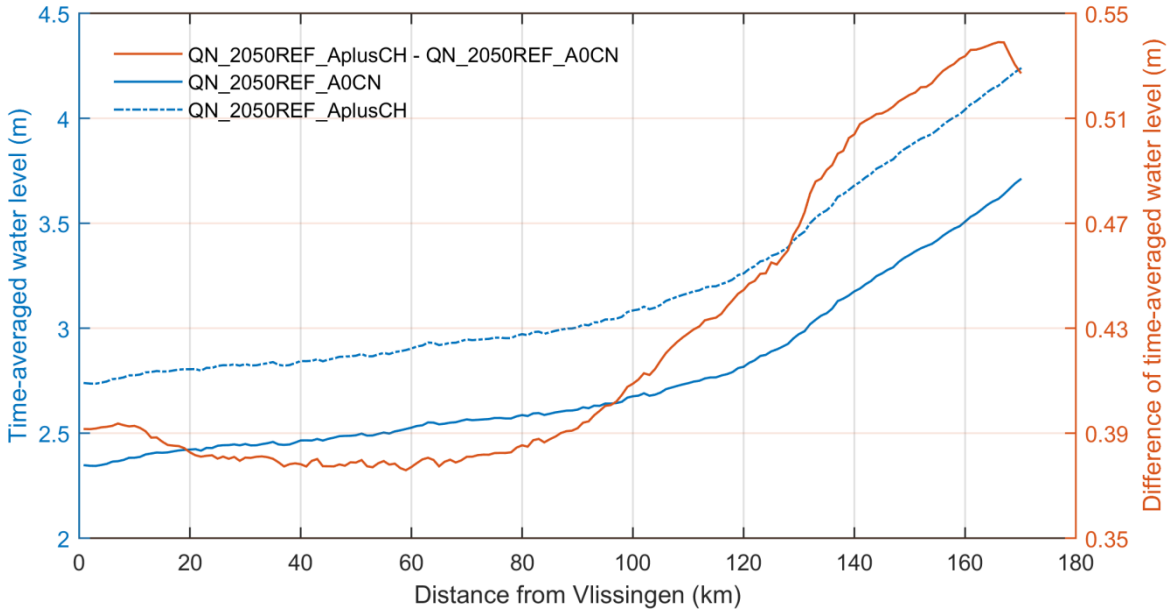

Figure 86 – Comparison of time-averaged water level between 2050_REF_A0CN and 2050_REF_AplusCH

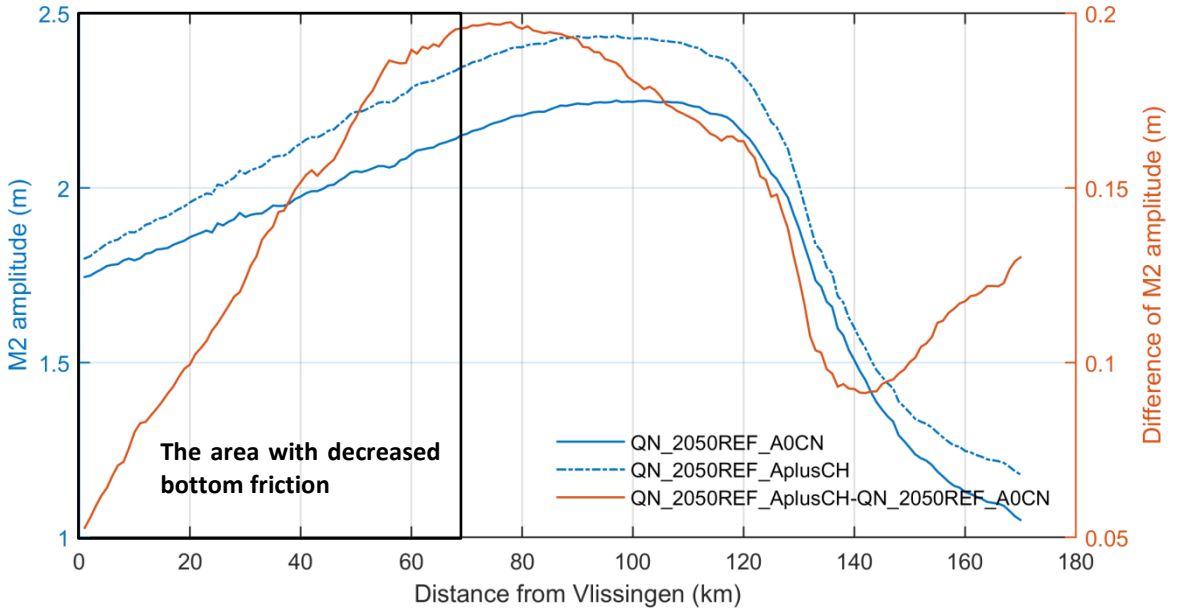

Figure 87 – Comparison of M2 amplitude between 2050_REF_A0CN and 2050_REF_AplusCH

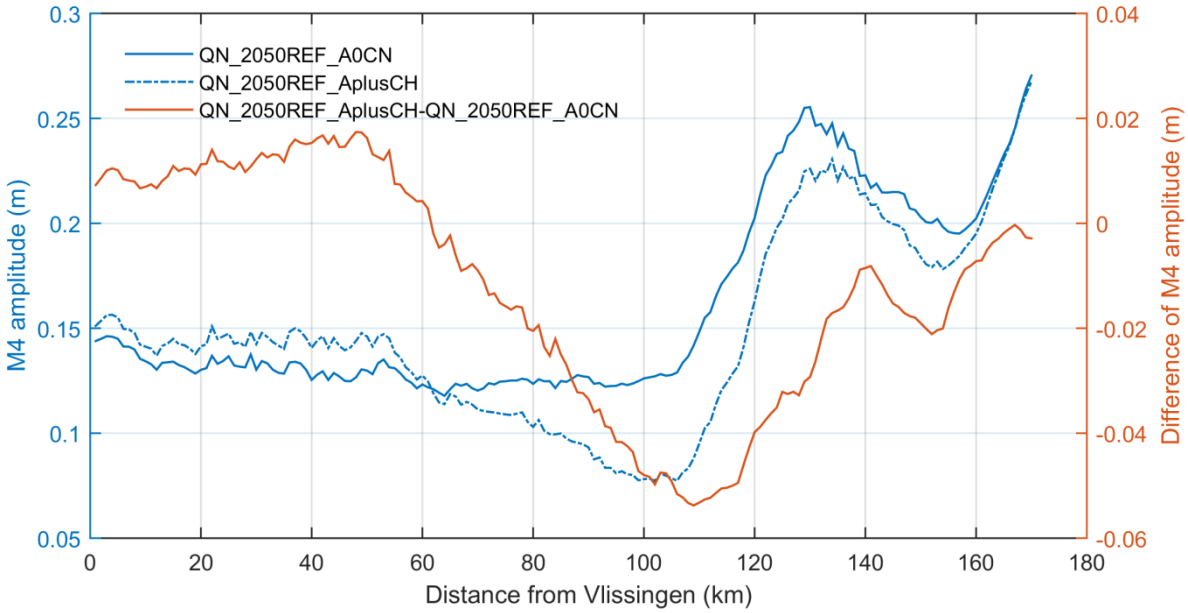

Figure 88 – Comparison of M4 amplitude between 2050_REF_A0CN and 2050_REF_AplusCH

Harmonic analysis is performed on the cross-sectionally averaged velocity. As shown in Figure 89, the velocity M_2 amplitude becomes larger in 2050_REF_AplusCH, due to the fact that the bottom friction is reduced in the Western Scheldt. Another influence could be the increased water level along the Scheldt, resulting in lower friction as well.

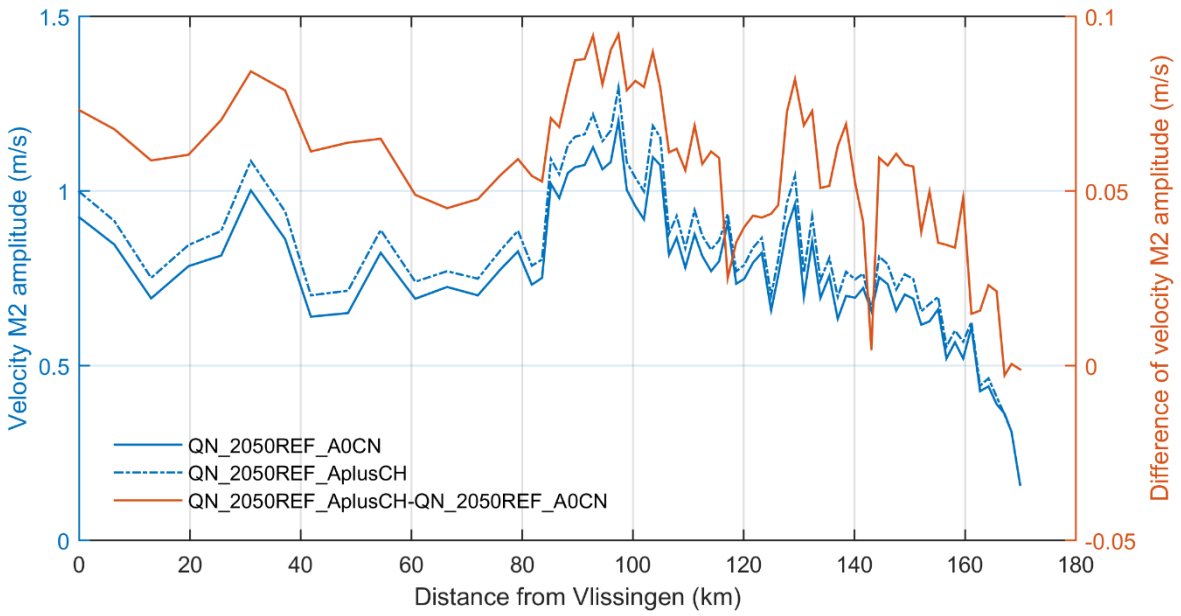

Figure 89 – Comparison of M2 amplitude of cross-sectionally averaged velocity between 2050_REF_A0CN and 2050_REF_AplusCH

(2). The change of tidal asymmetry

All the tidal asymmetry indicators as mentioned in §4.8, are calculated in this section. These indicators, 8 in total, are organized in 3 groups, based on time duration, velocity magnitude and skewness, respectively.

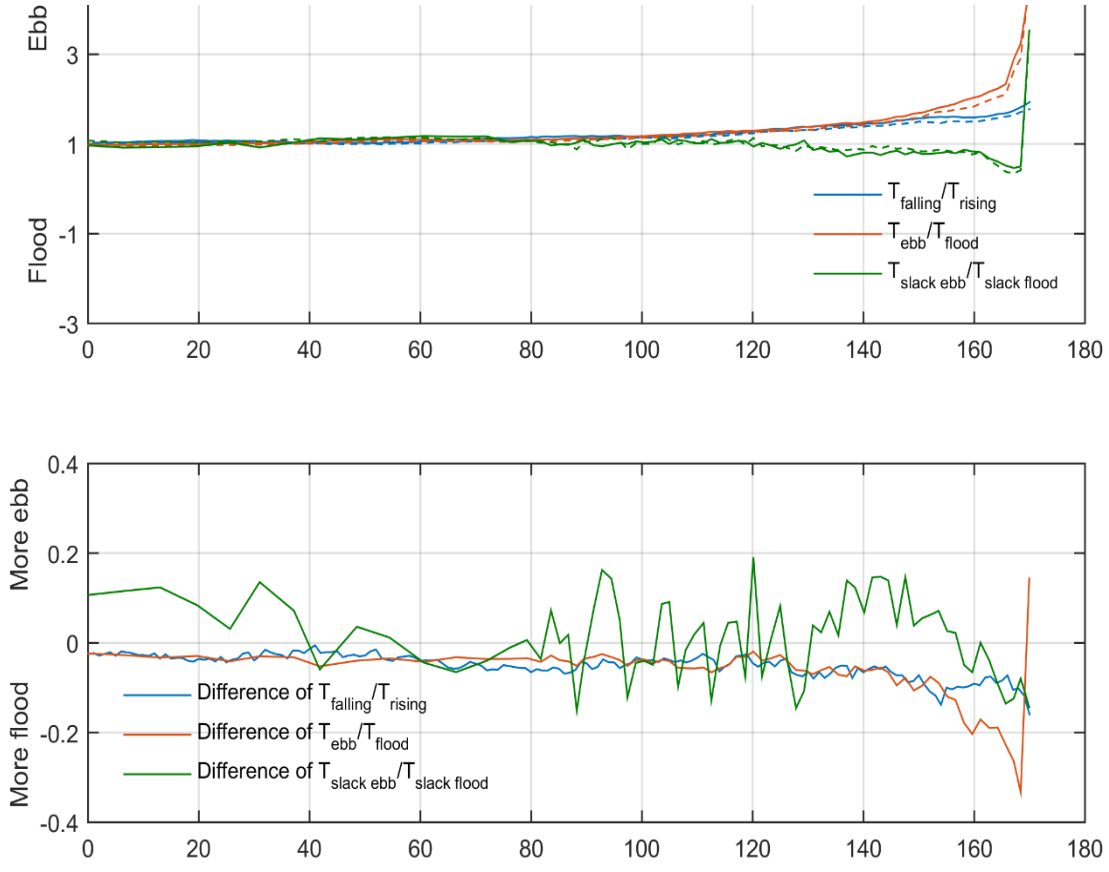

Figure 90 – Indicators of tidal asymmetry (durations).
Solid lines represent the reference 2050_REF_A0CN, dashed lines represent the scenario 2050_REF_AplusCH.

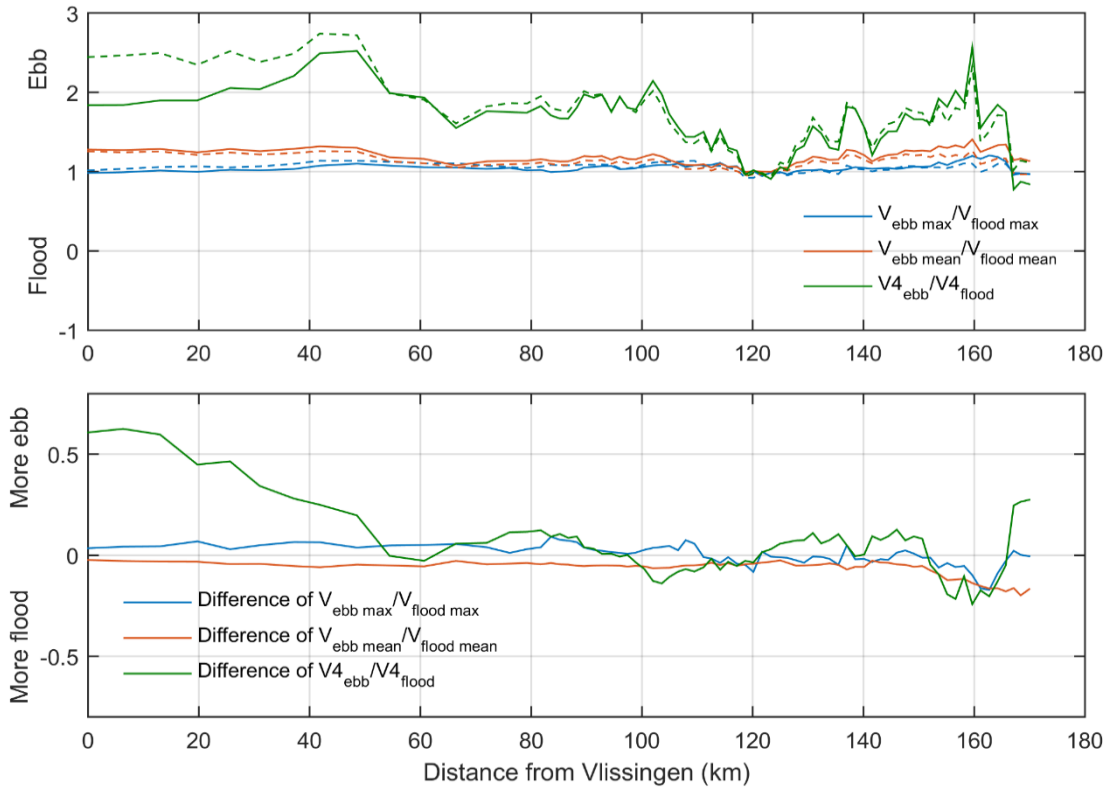

Figure 91 – Indicators of tidal asymmetry (velocities).
Solid lines represent the reference 2050_REF_A0CN, dashed lines represent the scenario 2050_REF_AplusCH.

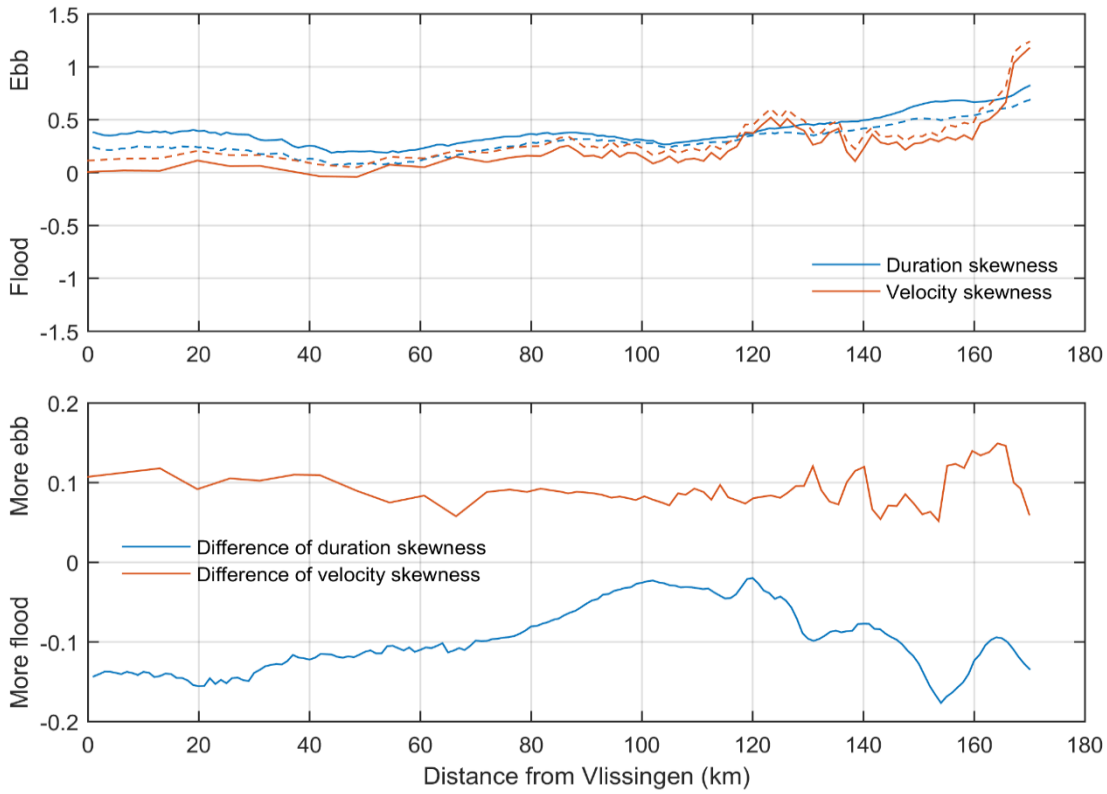

Figure 92 – Indicators of tidal asymmetry (skewness).
Solid lines represent the reference 2050_REF_A0CN, dashed lines represent the scenario 2050_REF_AplusCH.

(3). Sediment Transport Decomposition

Figure 93 shows the sediment transport decomposed according to §4.7. From 170 km to 110 km, total sediment transport is increased, meaning more transported downstream. In this region, QA is dominant, suggesting discharge is the most influential factor.

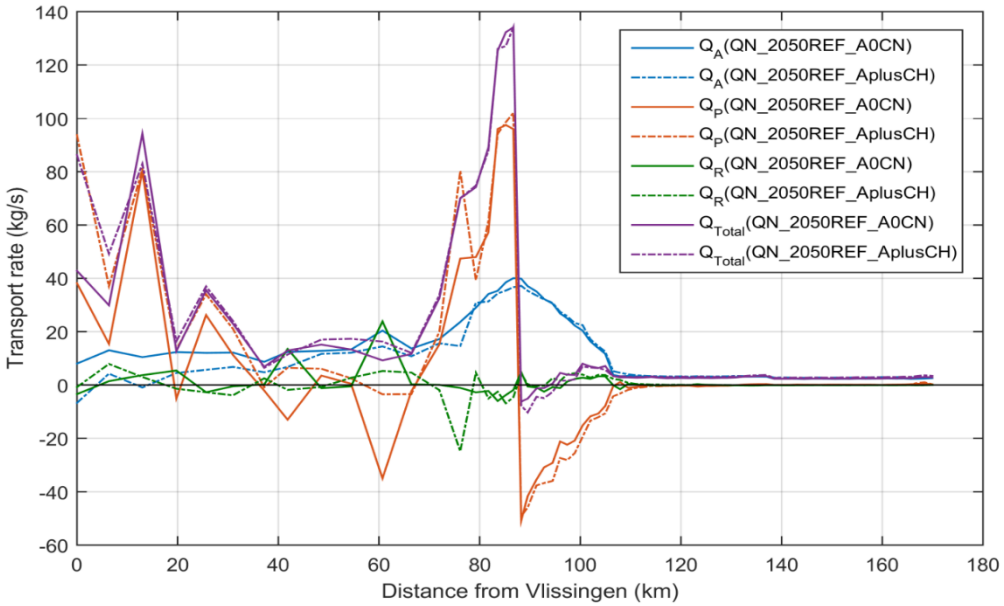

Figure 93 – Time-averaged decomposed sediment transport rate QA, QP and QR.
Positive sign means downstream direction and negative means upstream direction.

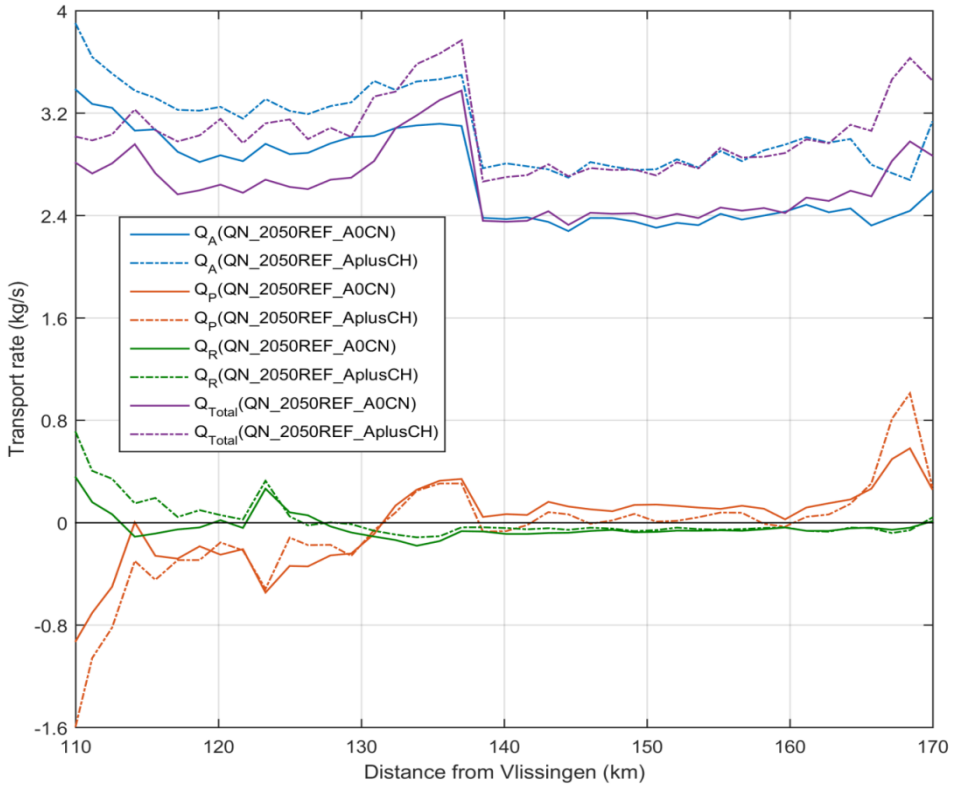

Figure 94 – Time-averaged decomposed sediment transport rate QA, QP and QR in the Upper Sea Scheldt.
Positive sign means downstream direction and negative means upstream direction.

(4). Erosion-deposition map

The difference of sedimentation rate is calculated between the run 2050_REF_AplusCH and 2050_REF_A0CN using the bed layer thickness given in the result files. The sedimentation rate is based on the production period of the last 20 days and it is converted to cm/yr.

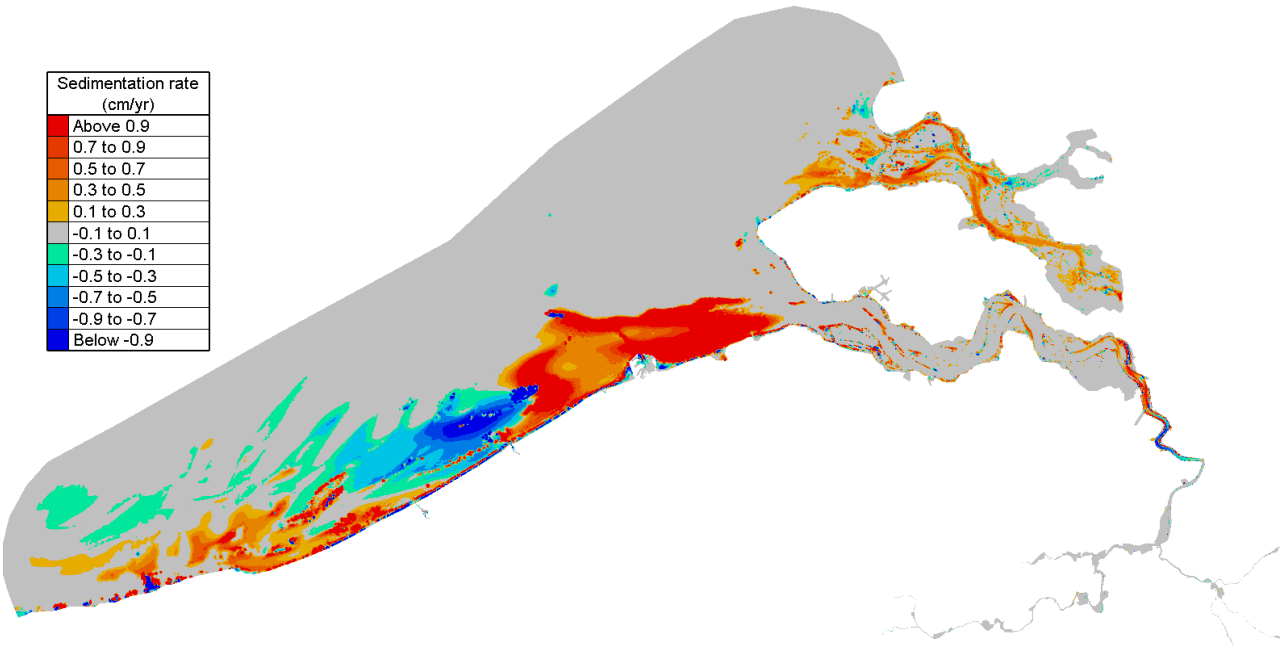

Figure 95 – Difference of sedimentation rate (2050_REF_AplusCH-2050_REF_A0CN) – overview

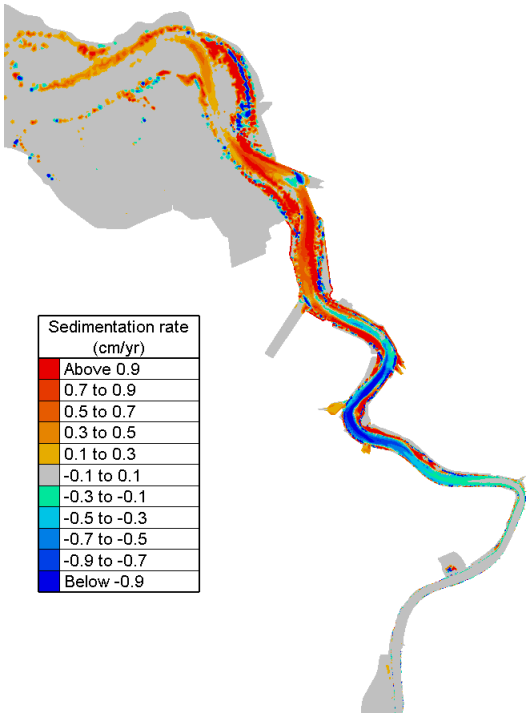

Figure 96 – Difference of sedimentation rate (2050_REF_AplusCH-2050_REF_A0CN) – Lower Sea Scheldt

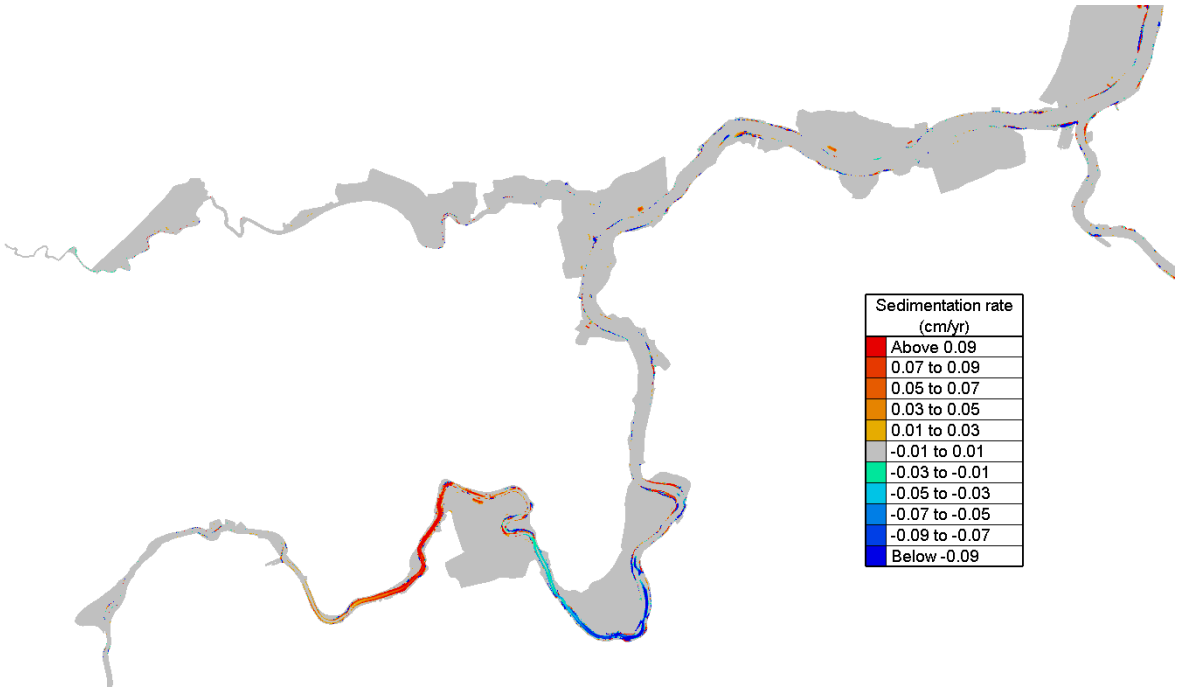

Figure 97 – Difference of sedimentation rate (2050_REF_AplusCH-2050_REF_A0CN) – Upper Sea Scheldt (part 1)

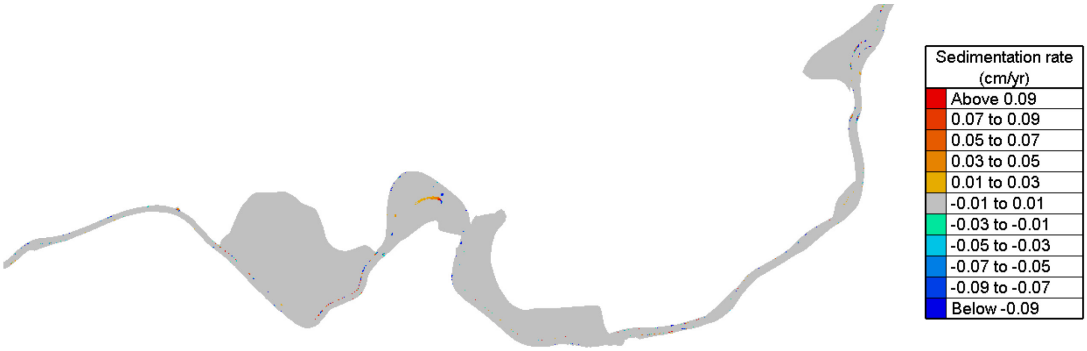

Figure 98 – Difference of sedimentation rate (2050_REF_AplusCH-2050_REF_A0CN) – Upper Sea Scheldt (part 2)

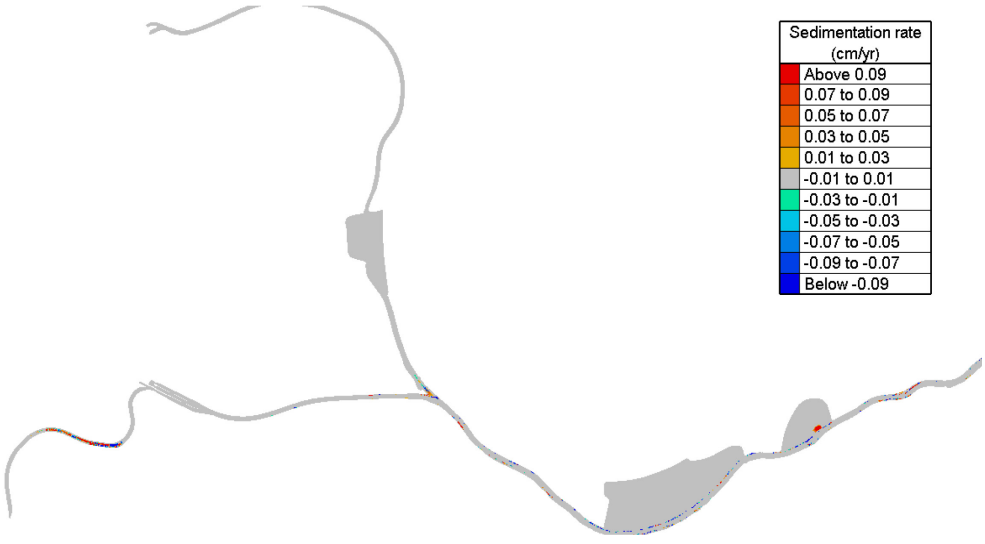

Figure 99 – Difference of sedimentation rate (2050_REF_AplusCH-2050_REF_A0CN) – Upper Sea Scheldt (part 3)

With higher sea level rise in 2050_REF_AplusCH, there is even larger impact in the North Sea and Belgian coast compared. In the Western Scheldt and the Lower Sea Scheldt, there are more intertidal areas with larger sedimentation rate. Also increased sedimentation rates at the sills of Hansweert and Frederik can be observed. But in the downstream of Antwerp, sedimentation rate becomes smaller in the navigation channel compared to 2050_REF_A0CN. In the Upper Sea Scheldt, smaller sedimentation rate is again found in Baasrode. But this time there is another area showing the difference, with slightly larger sedimentation rate near Vlassenbroek.

(5). Bed shear stress

Changes in bottom shear stress lead to changes in sedimentation/erosion patterns and habitat suitability. Therefore maps are made in the study area of exceedance time (%) of a threshold value of 1 Pa during a spring-neap cycle. A difference map (in %-points) shows the spatial changes.

Note that changes in shear stress in the Western Scheldt are an artefact and related to the way the Aplus amplitude increase is implemented.

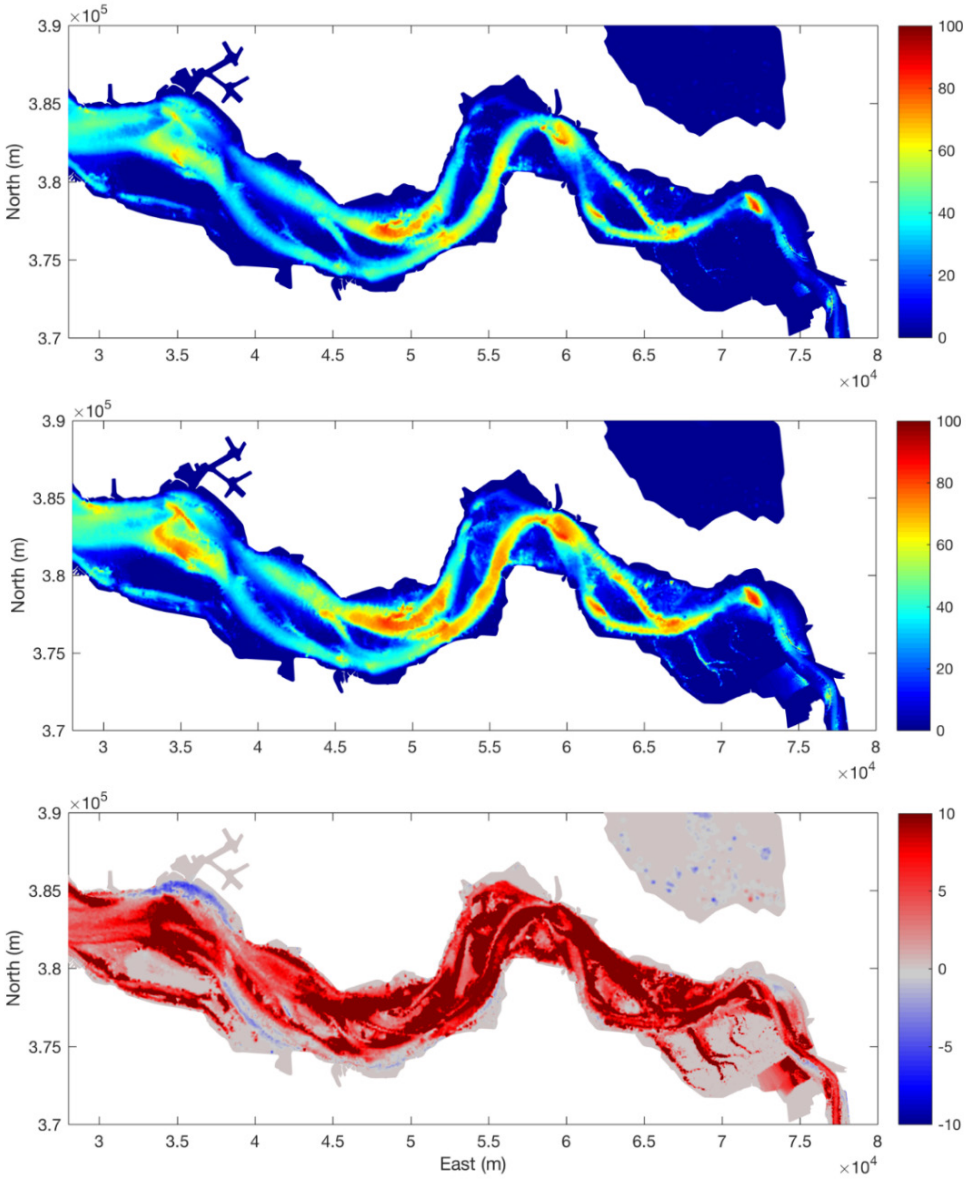

Figure 100 – Exceedance time of bed shear stress >1Pa (%) during a spring-neap cycle in Western Scheldt.
From top to bottom: the reference 2050_REF_A0CN; the scenario 2050_REF_AplusCH;
the difference 2050_REF_AplusCH - 2050_REF_A0CN.

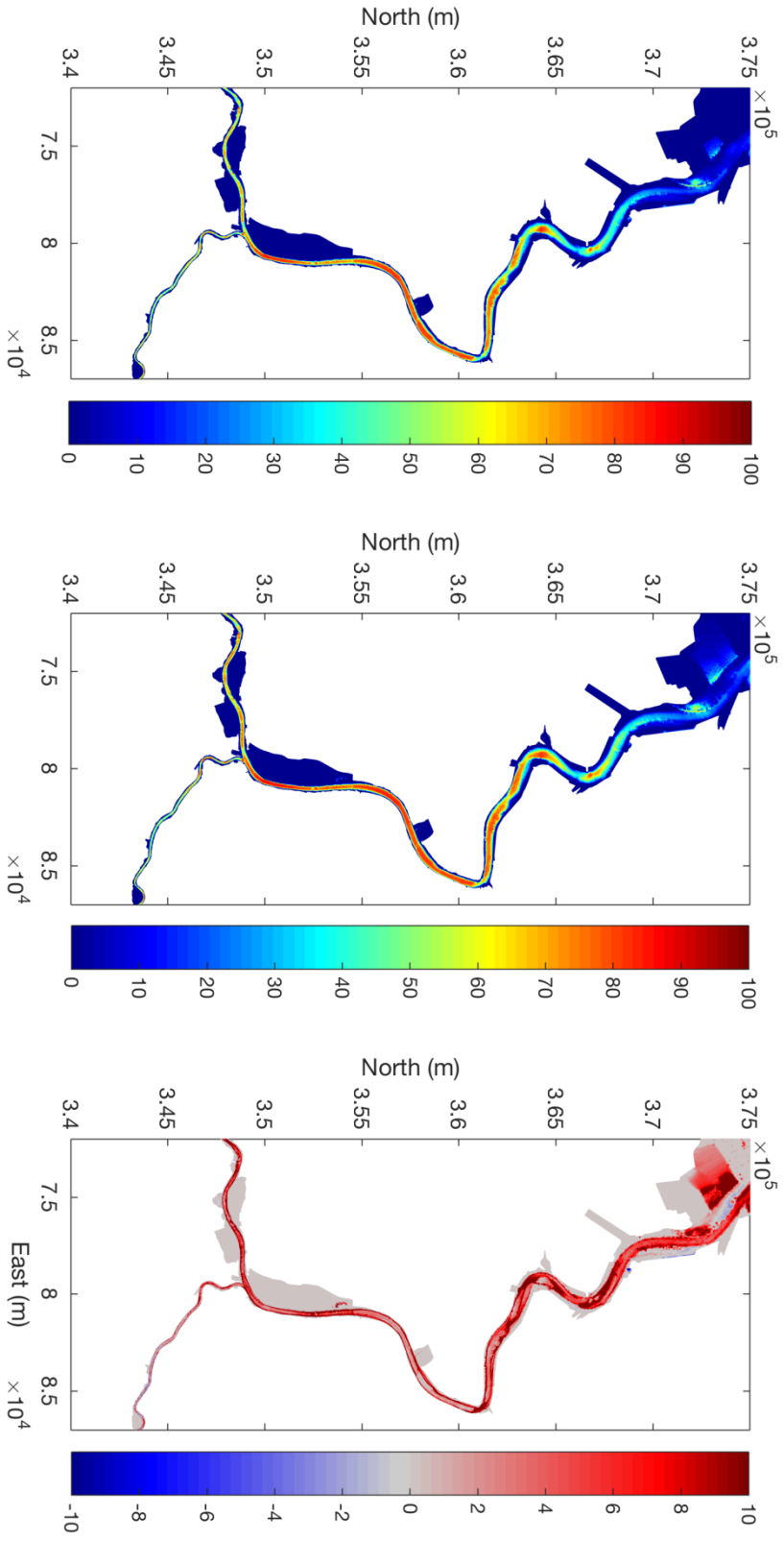

Figure 101 – Exceedance time of bed shear stress >1Pa (%) during a spring-neap cycle in Lower Sea Scheldt.
From top to bottom: the reference 2050_REF_A0CN; the scenario 2050_REF_AplusCH;
the difference 2050_REF_AplusCH - 2050_REF_A0CN.

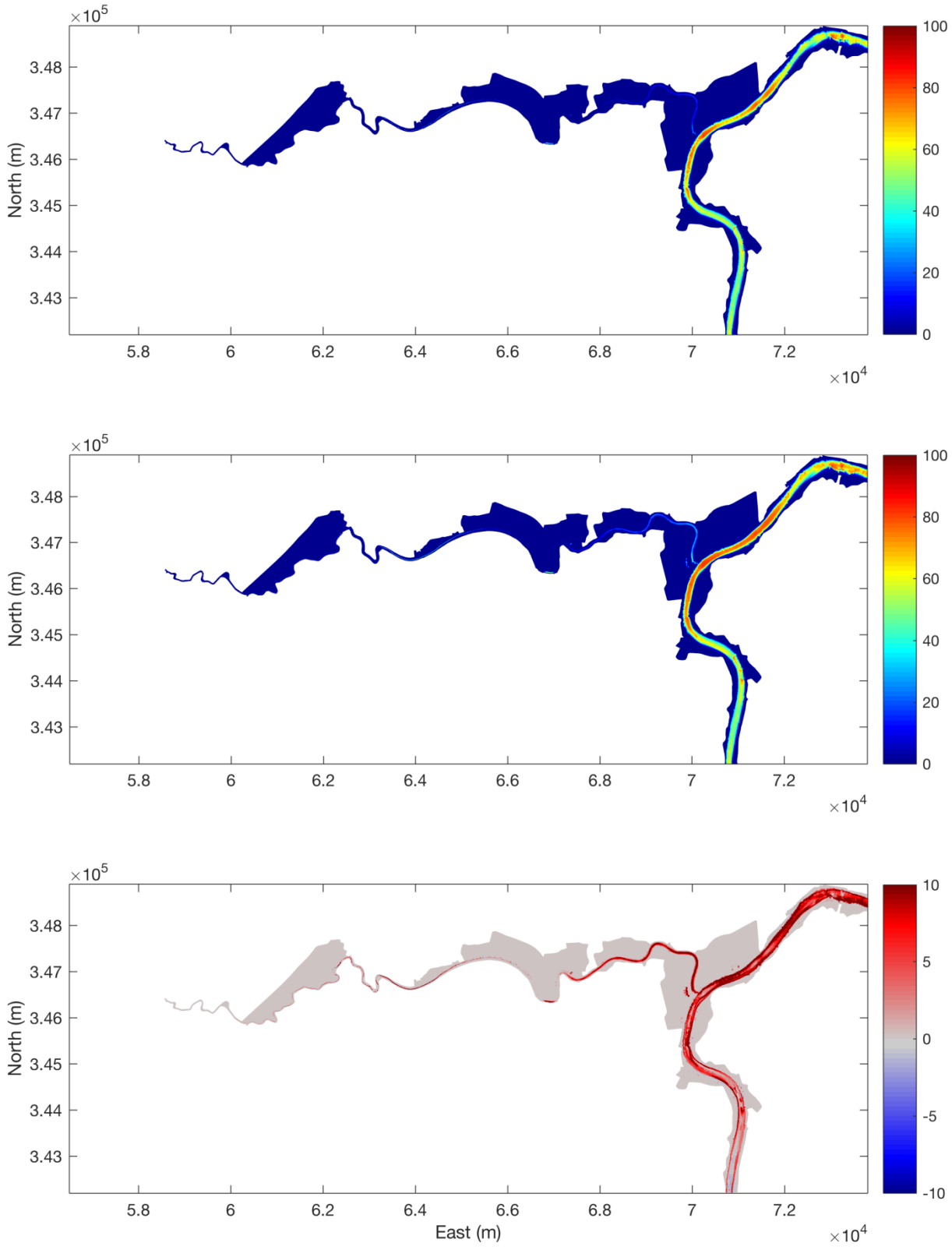

Figure 102 – Exceedance time of bed shear stress >1Pa (%) during a spring-neap cycle in Upper Sea Scheldt.
From top to bottom: the reference 2050_REF_A0CN; the scenario 2050_REF_AplusCH;
the difference 2050_REF_AplusCH - 2050_REF_A0CN.

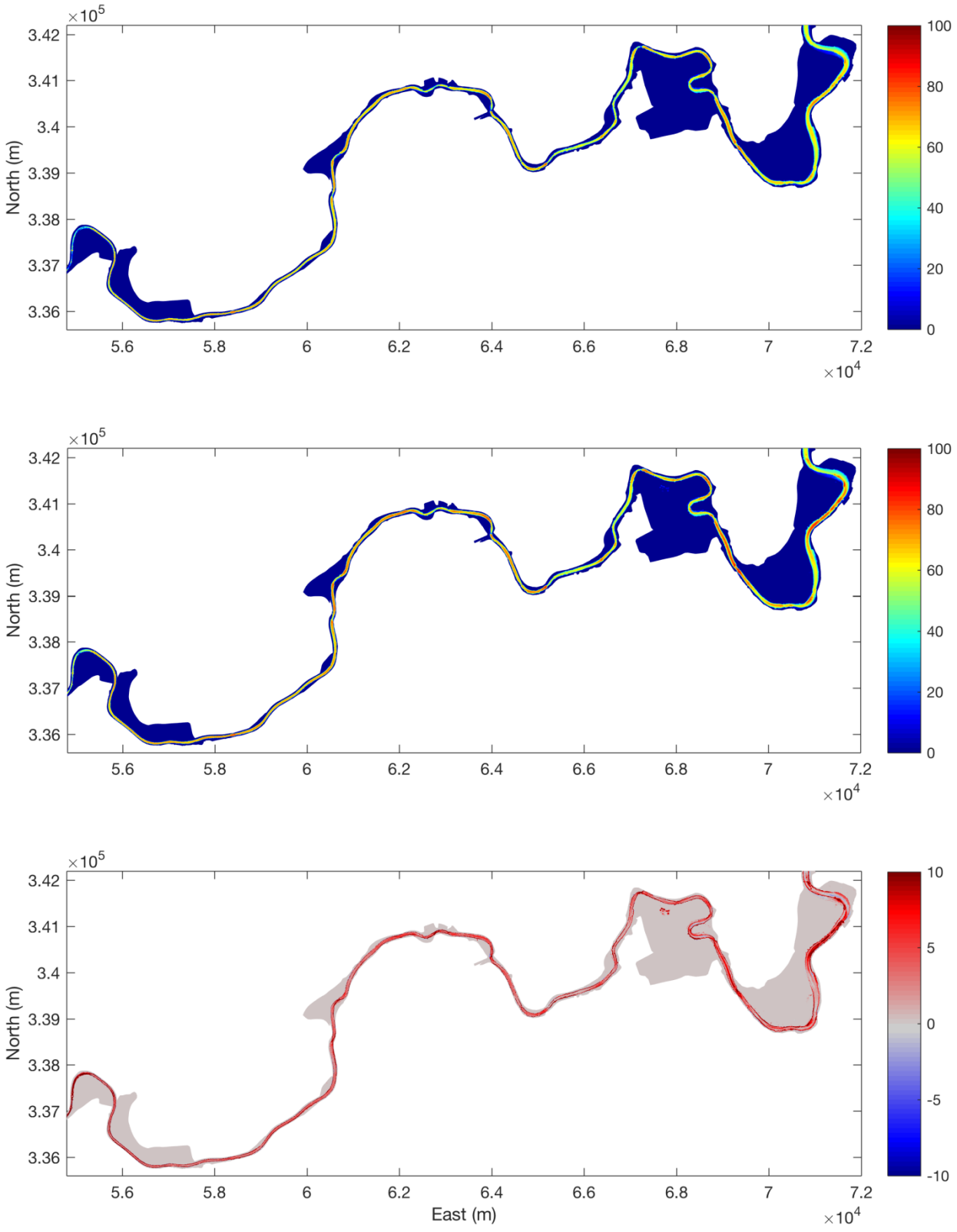

Figure 103 – Exceedance time of bed shear stress >1Pa (%) during a spring-neap cycle in Upper Sea Scheldt.
From top to bottom: the reference 2050_REF_A0CN; the scenario 2050_REF_AplusCH;
the difference 2050_REF_AplusCH - 2050_REF_A0CN.

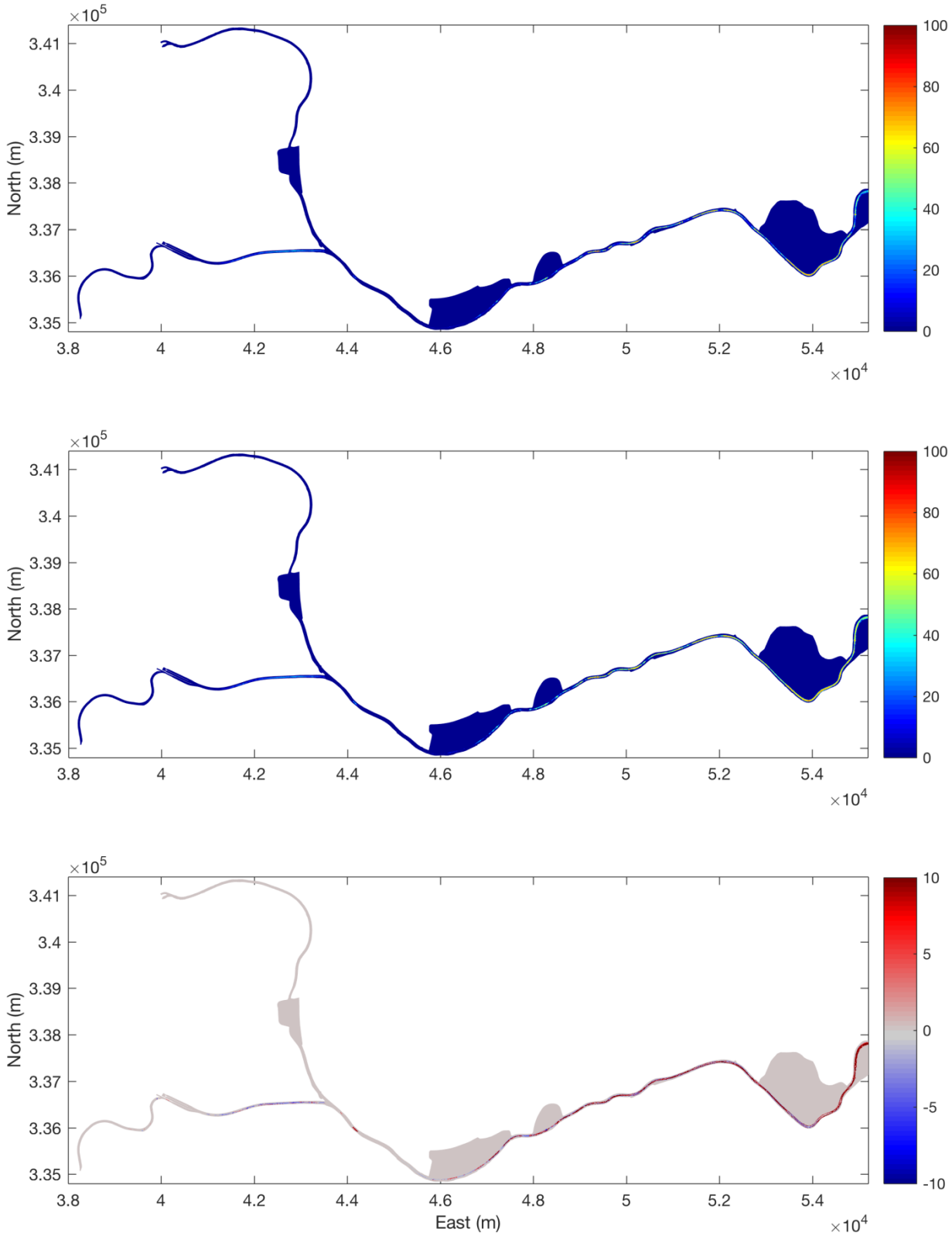

Figure 104 – Exceedance time of bed shear stress >1Pa (%) during a spring-neap cycle in Upper Sea Scheldt.
From top to bottom: the reference 2050_REF_A0CN; the scenario 2050_REF_AplusCH;
the difference 2050_REF_AplusCH - 2050_REF_A0CN.

(6). Delta SSC

The Delta SSC is calculated based on equation described in §5.1 and the time averaged Delta SSC is given for each box of the ecosystem model in Figure 105.

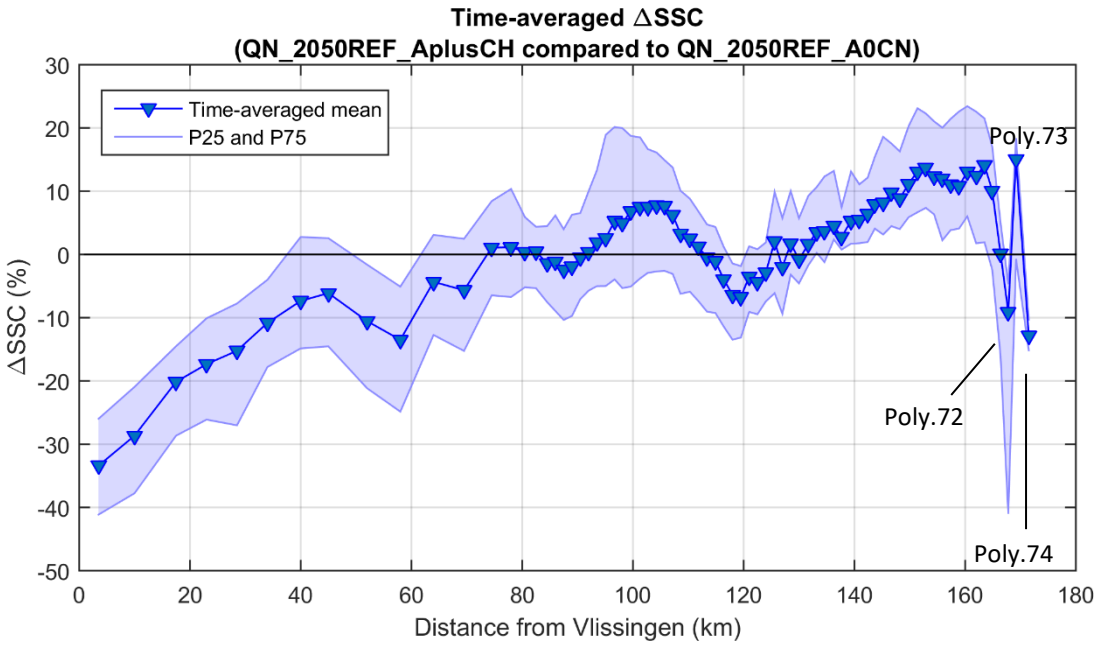

Figure 105 – 2050_REF_AplusCH compared to 2050_REF_A0CN

(7). Discussion

The influences of higher upstream discharge, increased tidal amplitude and sea level rise (+40cm) are combined in the scenario 2050_REF_AplusCH and affect hydrodynamics and sediment transport together in the model.

Starting from the most upstream points in the delta SSC figure (Figure 105), a similar pattern can be observed as in Figure 80, which is that the delta SSC is negative at 171.5 km in Polygon 74, then it increases sharply towards downstream, with a local peak found at 169.2 km in Pylogon 73, and then followed a sharp decrease further downstream at 167.8 km in polygon 72. The reader is referred to §5.1.2.6 for the discussion.

From 163.5 km to 133.2 km, the general trend for delta SSC is to be positive and decreasing, with minor fluctuations in between. The main reason for this decreasing trend is that, the influence of higher upstream discharge or larger sediment input decays towards downstream due to increasing cross sectional area. Some fluctuations are possibly due to the spatial change in the bed shear shtress as shown in Figure 103 and Figure 104. For instance, the maximum bed shear stress becomes larger from 158 km to 152 km, hence the delta SSC goes up as well. From 152 km to 143 km, bed shear stress becomes smaller again, in the same region delta SSC also decreases.

At the entrance of Durme (about 118 km), there is less sediment entering upstream of Durme in the scenario 205_REF_AplusCH comparing to the reference case. The result shows there is 890.53 KT/yr less sediment entering the Durme. Thus, more sediment remains in the main channel and supply the nearby area. Hence, delta SSC increases in the neibouring downstream areas.

There is a point souce placed at about 88 km, constantly releasing sediment into the channel at the same rate as in the reference. This dominates the solution, attracting Delta SSC to zero in this region.

The peak of delta SSC at about 103 km can also be explained from the difference of total sediment flux. Figure 106 shows that the difference of yearly sediment transport from both directions indeed converges at about 103 km.

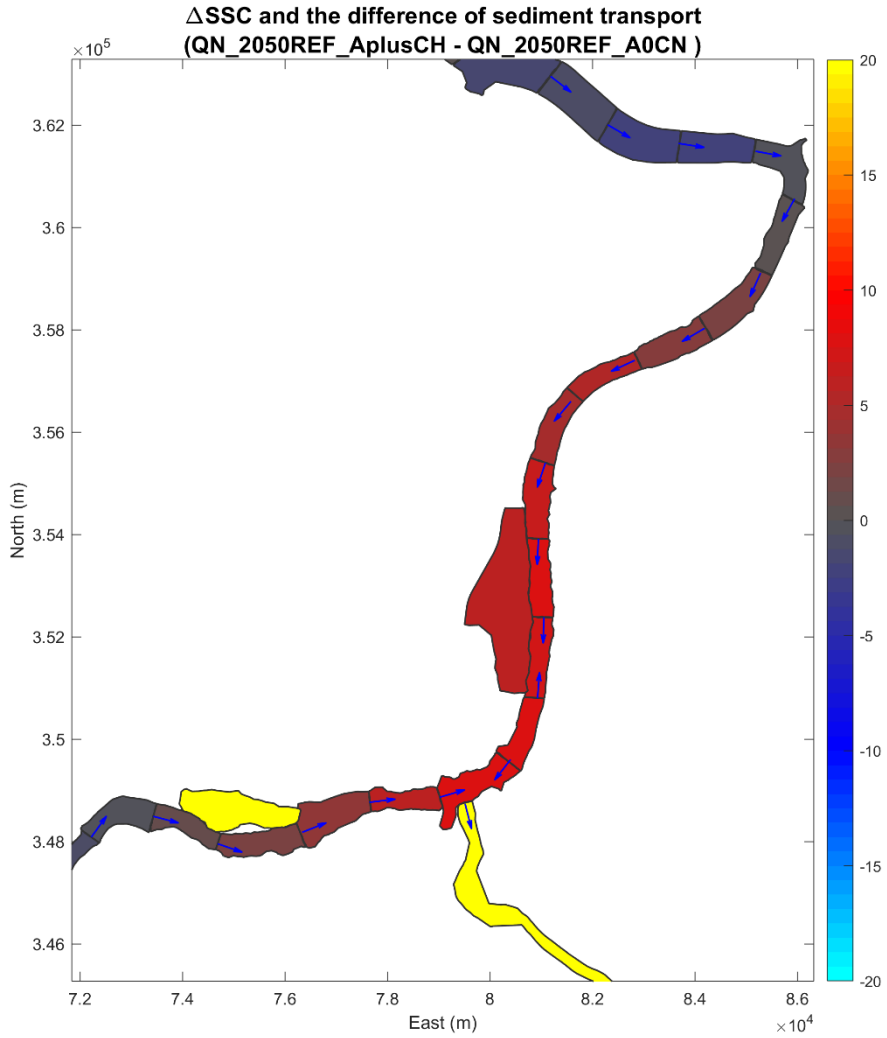

Figure 106 – Delta SSC and the difference of sediment transport. (Colour patch indicates delta SSC, arrow pointing upstream means the sediment transport is less towards downstream or more towards upstream)

5.1.4 Conclusion: from 2013 to 2050

The mud transport model used in the scenario analysis has several shortcomings, e.g. the sedimentation rate in shallow areas is not accurately represented, the SSC level is not well reproduced when comparing with measurements at Driegoten, and the model settings are not fine-tuned for the Western Scheldt and coastal area. However, it seems still capable to give reasonable system response against bathymetric changes, sea level rise, change of tidal range and increased upstream discharge.

(1). Influence on delta SSC

In the Western Scheldt from 0 km to about 70 km, the change of tidal range (implemented by changing the bottom roughness in the HD calculation) has the most significant influence.

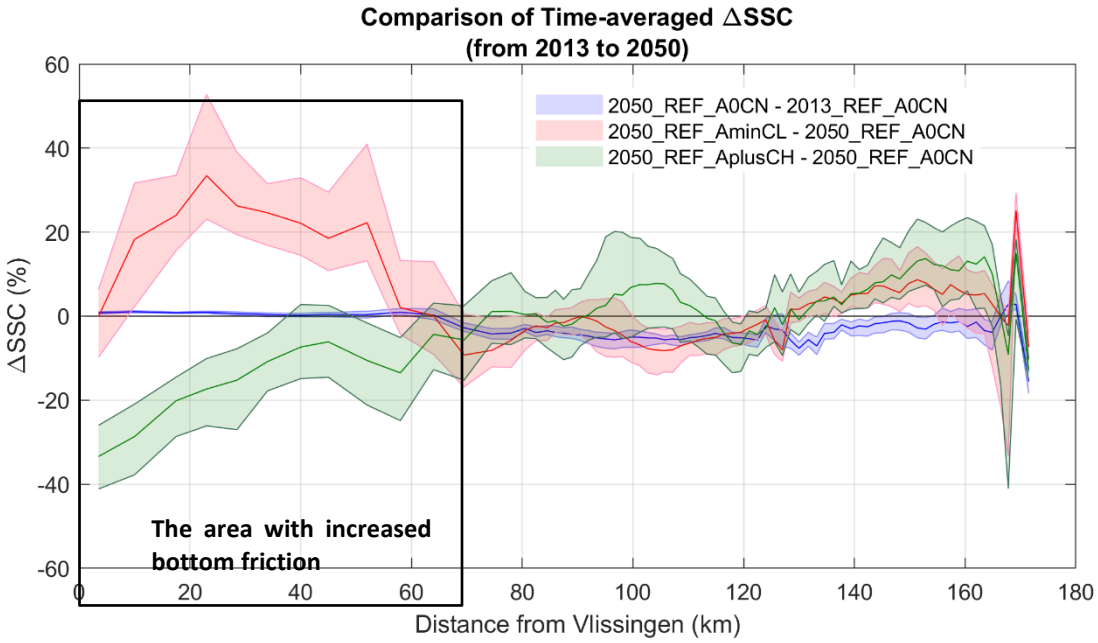

Figure 107 – Delta SSC in the three scenarios from 2013 to 2050

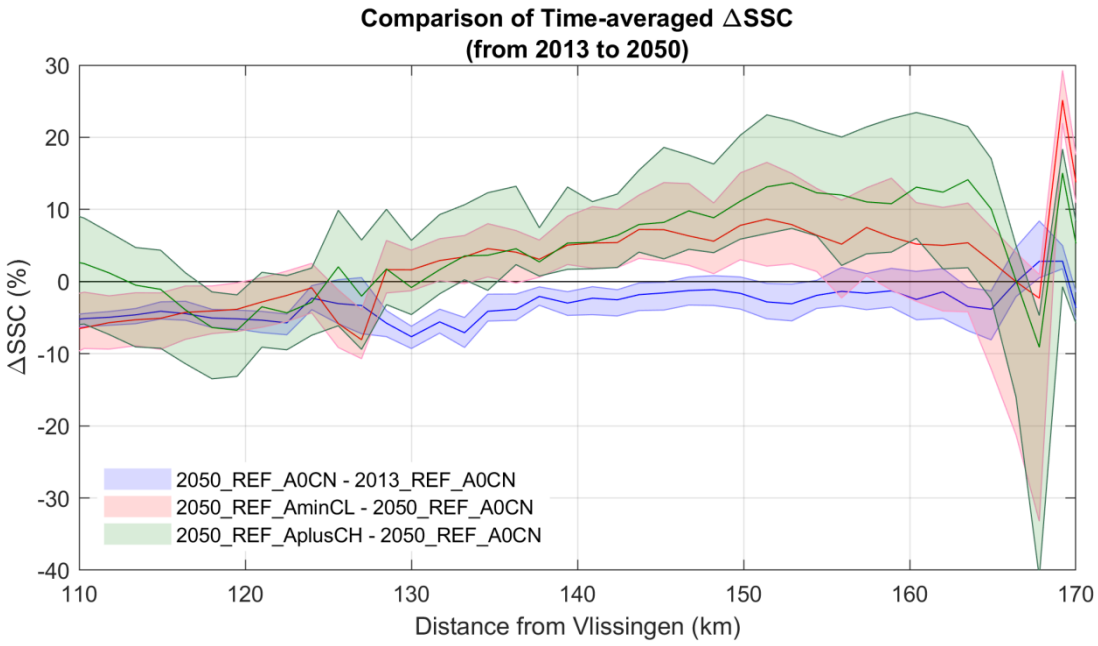

Figure 108 – Delta SSC in the three scenarios from 2013 to 2050 - Upper Sea Scheldt

The most important influential factors can be summarised as follows.

Sustainable bathymetry

Implementing the sustainable bathymetry gives a negative delta SSC in most area of the Upper Sea Scheldt. An influential factor on the general trend of delta SSC being negative between 110 km to 170 km is that the bed shear stress (from Figure 54 to Figure 56) is lower in this region due to the changes in hydrodynamics. The change of maximum bed shear stress is consistent with the difference of velocity M_2 amplitude.

Upstream discharge

One of the important effects on delta SSC is the higher upstream discharge in 2050 relative to 2013. It means higher downstream sediment transport in the Upper Sea Scheldt. Since constant SSC values are imposed at the upstream boundary, the sediment flux from the boundary is proportional to the discharge.

The change of upstream discharge will affect the amount of the sediment input of the system. This leads to a positive delta SSC. But the influence becomes weaker and weaker when it is further away from the upstream boundary, where discharge is not dominant anymore. This is also revealed by the decomposed sediment flux discussed before.

Note that the effect of discharge on ETM location is smaller than is observed in the measurements. This has also been observed in other, sediment transport models of the Scheldt estuary. One hypothesis is that the seasonality of settling velocities and erosion coefficients plays an important role in ETM location. the settling velocities and erosion coefficients are kept constant in the model though, so any biological feedback is not included.

(2). Sedimentation on tidal flats

Figure 109 shows the difference of mass deposited on tidal flats in the Upper Sea Scheldt from 2013 to 2050. As can be seen, the differences are noticeable at around 165km - 160 km, 144 km – 139 km, and become significant at 130 km - 100 km, where larger tidal flats can be found on the sides of the channel.

In general, the most influential factors on the sedimentation on tidal flats are the change of SSC and the change of flooded areas of tidal flats. If SSC decreases due to certain reasons, as seen from 2013_REF_A0CN to 2050_REF_A0CN from 100 km to 130 km, the amount of sedimentation on tidal flats also decreases. If larger area of tidal flats is flooded due to sea level rise, this means sediment deposits on larger areas, thus total amount of sedimentation on tidal flats increases. This is true in both 2050_REF_AminCL and 2050_REF_AplusCH.

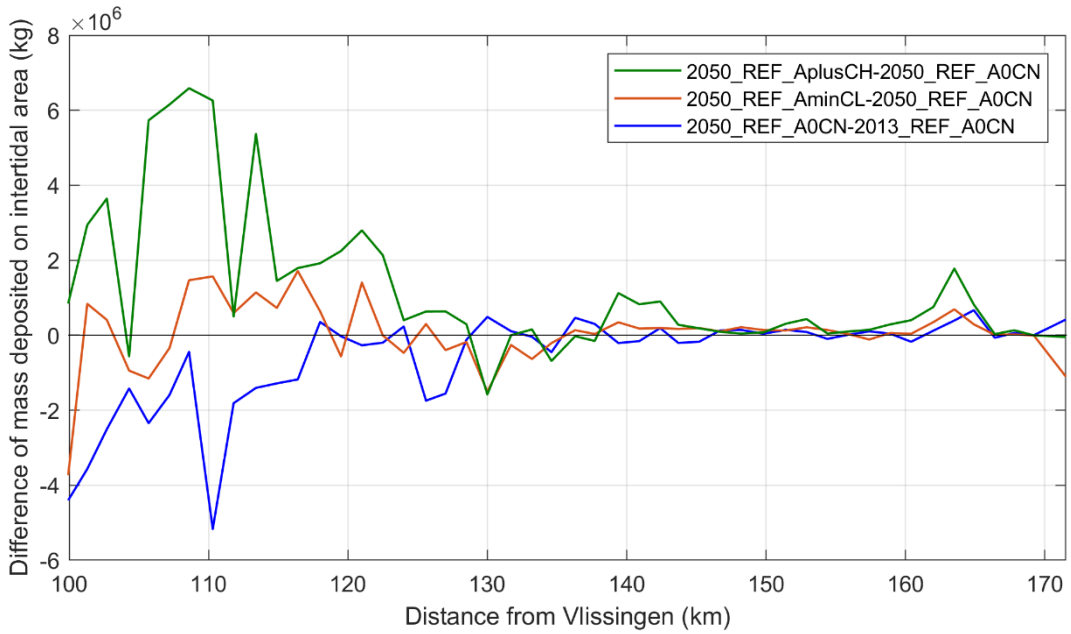

Figure 109 – Comparison of mass deposited on tidal flats (from 2013 to 2050)

(3). Influence on dredging

Lower Sea Scheldt

As shown in Table 6, shifting from 2013 bathymetry to 2050 sustainable bathymetry in the mud model causes the sedimentation rate to decrease by 2.36%. This is consistent with the negative trend in delta SSC. To be more specifically, the decrease trend can be observed at Deurganckdock, Entrance Zandvliet and Entrance Kallo lock.

The influence of sea level rise on the dredging can only be deduced indirectly from the model results (Figure 110). Based on the difference of sedimentation in 2050_REF_AminCL and 2050_REF_AplusCH, it seems that sea level rise tends to counteract the effect of decreasing the bottom friction in 2050_REF_AplusCH, which means sea level rise maybe could result in less sedimentation in the access channels and DGD. The explanation could be the bottom friction becoming smaller due to larger water depth, hence smaller bed shear stress, lower SSC and less sedimentation.

Table 6 – Sedimentation rate and the comparison between the scenarios in Lower Sea Scheldt (from 2013 to 2050)

Runs	Sedimentation (MT/yr)	Difference compared to 2013_REF_A0CN	Difference compared to 2050_REF_A0CN
2013_REF_A0CN	3.2143	/	/
2050_REF_A0CN	3.1385	-2.36%	/
2050_REF_AminCL	3.0129	/	-4.00%
2050_REF_AplusCH	3.1257	/	-0.41%

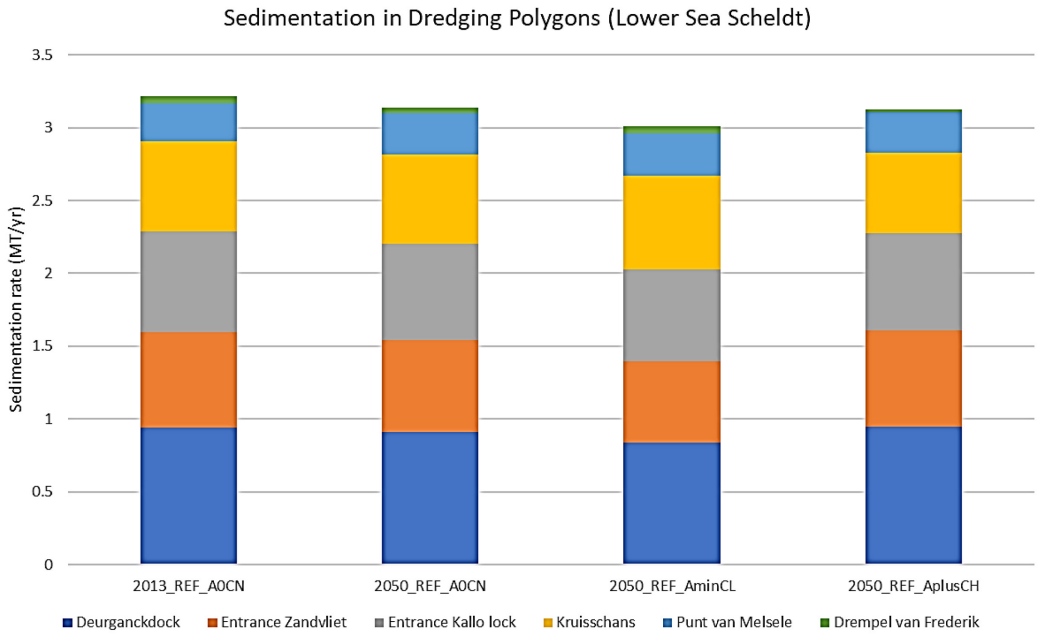

Figure 110 – Comparison of sedimentation rate in the Lower Sea Scheldt (from 2013 to 2050)

Upper Sea Scheldt

It can be seen in Table 7 that the influence of scenarios on sedimentation in the Upper Sea Scheldt is similar as in the Lower Sea Scheldt, although the absolute differences are not the same. Figure 111 shows the sedimentation rate in each dredging polygon in the Upper Sea Scheldt.

Shifting from 2013 bathymetry to 2050 sustainable bathymetry in the mud model gives lower sedimentation. As shown in the sedimentation-erosion map (Figure 49), the differences can found downstream the sluice at Heusden, and a spatial shift in sedimentation rates near Baasrode. It can also be seen in Figure 111 that smaller sedimentation rate is found in Durme, and slightly higher in Ringvaart.

Comparisons between three "2050_REF" runs reveal the influence of different climate scenarios plus sea level rise on the sedimentation in the Upper Sea Scheldt. Similarly as in the Lower Sea Scheldt, 2050_REF_AminCL tends to give lower sedimentation rate whereas 2050_REF_AplusCH tends to have higher sedimentation rate. Because these areas are far away from Western Scheldt, the influence of changing bottom friction (seen as an artefact) becomes less. In both comparisons, the differences are mainly observed in the channel sections near Baasrode and in the tidal arm near Zwijnaarde.

Table 7 – Sedimentation rate and the comparison between the scenarios in Upper Sea Scheldt (from 2013 to 2050)

Runs	Sedimentation (MT/yr)	Difference compared to 2013_REF_A0CN	Difference compared to 2050_REF_A0CN
2013_REF_A0CN	0.0281	/	/
2050_REF_A0CN	0.0276	-1.78%	/
2050_REF_AminCL	0.0271	/	-1.81%
2050_REF_AplusCH	0.0289	/	+4.71%

Moreover, Figure 112 reveals in detail the changes of sedimentation rate between 2050_REF_AminCL and 2050_REF_AplusCH, comparing to the reference 2050_REF_A0CN. It can be found that climate scenario AminCL tends to reduce sedimentation rate in Wintam, Gentbrugge, Ringvaart and Tijarm Zwijnaarde except in Durme, whereas increase it in Durme; AplusCH tends to do the opposite, increasing sedimentation rate in all the other locations while decreasing it in Durme.

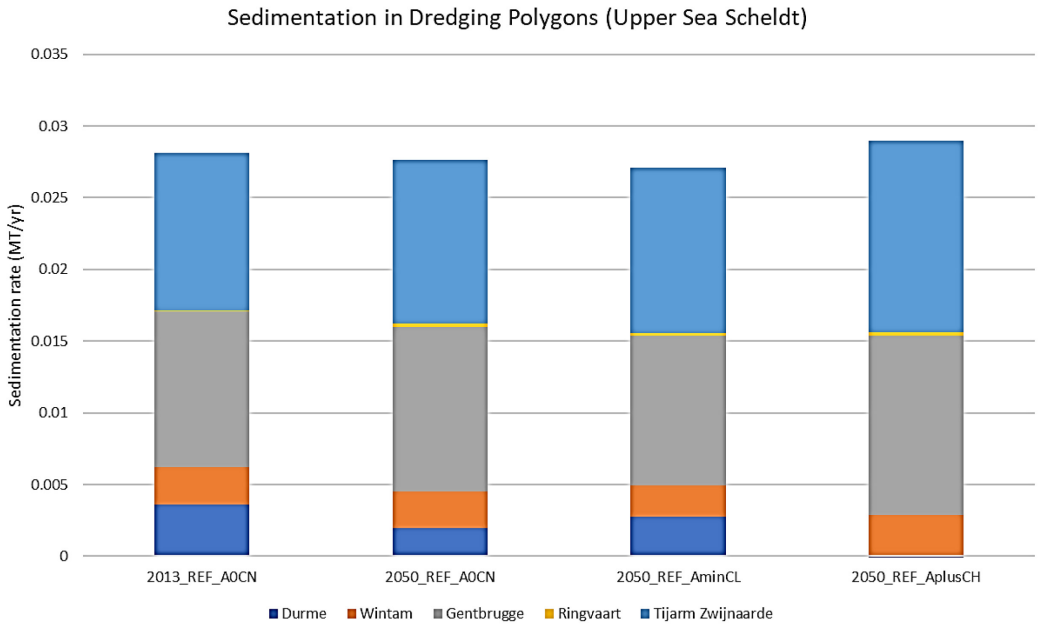

Figure 111 – Comparison of sedimentation rate in the Upper Sea Scheldt (from 2013 to 2050)

5.2 Effect of VaG

The VaG scenario has the most dramatic bathymetry change among the three B-alternatives (VaG, VaH and Chafing). It consists of deepening and/or widening channels and straightening bends in the Upper Sea Scheldt. The change in bathymetry is detailed in §3.5.4.

5.2.1 The effect of VaG in AminCL boundary conditions

(1). The difference in hydrodynamics

The change of bathymetry begins at about 118 km away from Vlissingen, and continues up until about 170 km. Thus, it is expected to have minor influence in the region from 0 km to 118 km, especially in the Western Scheldt.

As seen in Figure 112, water level M2 amplitude decreases slightly in the area from 70 km to 130 km. However, the larger difference is found in the Upper Sea Scheldt, from 130 km to 170 km. Water level M2 amplitude becomes larger compared to the reference case. Due to the bathymetric changes in the VaG scenario, the tidal wave can penetrate deeper in the estuary. A secondary effect is a higher M4 amplitude in the Upper Sea Scheldt (Figure 113).

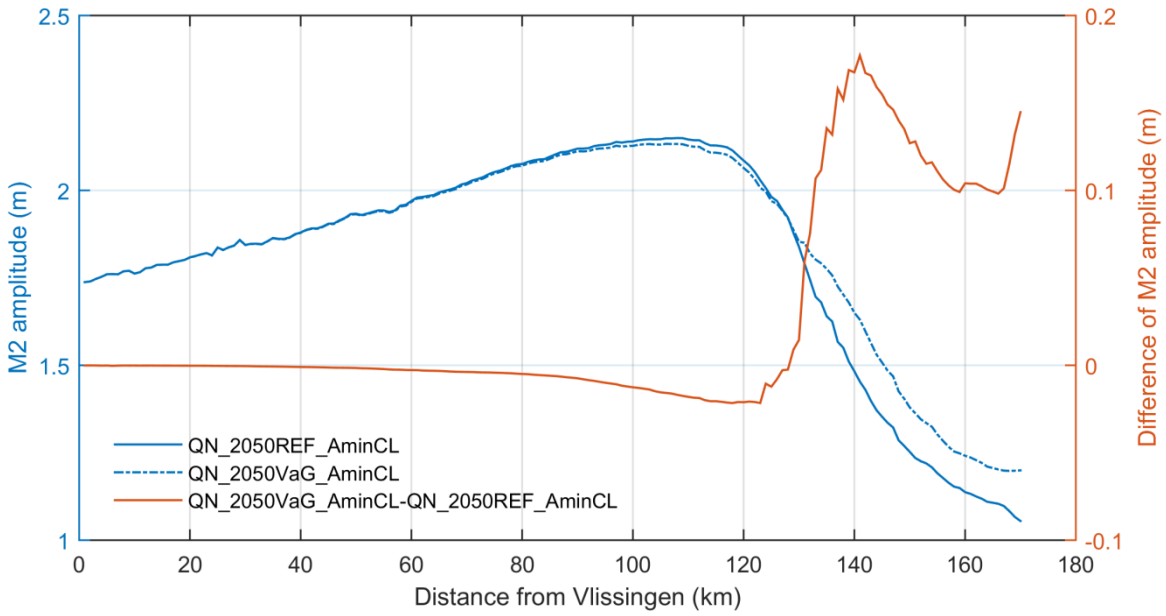

Figure 112 – Comparison of M2 amplitude between 2050_REF_AminCL and 2050_VaG_AminCL

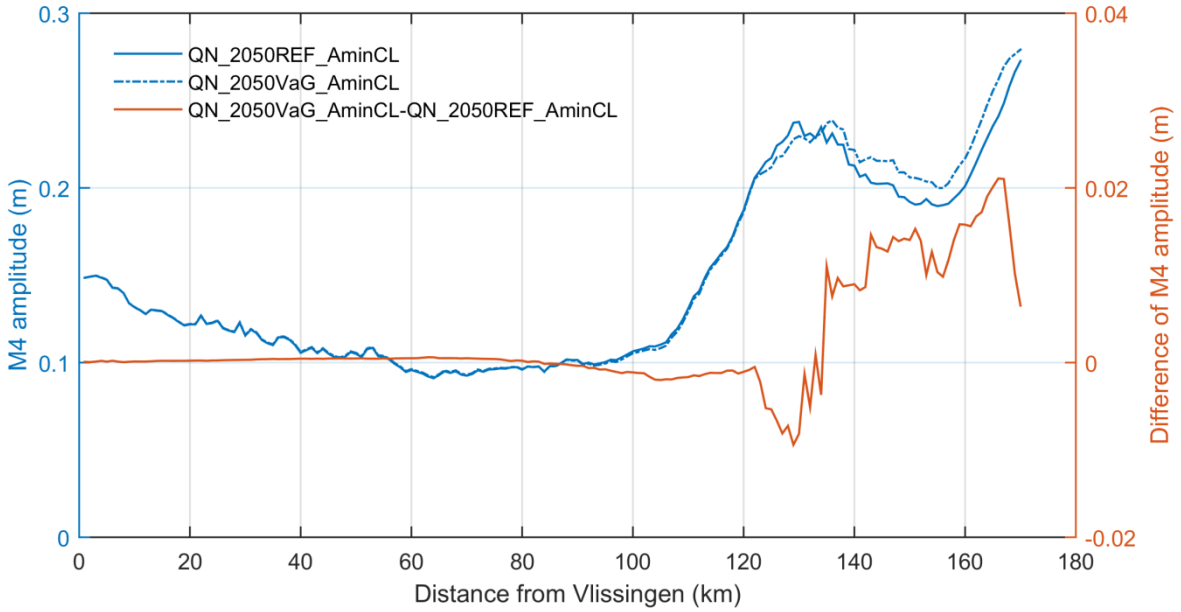

Figure 113 – Comparison of M4 amplitude between 2050_REF_AminCL and 2050_VaG_AminCL

In terms of cross-sectionally averaged velocity amplitude, the changes are mostly due to local bathymetric changes. This has influence to sediment transport and will be discussed in the following sections.

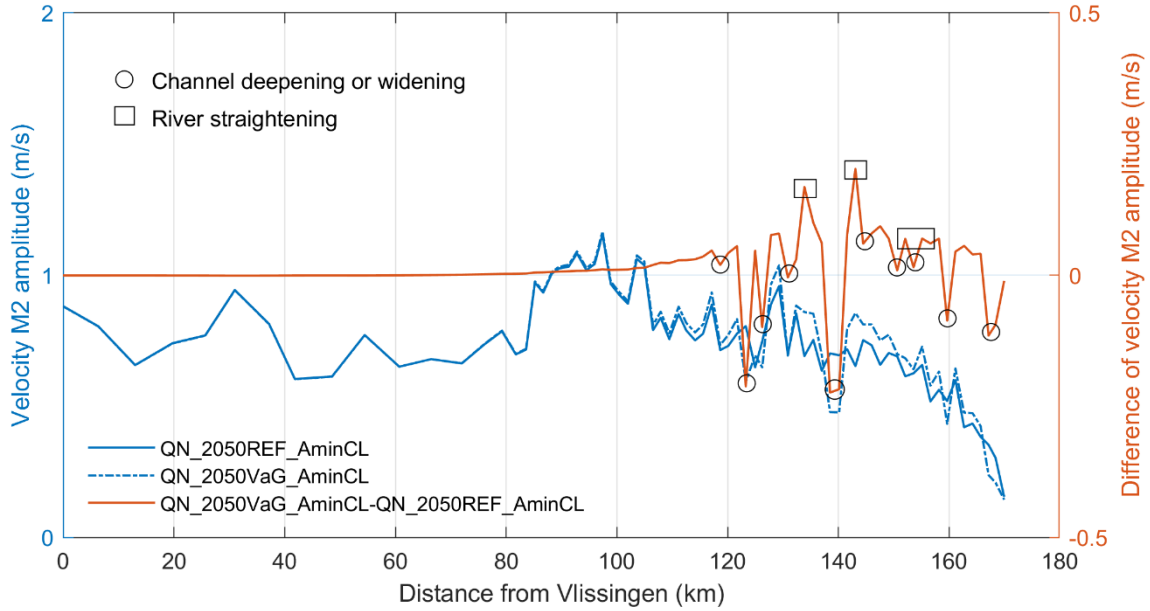

Figure 114 – Comparison of velocity M2 amplitude of cross-sectionally averaged velocity between 2050_REF_AminCL and 2050_VaG_AminCL

(2). The change of tidal asymmetry

All the tidal asymmetry indicators as mentioned in §4.8, are calculated in this section. These indicators, 8 in total, are organized in 3 groups, based on time duration, velocity magnitude and skewness, respectively.

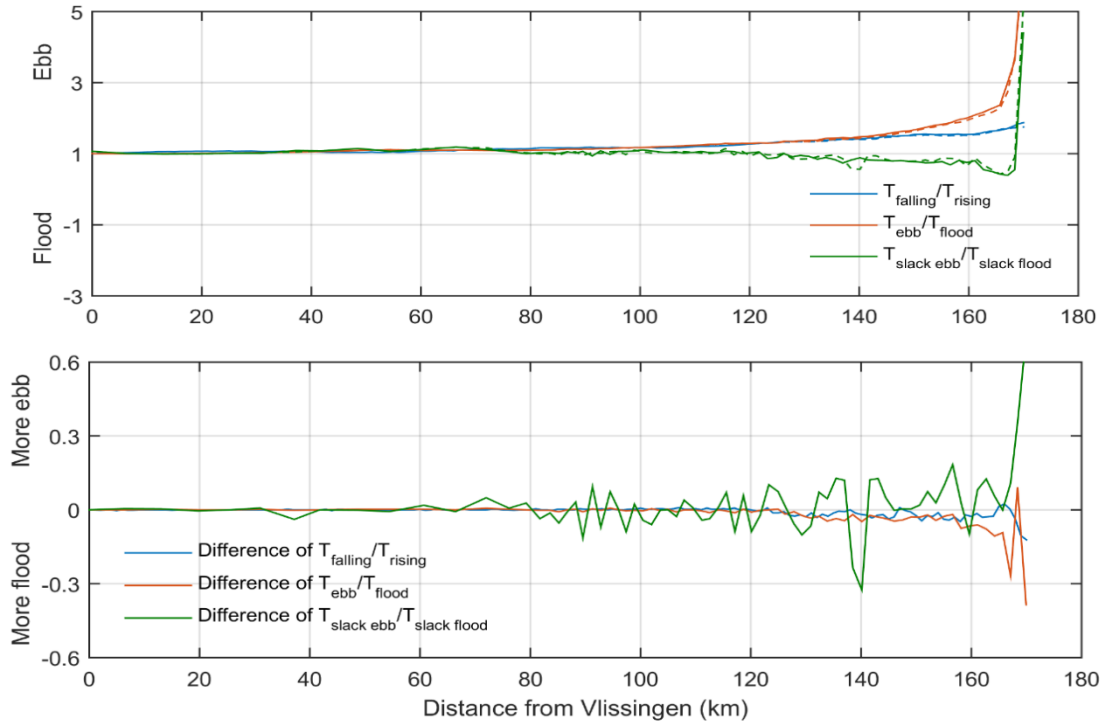

Figure 115 – Indicators of tidal asymmetry (durations). Solid lines represent the reference 2050_REF_AminCL, dashed lines represent the scenario 2050_VaG_AminCL.

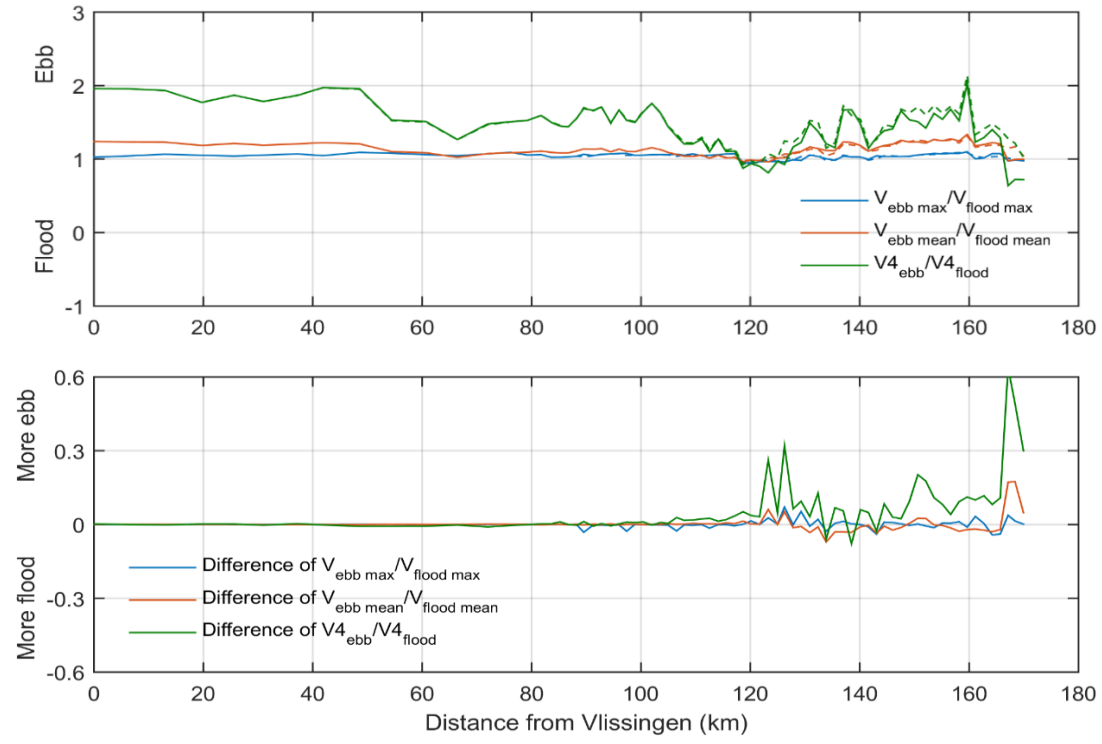

Figure 116 – Indicators of tidal asymmetry (velocities). Solid lines represent the reference 2050_REF_AminCL, dashed lines represent the scenario 2050_VaG_AminCL.

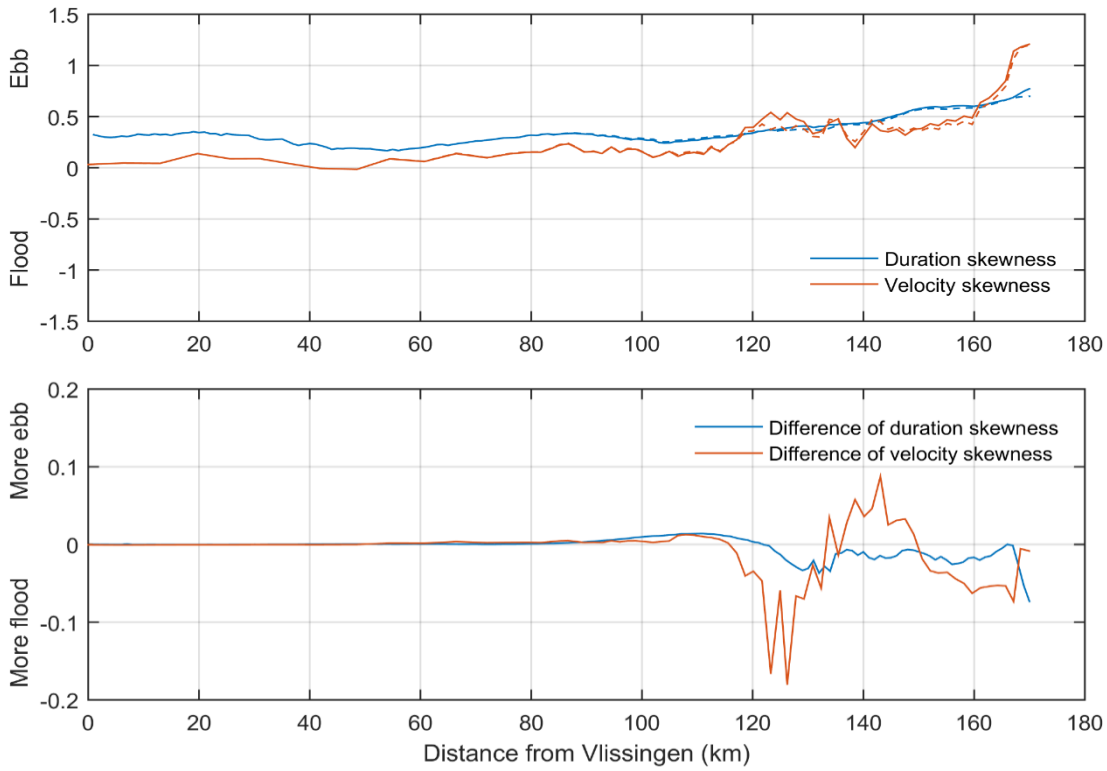

Figure 117 – Indicators of tidal asymmetry (skewness). Solid lines represent the reference 2050_REF_AminCL, dashed lines represent the scenario 2050_VaG_AminCL.

(3). Sediment Transport Decomposition

Figure 118 shows the sediment transport decomposed according to §4.7

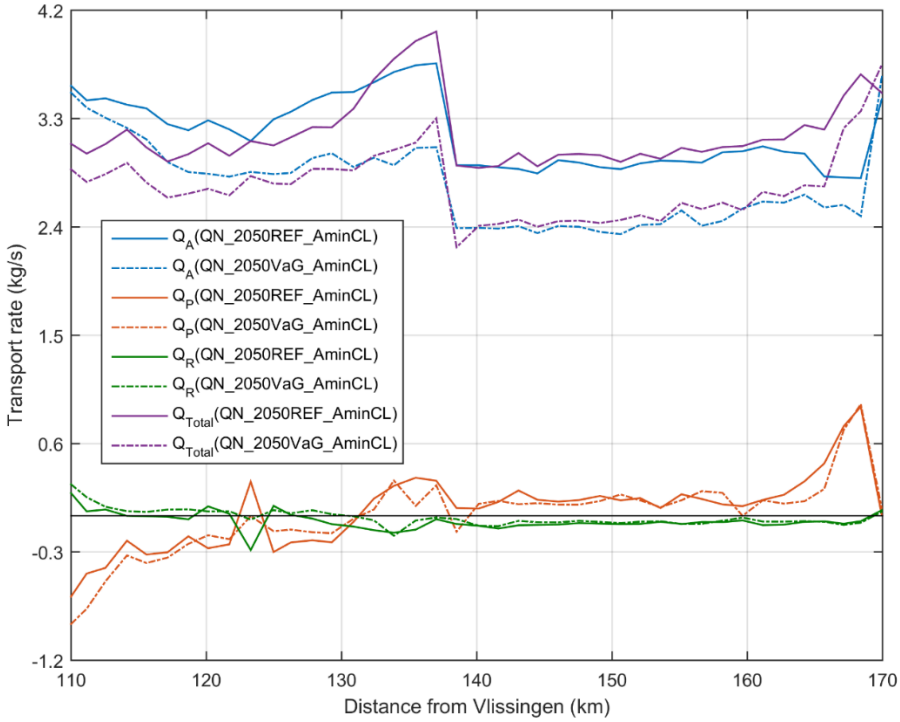

Figure 118 – Time-averaged decomposed sediment transport rate QA, QP and QR in the Upper Sea Scheldt. Positive sign means downstream direction and negative means upstream direction

Note the decrease in downstream sediment transport. This is due to the influence of the bathymetric changes near the upstream boundary in VaG. The consequences in general are a less ebb dominant system in this region compared to the reference case.

(4). Erosion-deposition map

The difference of sedimentation rate is calculated between the run 2050_VaG_AminCL and 2050_REF_AminCL using the bed layer thickness given in the result files. The sedimentation rate is based on the production period of the last 20 days and it is converted to cm/yr.

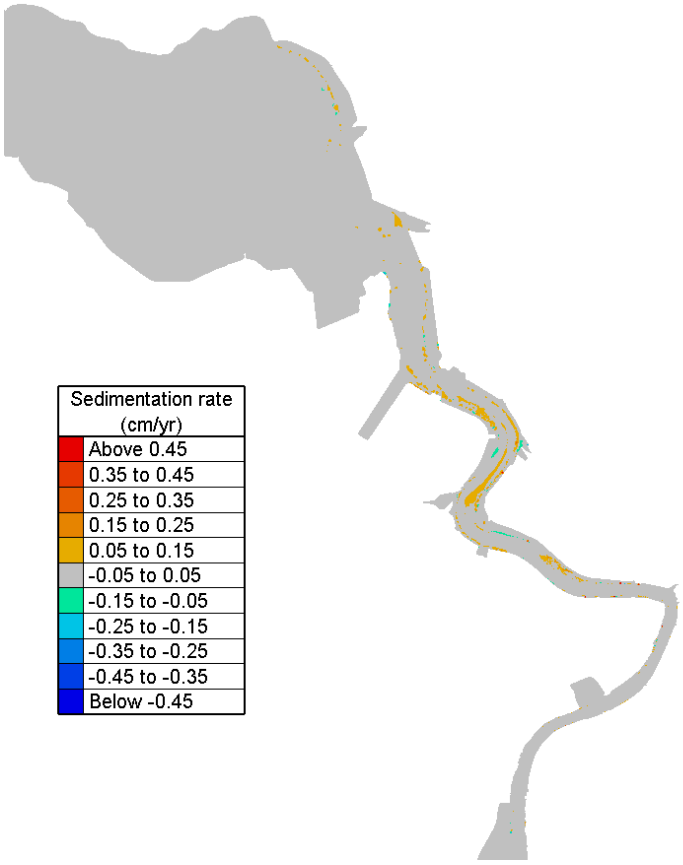

Figure 119 – Difference of sedimentation rate (2050_VaG_AminCL-2050_REF_AminCL) – part 1

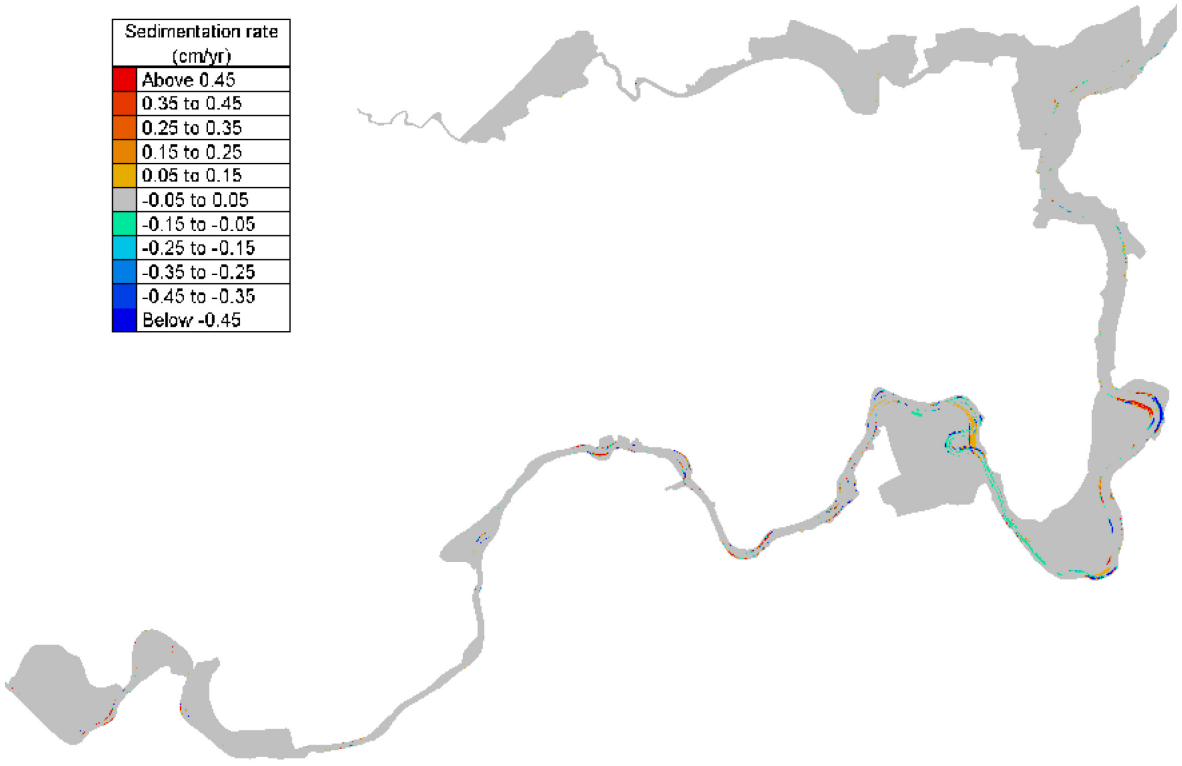

Figure 120 – Difference of sedimentation rate (2050_VaG_AminCL-2050_REF_AminCL) – part 2

Figure 121 – Difference of sedimentation rate (2050_VaG_AminCL-2050_REF_AminCL) – part 3

Compared to the reference case, the differences in the Upper Sea Scheldt are found where bathymetric changes are intensive. In the Lower Sea Scheldt, downstream of Antwerp, there are also slight differences in the sedimentation rate, possibly due to the impact on tidal amplitude.

(5). Bed shear stress

Changes in bottom shear stress lead to changes in sedimentation/erosion patterns and habitat suitability. Therefore maps are made in the study area of exceedance time (%) of a threshold value of 1 Pa during a spring-neap cycle. A difference map (in %-points) shows the spatial changes.

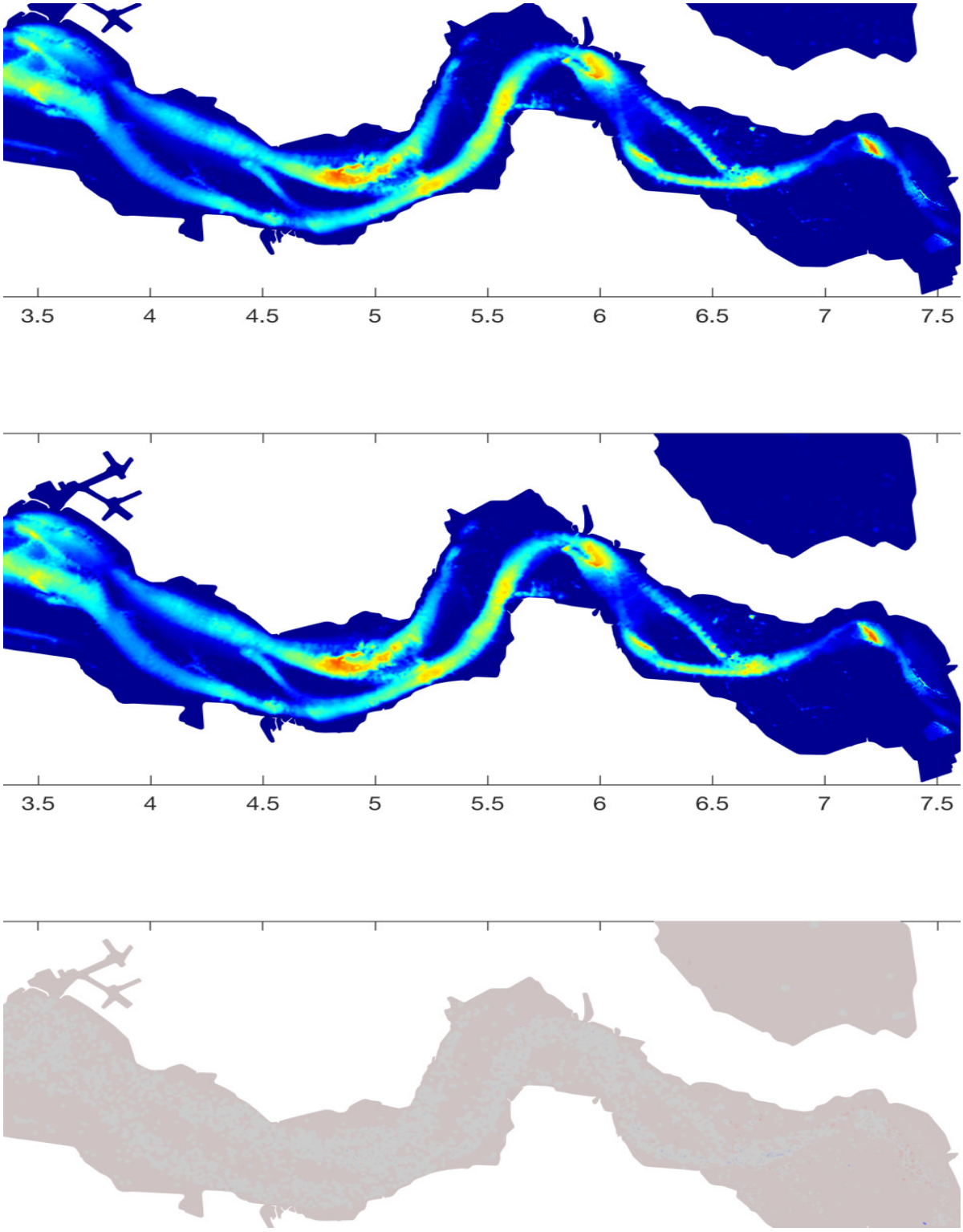

Figure 122 – Exceedance time of bed shear stress >1Pa (%) during a spring-neap cycle in Western Scheldt.
From top to bottom: the reference 2050_REF_AminCL; the scenario 2050_VaG_AminCL;
the difference 2050_VaG_AminCL - 2050_REF_AminCL.

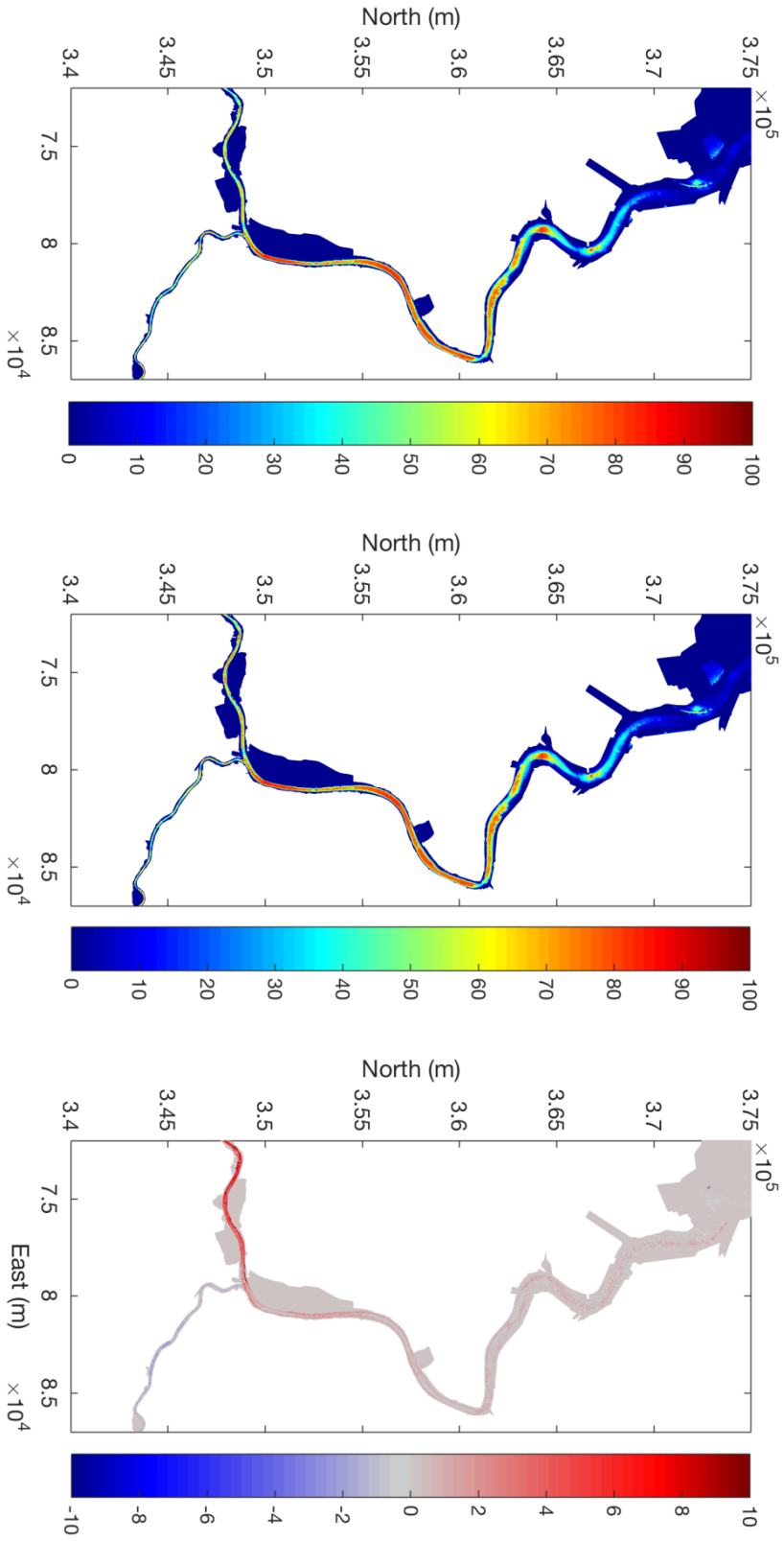

Figure 123 – Exceedance time of bed shear stress >1Pa (%) during a spring-neap cycle in Lower Sea Scheldt.
From top to bottom: the reference 2050_REF_AminCL; the scenario 2050_VaG_AminCL;
the difference 2050_VaG_AminCL - 2050_REF_AminCL.

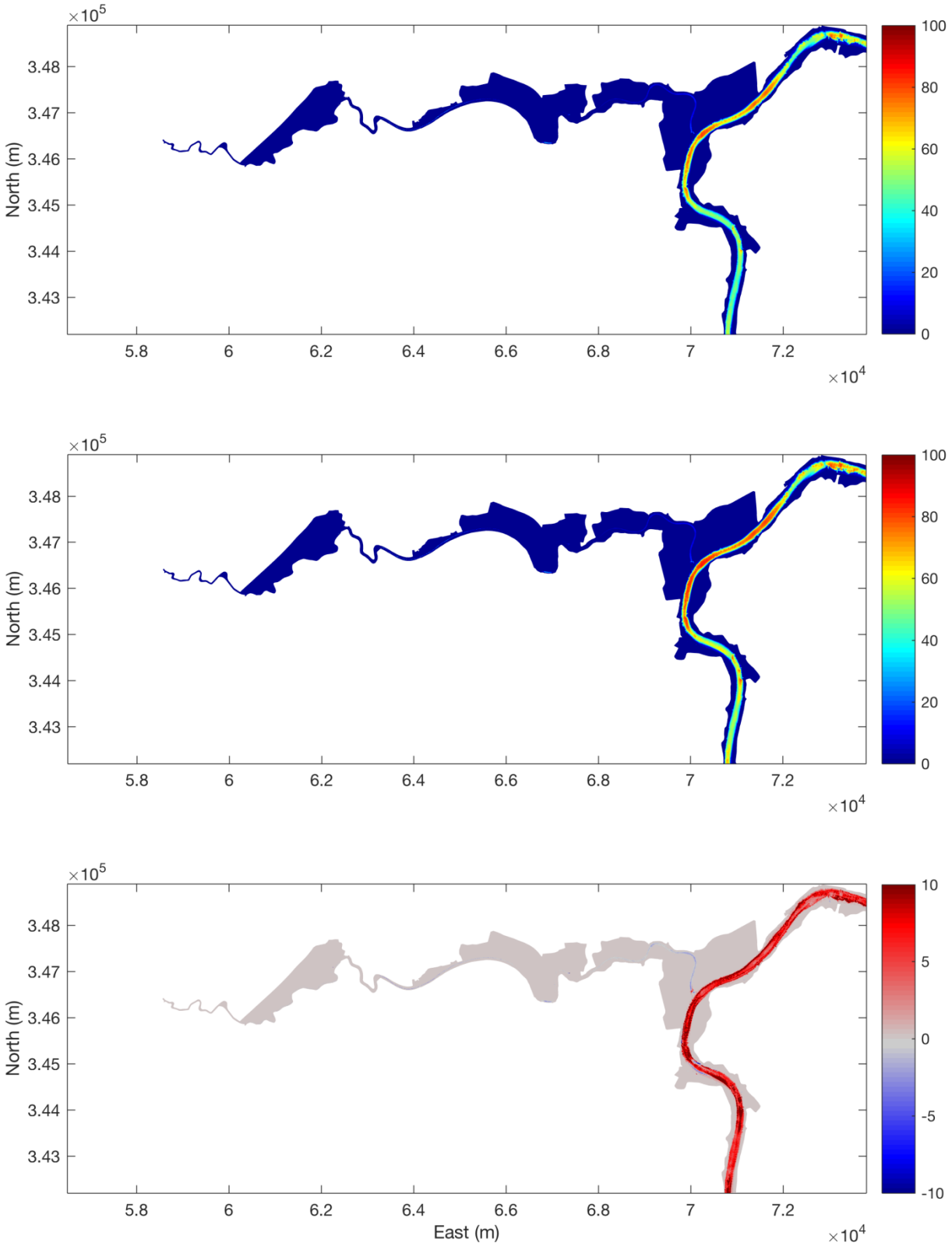

Figure 124 – Exceedance time of bed shear stress >1Pa (%) during a spring-neap cycle in Upper Sea Scheldt.
From top to bottom: the reference 2050_REF_AminCL; the scenario 2050_VaG_AminCL;
the difference 2050_VaG_AminCL - 2050_REF_AminCL.

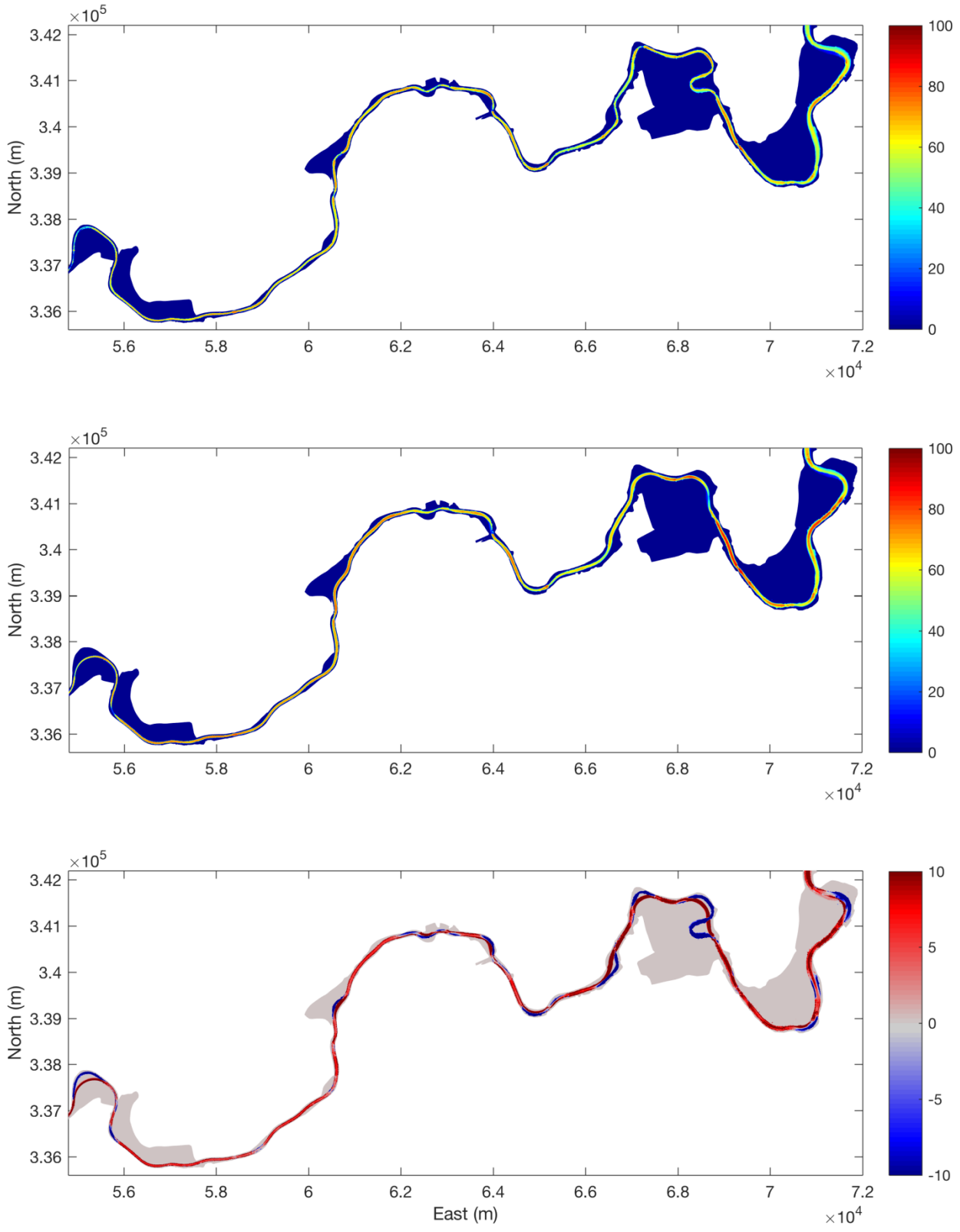

Figure 125 – Exceedance time of bed shear stress >1Pa (%) during a spring-neap cycle in Upper Sea Scheldt.
From top to bottom: the reference 2050_REF_AminCL; the scenario 2050_VaG_AminCL;
the difference 2050_VaG_AminCL - 2050_REF_AminCL.

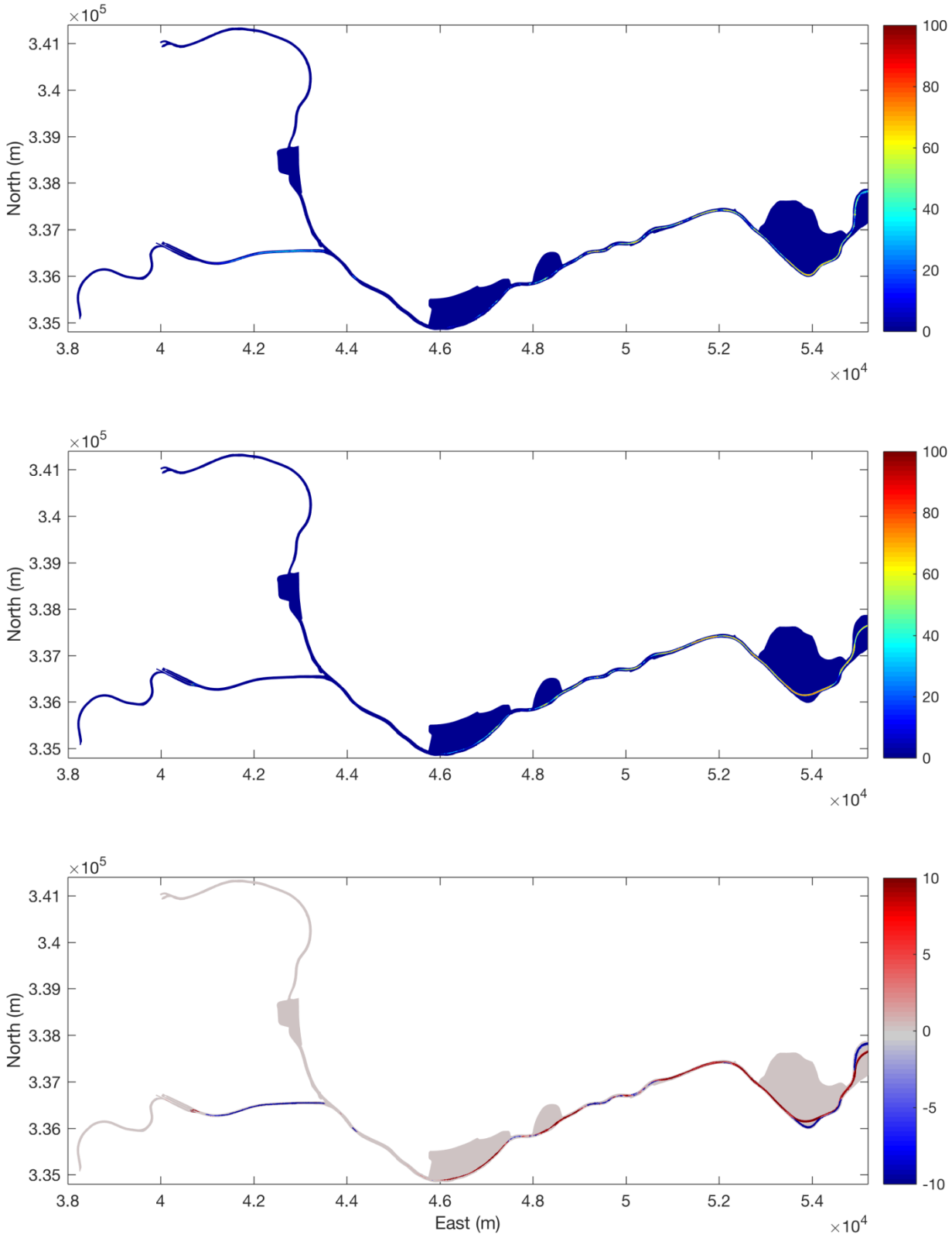

Figure 126 – Exceedance time of bed shear stress >1Pa (%) during a spring-neap cycle in Upper Sea Scheldt.
From top to bottom: the reference 2050_REF_AminCL; the scenario 2050_VaG_AminCL;
the difference 2050_VaG_AminCL - 2050_REF_AminCL.

(6). Delta SSC

The Delta SSC is calculated based on equation described in §5.1 and the time averaged Delta SSC is given for each box of the ecosystem model in Figure 127.

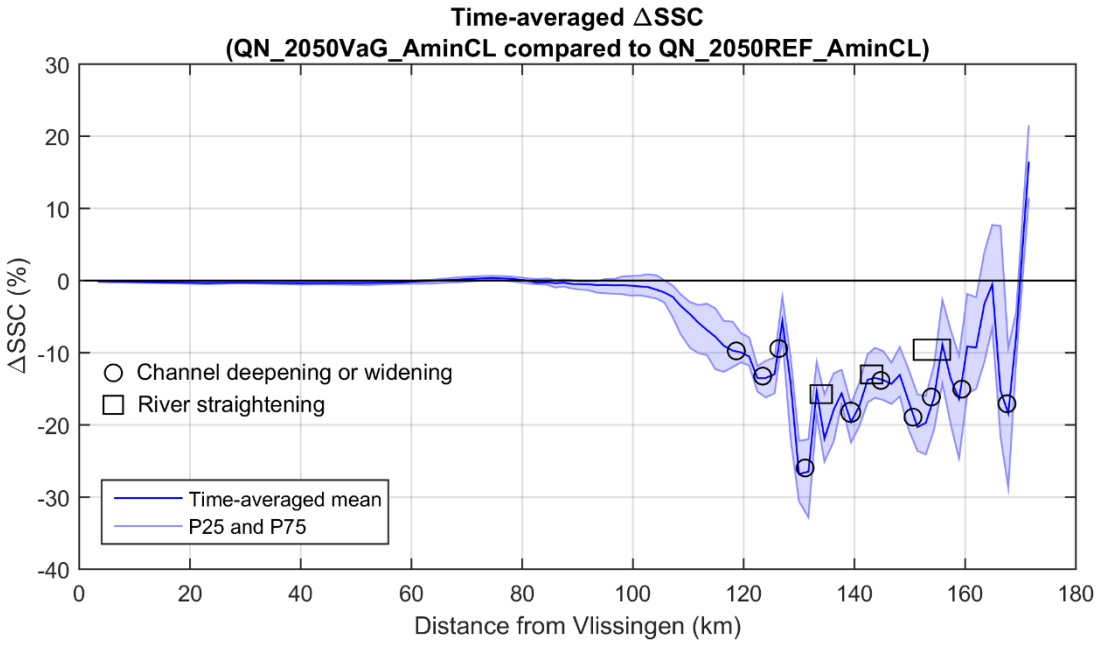

Figure 127 – Time-averaged delta SSC (2050_VaG_AminCL compared to 2050_REF_AminCL)

It can be seen from above figure that delta SSC is almost zero in the Western Scheldt (from 0 km to 70 km). It starts to deviate from zero at about 80 km, and further upstream the delta SSC is negative in most of the area. The trend changes again at locations from about 167 km to 170 km, with delta SSC increasing and being positive near the upstream boundary. The locations with intensive bathymetric changes are also plotted in the above figure. In general, channel deepening leads to lower SSC and the cutting of a river bend tends to increase SSC. This is discussed in detail in following section.

5.2.2 The effect of VaG in AplusCH boundary conditions

The scenario 2050_VaG_AplusCH has the same bathymetry as in 2050_VaG_AminCL. The difference in this case is the sea level rise is taken from a more severe scenario, which is 40cm instead of 15cm in the previous case. The tidal range is increased by reducing bottom friction in the Western Scheldt. For the rest the model settings are the same.

(1). The difference in hydrodynamics

Harmonic analysis is performed on time series of water levels along the thalweg of the Scheldt. Figure 128 and Figure 129 show the water level M2 and M4 amplitudes. The effect is similar as found with AminCL boundary conditions. Water level M2 amplitude has a slight decrease from about 70 km to 130 km, then the trend is reversed from 130 km to 170 km, with an increase up to 20cm in the Upper Sea Scheldt.

Water level M4 amplitude decreases from 122 km to 135 km, then it increases again further upstream.

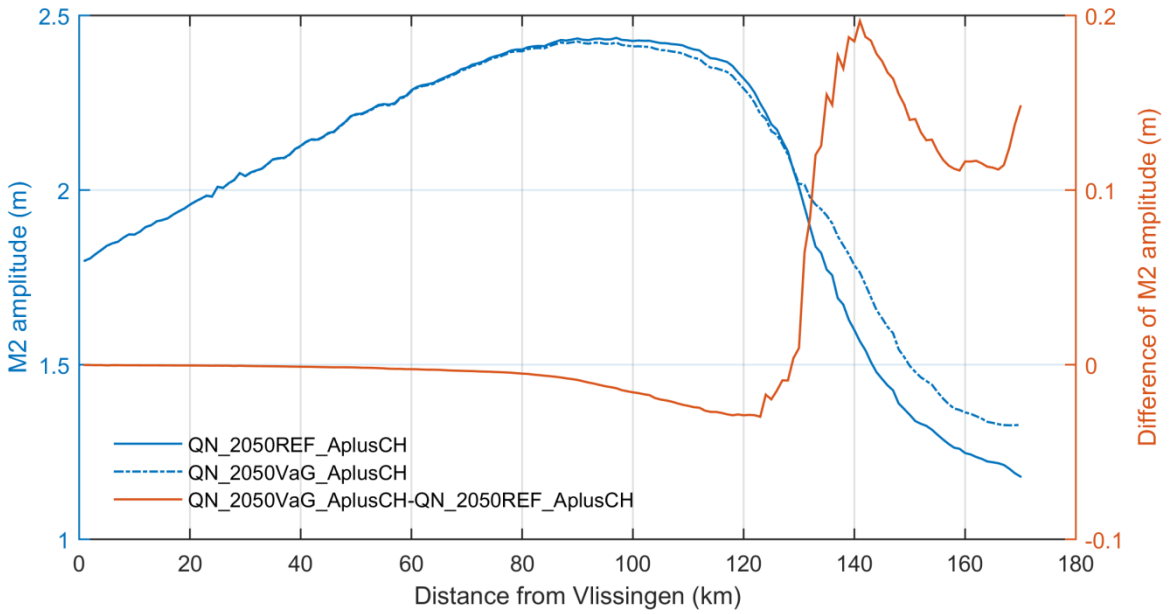

Figure 128 – Comparison of M2 amplitude between 2050_REF_AplusCH and 2050_VaG_AplusCH

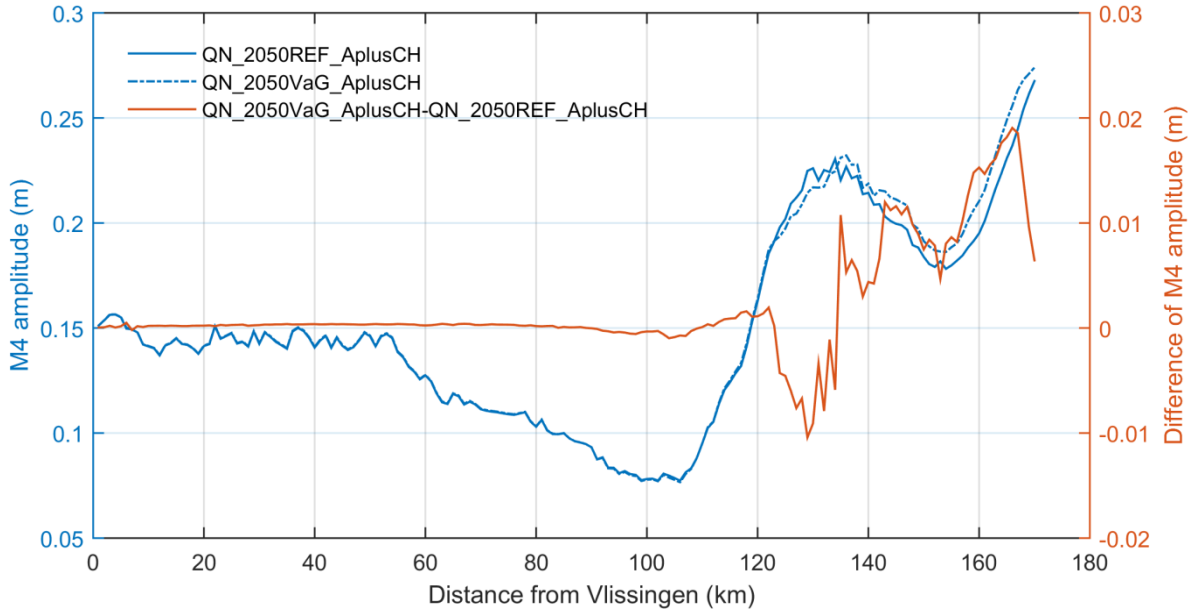

Figure 129 – Comparison of M4 amplitude between 2050_REF_AplusCH and 2050_VaG_AplusCH

The effect on M2 velocity amplitude is shown in Figure 130.

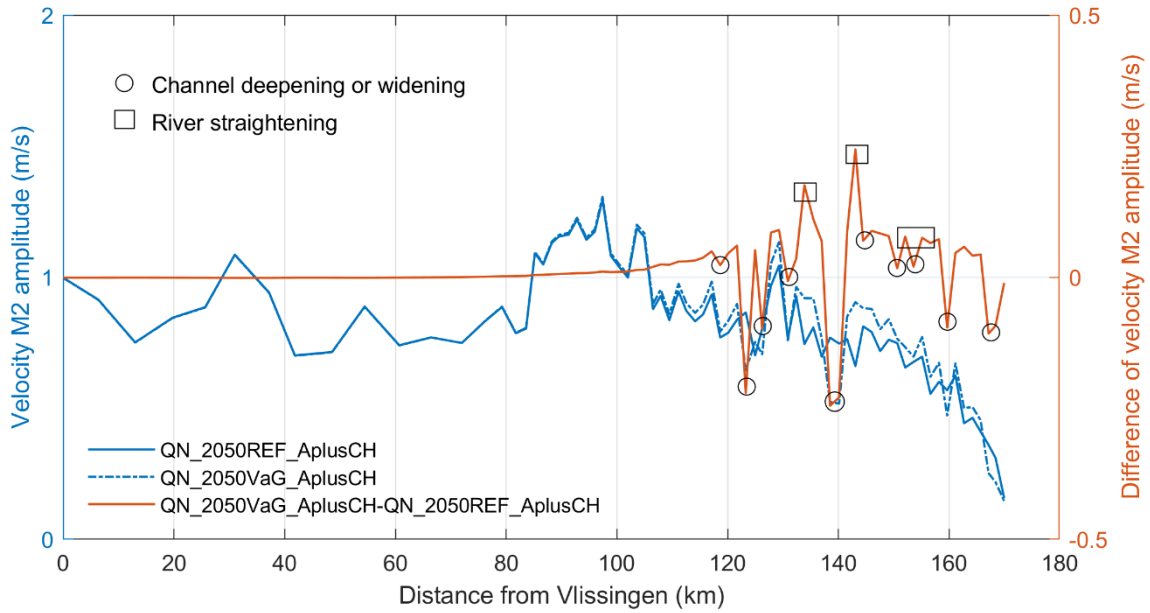

Figure 130 – Comparison of M2 amplitude of cross-sectionally averaged velocity between 2050_REF_AplusCH and 2050_VaG_AplusCH

(2). The change of tidal asymmetry

All the tidal asymmetry indicators as mentioned in §4.8, are calculated in this section. These indicators, 8 in total, are organized in 3 groups, based on time duration, velocity magnitude and skewness, respectively.

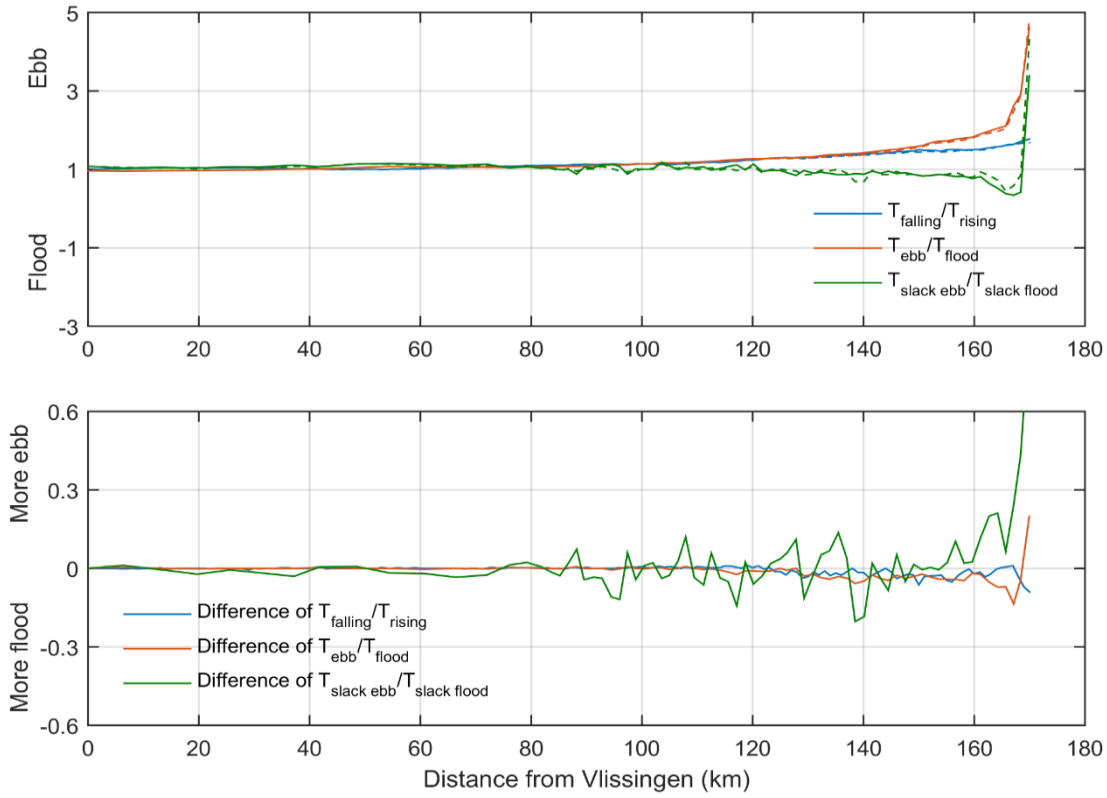

Figure 131 – Indicators of tidal asymmetry (durations).
Solid lines represent the reference 2050_REF_AplusCH, dashed lines represent the scenario 2050_VaG_AplusCH.

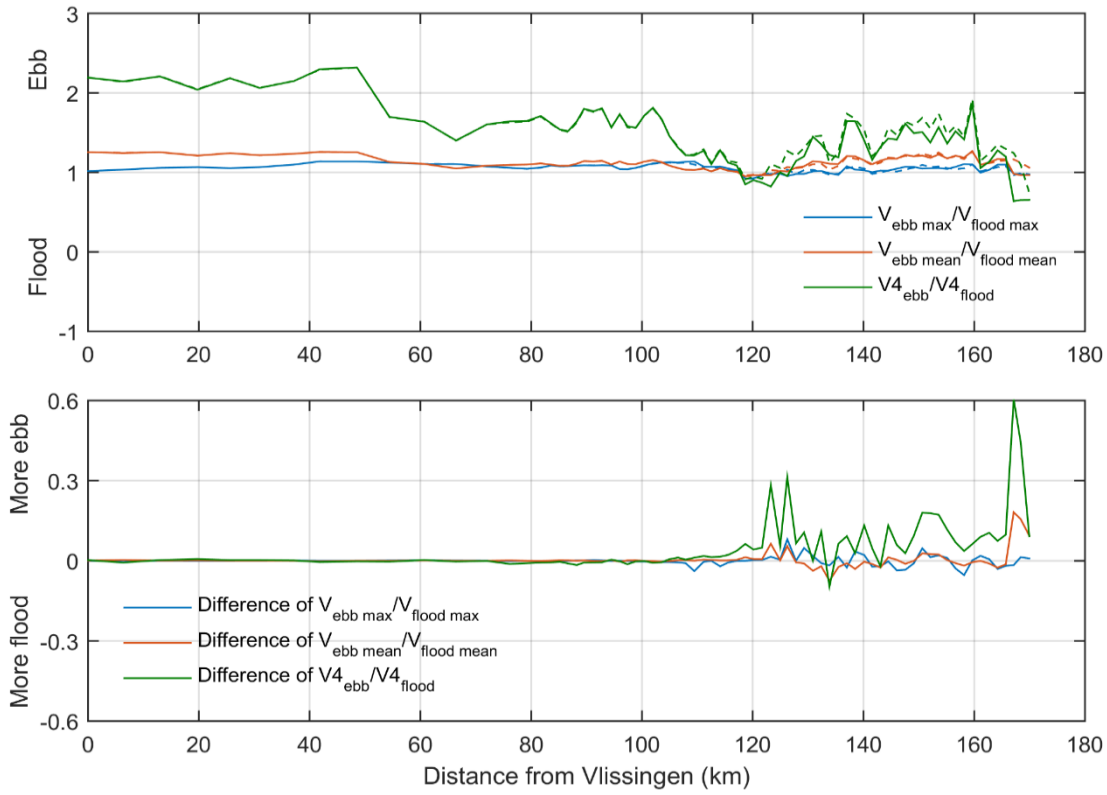

Figure 132 – Indicators of tidal asymmetry (velocities).
Solid lines represent the reference 2050_REF_AplusCH, dashed lines represent the scenario 2050_VaG_AplusCH.

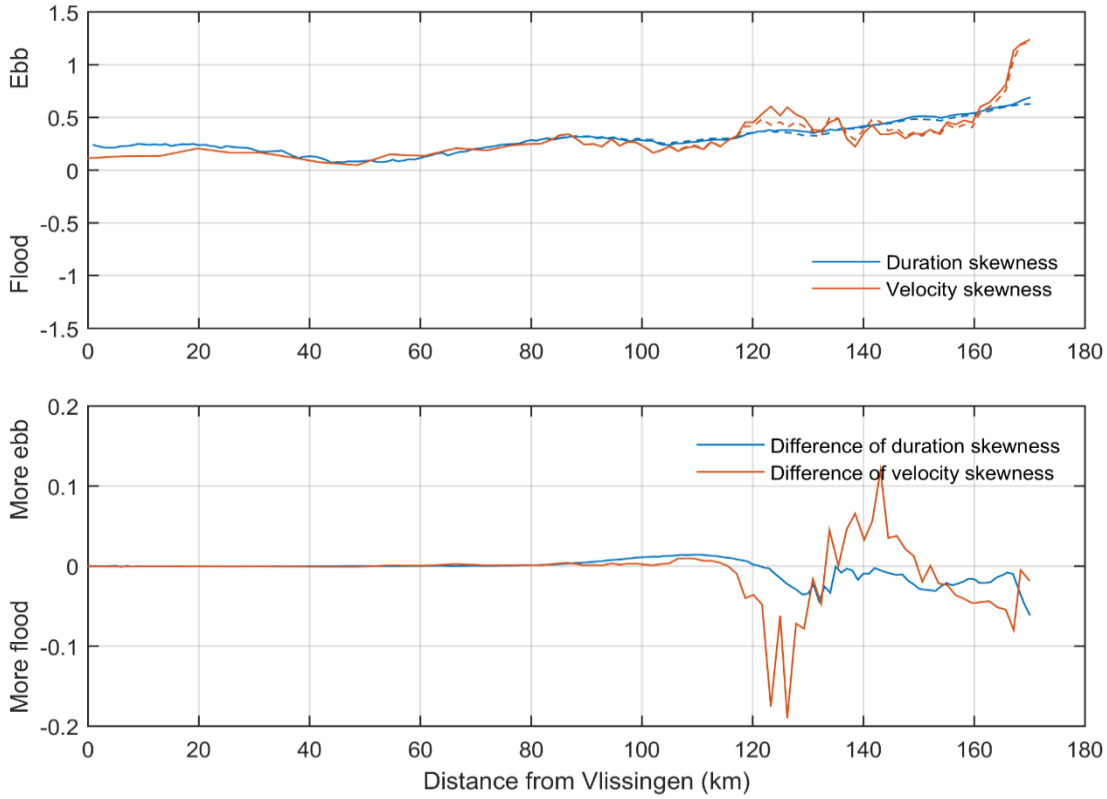

Figure 133 – Indicators of tidal asymmetry (skewness).
Solid lines represent the reference 2050_REF_AplusCH, dashed lines represent the scenario 2050_VaG_AplusCH.

(3). Sediment Transport Decomposition

Figure 134 shows the sediment transport decomposed according to §4.7

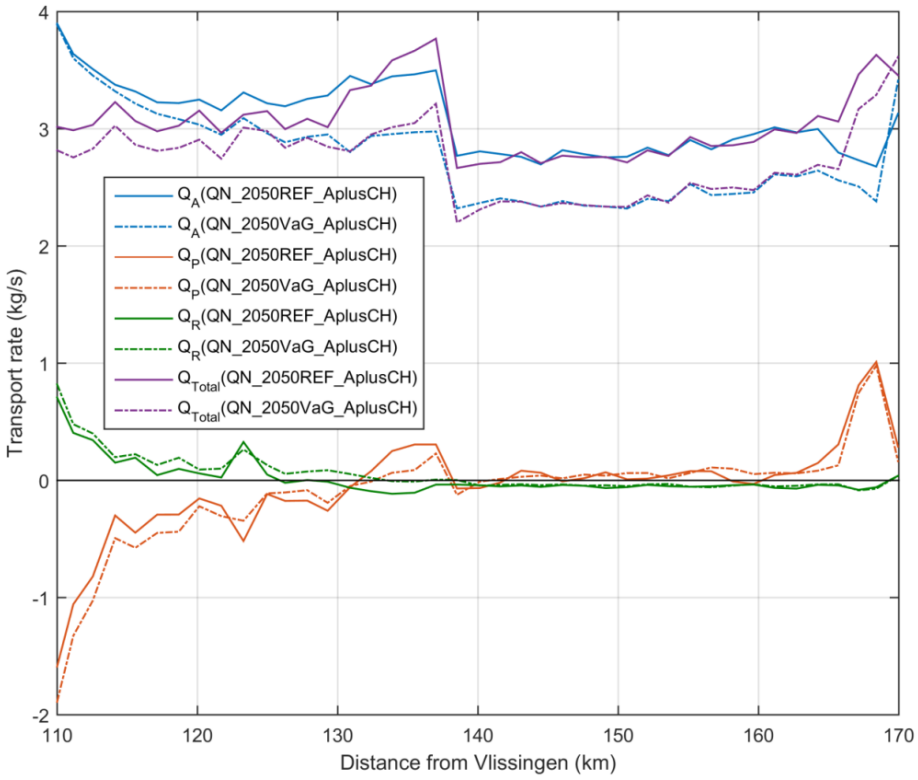

Figure 134 – Time-averaged decomposed sediment transport rate QA, QP and QR in the Upper Sea Scheldt. Positive sign means downstream direction and negative means upstream direction

It can be seen in the above figure, the VaG scenario combined with AplusCH (sea level rise of 40cm and increased tidal range) tends to have more influence on sediment transport, even in the Lower Sea Scheldt. However, when VaG is combined with AminCL (sea level rise 15cm and decreased tidal range), the influence on sediment transport are less.

(4). Erosion-deposition map

The difference of sedimentation rate is calculated between the run 2050_VaG_AplusCH and 2050_REF_A0CN using the bed layer thickness given in the result files. The sedimentation rate is based on the production period of the last 20 days and it is converted to cm/yr.

Figure 135 – Difference of sedimentation rate (2050_VaG_AplusCH-2050_REF_AplusCH) – part 1

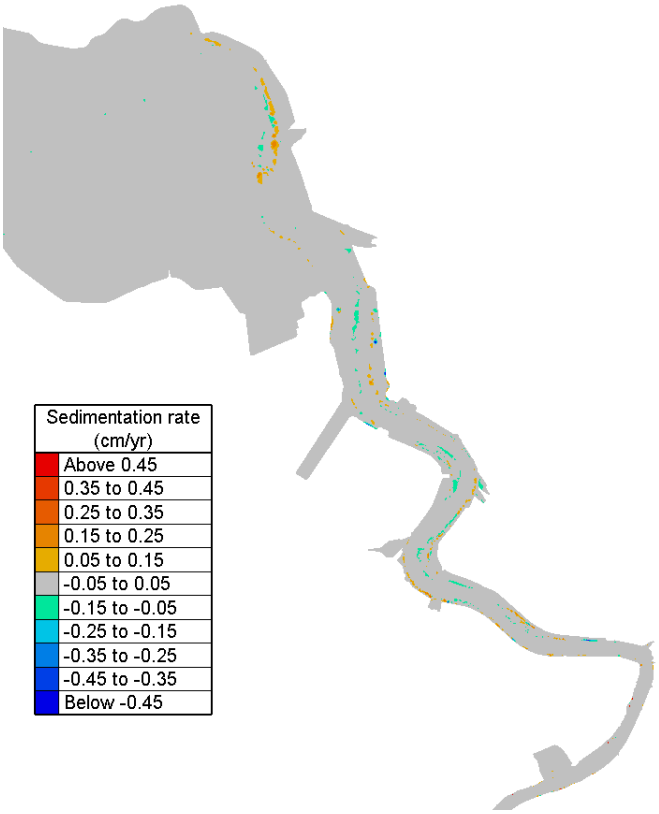

Figure 136 – Difference of sedimentation rate (2050_VaG_AplusCH-2050_REF_AplusCH) – part 2

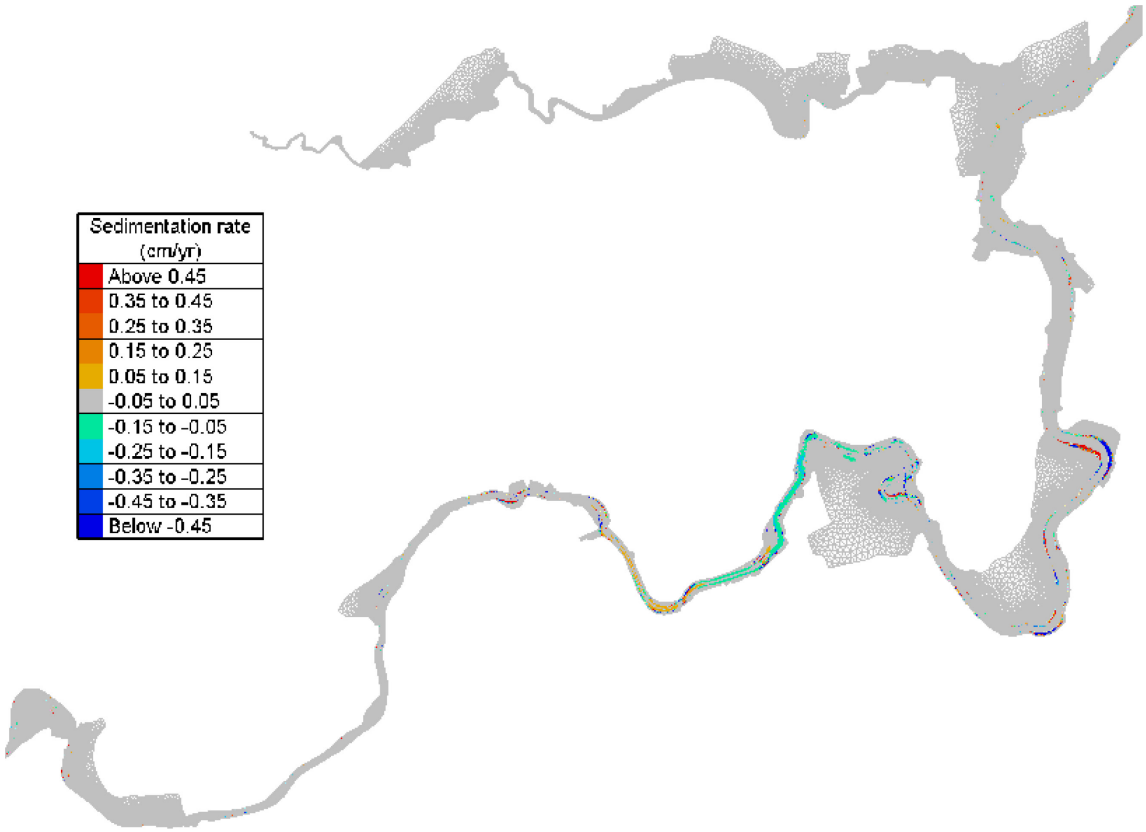

Figure 137 – Difference of sedimentation rate (2050_VaG_AplusCH-2050_REF_AplusCH) – part 3

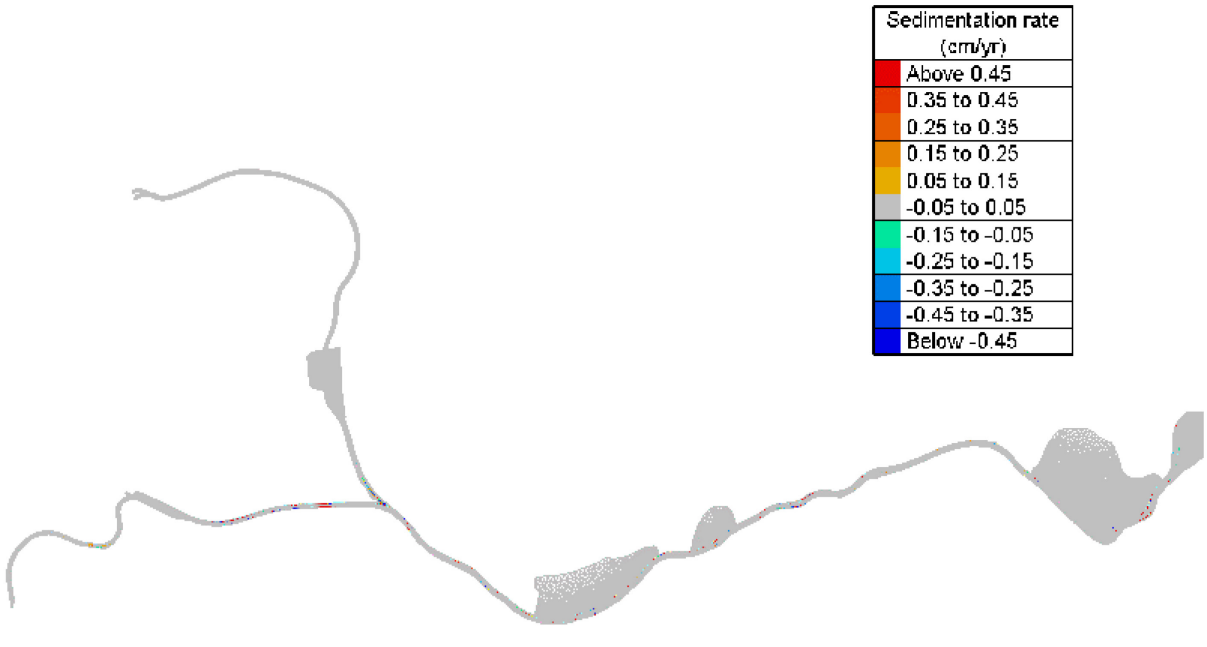

Figure 138 – Difference of sedimentation rate (2050_VaG_AplusCH-2050_REF_AplusCH) – part 4

Compared to the reference case, the most differences are found in the Upper Sea Scheldt where bathymetric changes are intensive. This is similar as in §6.2.1. In the Lower Sea Scheldt, downstream of Antwerp, there are also slight differences in the sedimentation rate, probably due to the influence from the upstream. For the coastal area and the Western Scheldt, the difference is not obvious.

(5). Bed shear stress

Changes in bottom shear stress lead to changes in sedimentation/erosion patterns and habitat suitability. Therefore maps are made in the study area of exceedance time (%) of a threshold value of 1 Pa during a spring-neap cycle. A difference map (in %-points) shows the spatial changes.

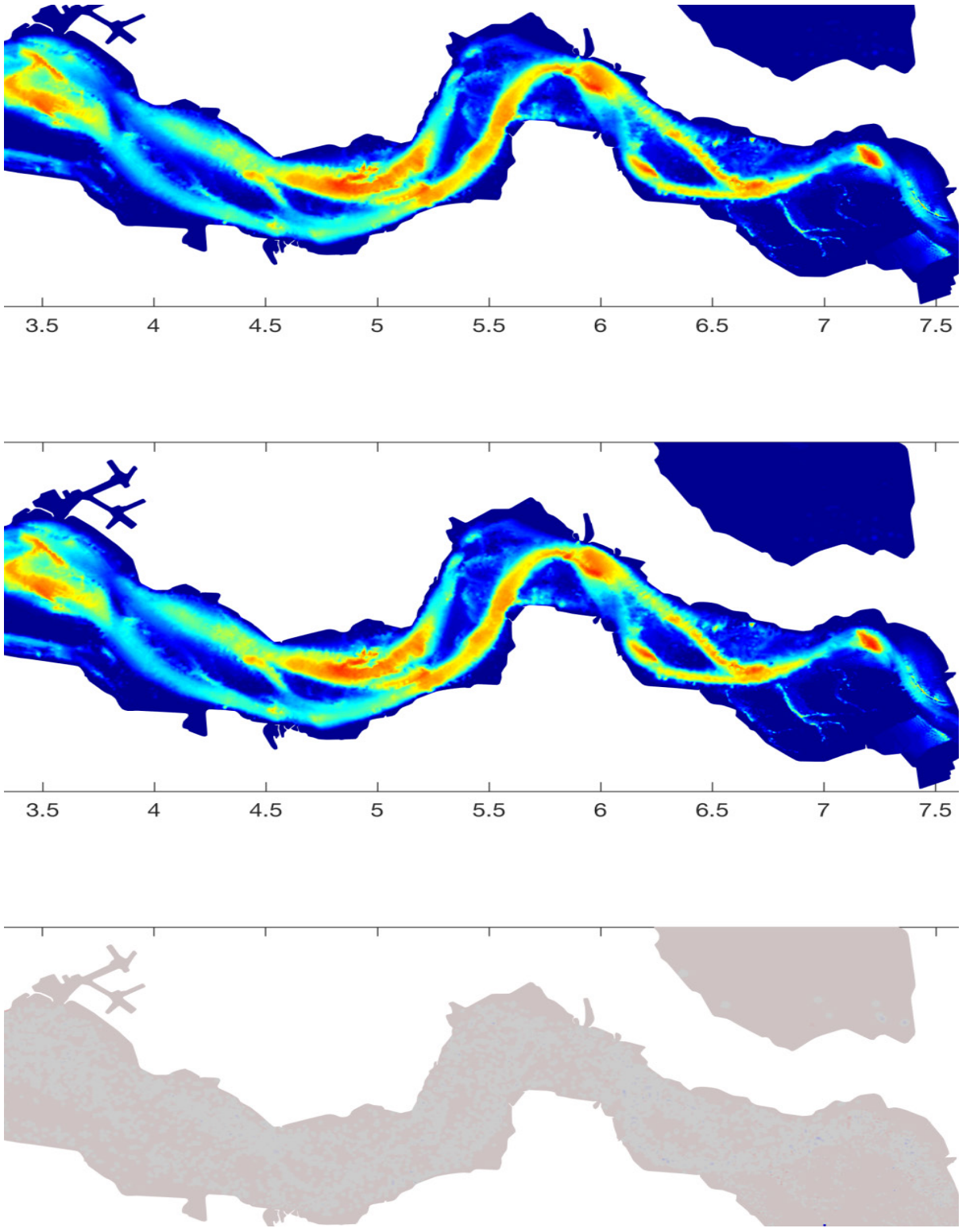

Figure 139 – Exceedance time of bed shear stress >1Pa (%) during a spring-neap cycle in Western Scheldt.
From top to bottom: the reference 2050_REF_AplusCH; the scenario 2050_VaG_AplusCH;
the difference 2050_VaG_AplusCH - 2050_REF_AplusCH.

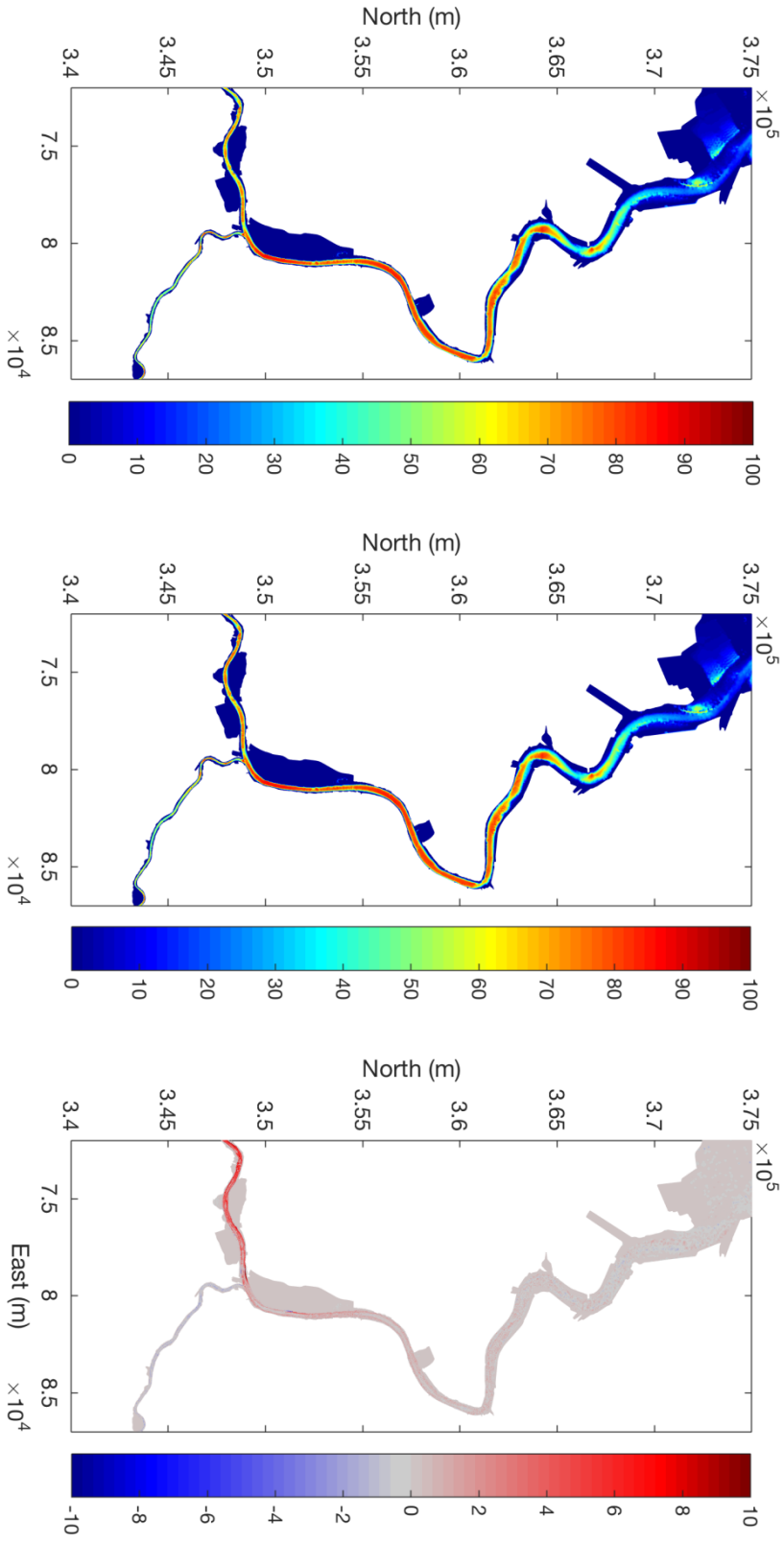

Figure 140 – Exceedance time of bed shear stress >1Pa (%) during a spring-neap cycle in Lower Sea Scheldt.
From top to bottom: the reference 2050_REF_AplusCH; the scenario 2050_VaG_AplusCH;
the difference 2050_VaG_AplusCH - 2050_REF_AplusCH.

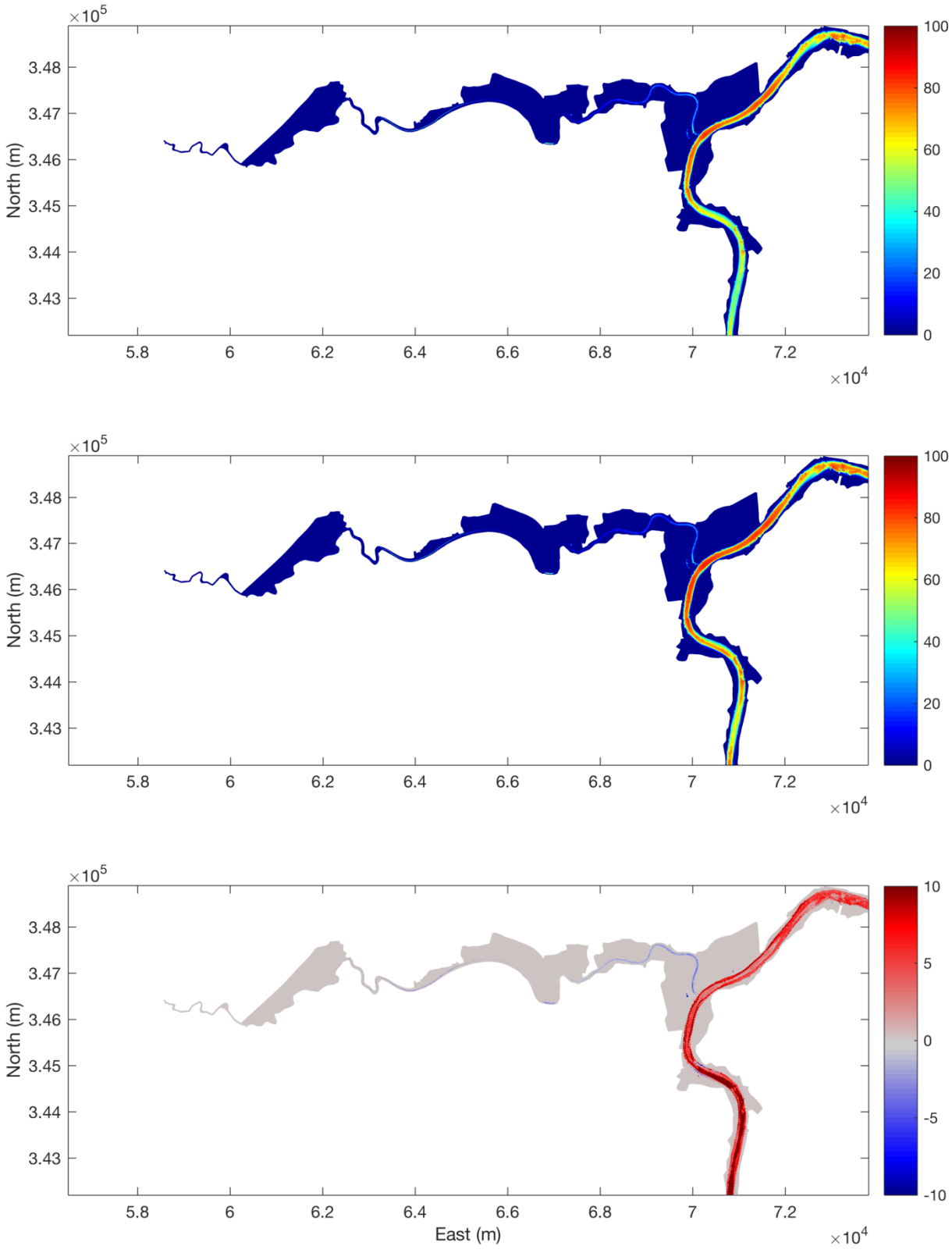

Figure 141 – Exceedance time of bed shear stress >1Pa (%) during a spring-neap cycle in Upper Sea Scheldt.
From top to bottom: the reference 2050_REF_AplusCH; the scenario 2050_VaG_AplusCH;
the difference 2050_VaG_AplusCH - 2050_REF_AplusCH.

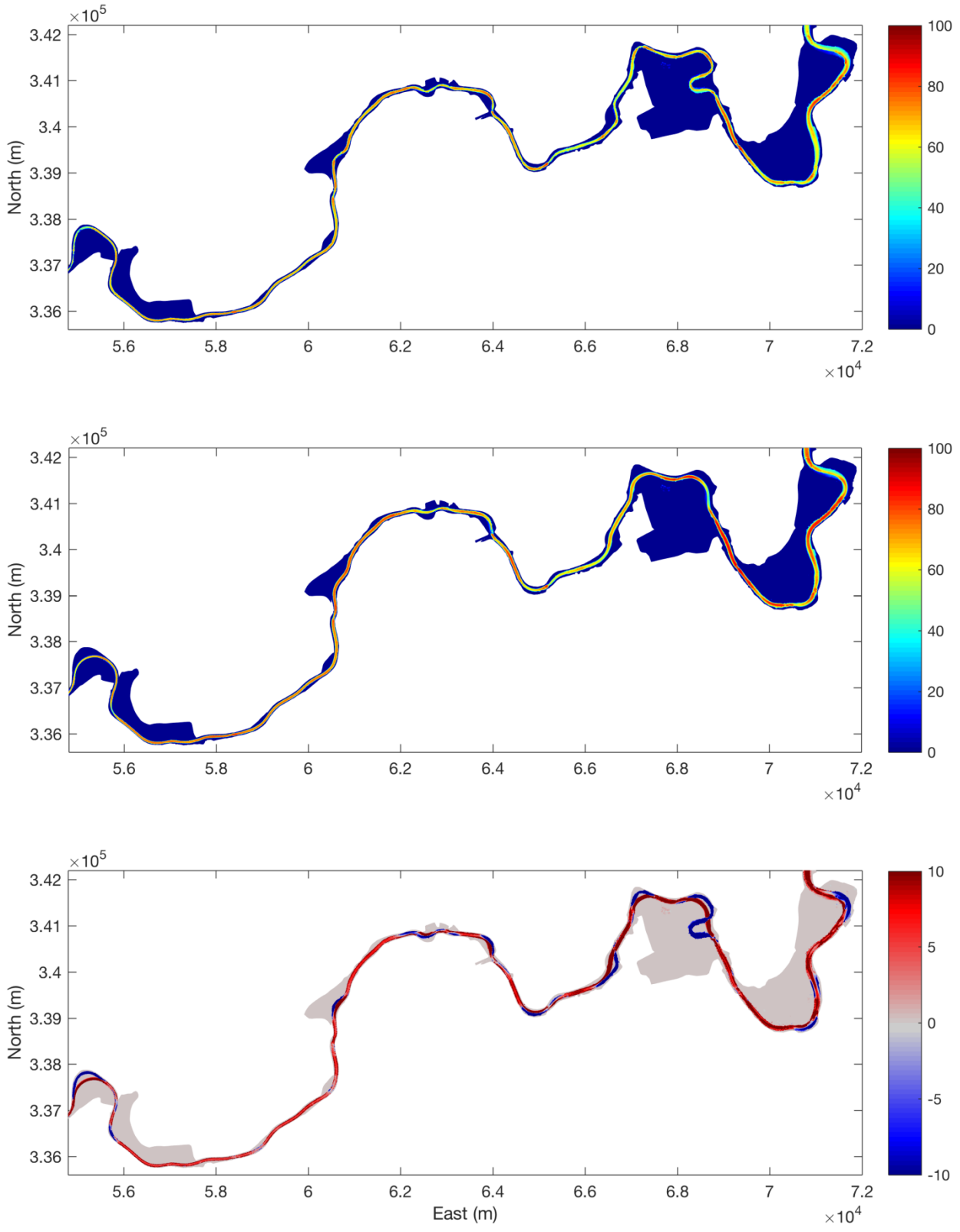

Figure 142 – Exceedance time of bed shear stress >1Pa (%) during a spring-neap cycle in Upper Sea Scheldt.
From top to bottom: the reference 2050_REF_AplusCH; the scenario 2050_VaG_AplusCH;
the difference 2050_VaG_AplusCH – 2050_REF_AplusCH.

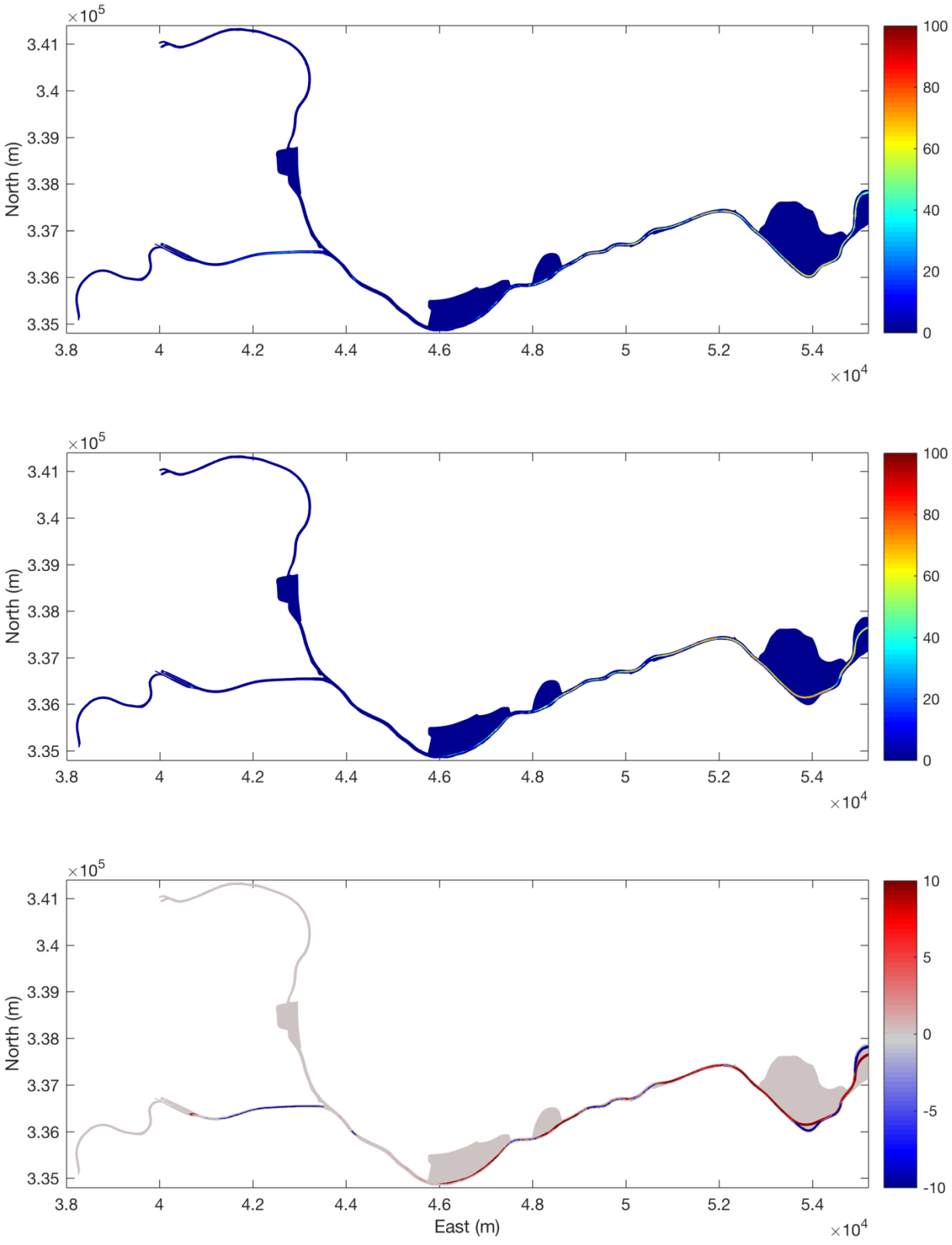

Figure 143 – Exceedance time of bed shear stress >1Pa (%) during a spring-neap cycle in Upper Sea Scheldt.
From top to bottom: the reference 2050_REF_AplusCH; the scenario 2050_VaG_AplusCH;
the difference 2050_VaG_AplusCH - 2050_REF_AplusCH.

(6). Delta SSC

The Delta SSC is calculated based on equation described in §5.1 and the time averaged Delta SSC is given for each box of the ecosystem model in Figure 144.

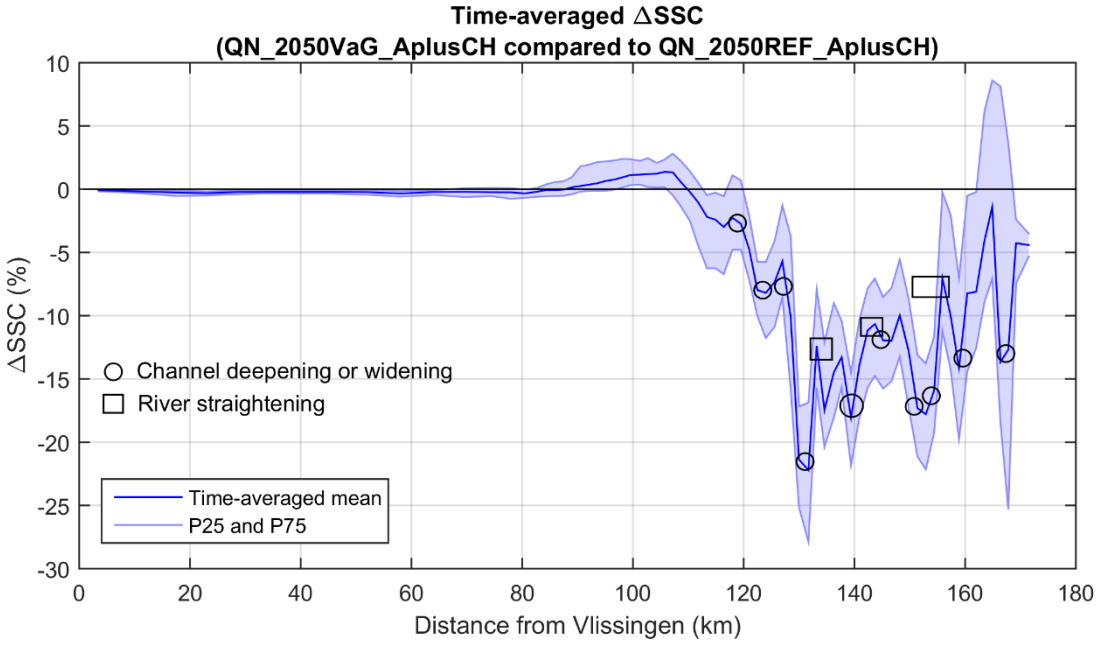

Figure 144 – Delta SSC (2050_VaG_AplusCH compared to 2050_REF_AplusCH)

It can be seen from above figure that delta SSC remains nearly zero in the Western Scheldt (from 0 km to 70 km). It starts to deviate from zero (also shows temporal variations) at about 80 km, and further upstream the mean delta SSC becomes negative in the entire Upper Sea Scheldt, with temporal variations sometimes above zeros from 160 km to 170 km. The locations with intensive bathymetric changes are also plotted in the above figure. In general, channel deepening leads to lower SSC and cutting of river bend tends to increase SSC.

5.2.3 Discussion

The effects of VaG in AminCL and AplusCH scenarios are similar to each other. In both cases, the difference of cross-sectionally averaged velocity M_2 amplitude can be seen in Figure 114 and Figure 130. Analysis of cross-sectionally averaged velocity magnitude (presented as M_2 amplitude) shows that straightening river bends tends to increase local velocity (the length is reduced and less friction loss along the channel) while deepening and/or widening channels tends to reduce velocity (channel depth and/or width is increased and velocity decreases due to continuity).

The change of velocity has influences on sediment transport and delta SSC. When velocity is reduced, the bed shear stress decreases as well. Thus more sediment deposits to the bed and less remaining in suspension, which means delta SSC could decrease. If velocity becomes larger, both suspension capacity and erosion capability will increase. If there is enough supply from the source, it will be able to maintain higher suspension concentration in water column. Therefore, based on above reasoning, it is not a surprise that the change of velocity magnitude could affect delta SSC. Figure 127 and Figure 144 shows that in the locations where there are channel deepening or widening, both velocity M_2 amplitude and delta SSC are changed accordingly.

In both cases, delta SSC is negative from 165 km to 170 km. This is due to deepening of the channel near Merelbeke. The channel deepening reduces velocity magnitude here, thus more sediment deposits to the bed and less sediment remains available for being transported downstream (Figure 145 and Figure 146).

Delta SSC remains negative in the entire Upper Sea Scheldt. Part of the explanation is that, SSC in this region is mainly determined by the input from upstream. More sediment deposited near Merelbeke means less sediment is transported downstream.

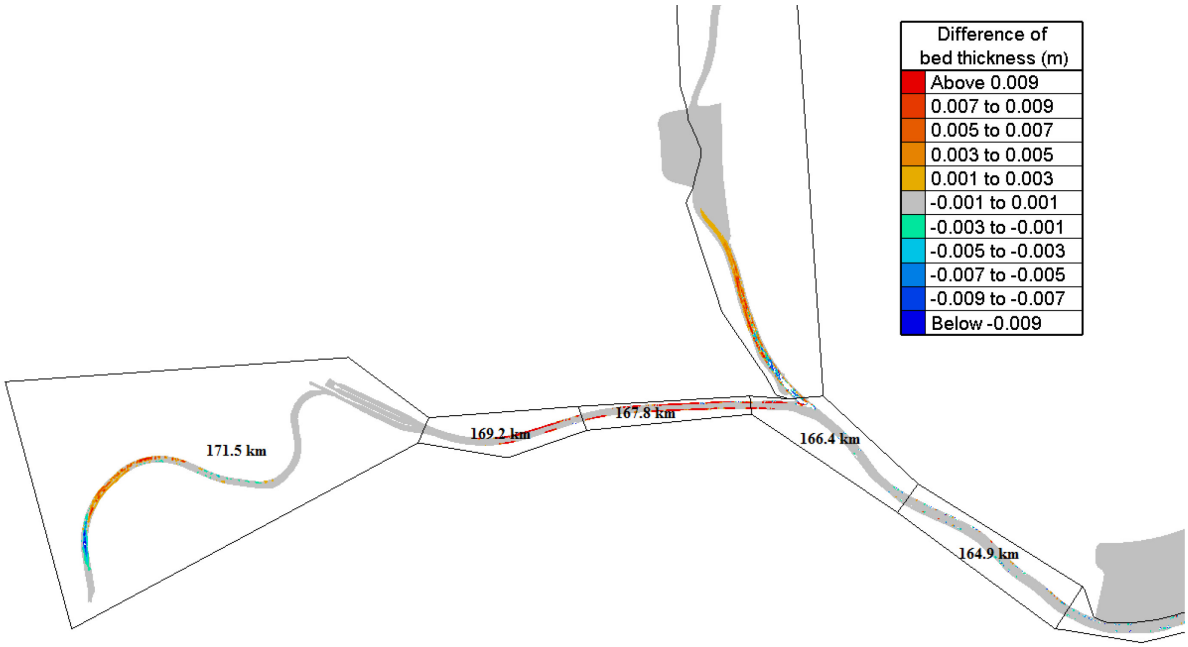

Figure 145 – Difference of bed thickness in Upper Sea Scheldt (165 km – 171 km) in 2050_VaG_AminCL

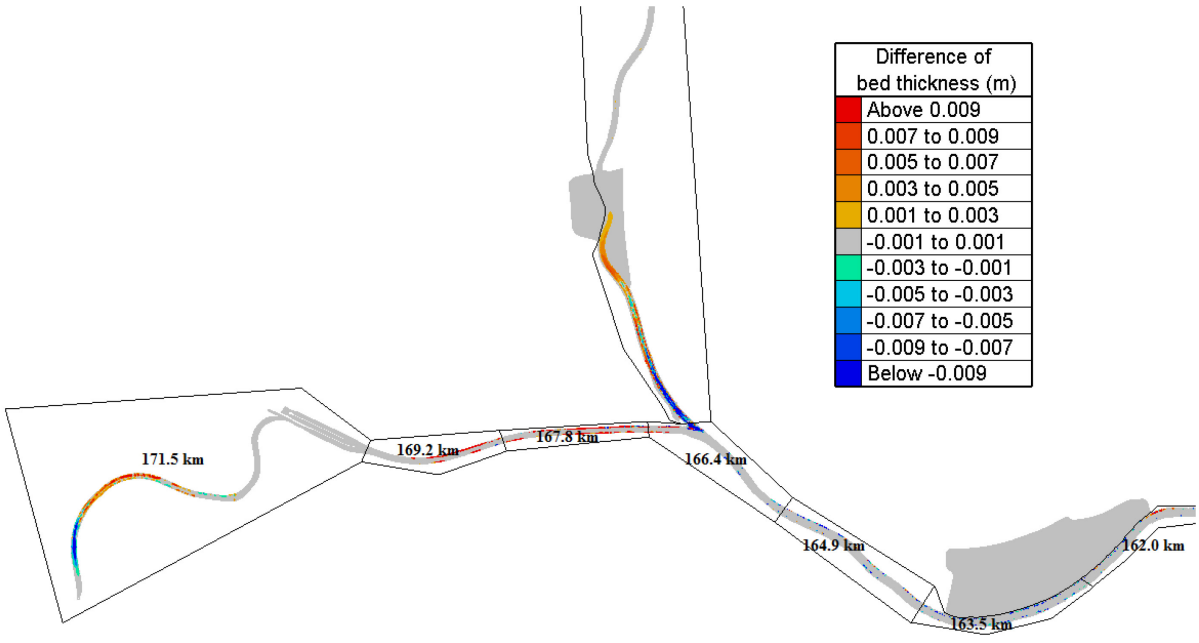

Figure 146 – Difference of bed thickness in Upper Sea Scheldt (162 km – 171 km) in 2050_VaG_AplusCH

The general trend of delta SSC is explained above. However, there are some local peaks and variations (from 110 km – 170 km) that can only be explained by the local bathymetry changes. As stated before, the main influencing factor is cross-sectionally averaged velocity magnitude (shown as velocity M2 amplitude). Reduction of delta SSC is mostly caused by decrease of velocity , thus more locally deposition of sediment. The bathymetry is intensively altered from 120 km to 142 km, and 150 km to 160 km. Therefore, delta SSC goes down deeply in those areas. There are more deposition happening from 120 km to 142 km, thus lower delta SSC compared to the rest part of Upper Sea Scheldt (Figure 147 to Figure 150).

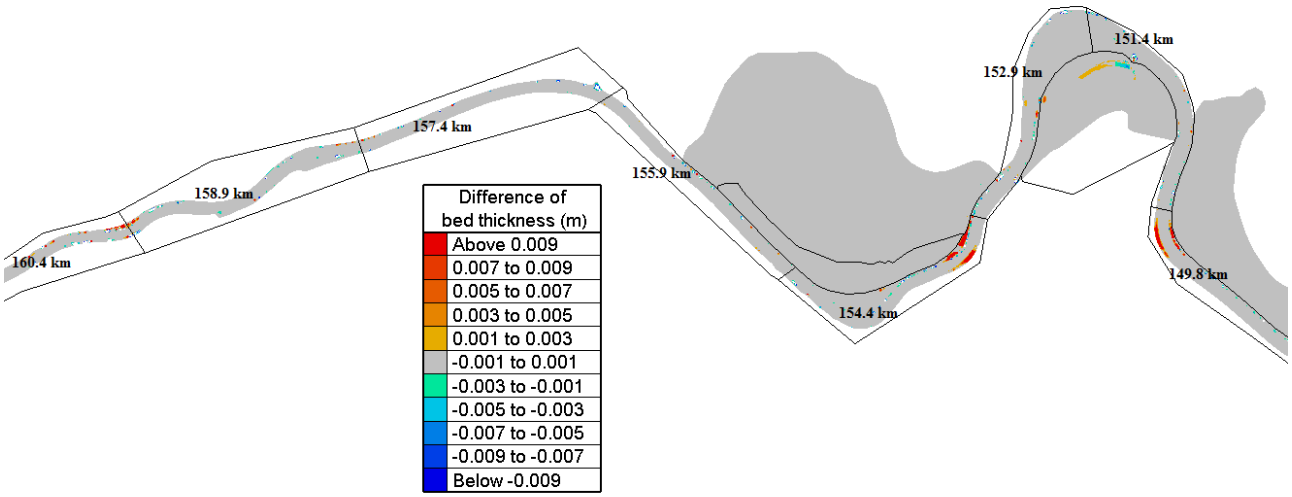

Figure 147 – Difference of bed thickness in Upper Sea Scheldt (150 km – 160 km) in 2050_VaG_AminCL

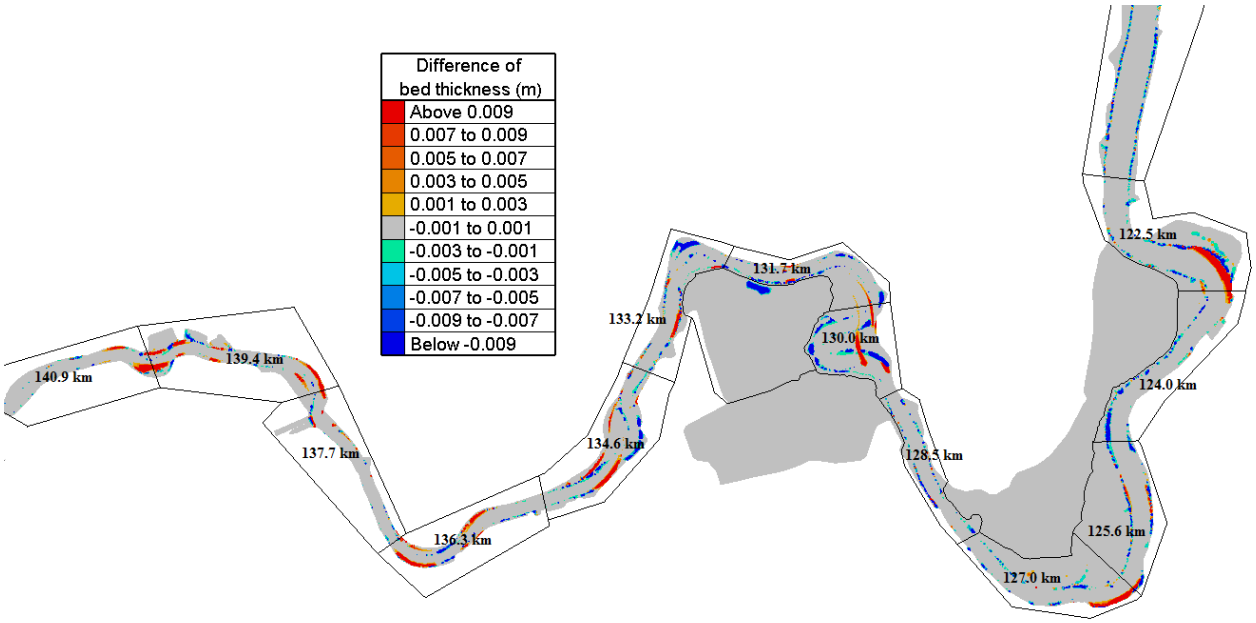

Figure 148 – Difference of bed thickness in Upper Sea Scheldt (120 km – 140 km) in 2050_VaG_AminCL

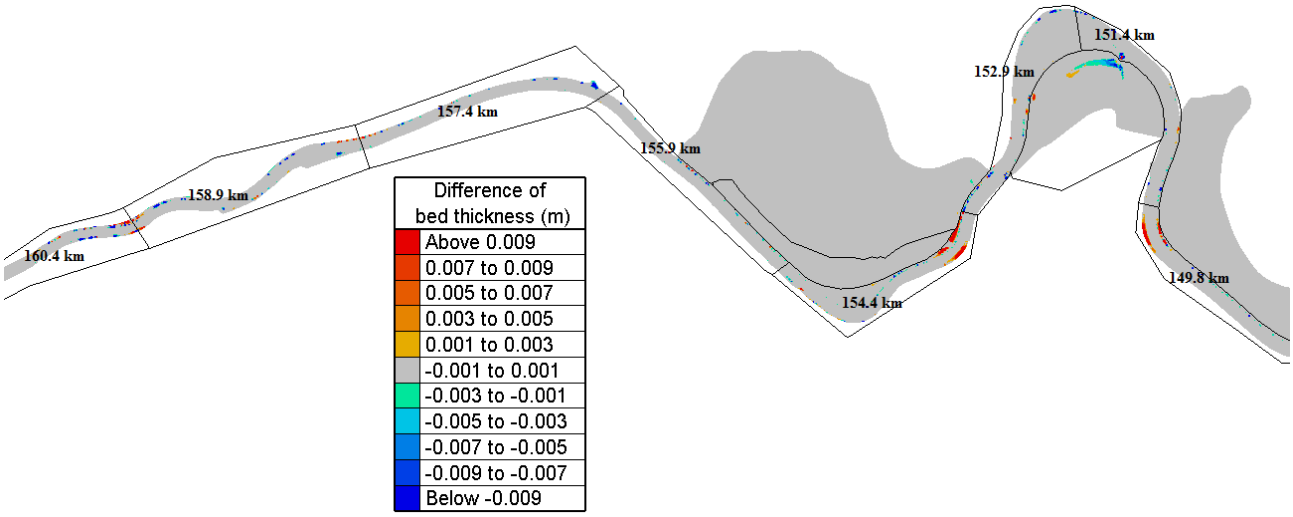

Figure 149 – Difference of bed thickness in Upper Sea Scheldt (150 km – 160 km) in 2050_VaG_AplusCH

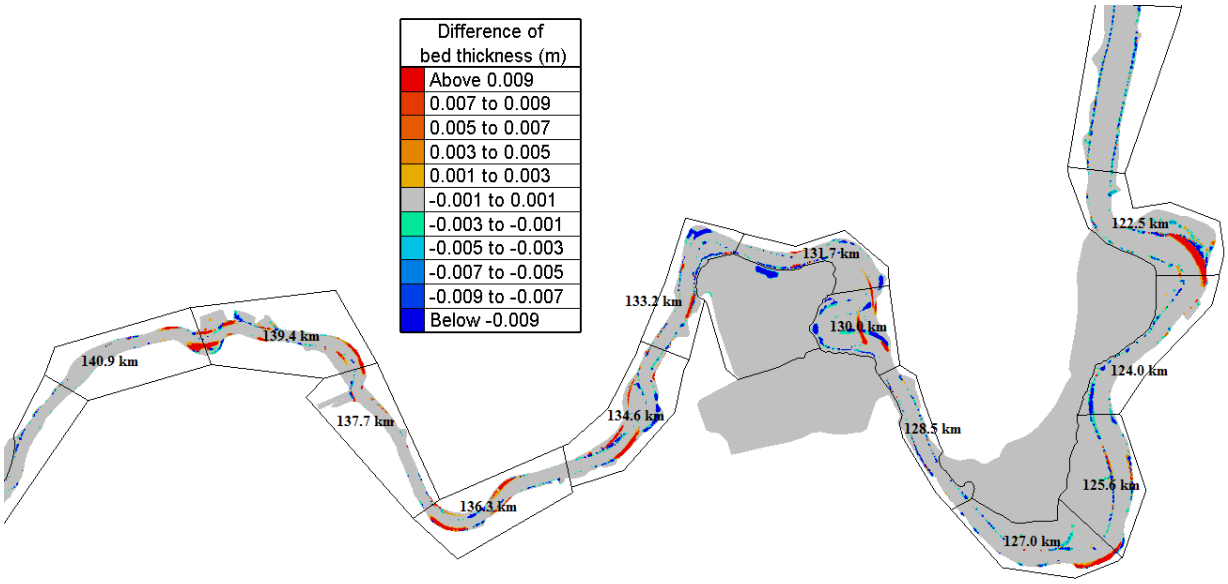

Figure 150 – Difference of bed thickness in Upper Sea Scheldt (122 km – 141 km) in 2050_VaG_AplusCH

5.3 Effect of VaH

The scenario 2050_VaH_AplusCH has less intensive bathymetry changes compared to 2050_VaG_AplusCH. It consists of mainly deepening and/or widening channels in the Upper Sea Scheldt. 2050_VaH_AplusCH is compared to the reference 2050_REF_AplusCH in order to show the effect of the VaH bathymetry.

(1). The difference in hydrodynamics

Harmonic analysis is performed on time series of water levels at each thalweg points along Scheldt. Figure 151 and Figure 152 show the water level M_2 and M_4 amplitudes. The difference between 2050_VaH_AplusCH and 2050_REF_AplusCH is not as much as in the VaG scenarios because of less drastic bathymetric changes in the Upper Sea Scheldt. Water level M_2 amplitude has a slight decrease from about 90 km to 130 km, then it starts to increase from 130 km to 170 km, with a peak near the upstream boundary.

The difference in water level M_4 amplitude also appears less compared to VaG cases. The noticeable changes are usually in the location where bottom alternations are found because it is more related to the change of bottom friction or bottom elevation

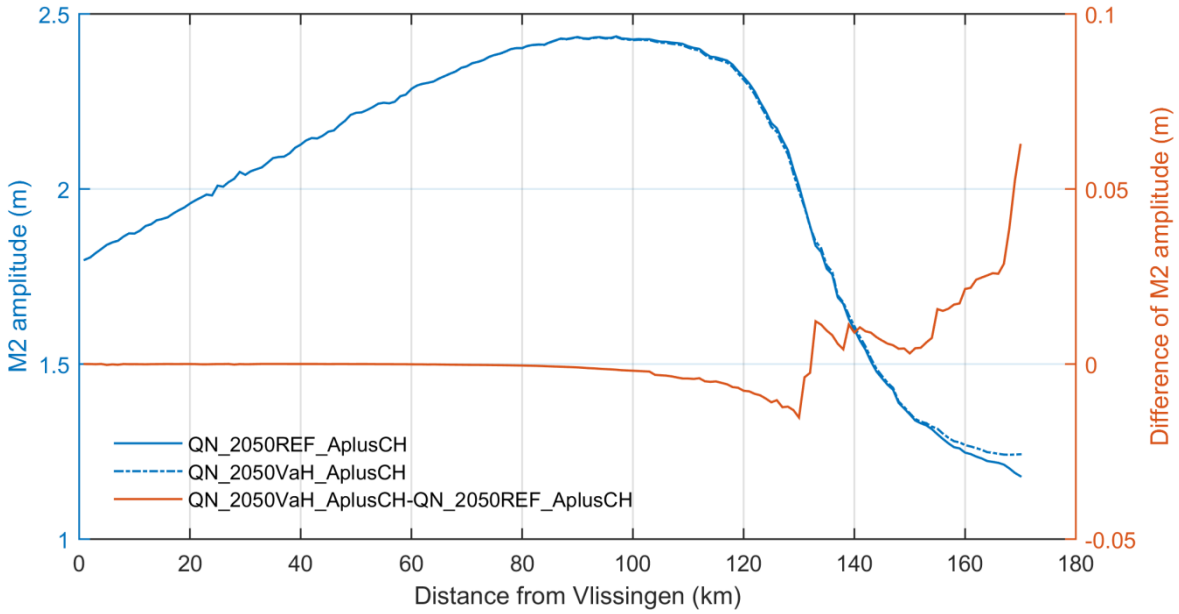

Figure 151 – Comparison of M2 amplitude between 2050_REF_AplusCH and 2050_VaH_AplusCH

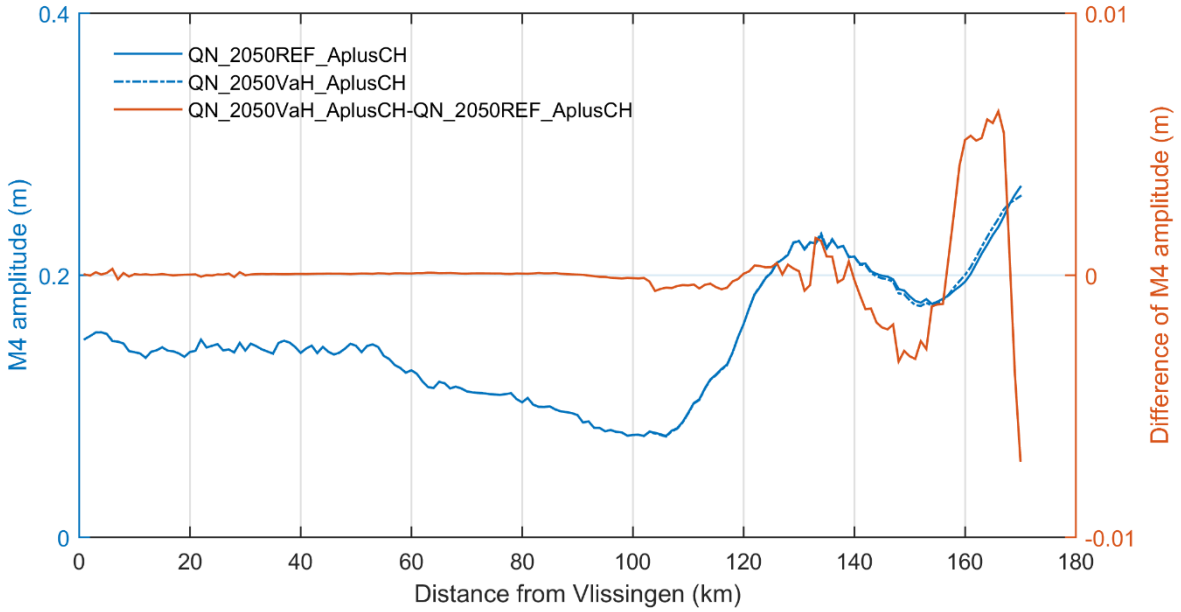

Figure 152 – Comparison of M4 amplitude between 2050_REF_AplusCH and 2050_VaH_AplusCH

The effect on M2 velocity amplitude is shown in Figure 153.

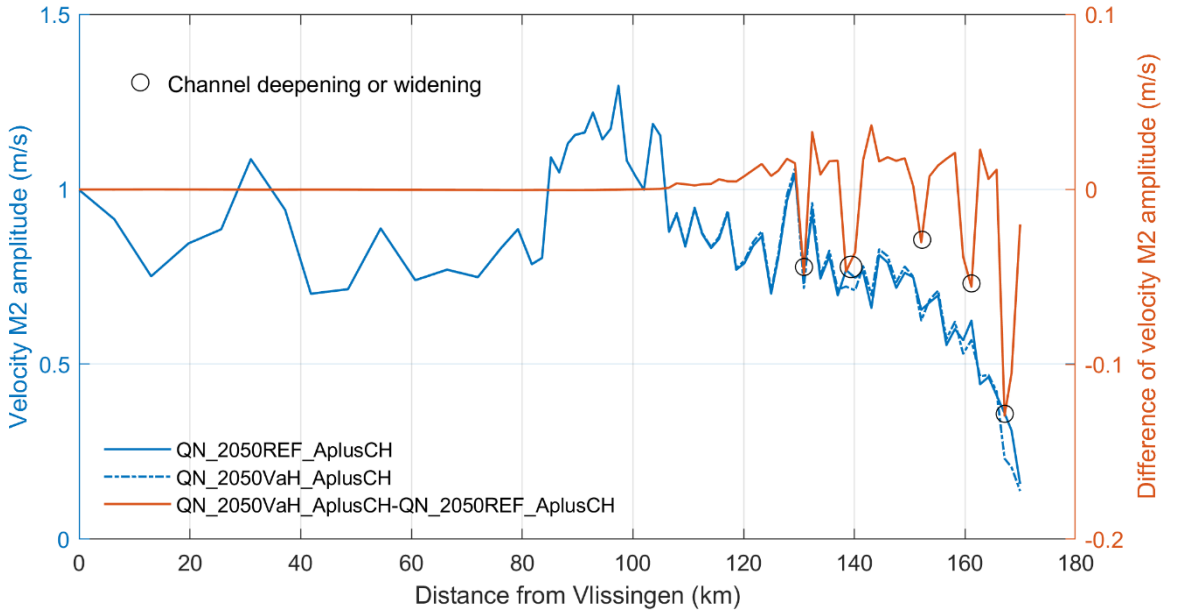

Figure 153 – Comparison of M2 amplitude of cross-sectionally averaged velocity between 2050_REF_AplusCH and 2050_VaH_AplusCH

(2). The change of tidal asymmetry

All the tidal asymmetry indicators as mentioned in §4.8, are calculated in this section. These indicators, 8 in total, are organized in 3 groups, based on time duration, velocity magnitude and skewness, respectively.

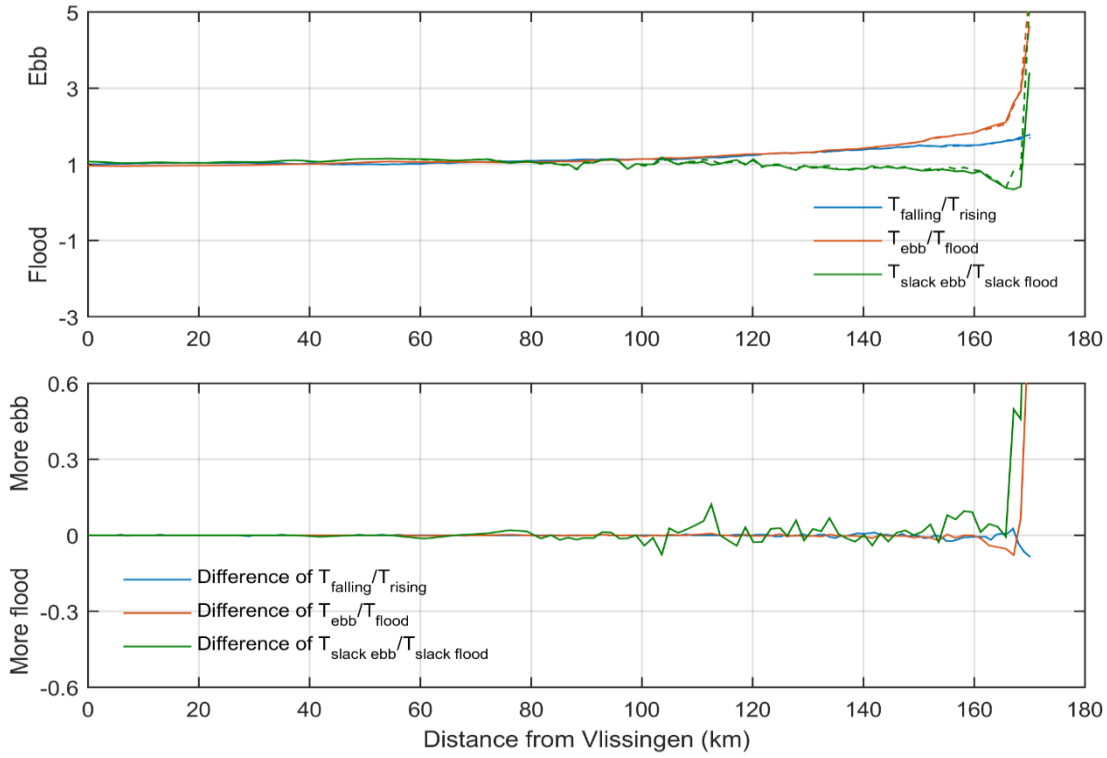

Figure 154 – Indicators of tidal asymmetry (durations).
Solid lines represent the reference 2050_REF_AplusCH, dashed lines represent the scenario 2050_VaH_AplusCH.

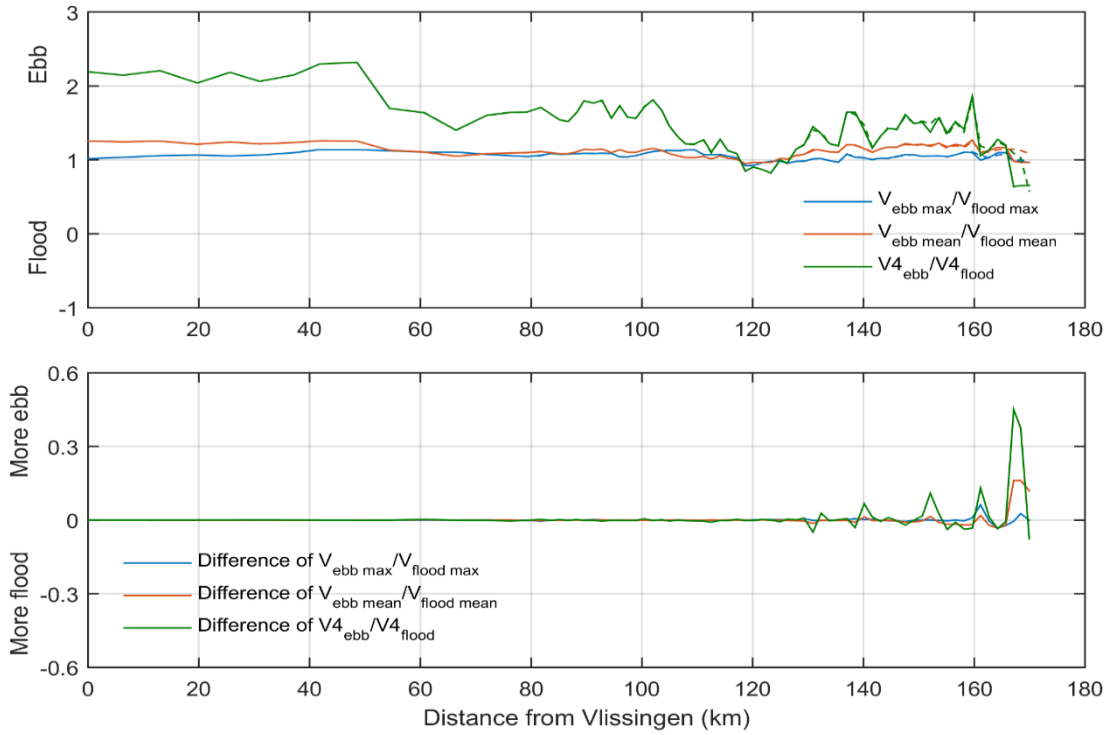

Figure 155 – Indicators of tidal asymmetry (velocities).
Solid lines represent the reference 2050_REF_AplusCH, dashed lines represent the scenario 2050_VaH_AplusCH.

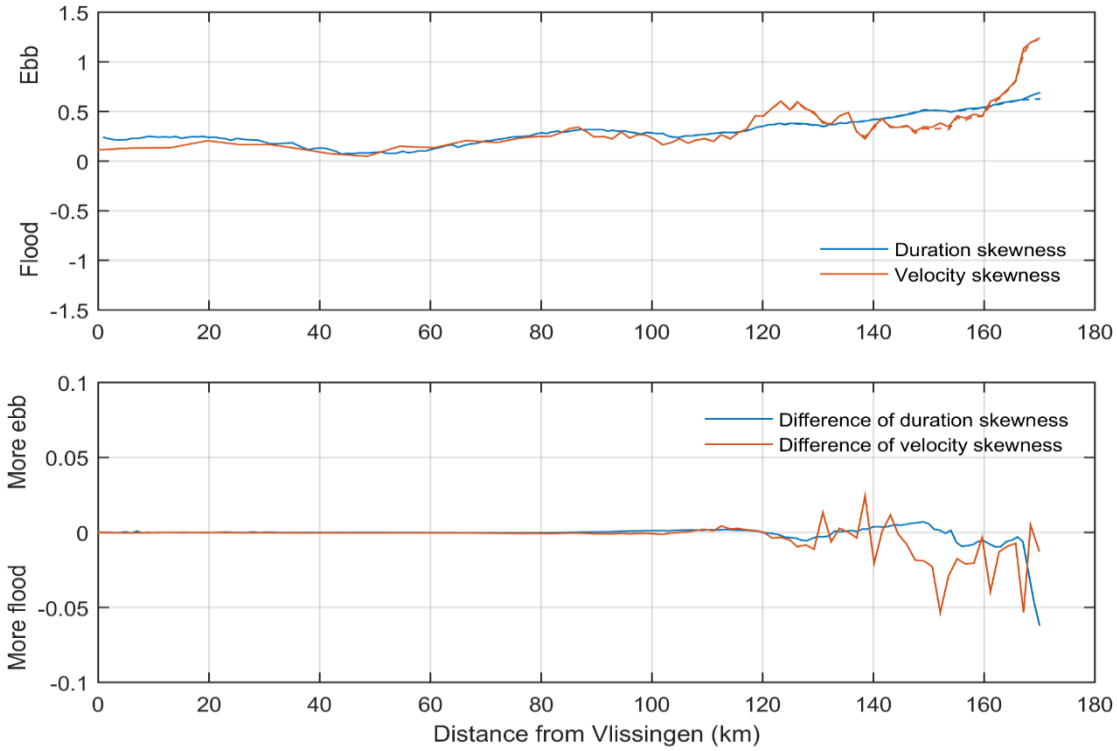

Figure 156 – Indicators of tidal asymmetry (skewness).
Solid lines represent the reference 2050_REF_AplusCH, dashed lines represent the scenario 2050_VaH_AplusCH.

(3). Sediment Transport Decomposition

Figure 157 shows the sediment transport decomposed according to §4.7. It can be seen that the sediment transport is initially higher at the upstream boundary in 2050_VaH_AplusCH due the change of tidal asymmetry (Figure 154). At the upstream boundary T_{ebb}/T_{flood} shows it becomes more ebb dominant, thus larger downstream transport comparing to reference case. The difference becomes smaller when we move further downstream.

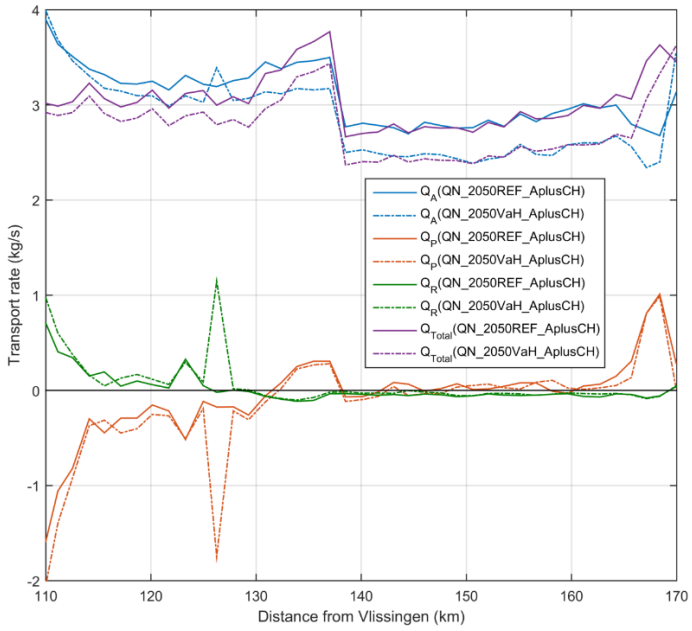

Figure 157 – Time-averaged decomposed sediment transport rate QA, QP and QR in the Upper Sea Scheldt.
Positive sign means downstream direction and negative means upstream direction

(4). Erosion-deposition map

The difference of sedimentation rate is calculated between the run 2050_VaH_AplusCH and 2050_REF_AplusCH using the bed layer thickness given in the result files. The sedimentation rate is based on the production period of the last 20 days and it is converted to cm/yr.

Figure 158 – Difference of sedimentation rate (2050_VaH_AplusCH-2050_REF_AplusCH) – part 1

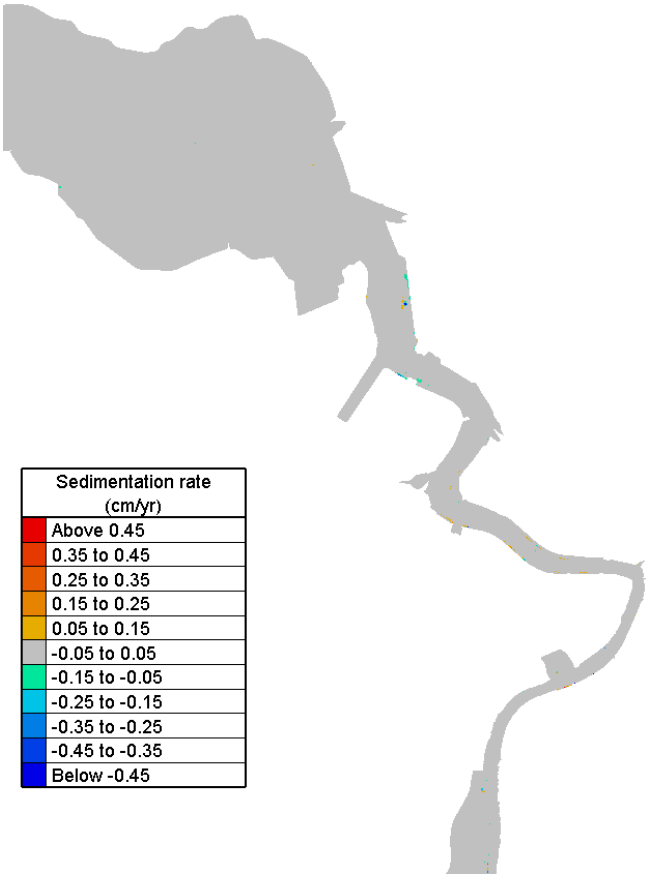

Figure 159 – Difference of sedimentation rate (2050_VaH_AplusCH-2050_REF_AplusCH) – part 2

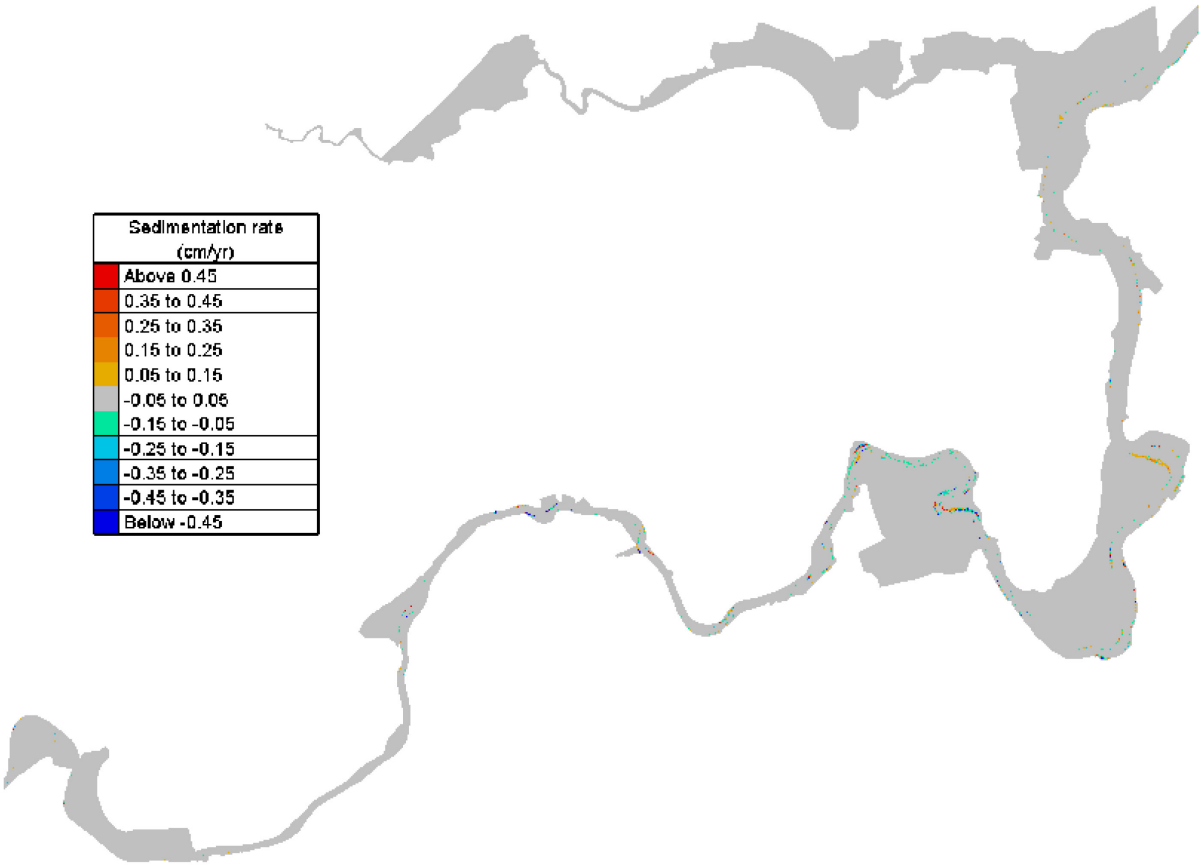

Figure 160 – Difference of sedimentation rate (2050_VaH_AplusCH-2050_REF_AplusCH) – part 3

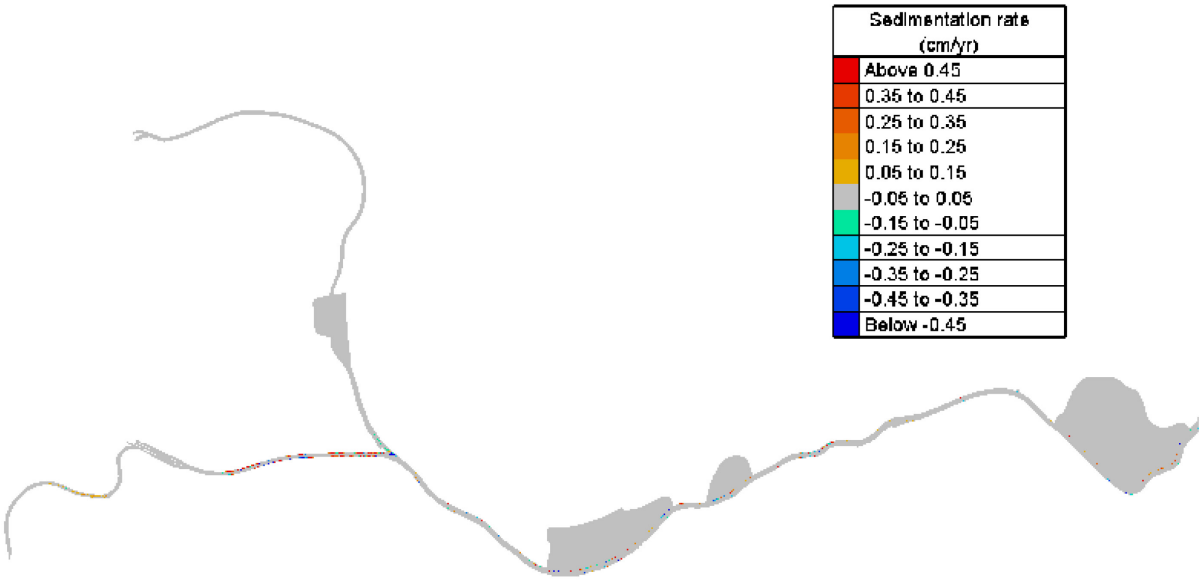

Figure 161 – Difference of sedimentation rate (2050_VaH_AplusCH-2050_REF_AplusCH) – part 4

The VaH alternative has minor influence on the sedimentation rate in general. As shown in the above figures, the differences in most of the domain are negligible. The same as in VaH scenario, the most differences are found in the Upper Sea Scheldt where bathymetric changes are intensive.

(5). Bed shear stress

Changes in bottom shear stress lead to changes in sedimentation/erosion patterns and habitat suitability. Therefore maps are made in the study area of exceedance time (%) of a threshold value of 1 Pa during a spring-neap cycle. A difference map (in %-points) shows the spatial changes.

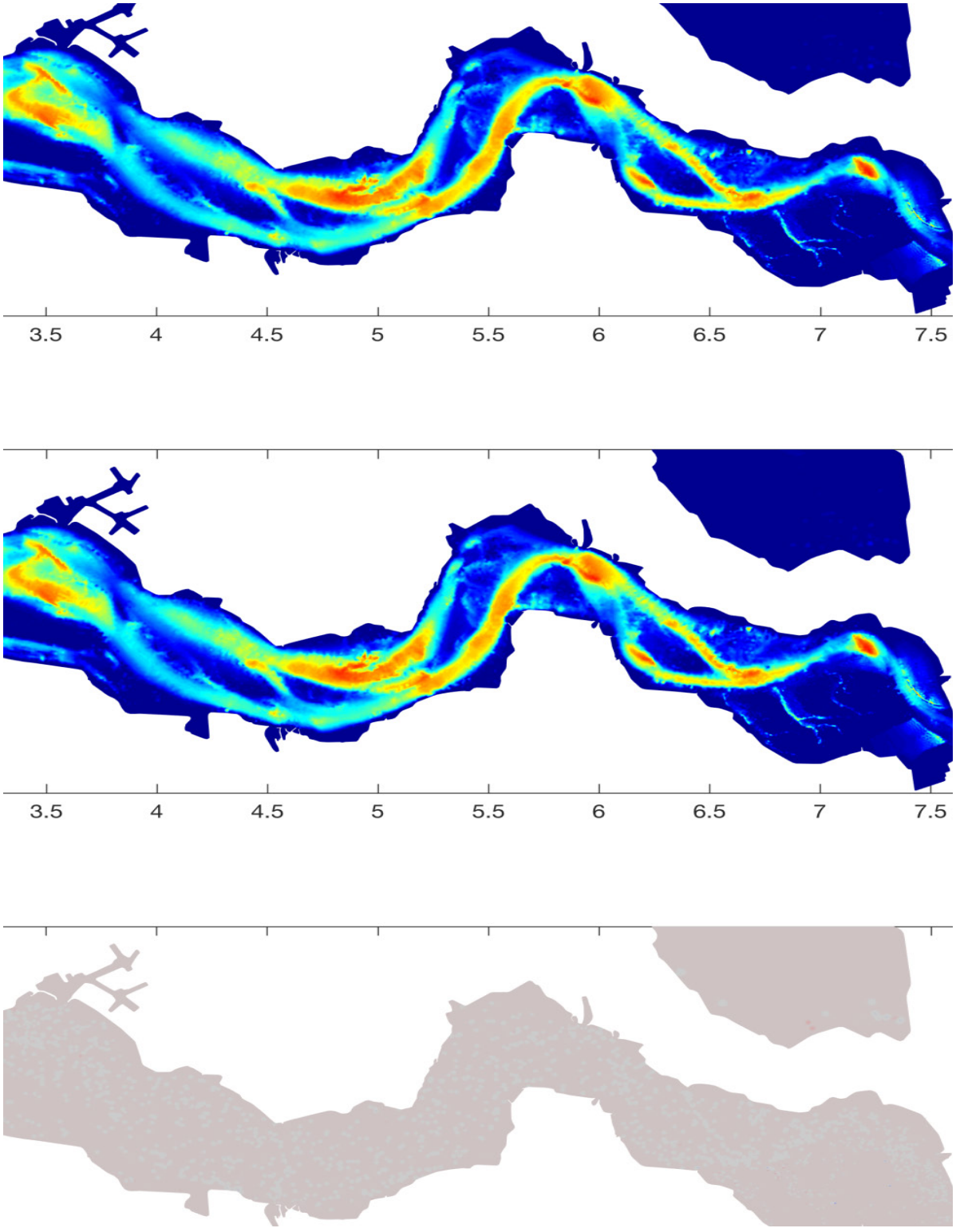

Figure 162 – Exceedance time of bed shear stress >1Pa (%) during a spring-neap cycle in Western Scheldt.
From top to bottom: the reference 2050_REF_AplusCH; the scenario 2050_VaH_AplusCH;
the difference 2050_VaH_AplusCH - 2050_REF_AplusCH.

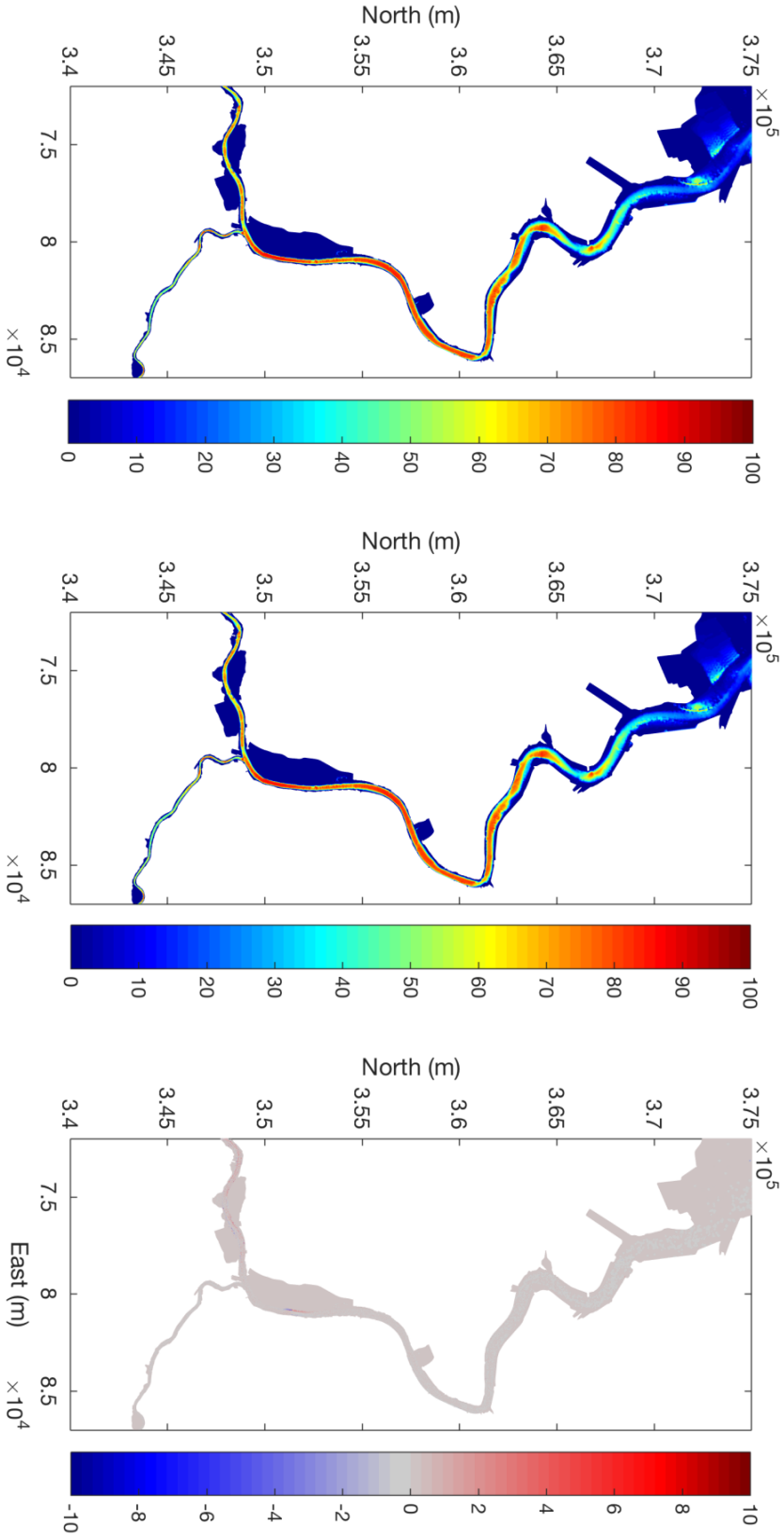

Figure 163 – Exceedance time of bed shear stress >1Pa (%) during a spring-neap cycle in Lower Sea Scheldt.
From top to bottom: the reference 2050_REF_AplusCH; the scenario 2050_VaH_AplusCH;
the difference 2050_VaH_AplusCH - 2050_REF_AplusCH.

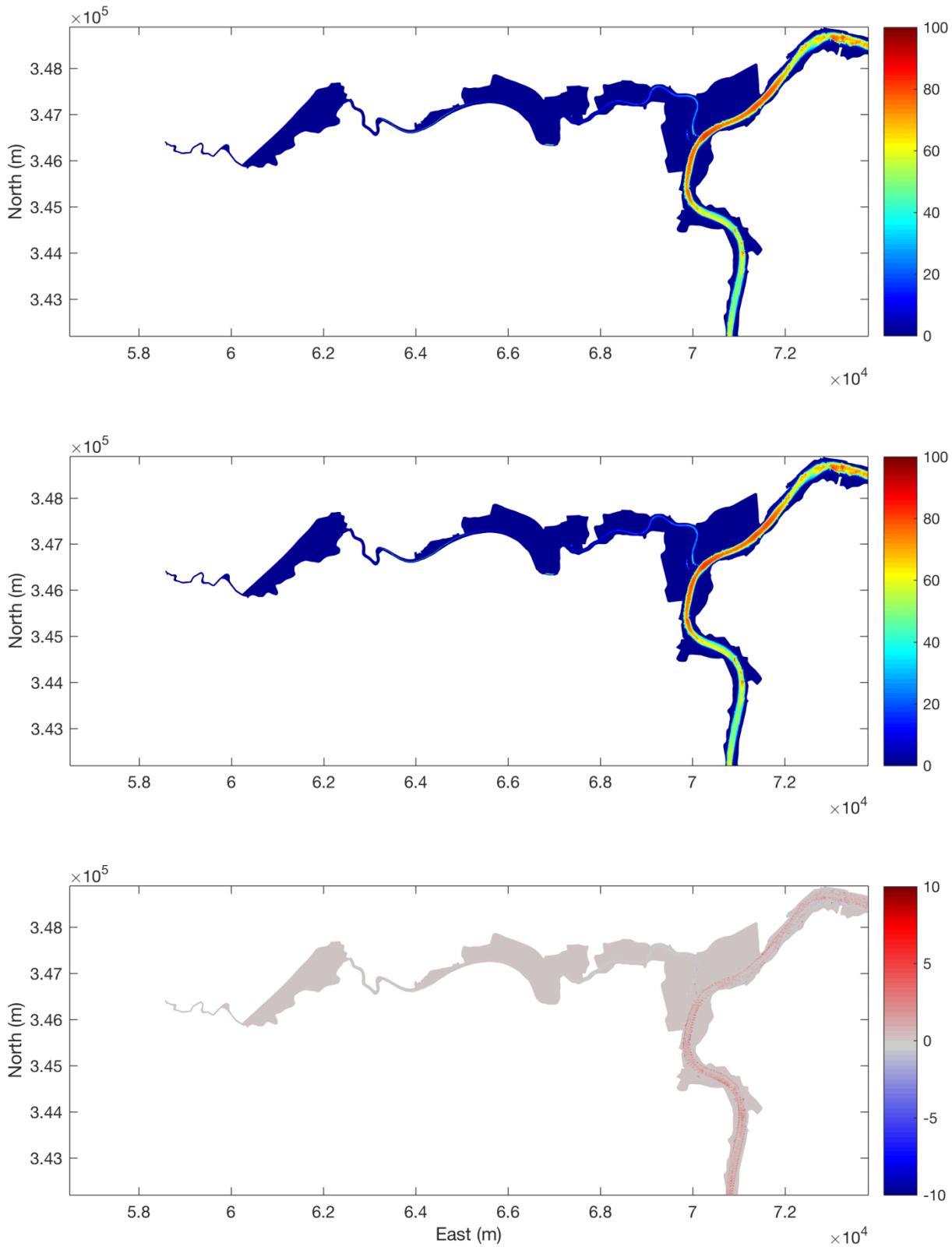

Figure 164 – Exceedance time of bed shear stress >1Pa (%) during a spring-neap cycle in Upper Sea Scheldt.
From top to bottom: the reference 2050_REF_AplusCH; the scenario 2050_VaH_AplusCH;
the difference 2050_VaH_AplusCH - 2050_REF_AplusCH.

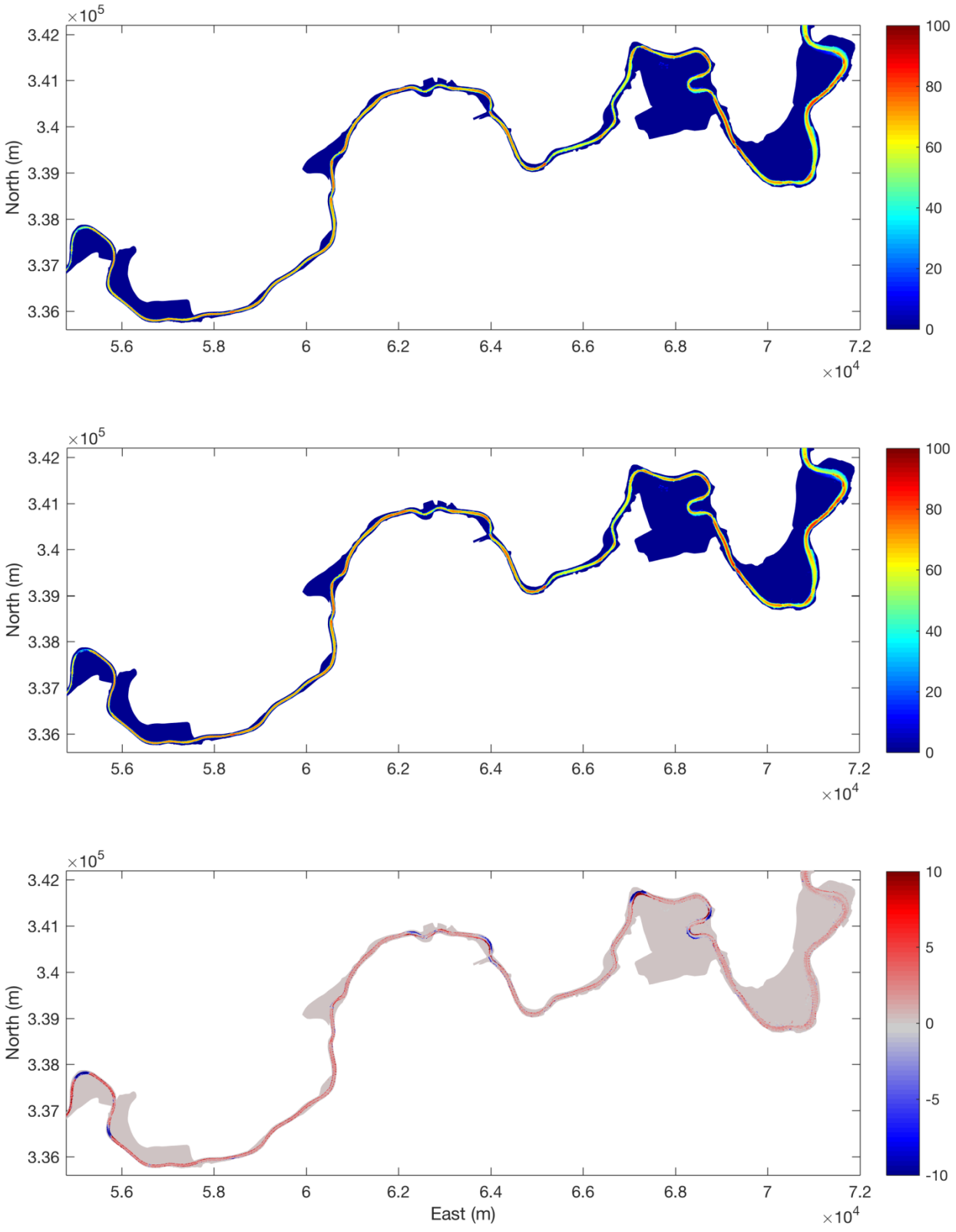

Figure 165 – Exceedance time of bed shear stress >1Pa (%) during a spring-neap cycle in Upper Sea Scheldt.
From top to bottom: the reference 2050_REF_AplusCH; the scenario 2050_VaH_AplusCH;
the difference 2050_VaH_AplusCH – 2050_REF_AplusCH.

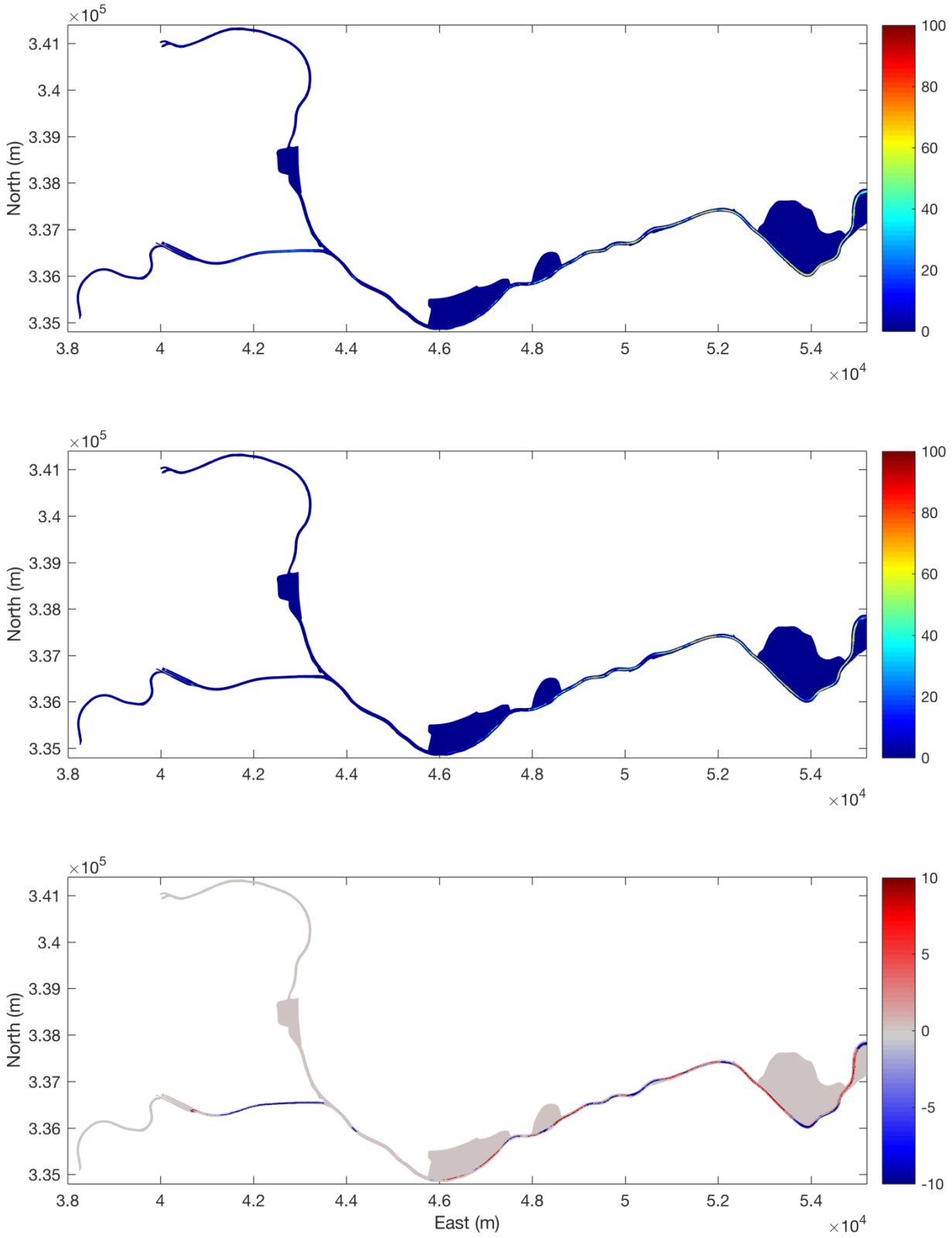

Figure 166 – Exceedance time of bed shear stress >1Pa (%) during a spring-neap cycle in Upper Sea Scheldt.
From top to bottom: the reference 2050_REF_AplusCH; the scenario 2050_VaH_AplusCH;
the difference 2050_VaH_AplusCH - 2050_REF_AplusCH.

(6). Delta SSC

The Delta SSC is calculated based on the equation described in §5.1 and the time averaged Delta SSC is given for each box of the ecosystem model in Figure 167. As it is shown in the figure, the SSC barely changes in the Western Scheldt (from 0 km to 70 km), therefore, the delta SSC stays almost zero in this region. It starts to deviate from zero (also shows temporal variations) at about 110 km compared to 80 km in VaG cases, which suggests the bathymetry changes are generally not as intensive as in VaG scenarios. And further upstream the mean delta SSC becomes negative in the entire Upper Sea Scheldt, except near the upstream boundary at about 170 km.

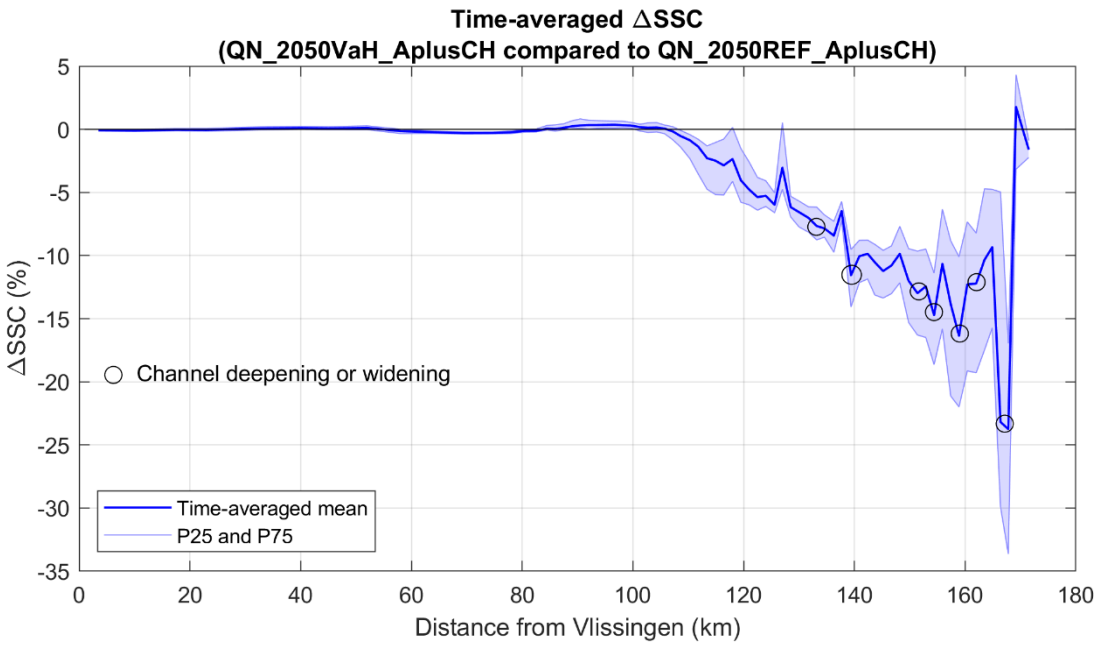

Figure 167 – Delta SSC (2050_VaH_AplusCH compared to 2050_REF_AplusCH)

The locations with intensive bathymetric changes are also plotted in the above figure. In general, channel deepening leads to lower SSC. This is discussed in detail in following section.

(7). Discussion

The bathymetric changes cause changes in velocity as shown in Figure 153. The change of velocity has influences on sediment transport and delta SSC. When velocity is reduced, the bed shear stress decreases as well. Thus more sediment deposits to the bed and less remaining in suspension, which means delta SSC could decrease. If velocity becomes larger, both suspension capacity and erosion capability will increase. If there is enough supply from the source, it will be able to maintain higher suspension concentration in water column. Therefore, based on above reasoning, it is not a surprise that the change of velocity magnitude could affect delta SSC. Figure 153 and Figure 167 shows that in the locations where there are channel deepening or widening, both velocity M_2 amplitude and delta SSC are changed accordingly.

Delta SSC is negative from 165 km to 170 km. This is due to deepening of the channel near Merelbeke. The channel deepening reduces velocity magnitude here, thus more sediment deposits to the bed and less sediment remains available for being transported downstream (Figure 168).

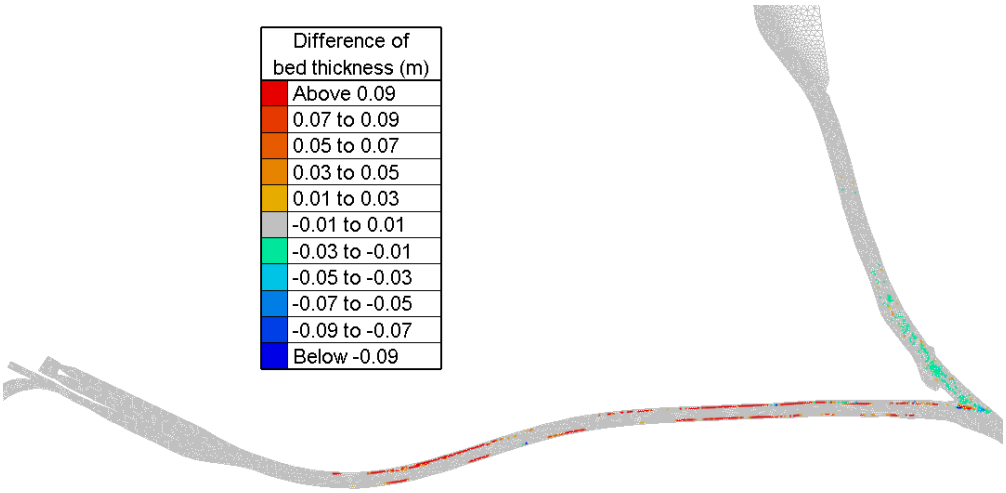

Figure 168 – Difference of bed thickness in the part of channel close to Merelbeke

Delta SSC remains negative in the entire Upper Sea Scheldt. Part of the explanation is that, SSC in this region is mainly determined by the input from upstream. More sediment deposited near Merelbeke means less sediment is transported downstream

5.4 Effect of Chafing

The scenario 2050_Chafing_AplusCH has less intensive bathymetry changes compared to 2050_VaG_AplusCH. Actually this scenario is similar to 2050_VaH_AplusCH, consisting of only deepening and/or widening channels in the Upper Sea Scheldt. For the rest of the model settings, they are identical to the reference 2050_REF_AplusCH.

(1). The difference in hydrodynamics

The water level M2 and M4 amplitudes are shown in Figure 169 and Figure 170. As seen in these figures, the differences are smaller than they are found in the VaG and VaH scenarios, because the Chafing scenario has the least intensive bathymetric changes among all the three B-alternatives. Generally speaking, both M2 and M4 amplitudes becomes larger between 130 km and 170 km, which is possibly due to higher water depth, thus smaller bottom friction caused by bottom alternations.

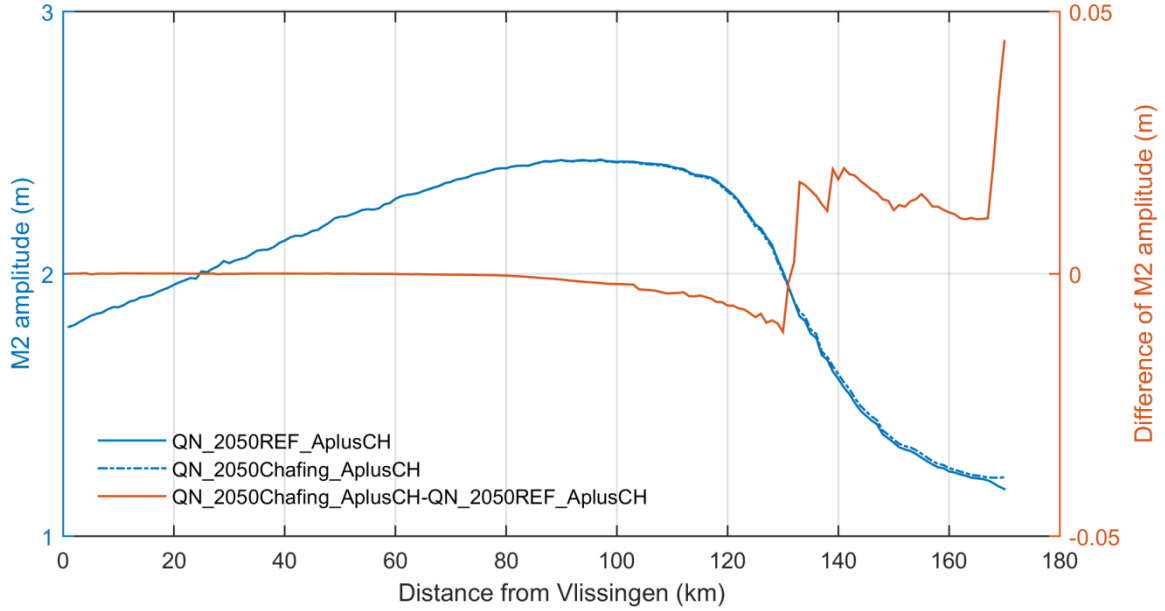

Figure 169 – Comparison of M2 amplitude between 2050_REF_AplusCH and 2050_Chafing_AplusCH

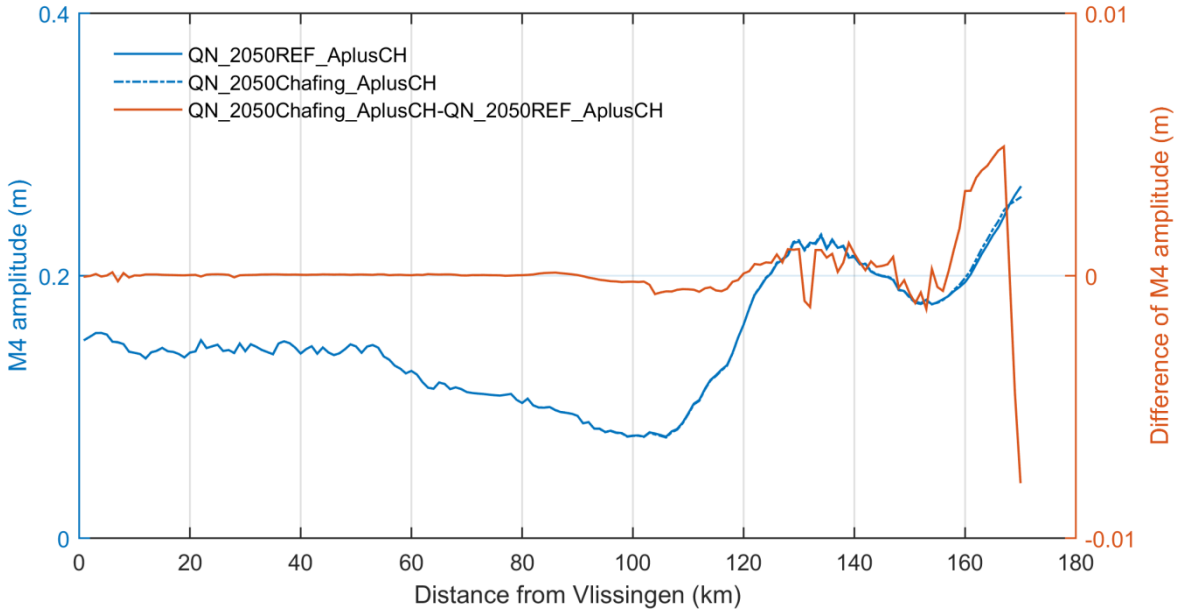

Figure 170 – Comparison of M4 amplitude between 2050_REF_AplusCH and 2050_Chafing_AplusCH

The effect on M2 velocity amplitude is shown in Figure 171.

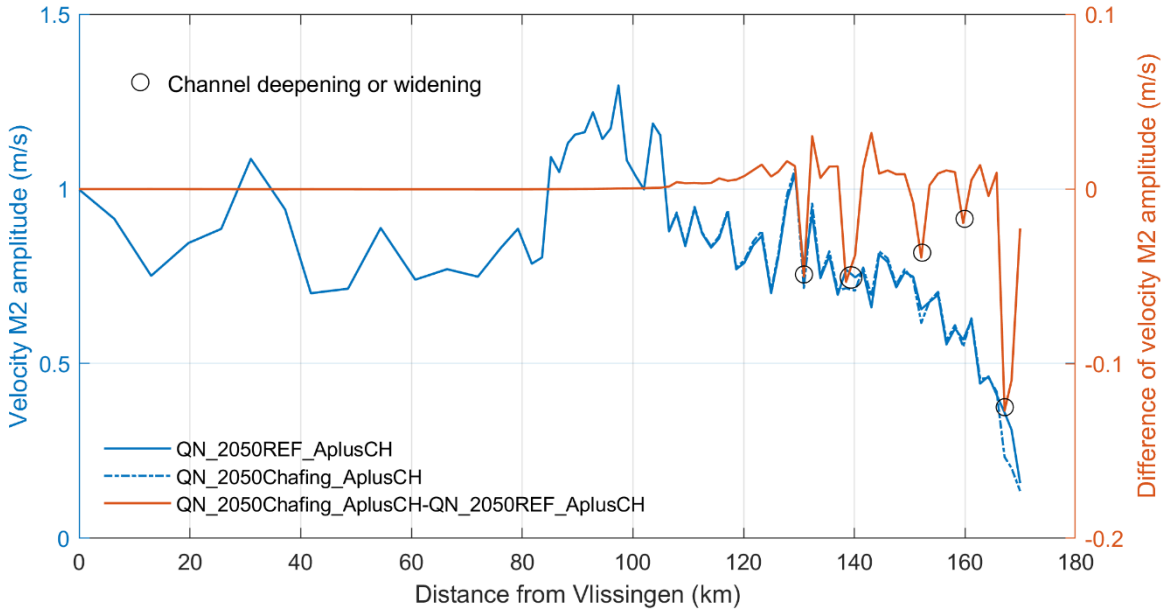

Figure 171 – Comparison of M2 amplitude of cross-sectionally averaged velocity between 2050_REF_AplusCH and 2050_Chafing_AplusCH

(2). The change of tidal asymmetry

All the tidal asymmetry indicators as mentioned in §4.8, are calculated in this section. These indicators, 8 in total, are organized in 3 groups, based on time duration, velocity magnitude and skewness, respectively.

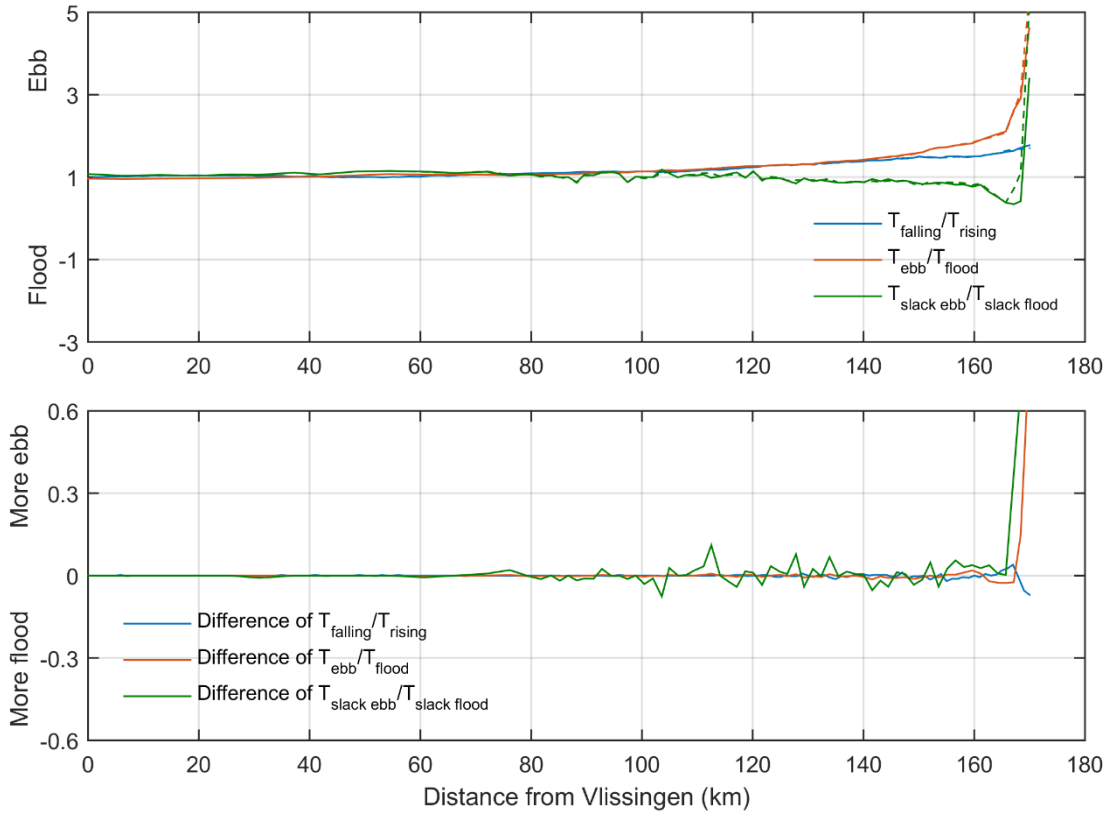

Figure 172 – Indicators of tidal asymmetry (durations).
Solid lines represent the reference 2050_REF_AplusCH, dashed lines represent the scenario 2050_Chafing_AplusCH.

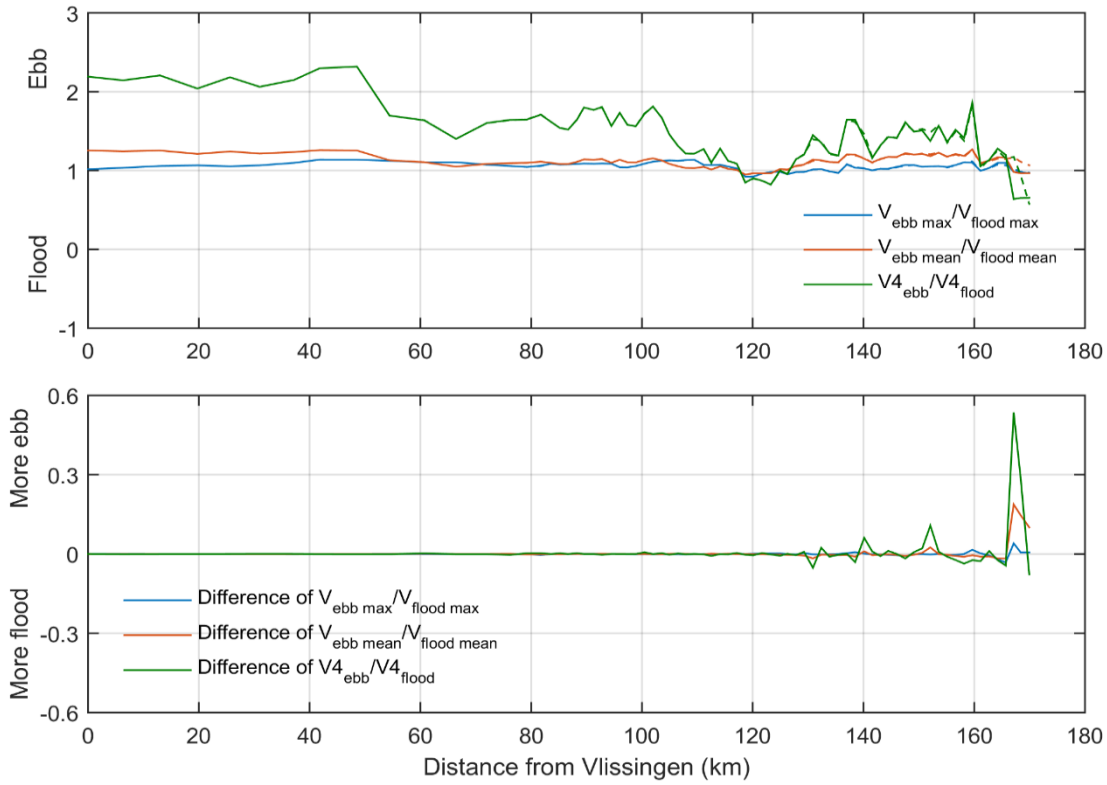

Figure 173 – Indicators of tidal asymmetry (velocities).
Solid lines represent the reference 2050_REF_AplusCH, dashed lines represent the scenario 2050_Chafing_AplusCH.

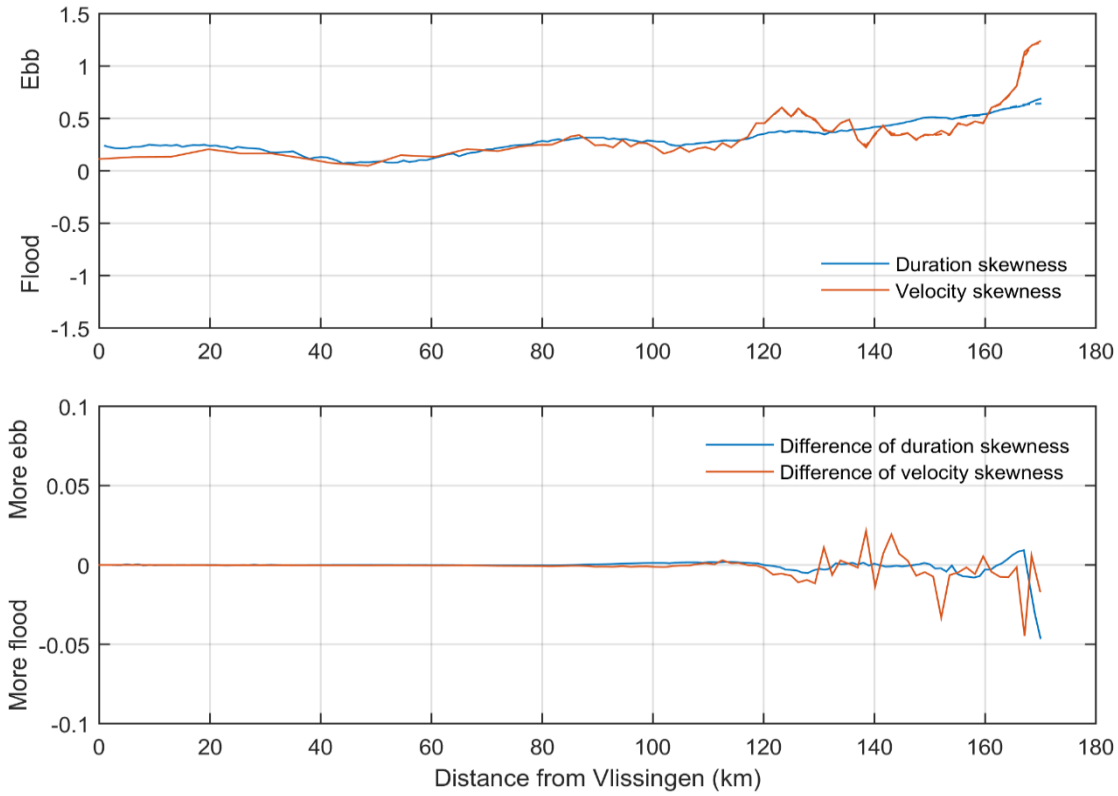

Figure 174 – Indicators of tidal asymmetry (skewness).
Solid lines represent the reference 2050_REF_AplusCH, dashed lines represent the scenario 2050_Chafing_AplusCH.

(3). Sediment Transport Decomposition

Figure 175 shows the sediment transport decomposed according to §4.7. It shows a very similar pattern as in the comparison of 2050_VaH_AplusCH to the reference case. A slightly higher sediment input at upstream boundary due to the change of tidal asymmetry and the total sediment transport becomes lower due to the deepening of the channel from 170 km to 165 km.

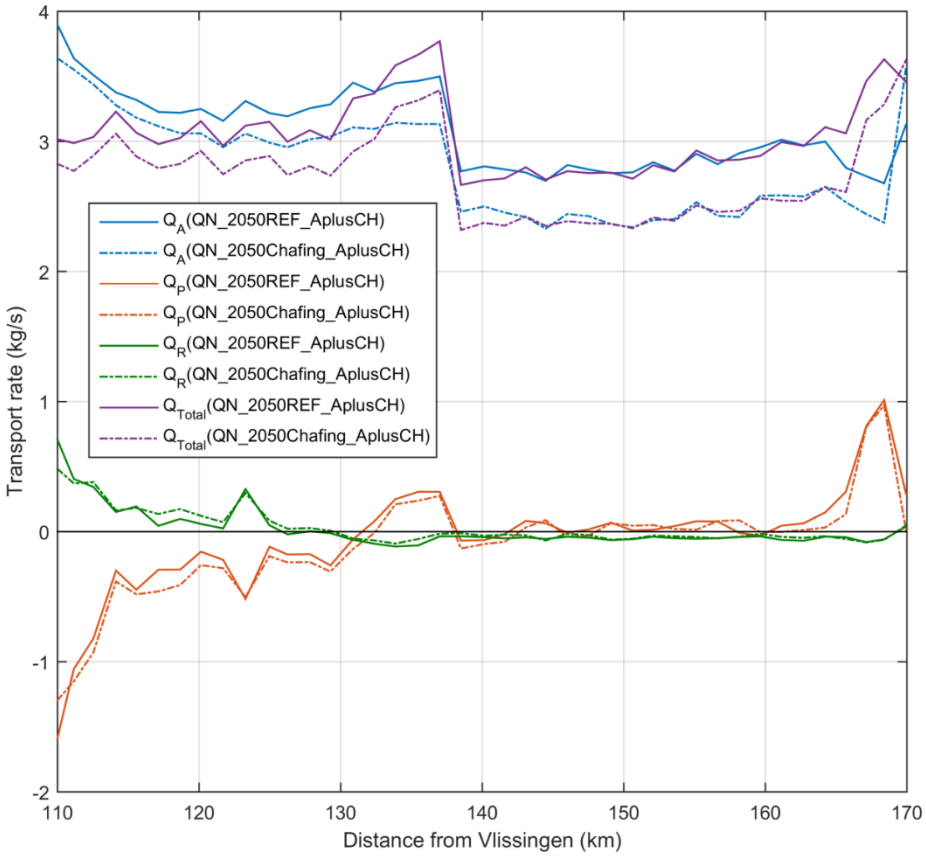

Figure 175 – Time-averaged decomposed sediment transport rate QA, QP and QR in the Upper Sea Scheldt.
Positive sign means downstream direction and negative means upstream direction

In general, Chafing has less intensive bathymetric changes as in VaH and VaG, thus, less differences in the decomposed sediment flux.

(4). Erosion-deposition map

The difference of sedimentation rate is calculated between the run 2050_Chafing_AplusCH and 2050_REF_A0CN using the bed layer thickness given in the result files. The sedimentation rate is based on the production period of the last 20 days and it is converted to cm/yr.

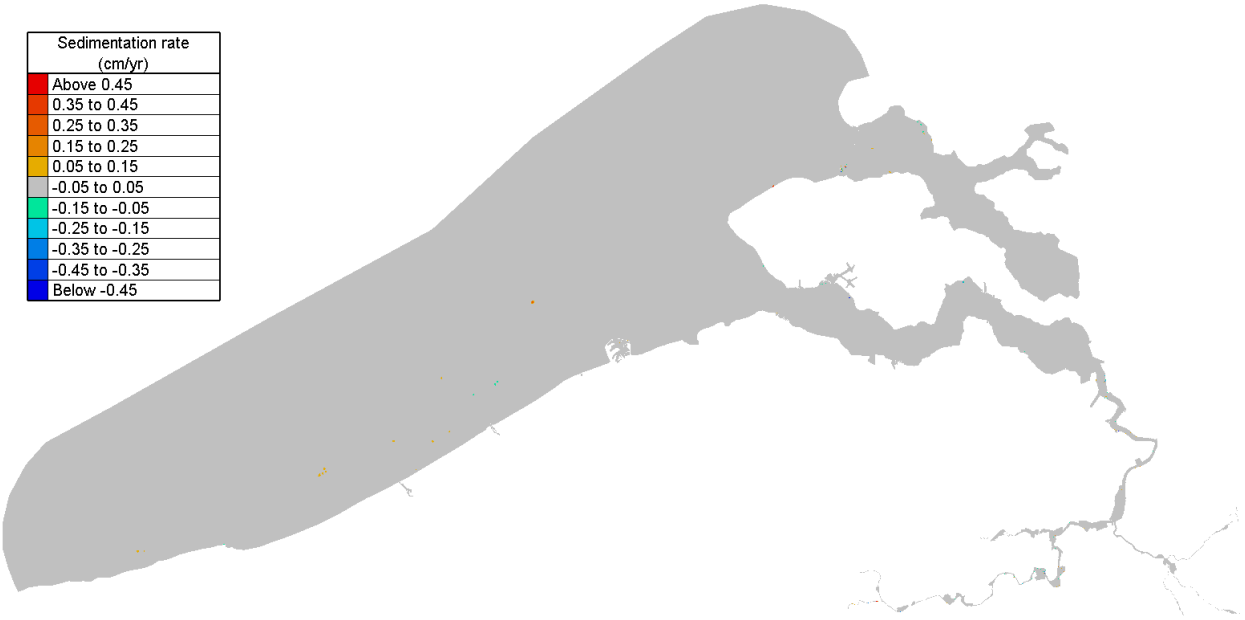

Figure 176 – Difference of sedimentation rate (2050_Chafing_AplusCH-2050_REF_AplusCH) – part 1

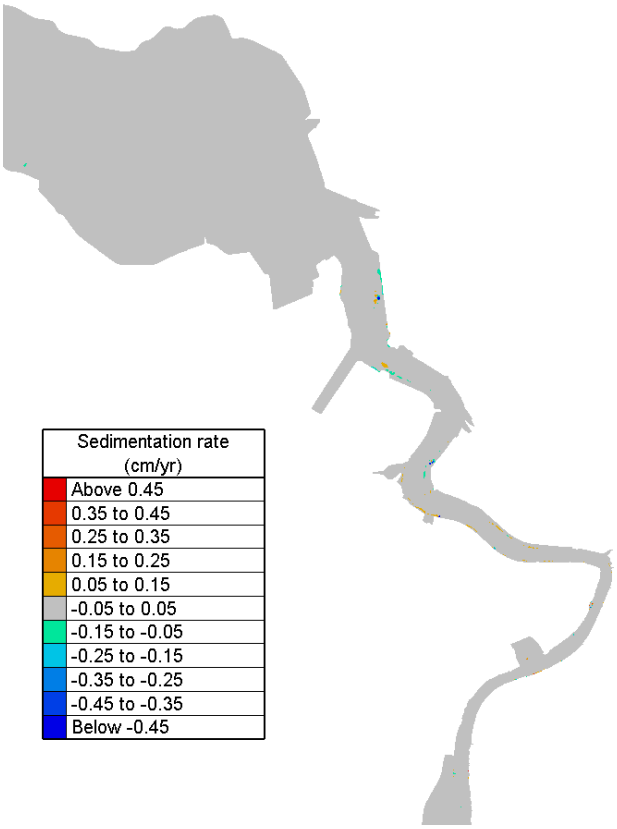

Figure 177 – Difference of sedimentation rate (2050_Chafing_AplusCH-2050_REF_AplusCH) – part 2

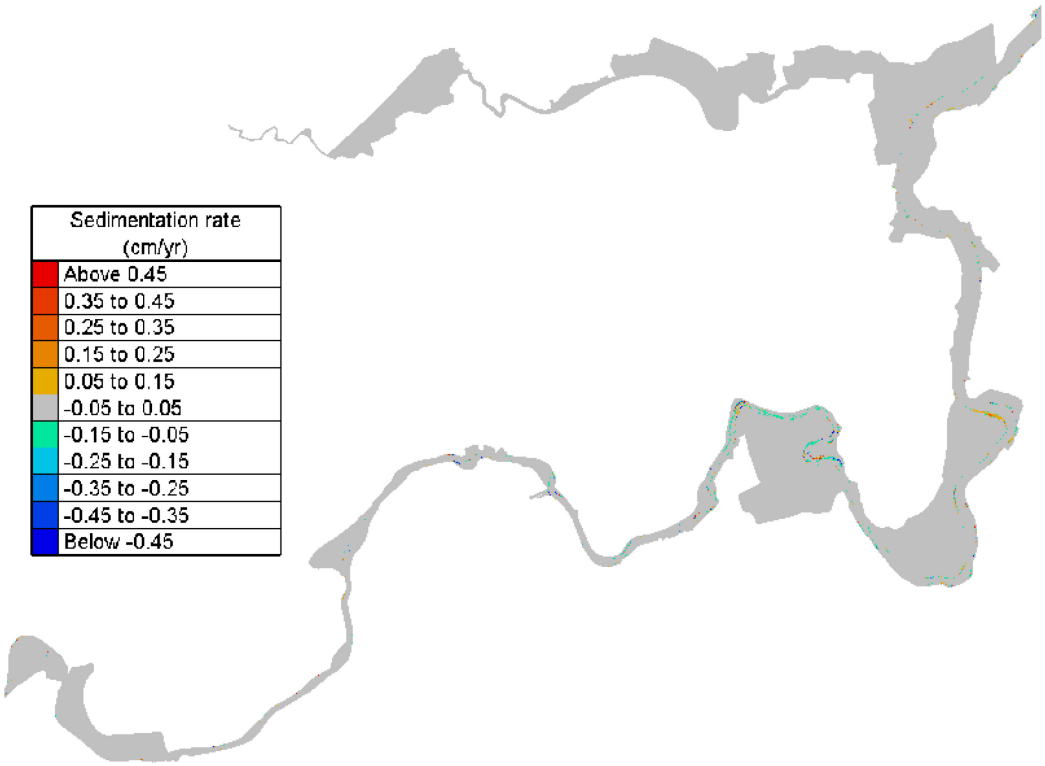

Figure 178 – Difference of sedimentation rate (2050_Chafing_AplusCH-2050_REF_AplusCH) – part 3

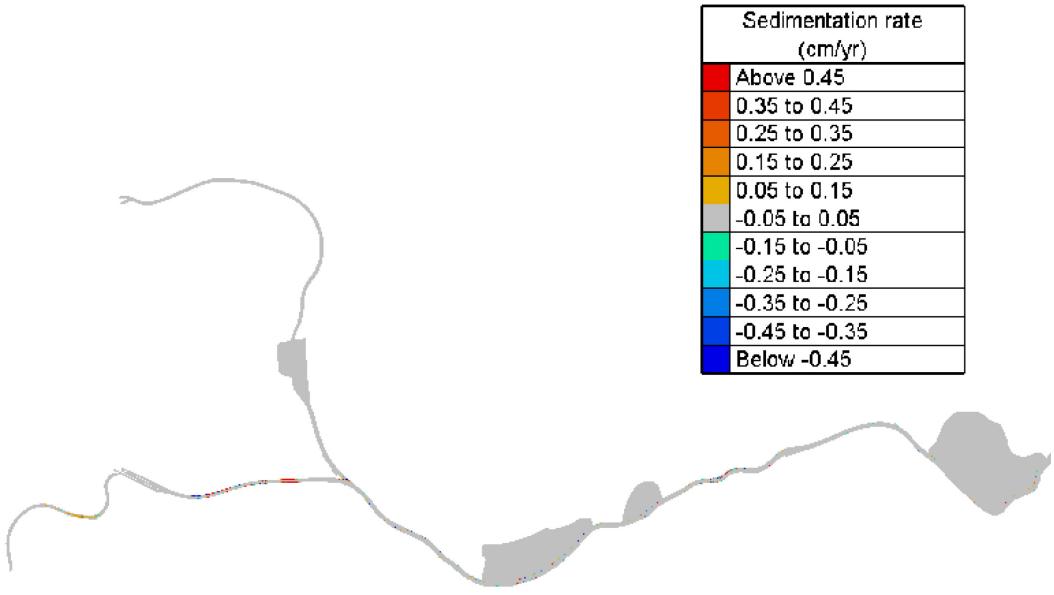

Figure 179 – Difference of sedimentation rate (2050_Chafing_AplusCH-2050_REF_AplusCH) – part 4

The Chafing alternative is similar to VaH scenario in terms of the influence on sedimentation rate. As shown in the above figures, the differences in most of the domain are negligible, except that the most differences are found in the Upper Sea Scheldt where bathymetric changes are intensive.

(5). Bed shear stress

Changes in bottom shear stress lead to changes in sedimentation/erosion patterns and habitat suitability. Therefore maps are made in the study area of exceedance time (%) of a threshold value of 1 Pa during a spring-neap cycle. A difference map (in %-points) shows the spatial changes.

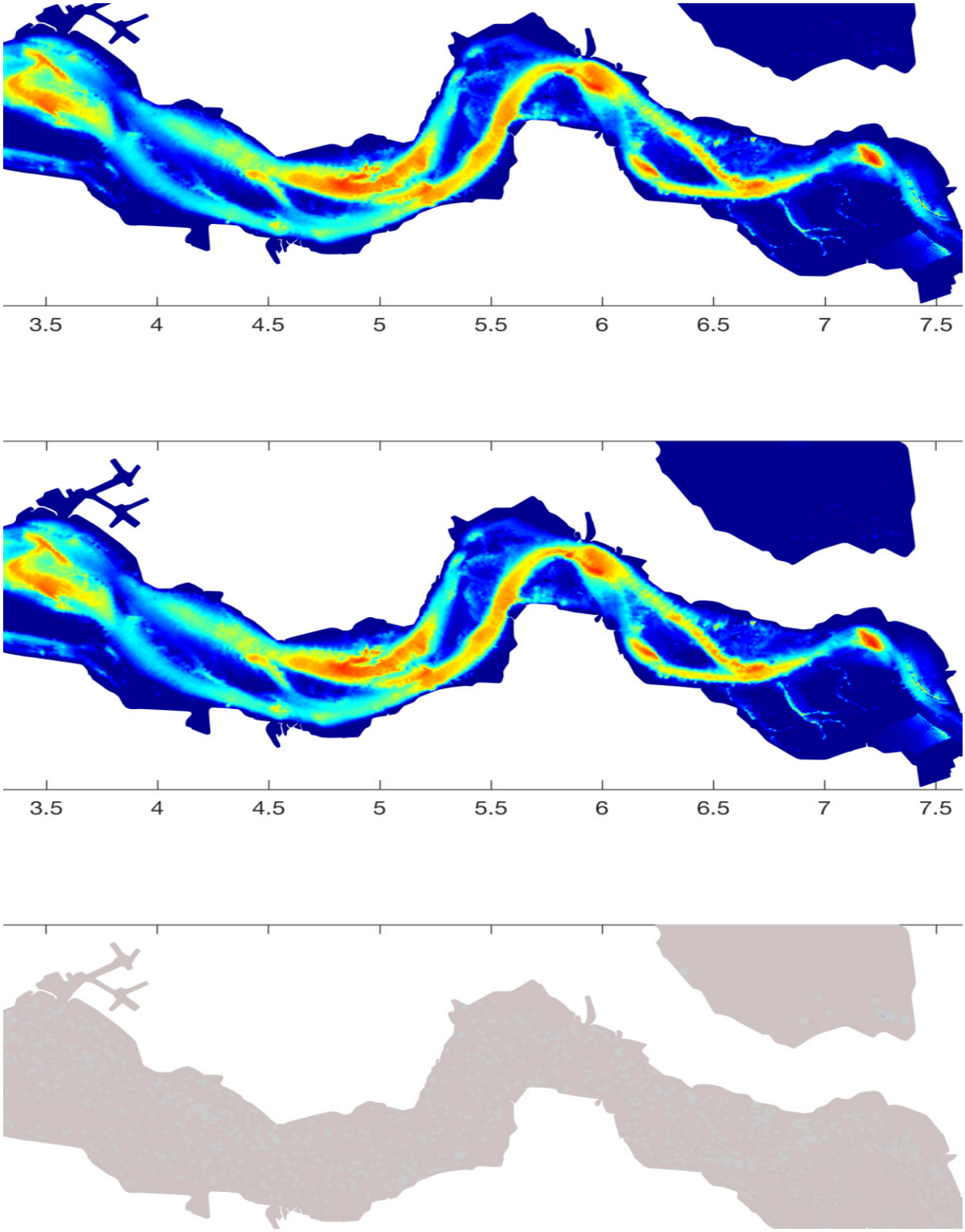

Figure 180 – Exceedance time of bed shear stress >1Pa (%) during a spring-neap cycle in Western Scheldt.
From top to bottom: the reference 2050_REF_AplusCH; the scenario 2050_Chafing_AplusCH;
the difference 2050_Chafing_AplusCH – 2050_REF_AplusCH.

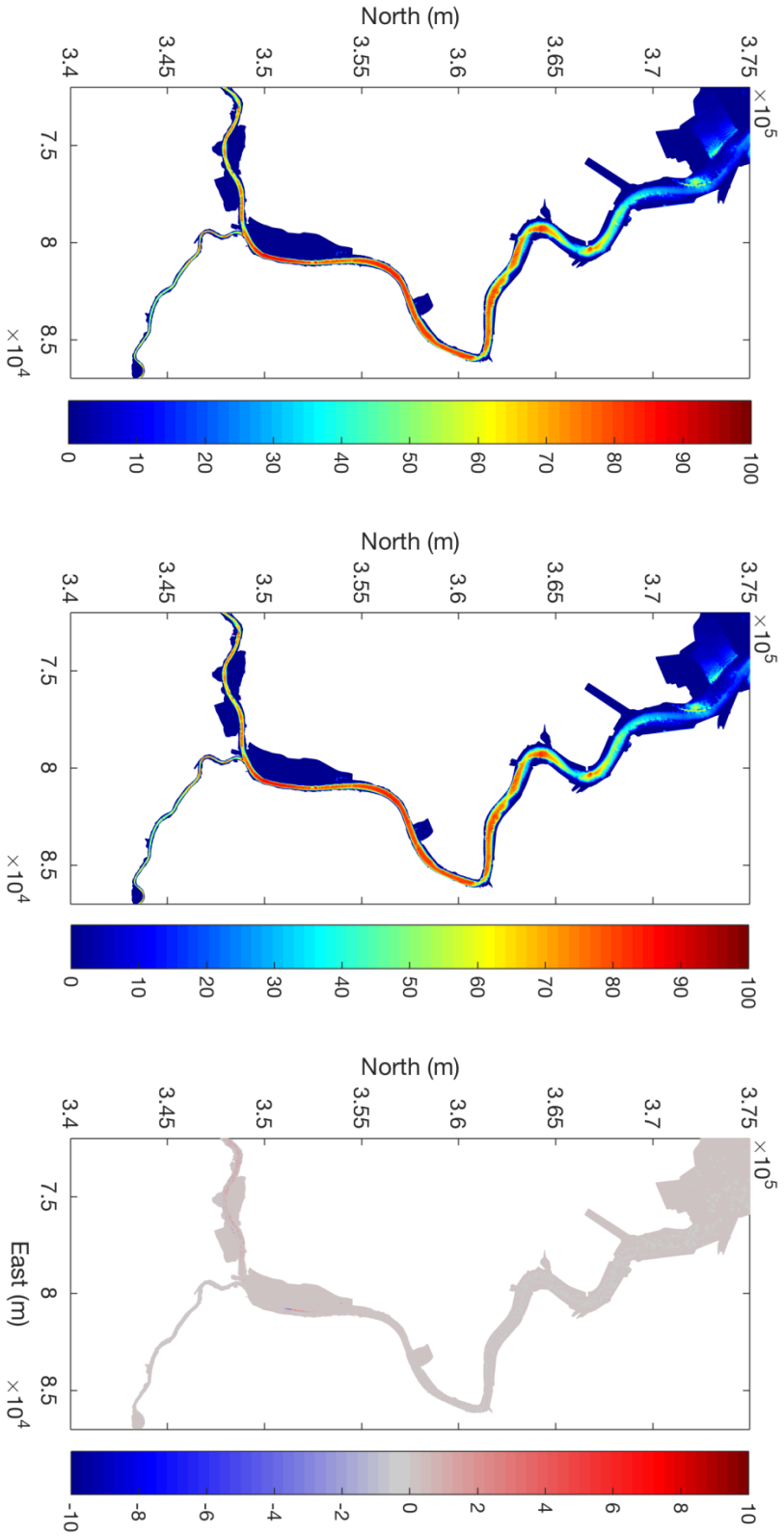

Figure 181 – Exceedance time of bed shear stress >1Pa (%) during a spring-neap cycle in Lower Sea Scheldt.
From top to bottom: the reference 2050_REF_AplusCH; the scenario 2050_Chafing_AplusCH;
the difference 2050_Chafing_AplusCH - 2050_REF_AplusCH.

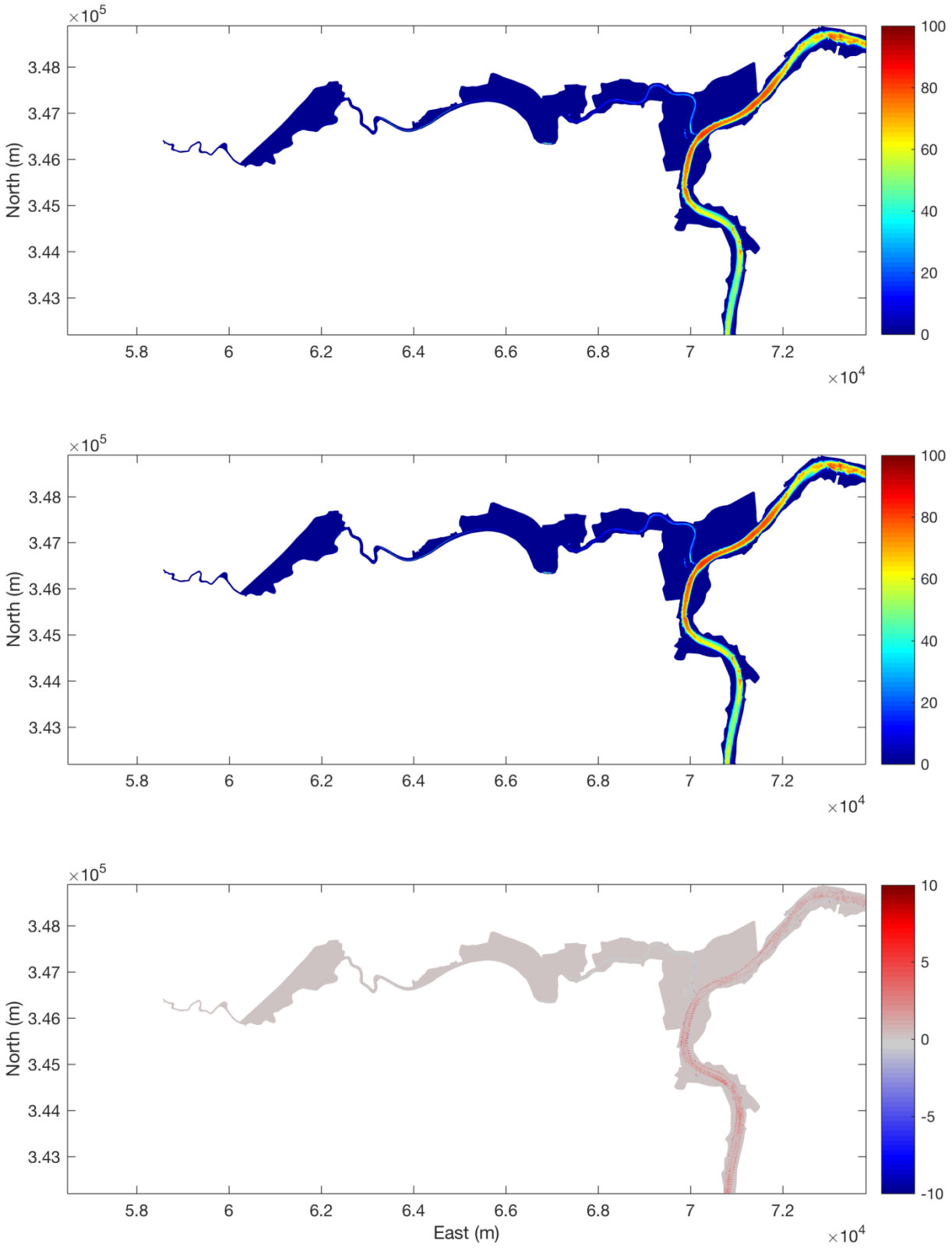

Figure 182 – Exceedance time of bed shear stress >1Pa (%) during a spring-neap cycle in Upper Sea Scheldt.
From top to bottom: the reference 2050_REF_AplusCH; the scenario 2050_Chafing_AplusCH;
the difference 2050_Chafing_AplusCH - 2050_REF_AplusCH.

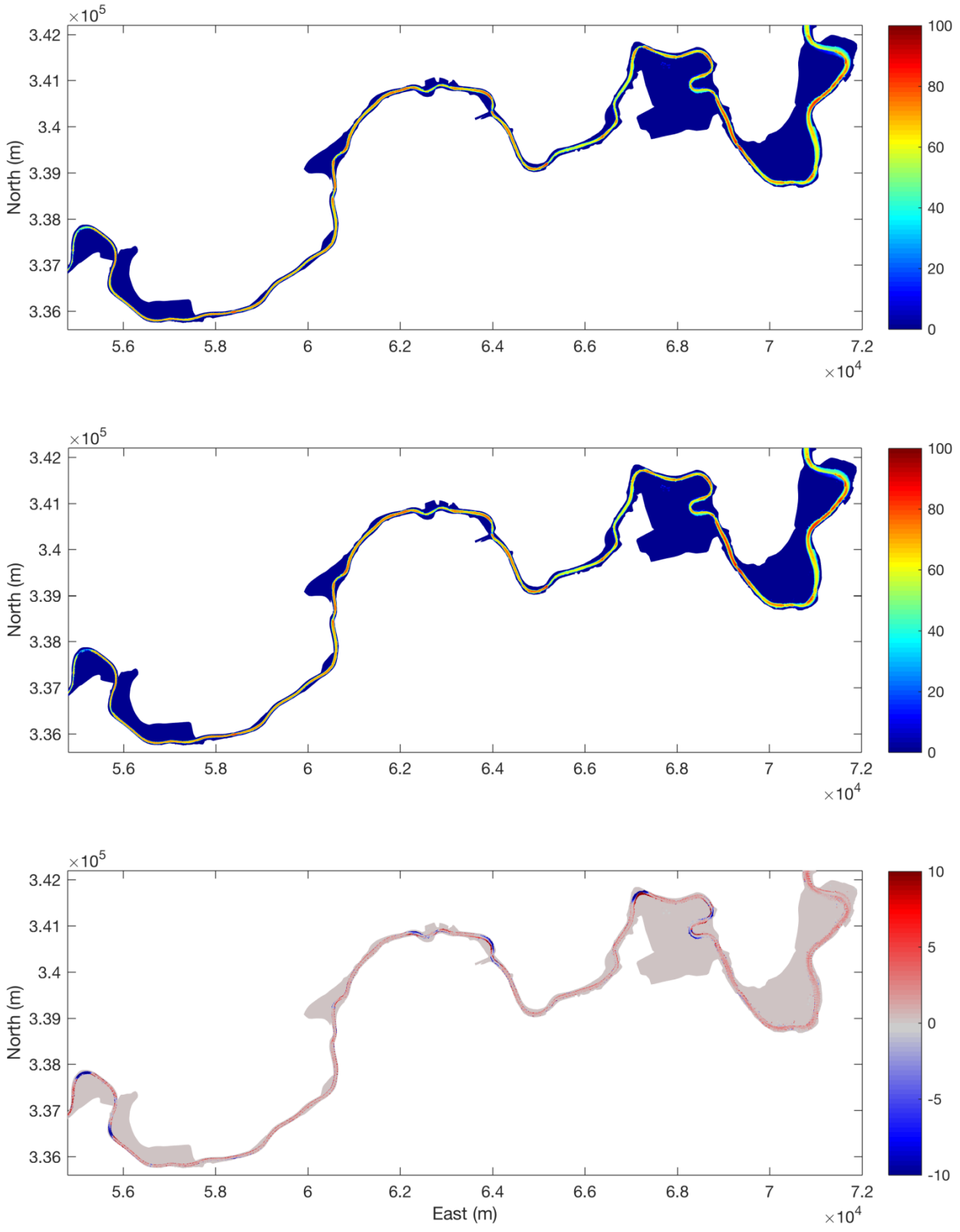

Figure 183 – Exceedance time of bed shear stress >1Pa (%) during a spring-neap cycle in Upper Sea Scheldt.
From top to bottom: the reference 2050_REF_AplusCH; the scenario 2050_Chafing_AplusCH;
the difference 2050_Chafing_AplusCH – 2050_REF_AplusCH.

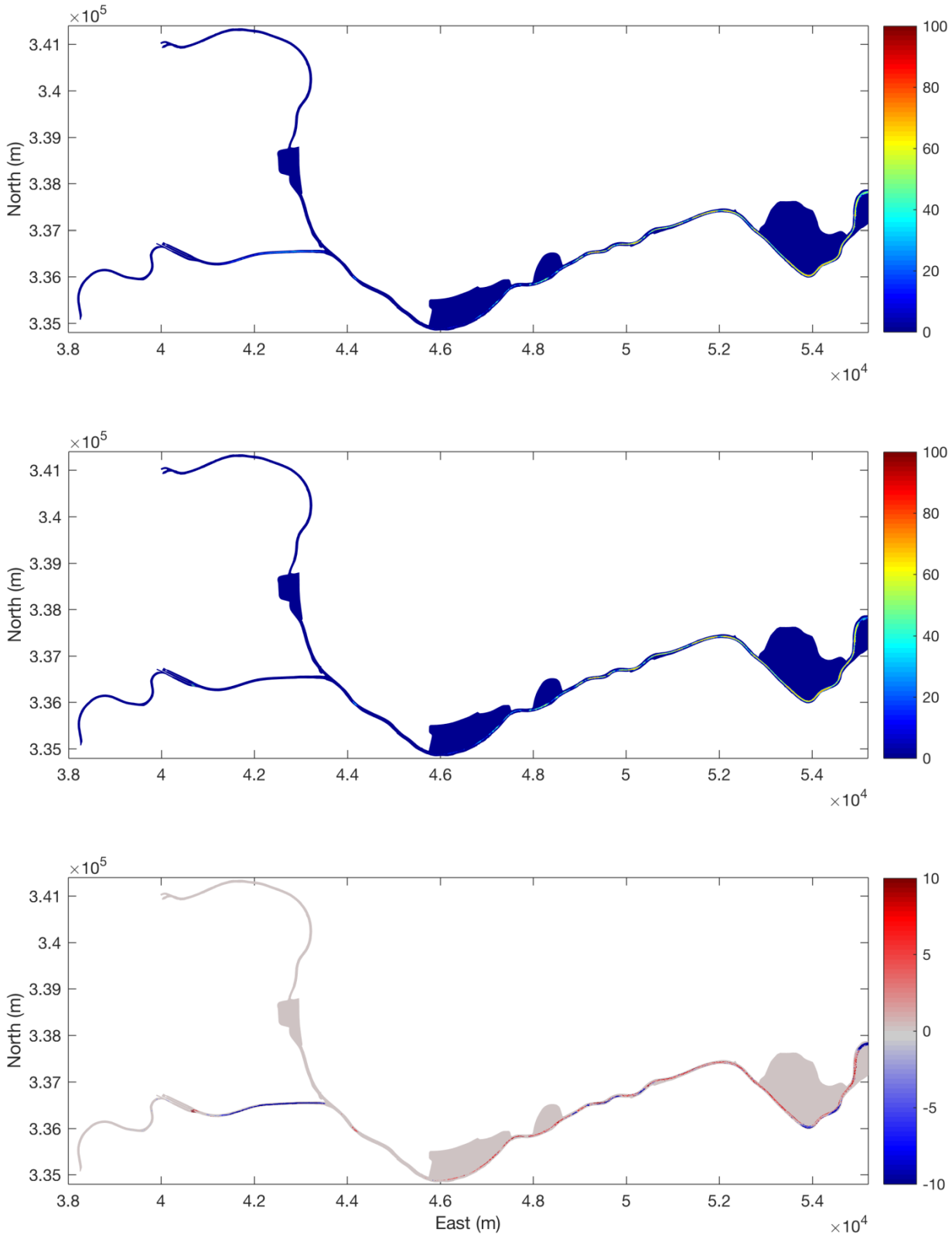

Figure 184 – Exceedance time of bed shear stress >1Pa (%) during a spring-neap cycle in Upper Sea Scheldt.
From top to bottom: the reference 2050_REF_AplusCH; the scenario 2050_Chafing_AplusCH;
the difference 2050_Chafing_AplusCH - 2050_REF_AplusCH.

(6). Delta SSC

The Delta SSC is calculated based on equation described in §5.1 and the time averaged Delta SSC is given for each box of the ecosystem model in Figure 185.

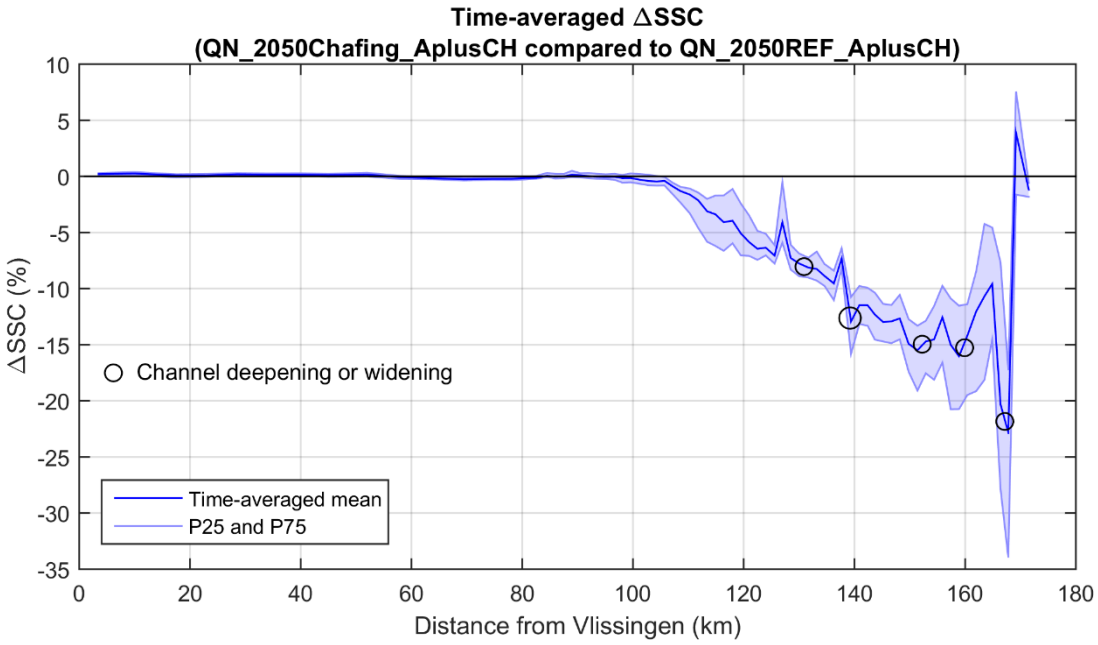

Figure 185 – Delta SSC (2050_Chafing_AplusCH compared to 2050_REF_AplusCH)

As it is shown in the figure, the SSC stays almost the same as in the reference case in the area from 0 km to 130 km, therefore, the delta SSC stays almost zero in this region. It starts to deviate from zero (also shows temporal variations) at about 100 km. And further upstream the mean delta SSC becomes negative in the entire Upper Sea Scheldt, except near the upstream boundary at about 170 km. The locations with intensive bathymetric changes are also plotted in the above figure. In general, channel deepening leads to lower SSC. This is discussed in detail in following section.

(7). Discussion

The bathymetric changes cause changes in velocity as shown in Figure 171. The change of velocity has influences on sediment transport and delta SSC. When velocity is reduced, the bed shear stress decreases as well. Thus more sediment deposits to the bed and less remaining in suspension, which means delta SSC could decrease. If velocity becomes larger, both suspension capacity and erosion capability will increase. If there is enough supply from the source, it will be able to maintain higher suspension concentration in water column. Therefore, based on above reasoning, it is not a surprise that the change of velocity magnitude could affect delta SSC. Figure 171 and Figure 185 shows that in the locations where there are channel deepening or widening, both velocity M_2 amplitude and delta SSC are changed accordingly.

Delta SSC is negative from 165 km to 170 km. This is due to deepening of the channel near Merelbeke, which is the same situation as in VaH and VaG. The channel deepening reduces velocity magnitude here, thus more sediment deposits to the bed and less sediment remains available for being transported downstream (Figure 186). This means less sediment will be transported downstream. This is consistent with the trend found in the analysis of decomposed sediment fluxes.

Delta SSC remains negative in the entire Upper Sea Scheldt. Part of the explanation is that, SSC in this region is mainly determined by the input from upstream. More sediment deposited near Merelbeke means less sediment is transported downstream.

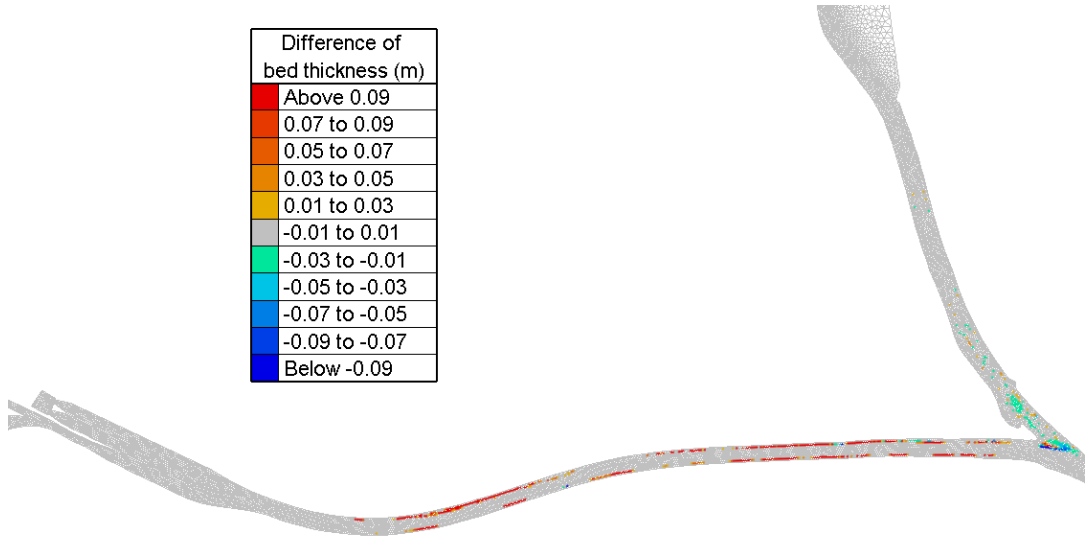

Figure 186 – Difference (alternative – reference) of bed thickness at the end of the run, in the part of channel close to Merelbeke. Positive values mean more deposition in the alternative.

5.5 Conclusion: the B-alternatives

5.5.1 Influence on delta SSC

All the three B-alternatives give negative delta SSC in the Upper Sea Scheldt, except near the upstream boundary at 170 km. However, their influence in the rest of the domain, from 0 km to 100 km is not noticeable.

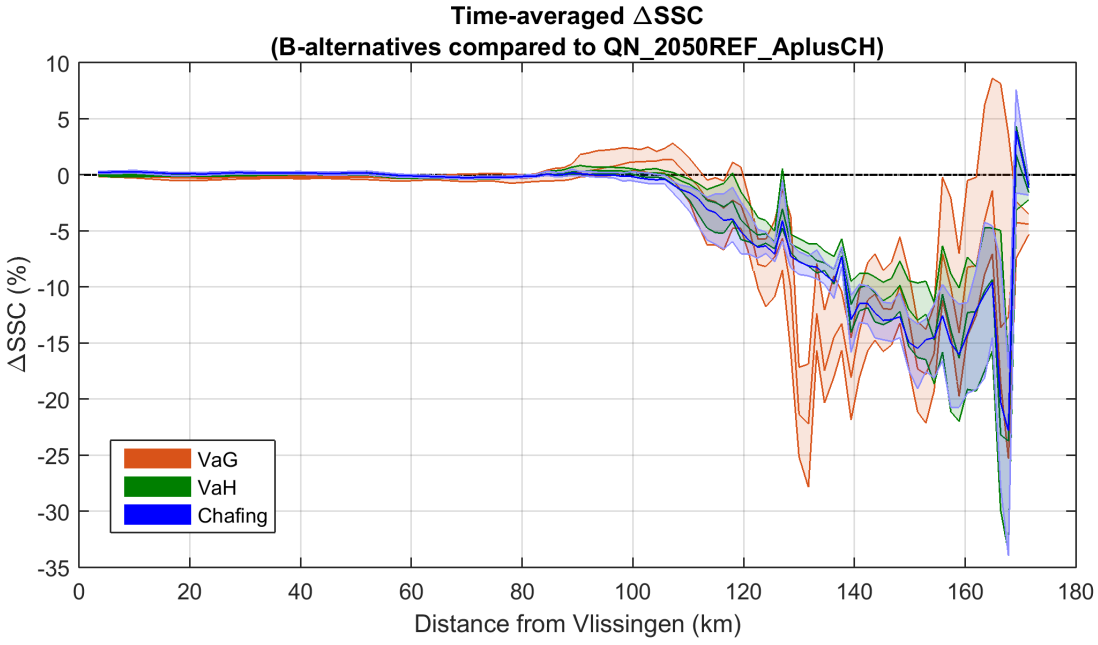

Figure 187 – Time-averaged Delta SSC (B-alternatives compared to 2050_REF_AplusCH)

The bathymetric changes in all three B-alternatives have a clear local influence. They affect the local velocity, thus the available energy in the flow. This directly influences SSC.

The channel deepening near the upstream boundary, from approximately 165 km to 170 km plays an important role in all three scenarios. It acts like a sediment sink, causing less sediment transport downstream. This equals to a lower sediment input for the Upper Sea Scheldt. Note however that this is only the immediate effect. Since there is no feedback in the calculation from sediment deposition to bathymetry, the sediment sink can fill in indefinitely.

5.5.2 Sedimentation on tidal flats

Figure 188 shows the difference of mass deposited on tidal flats in 2050_VaG_AplusCH, 2050_VaH_AplusCH and 2050_Chafing_AplusCH, compared to the reference 2050_REF_AplusCH.

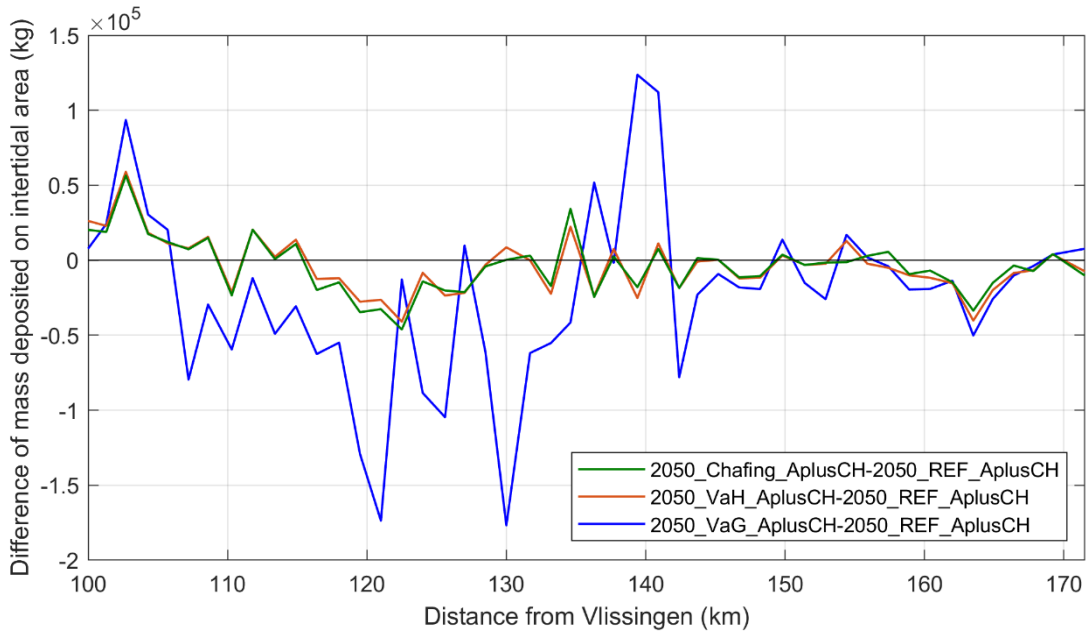

Figure 188 – Comparison of mass deposited on tidal flats
(2050_VaG_AplusCH, 2050_VaH_AplusCH and 2050_Chafing_AplusCH, compared to 2050_REF_AplusCH).

There are several reasons for the change of mass deposited on tidal flats. The most obvious is that a higher/lower SSC at certain locations leads to more/less deposition on the nearby tidal flats. In general, mass deposited on tidal flats tends decreases in all the three B-alternatives since SSC drops in all these scenarios. This is especially true in the areas from 105 km to 133 km, and from 158 km to 168 km. However, there are also some exceptions. For example, in VaG scenario, mass deposited on tidal flats becomes larger at about 140 km. This is due to complex changes in hydrodynamics in this area. As shown in Figure 189, the difference of flow velocity in VaG suggests the sediment is likely to be trapped on tidal flats due to the residual flow, whereas this is not the case in VaH (and in Chafing).

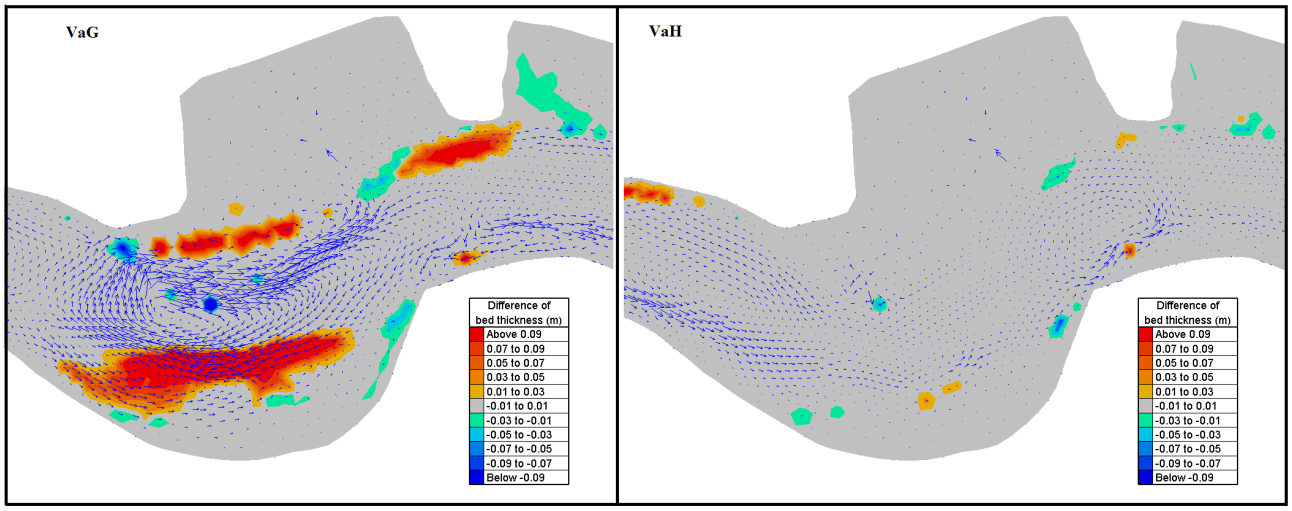

Figure 189 – Comparison of mass deposited on tidal flats between VaG and VaH alternatives at 140 km (arrows meaning the time-averaged difference of velocity vectors compared to 2050_REF_AplusCH)

5.5.3 Influence on dredging

Lower Sea Scheldt

The influence on the sedimentation in the access channels and Deurganck dock (DGD) is investigated. Their locations are indicated in Figure 32. It can be seen in Table 8 that the influence of B-alternatives on dredging in the Lower Sea Scheldt rate is negligible. None of them exceeds ±0.12%.

Table 8 – Sedimentation rate in the Lower Sea Scheldt and the comparison between the scenarios (B-alternatives)

Runs	Sedimentation (MT/yr)	Difference compared to 2050_REF_AminCL	Difference compared to 2050_REF_AplusCH
2050_REF_AminCL	3.0129	/	/
2050_VaG_AminCL	3.0152	+0.08%	/
2050_REF_AplusCH	3.1257	/	/
2050_VaG_AplusCH	3.1230	/	-0.09%
2050_VaH_AplusCH	3.1221	/	-0.12%
2050_Chafing_AplusCH	3.1221	/	-0.12%

The sedimentation rate in each dredging location is also calculated and shown in Figure 190. It can be seen that the total sedimentation rates in the runs under climate scenario AplusCH tend to be slightly more than those under AminCL scenarios.

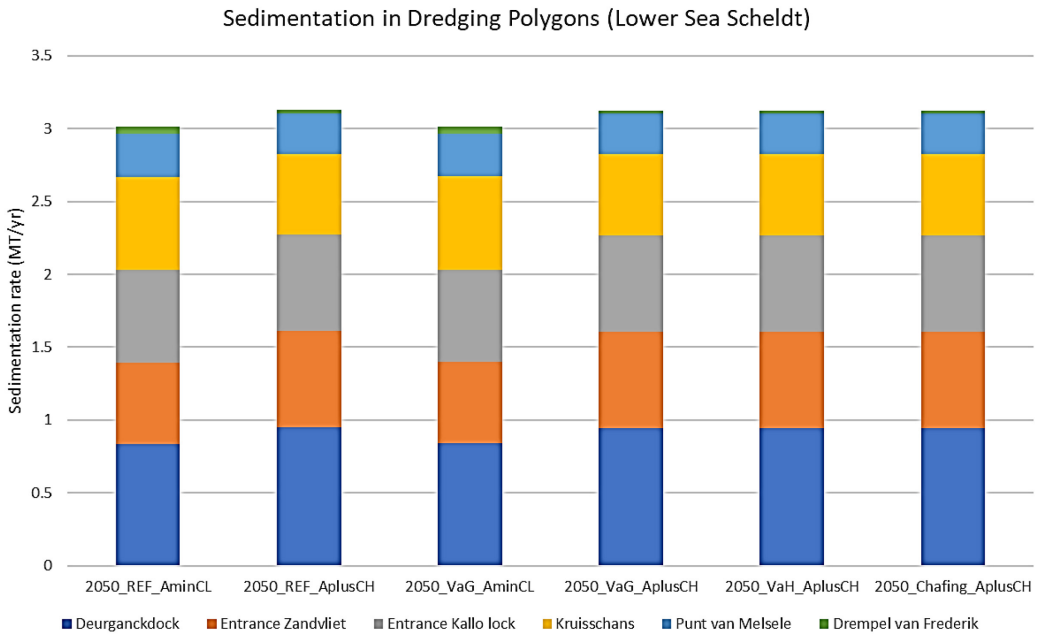

Figure 190 – Comparison of sedimentation rate in the Lower Sea Scheldt between B-alternatives and 2050 reference cases

Upper Sea Scheldt

The influence on the sedimentation rate in the Upper Sea Scheldt is investigated. The polygons considered are shown in Figure 33. Relative to the reference case (in percentage change), the effects of the alternatives on sedimentation in the Upper Sea Scheldt are much larger than in the Lower Sea Scheldt. In general, all three B-alternatives give higher sedimentation in the Upper Sea Scheldt. Also note that the expected change in sedimentation rate under VaG is larger in AminCL than in AplusCH.

Table 9 – Sedimentation rate in the Upper Sea Scheldt and the comparison between the scenarios (B-alternatives)

Runs	Sedimentation (MT/yr)	Difference compared to 2050_REF_AminCL	Difference compared to 2050_REF_AplusCH
2050_REF_AminCL	0.0271	/	/
2050_VaG_AminCL	0.0397	+46.49%	/
2050_REF_AplusCH	0.0289	/	/
2050_VaG_AplusCH	0.0393	/	+35.99%
2050_VaH_AplusCH	0.0383	/	+32.53%
2050_Chafing_AplusCH	0.0394	/	+36.33%

The main reason for having more sedimentation in the Upper Sea Scheldt in B-alternatives is the bathymetric changes, especially the channel deepening in the upstream end near Merelbeke from about 170 km to 167 km, which acts as a sediment trap. In this region, the sedimentation rate increases

significantly in all the B-alternatives comparing to the reference cases under both AminCL and AplusCH climate scenarios (Figure 191).

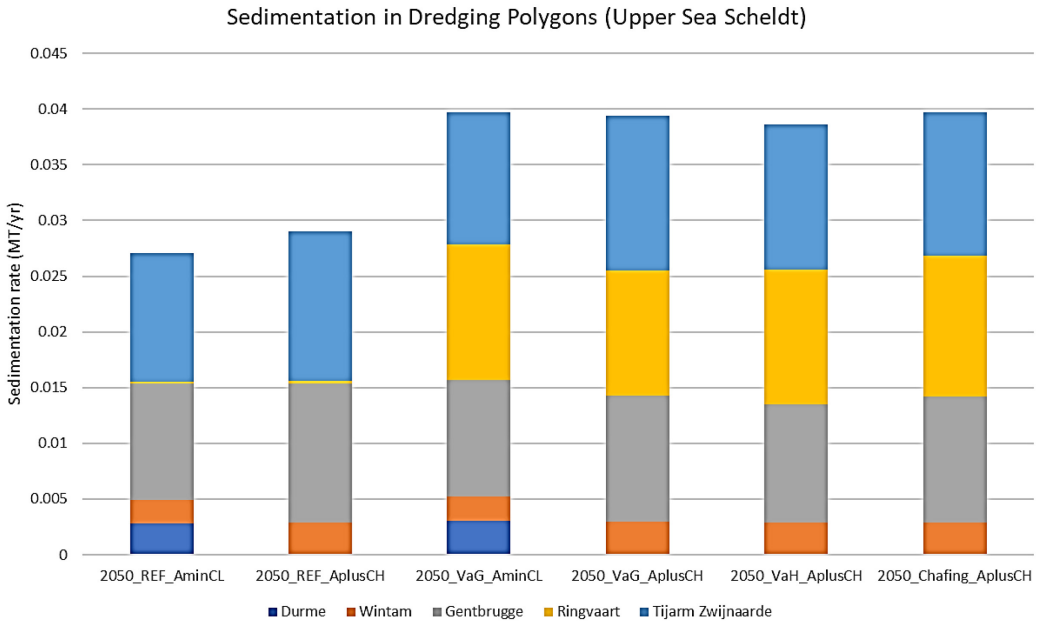

Figure 191 – Comparison of sedimentation rate in the Upper Sea Scheldt between B-alternatives and 2050 reference cases

The reason is that, due to the channel deepening in Ringvaart (existed in all the B-alternatives), velocity magnitudes become much smaller in these areas, which lead to smaller bed shear stress, thus lower suspension capacity and more sediment deposits to the bed.

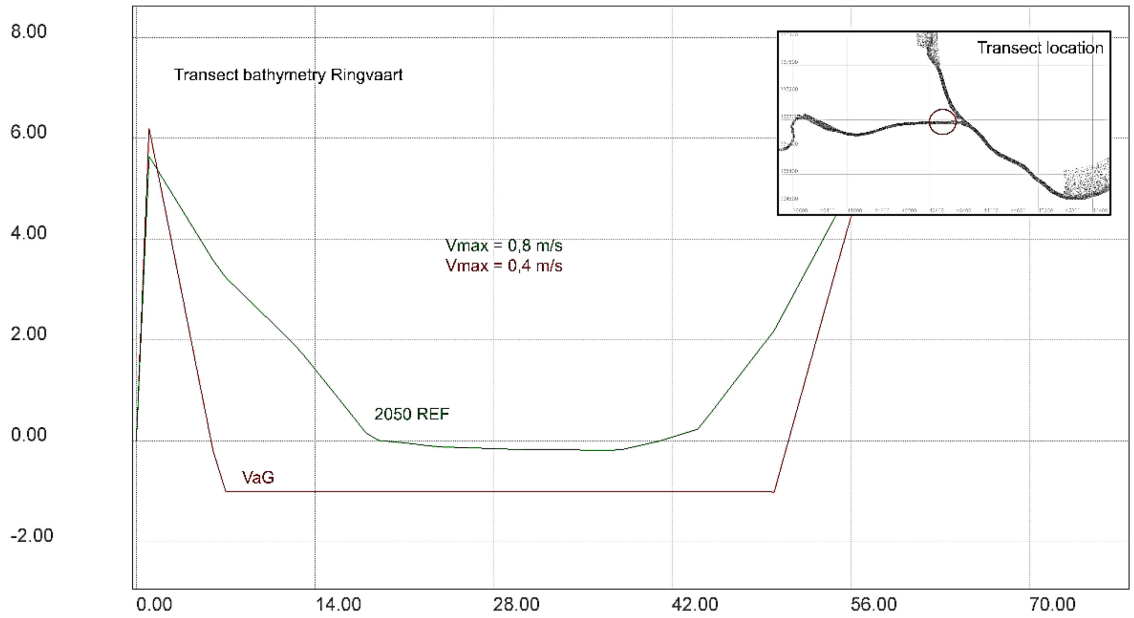

Figure 192 – Comparison of transect bathymetry and maximum velocity before and after channel deepening

6 Reanalysis of B-alternatives

The analysis of the effects of the B-alternatives is complicated by the presence of a deepened Ringvaart in all the B-alternative runs but not in the reference runs. The deepened Ringvaart acts as a sediment trap in the B-alternatives, which affects the sediment availability in the Upper Sea Scheldt. This reduces the sediment concentration in the downstream regions in the B-alternatives, making it difficult to assess the real impact to the system. In order to gain further insight in the effects of the B-alternatives, three additional runs were performed (Table 10).

Table 10 – List of additional runs

Run	Remark
2050_REF_AplusCH_DeepenedRV	With a deepened Ringvaart (the same as in B-alternatives)
2050_REF_AplusCH_DeepenedRV_NoSedPoly	With a deepened Ringvaart, and a polygon hampering sedimentation in this area
2050_VaG_AplusCH_NoSedPoly	With a deepened Ringvaart, and a polygon hampering sedimentation in this area

The additional runs have the same model settings as the previous runs, except the bathymetry in the Ringvaart and the addition of a polygon for reducing the settling velocity (Smolders et al., 2018) in the Ringvaart. To implement the deepening of the Ringvaart in 2050_REF_AplusCH_DeepenedRV, the bathymetry of the deepened Ringvaart from 2050_VaG_AplusCH is extracted from the model grid, then it is mapped to the grid of 2050_REF_AplusCH to create a new mesh file for this new run. Adding a polygon hampering sedimentation uses the similar way described in §5.11 in the report of the mud transport model (Smolders et al. 2018). A polygon that covers the Ringvaart is introduced, in which the settling velocity is fixed at 10^{-7} m/s. This is done by modifying the subroutine vitchu.f in Telemac-3D.

Based on these additional runs, the following comparisons are carried out (Table 11).

Table 11 – List of additional comparisons

	Reference	Scenario	Purpose
1	2050_REF_AplusCH	2050_REF_AplusCH_DeepenedRV	Effect of a deepened Ringvaart, see §6.1
2	2050_REF_AplusCH_DeepenedRV	2050_REF_AplusCH_DeepenedRV_NoSedPoly	Reveals what would happen if no sedimentation can occur in the Ringvaart, see §6.2
3	2050_REF_AplusCH_DeepenedRV	2050_VaG_AplusCH	Effect of VaG with the same deepened Ringvaart in both Reference and Scenario, see §6.3
4	2050_REF_AplusCH_DeepenedRV_NoSedPoly	2050_VaG_AplusCH_NoSedPoly	Similar to the third comparison, but now in the stricter case that no sedimentation can occur in the Ringvaart, see §6.3
5	2050_REF_AplusCH_DeepenedRV	2050_VaH_AplusCH	Effects of VaH with the new reference case after eliminating the difference of Ringvaart, see §6.4
6	2050_REF_AplusCH_DeepenedRV	2050_Chafing_AplusCH	Effects of Chafing with the new reference case after eliminating the difference of Ringvaart, see §6.5

6.1 Effect of a deepened Ringvaart

The comparison of two runs, 2050_REF_AplusCH and 2050_REF_AplusCH_DeepenedRV, for showing the effect of a deepened Ringvaart is discussed in this section.

The bathymetry of the deepened Ringvaart in the B-alternative (VaG) is implemented in the additional run 2050_REF_AplusCH_DeepenedRV. The rest of the model settings are the same as in the run 2050_REF_AplusCH. The difference of the bathymetry is shown in Figure 193. The deepened Ringvaart also has a different cross-section profile, which can be viewed in Figure 192.

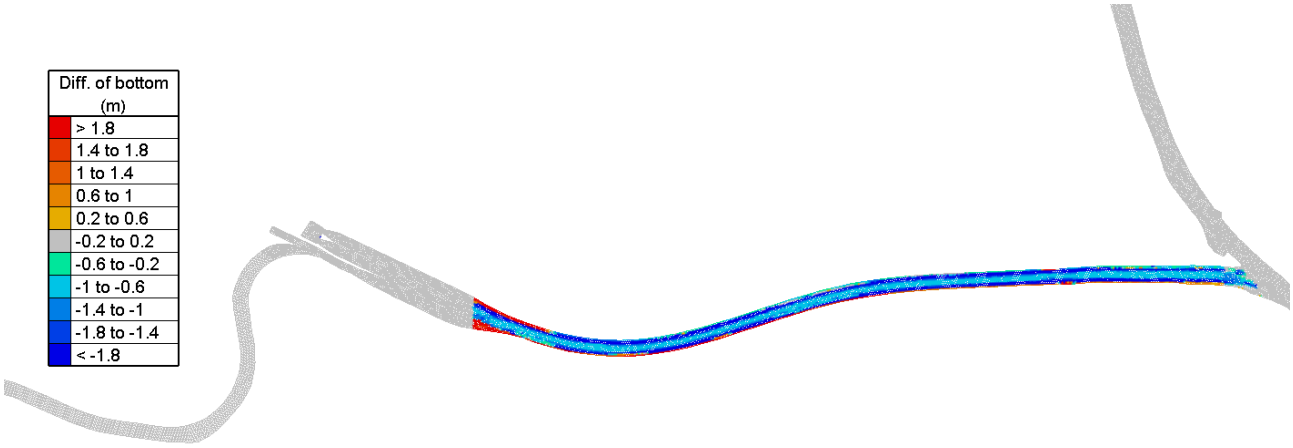

Figure 193 – Difference of the bathymetry
(2050_REF_AplusCH_DeepenedRV - 2050_REF_AplusCH)

In general, the deepened Ringvaart shows a similar effect on delta SSC as seen in the previous comparisons (Figure 194). There is a local decrease of the delta SSC and sediment is stored in the bed at the location where the Ringvaart is deepened. Due to the resulting reduction of the sediment input, the further downstream is also affected. The effect is visible up to 90 km from Vlissingen.

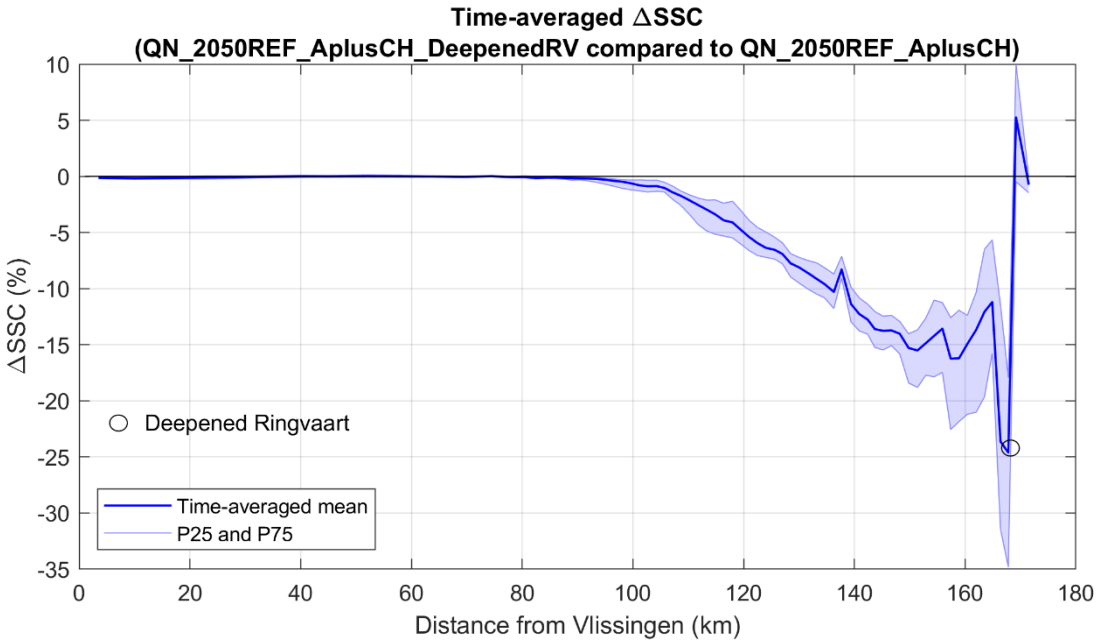

Figure 194 – Time-averaged delta SSC
(2050_REF_AplusCH_DeepenedRV compared to 2050_REF_AplusCH)

The deepened Ringvaart indeed results in more deposition in the local area. The deposited mass has been quantified in the polygons in the Upper Sea Scheldt as mentioned in Figure 33. The comparison is shown in Figure 195.

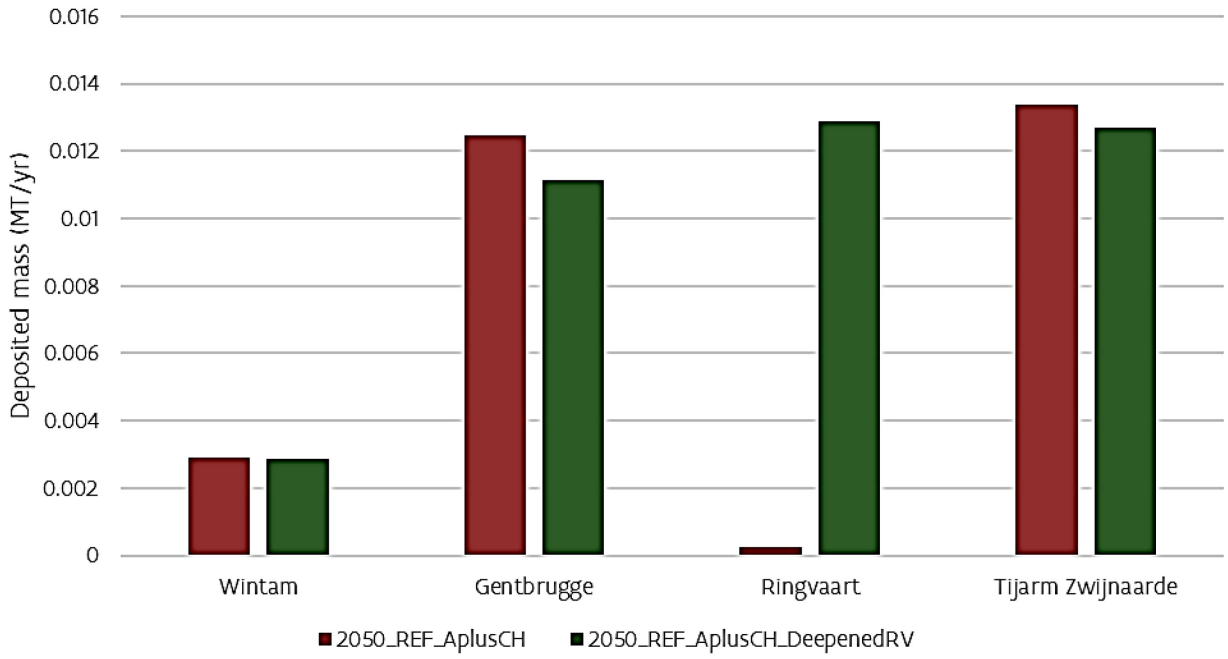

Figure 195 – Deposited mass in the Upper Sea Scheldt
(2050_REF_AplusCH_DeepenedRV compared to 2050_REF_AplusCH)

The effect of a deepened Ringvaart from this new comparison confirms what was suspected before. It acts as a sediment trap and has influence towards downstream.

6.2 Effect of reducing settling velocity in a deepened Ringvaart

In this comparison, the settling velocity is reduced to almost zero in the deepened Ringvaart in the run 2050_REF_AplusCH_DeepenedRV_NoSedPoly, and this is the only difference compared to the reference 2050_REF_AplusCH_DeepenedRV. The rest of the model settings remain the same.

As expected, there is no effect on hydrodynamics.

As shown in Figure 196, the time-averaged mean delta SSC drastically increases by up to 830% in the deepened Ringvaart where the settling velocity is reduced. With almost zero settling velocity, sediment is kept in suspension and no deposition is allowed. Hence, we also observe the sedimentation rate decreases in the same region.

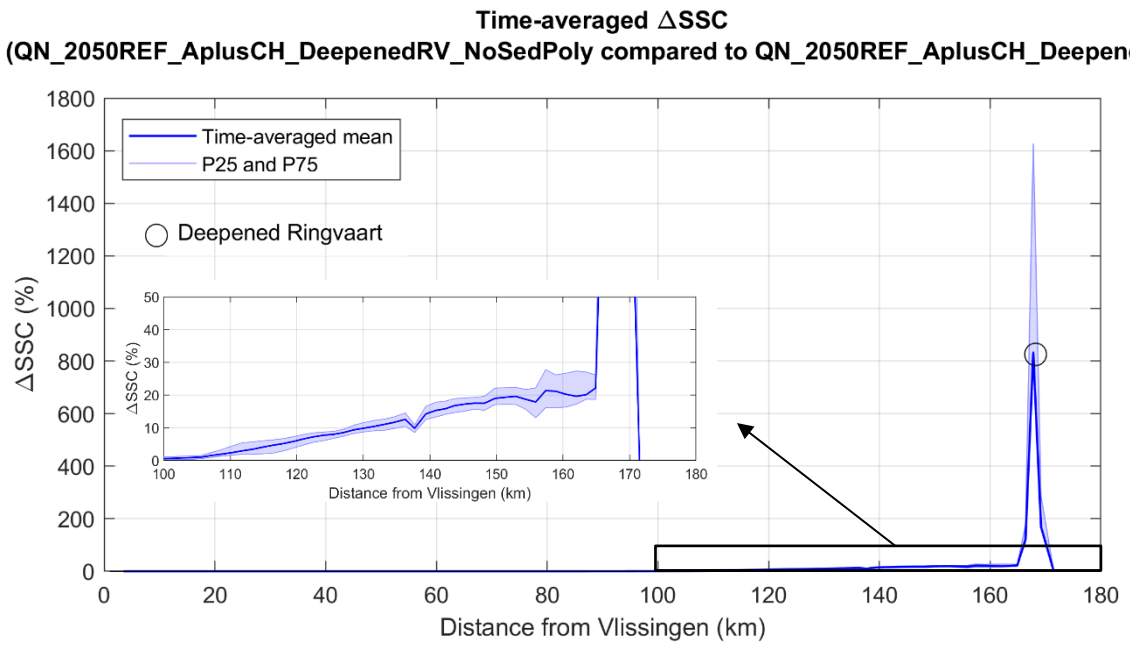

Figure 196 – Time-averaged delta SSC
(2050_REF_AplusCH_DeepenedRV_NoSedPoly compared to 2050_REF_AplusCH_DeepenedRV)

Comparison of sedimentation rate in four locations in the Upper Sea Scheldt are shown in Figure 197. There is no sedimentation in the deepened Ringvaart due to the reduced settling velocity in this region. But it is interesting to see the sedimentation rate becomes larger in Gentbrugge and Tijarm Zwijnaarde with increased sediment input from upstream.

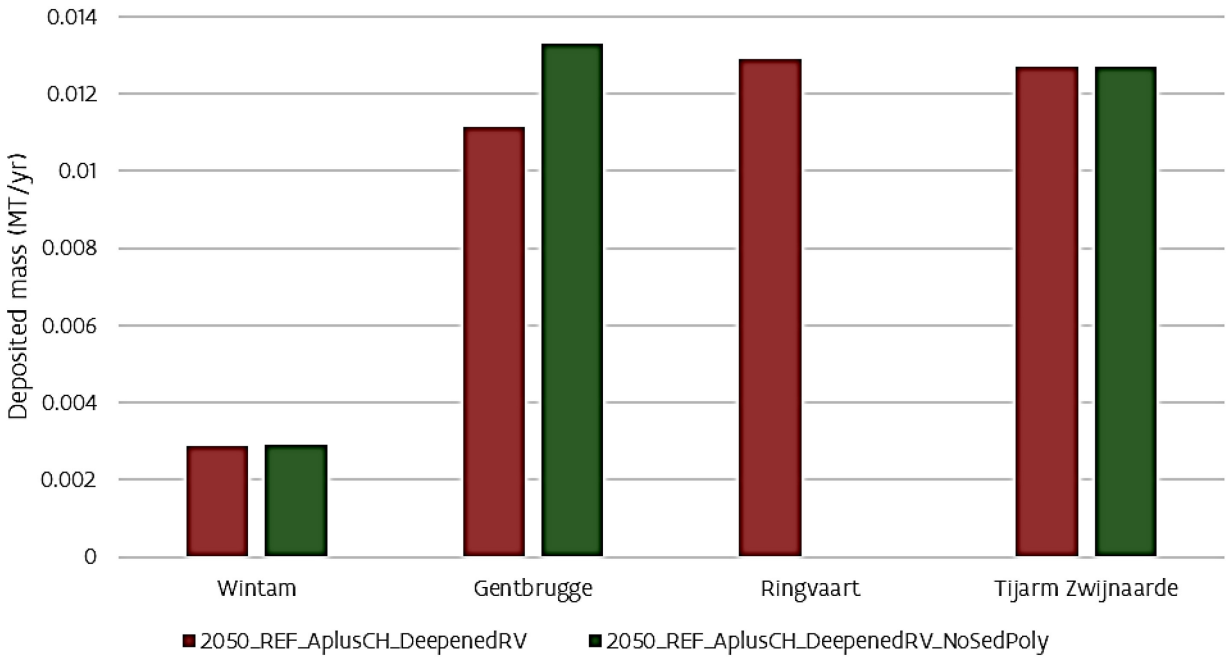

Figure 197 – Deposited mass in the Upper Sea Scheldt
(2050_REF_AplusCH_DeepenedRV_NoSedPoly compared to 2050_REF_AplusCH_DeepenedRV)

The sediment transport rate is calculated and decomposed into two main components according to difference mechanisms (see details in §4.7). The result is shown in Figure 198, in which positive value means downstream transport, negative value means upstream transport.

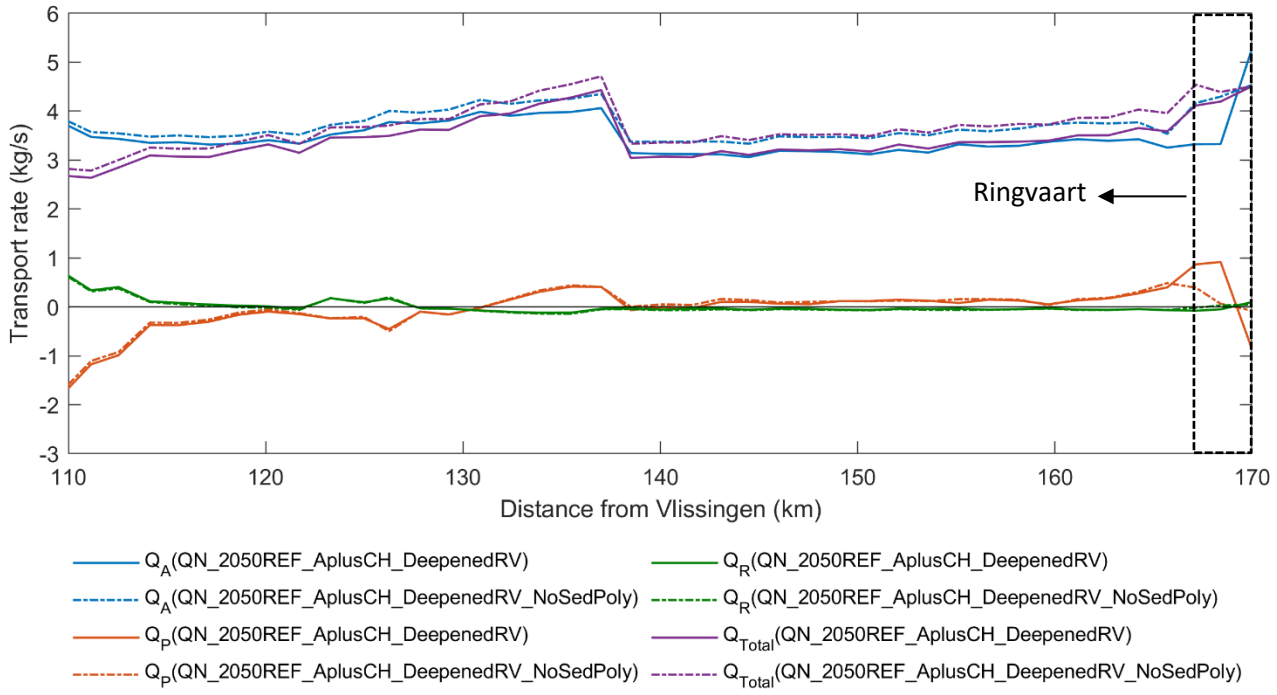

Figure 198 – Decomposed sediment transport rate (positive is downstream)
(2050_REF_AplusCH_DeepenedRV_NoSedPoly compared to 2050_REF_AplusCH_DeepenedRV)

Because of the reduced settling velocity in the area of Ringvaart (from 167 km to 170 km), the advective downstream transport increases, whereas the downstream sediment transport due to tidal pumping decreases. The two changes do not entirely cancel each other, resulting in an increased total sediment transport in this region.

Further downstream from 165 km to 110 km, the sediment transport due to tidal pumping does not show big changes, however, the advective downstream transport remains higher due to the larger SSC (as indicated in Figure 196), thus the total downstream transport is also higher.

It can be concluded that, reduced settling velocity in the area of Ringvaart indeed increases the sediment input for the Upper Sea Scheldt.

6.3 Effect of VaG

The previous comparison was done between the runs 2050_VaG_AplusCH and 2050_REF_AplusCH for showing the effect of VaG alternative. However, because 2050_REF_AplusCH does not have a deepened Ringvaart, the interpretation of the results was complicated. It was suspected that the deepened Ringvaart could act as a sediment trap and reduce sediment input enormously. Therefore, a new reference has been made and the same deepened Ringvaart is added in a new reference 2050_REF_AplusCH_DeepenedRV.

The new comparison indeed shows a different spatial pattern of delta SSC when the same deepened Ringvaart implemented in both runs. Near the upstream boundary, the delta SSC becomes positive by eliminating the difference of the Ringvaart.

Although the delta SSC being overall higher in the new comparison, the rest of the measures in the VaG alternative shows very similar effects as seen before. As revealed in Figure 199, the delta SSC decreases where the channel is deepened or widened, while it increases where the channel is straightened.

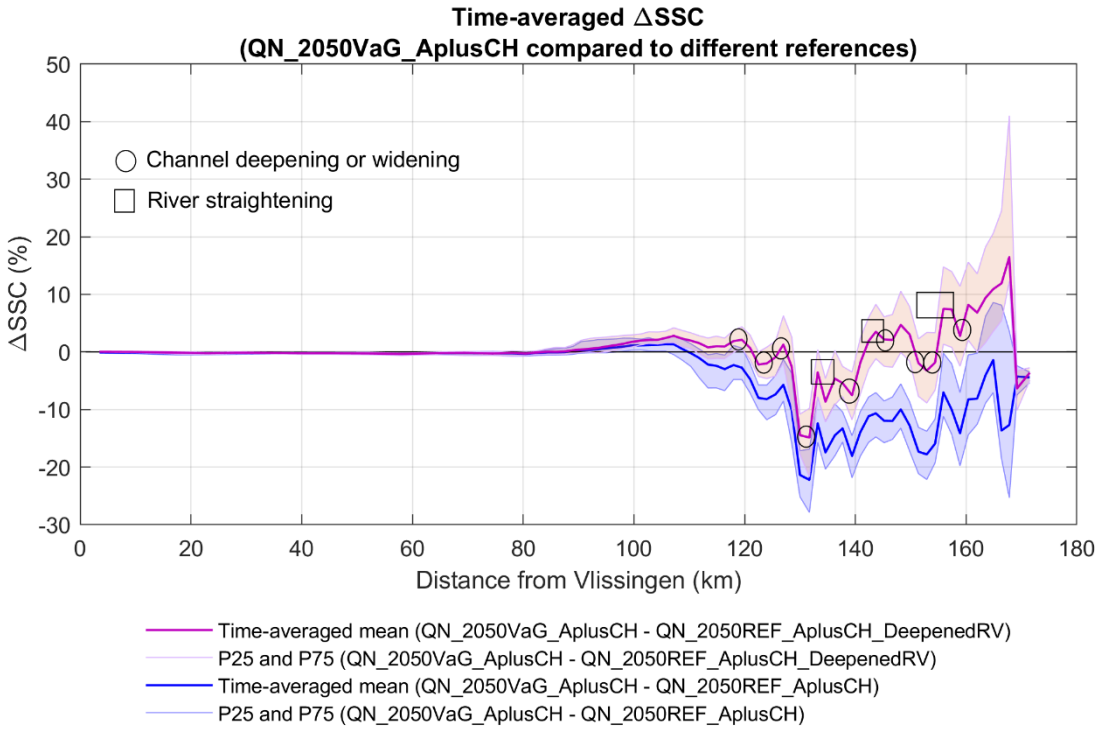

Figure 199 – Comparison of time-averaged delta SSC for VaG_AplusCH compared to different reference cases. The blue line was presented earlier in § 5.2.2. The magenta line is the new result.

The new comparison shows that, the system reactions to the measures in VaG alternative remain similar as in the previous comparisons. The local peaks and dips shown in the delta SSC still match the locations of different measures. But it also shows a different story in the upstream region from 150 km to 170 km, with higher and positive delta SSCs. This is believed to be caused by the changes in the hydrodynamics after implementing VaG alternative, which are discussed in detail in Figure 200.

The further comparison is done between 2050_VaG_AplusCH_NoSedPoly and the reference case 2050_REF_AplusCH_DeepenedRV_NoSedPoly. In both runs, a deepened Ringvaart is implemented, but now, the settling velocity is also reduced to nearly zero.

This comparison shows the effect of VaG under a slightly different situation with more sediment input from upstream.

The delta SSC profiles obtained from two comparisons are shown in Figure 200. It can be seen that when the Ringvaart stays the same in both comparisons (as mentioned in §6.3), the delta SSC profiles will also look similar to each other. After eliminating the difference of Ringvaart, both delta SSC profiles still show the same reactions to the measures in VaG (decreases where the channel is deepened or widened, while it increases where the channel is straightened).

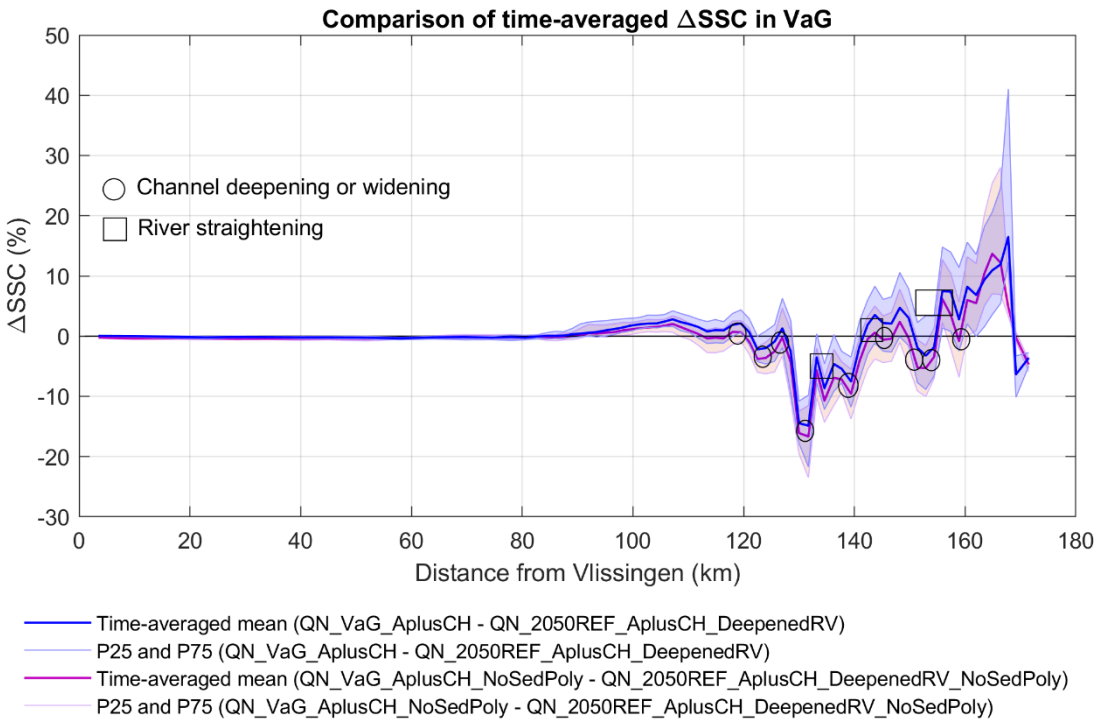

Figure 200 – Time-averaged delta SSC from two different comparisons

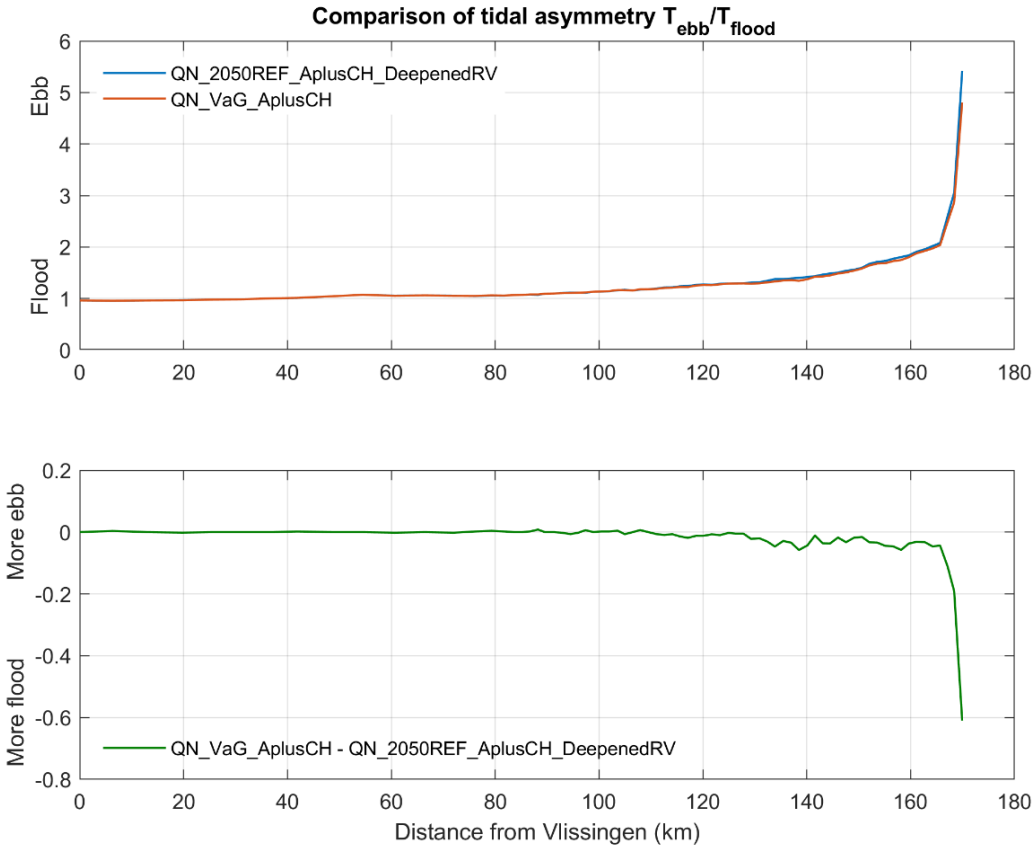

Figure 201 – Comparison of tidal asymmetry
(QN_VaG_AplusCH – QN_2050REF_AplusCH_DeepenedRV)

The similarity in delta SSC is due the fact that adding a no-deposition zone does not change the hydrodynamics. Hence, the change of tidal asymmetry stays the same in both comparisons. As shown in §6.3, because of all the measures in VaG (except the Ringvaart since the difference is eliminated here), the region from 150 km to 170 km becomes less ebb dominant compared to the reference case. This change of tidal asymmetry results in less transport during ebb, thus the SSC could become higher under the same input from upstream boundary.

This also suggests that delta SSC is a reliable index for showing the effect of B-alternatives. It represents the system reactions to the change of hydrodynamics.

Figure 200 also shows that the effect of a set of measures on SSC (the delta) is robust to the choice of the modeller on how to implement the Ringvaart. Because of this, the effects of VaH and Chafing are only re-calculated based on the new reference with a deepened Ringvaart.

6.4 Effect of VaH

The effect of VaH has also been reassessed by comparing the run QN_2050VaH_AplusCH to the new reference QN_2050REF_AplusCH_DeepenedRV, with the same deepened Ringvaart in both runs. The delta SSC is computed and shown in Figure 202.

Examining closely the patterns in the Figure 167 and Figure 202, similarity can be observed. In fact, in this new comparison, the locations of the dips in the delta SSC still matches well with the locations of the measures implemented in VaH alternative. The only major difference is that the delta SSC becomes higher in the Upper Sea Scheldt, after eliminating the difference of the Ringvaart.

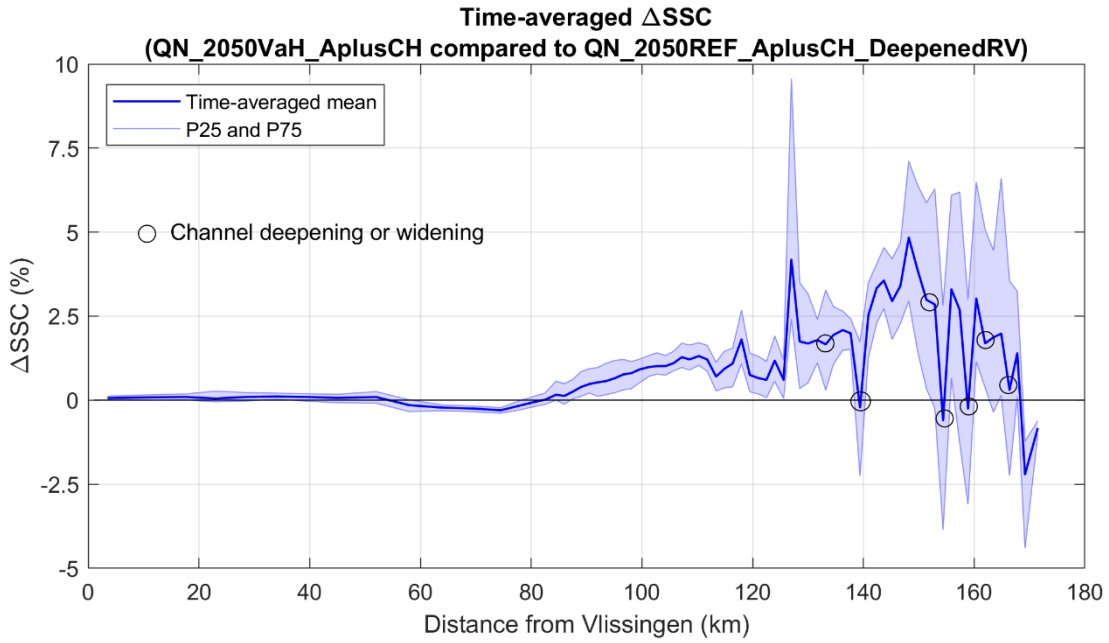

Figure 202 – Time-averaged delta SSC
(2050_VaH_AplusCH compared to 2050_REF_AplusCH_DeepenedRV)

The main reason of the delta SSC being higher in the most area of the Upper Sea Scheldt is the change in tidal asymmetry. To be more specifically, the ratio of ebb/flood duration changes in the upstream. Figure 203 shows the system becomes less ebb dominant from 170 km to 130 km, which will cause less sediment transport downstream, resulting in higher SSC under the same input from upstream boundary.

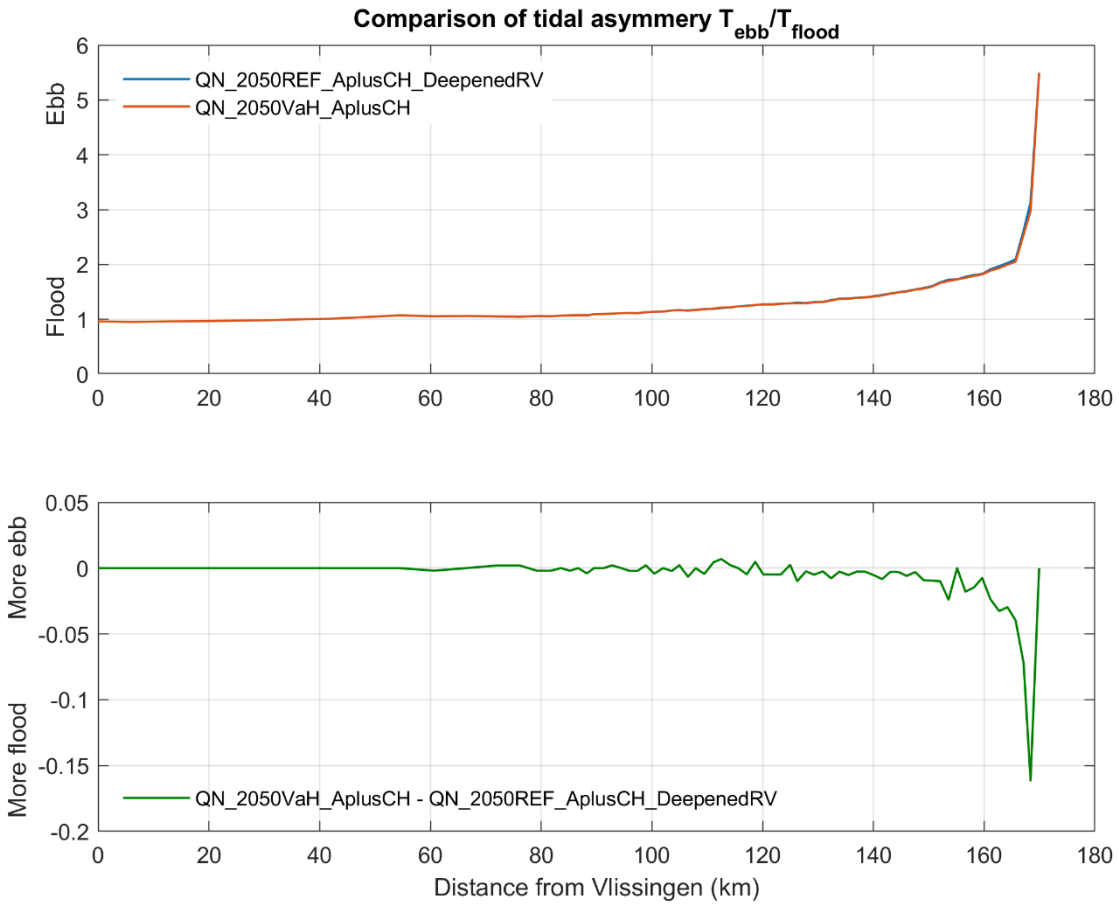

Figure 203 – Comparison of tidal asymmetry
(QN_2050VaH_AplusCH – QN_2050REF_AplusCH_DeepenedRV)

6.5 Effect of Chafing

The effect of the Chafing alternative is reanalysed by comparing the run QN_2050Chafing_AplusCH to the new reference QN_2050REF_AplusCH_DeepenedRV. The delta SSC is computed (Figure 204), as well as other differences in hydrodynamics, e.g. the change of tidal asymmetry (Figure 205).

Again, the new patterns seen in Figure 204 matches with the locations of the measures implemented in Chafing alternative, which is also seen in other B-alternatives. The most noticeable difference is the higher delta SSC in the Upper Sea Scheldt compared to the results shown in Figure 185.

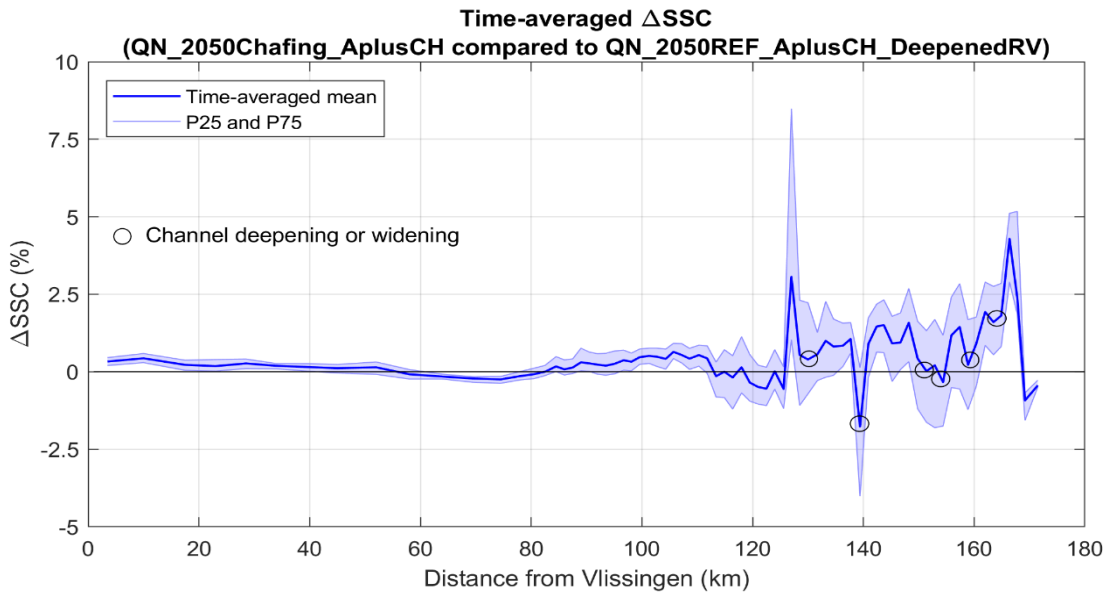

Figure 204 – Time-averaged delta SSC
(QN_2050Chafing_AplusCH compared to QN_2050REF_AplusCH_DeepenedRV)

The reason of having higher delta SSC in the Upper Sea Scheldt is also the change of tidal asymmetry due to the implementation of the measures. It can be seen that the duration ratio between ebb and flood changed noticeably in the upstream from 170 km to 140 km. This part of the system becomes less ebb dominant, thus, higher SSC is expected under the same sediment input. However, the difference of the ebb/flood duration is not as large as seen in Figure 201, therefore the change of delta SSC is also not as big as it is in Figure 200.

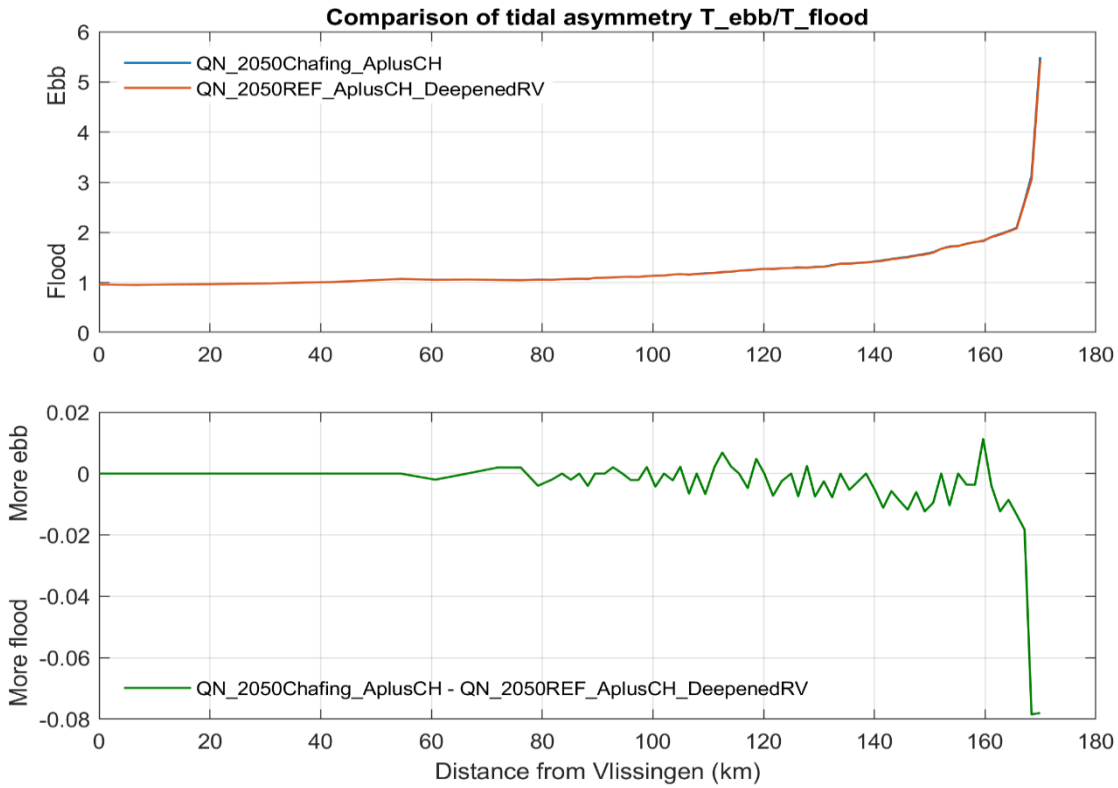

Figure 205 – Comparison of tidal asymmetry
(QN_2050VaH_AplusCH – QN_2050REF_AplusCH_DeepenedRV)

6.6 The influence of the peak discharge event

During the 40-day simulation period, a discharge event is imposed at the upstream boundary starting from about day 32 (Figure 1). The peak discharge is reached at about day 34, then it decreases gradually and restores to the constant value at about day 38. So in total the discharge event lasts about 6 days in total.

For better showing the effect of the peak discharge on the delta SSC, three periods are used for the time-averaging of the time series of delta SSC along the thalweg.

- The first period is from day 15.6 to day 30.4, which is a spring-neap cycle before the discharge event;
- The second period is the last 20 days including a peak discharge event;
- The third period is during the peak discharge event from day 32 to day 38.

The comparisons of delta SSCs are plotted in Figure 206, Figure 207 and Figure 208.

It can be seen in the comparisons, the differences of delta SSC between the three averaging periods, a spring-neap cycle and the last 20 days, are in general small. In both VaH and Chafing cases, the difference is less than 1%; in VaG case, the difference is also less than 1% in all the other locations, except at 167 km where the difference is about 4%. It could be that the discharge event is relatively short compared to the averaging period, hence it only affects little of the results.

The larger differences can be seen from the delta SSC averaged over only the peak discharge event.

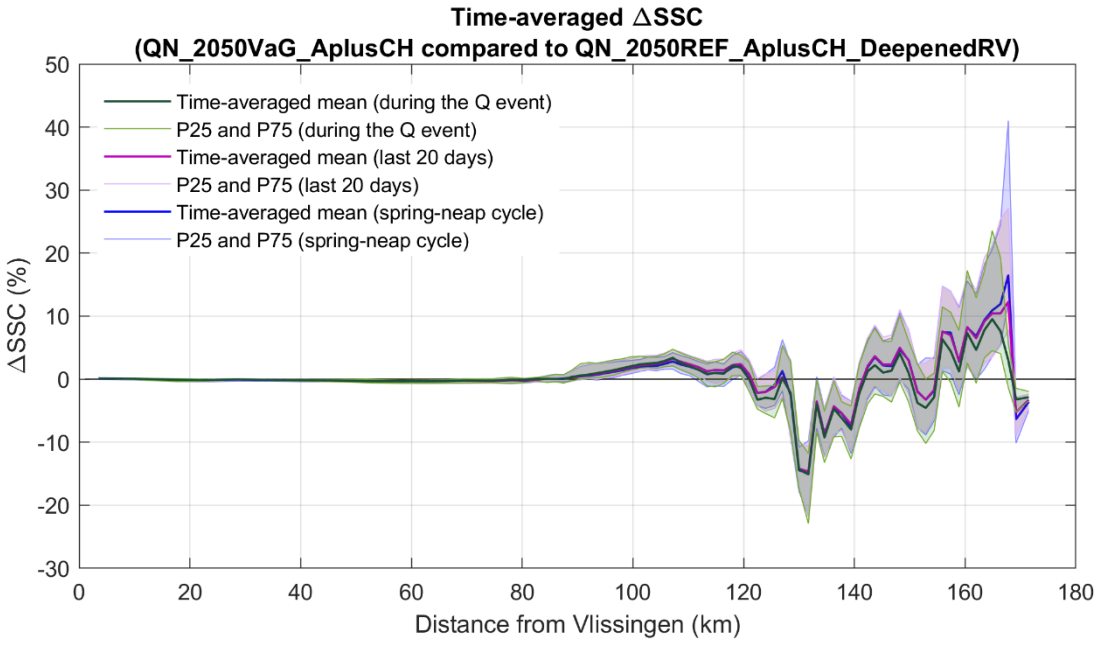

Figure 206 – Comparison of delta SSC of VaG in three different periods
(QN_2050VaG_AplusCH – QN_2050REF_AplusCH_DeepenedRV)

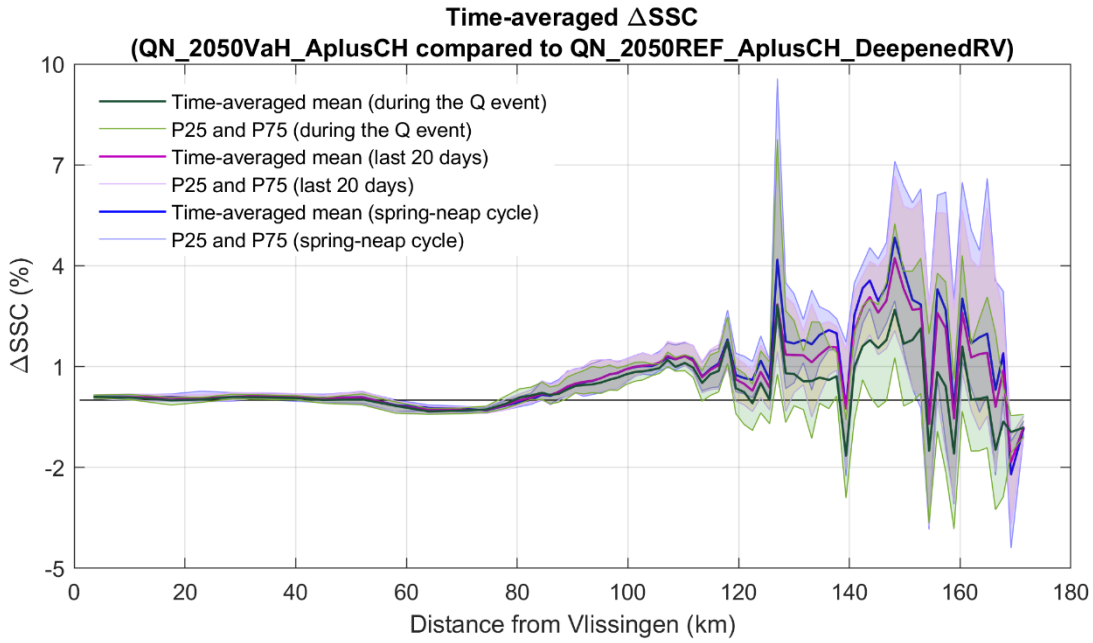

Figure 207 – Comparison of delta SSC of VaH in three different periods
(QN_2050VaH_AplusCH – QN_2050REF_AplusCH_DeepenedRV)

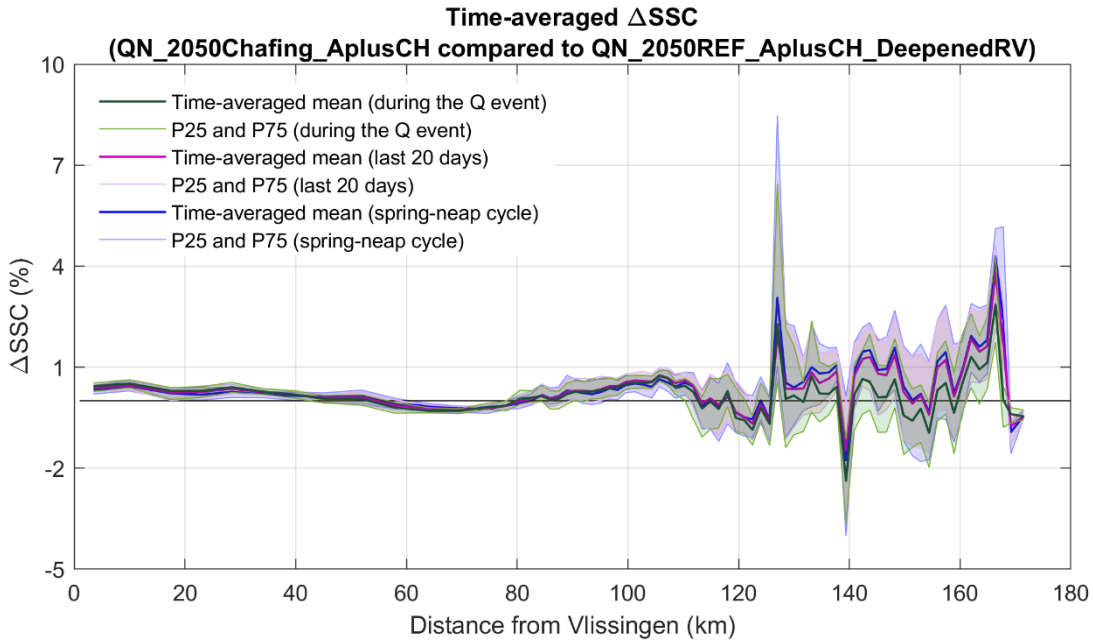

Figure 208 – Comparison of delta SSC of Chafing in three different periods
(QN_2050Chafing_AplusCH – QN_2050REF_AplusCH_DeepenedRV)

From the above three figures, one trend has to be noticed: calculating the delta SSC only during the period of peak discharge gives lower delta SSC in the Upper Sea Scheldt from about 110 km to 170 km. This could be due to the fact that during the discharge peak, sediment availability is higher. Furthermore, this delta is only calculated over a 6 day period, so you miss some of the spring-neap dynamics. As we're interested in average effects on SSC, the delta's calculated during the peak discharge event are for illustration purposes only.

6.7 Conclusion

Based on the four comparisons done in this chapter, the following conclusions can be drawn:

- The Deepening of the Ringvaart indeed acts as a sediment trap, reducing sediment availability in the model domain;
- Delta SSC becomes positive in the three B-alternatives, especially from 150 km to 170 km after the differences in schematisation of the Ringvaart are eliminated;
- There's no significant difference between calculating the delta SSC over a period with or without the discharge peak.

References

Blanton, J. O., G. Q. Lin, and S. A. Elston (2002), Tidal current asymmetry in shallow estuaries and tidal creeks, Cont. Shelf Res., 22, 1731–1743.

Burchard, H.; Schuttelaars, H.M.; Ralston, D.K. (2018). Sediment Trapping in Estuaries. Ann. Rev. Mar. Sci. 10(1): annurev-marine-010816-060535. doi:10.1146/annurev-marine-010816-060535

De Swart, H. E., & Zimmerman, J. T. F. (2009). Morphodynamics of tidal inlet systems. *Annual review of fluid mechanics*, *41*, 203-229.

Dronkers, J. (1986), Tidal asymmetry and estuarine morphology, Neth. J. Sea Res., 20, 117–131.

Emery, W. J. & Thomson, R. E. (2001). Data Analysis Methods in Physical Oceanography (Second and Revised Edition). Elsevier, Amsterdam, Netherland, pp.638.

Fettweis, M.; Du Four, I.; Zeelmaekers, E.; Baeteman, C.; Francken, F.; Houziaux, J.-S.; Mathys, M.; Nechad, B.; Pison, V.; Vandenberghe, N.; Van den Eynde, D.; Van Lancker, V.R.M.; Wartel, S. (2007). Mud Origin, Characterisation and Human Activities (MOCHA): Final report. Belgian Science Policy: Brussel. 59 pp.

Friedrichs, C. T., and D. G. Aubrey (1988), Non-linear tidal distortion in shallow well-mixed estuaries: A synthesis, Estuarine Coastal Shelf Sci., 27, 521–545.

Friedrichs, C. T. (2011). 3.06-Tidal Flat Morphodynamics: A Synthesis. *Virginia Institute of Marine Science: Gloucester Point, VA, USA*, 137-170.

Gatto, V.M.; van Prooijen, B.C.; Wang, Z.B. (2017). Net sediment transport in tidal basins: quantifying the tidal barotropic mechanisms in a unified framework. Ocean Dyn. ISBN 1023601710993 67(11): 1385–1406. doi:10.1007/s10236-017-1099-3.

Godin, G. (1966) Daily mean sea level and short-period seiches. International Hydrographic Review, 43, 75-89.

Hervouet, J. M. (2007). Hydrodynamics of free surface flows: modelling with the finite element method. John Wiley & Sons.

IMDC (2015). Bepalen van randvoorwaarden voor de referentiesituatie (2050) m.b.t. debiet en waterstand. I/NO/11448/15.128/TFR/

IMDC et al. (2018). Evaluation method for the Integrated Plan Upper Seascheldt.

Nidzieko, N. J., & Ralston, D. K. (2012). Tidal asymmetry and velocity skew over tidal flats and shallow channels within a macrotidal river delta. *Journal of Geophysical Research: Oceans*, *117*(C3).

Postma H. 1954. Hydrography of the Dutch Wadden Sea. *Arch. Néerl. Zool.* 10:405—511.

Postma, H. (1961), Transport and accumulation of suspended matter in the Dutch Wadden Sea, Neth. J. Sea Res., 1, 148–180.

Pritchard, D. (2005), Suspended sediment transport along an idealised tidal embayment: Settling lag, residual transport and the interpretation of tidal signals, Ocean Dyn., 55, 124–136, doi:10.1007/s10236-005-0004-7.

Seim, H. E., J. O. Blanton, and S. Elston (2006), Tidal circulation and energy dissipation in a shallow, sinuous estuary, Ocean Dyn., 56, 360–375, doi:10.1007/s10236-006-0078-x.

Smolders, S.; Maximova, T.; Vanlede, J.; Plancke, Y.; Verwaest, T.; Mostaert, F. (2016). Integraal Plan Bovenzeeschelde: Subreport 1 – SCALDIS: a 3D Hydrodynamic Model for the Scheldt Estuary. Version 5.0. WL Rapporten, 13_131. Flanders Hydraulics Research: Antwerp, Belgium.

Smolders, S.; Bi, Q.; Vanlede, J.; De Maerschalck, B.; Plancke, Y.; Schramkowski, G.; Mostaert, F. (2018). Integraal plan Boven-Zeeschelde: Sub report 6 – Scaldis Mud: a Mud Transport model for the Scheldt Estuary. Version 4.0. FHR Reports, 13_131_6. Flanders Hydraulics Research: Antwerp.

Scully, M.E.; Friedrichs, C.T. (2007). Sediment pumping by tidal asymmetry in a partially mixed estuary. J. Geophys. Res. Ocean. ISBN 01480227 (ISSN) 112(7): 1–12. doi:10.1029/2006JC003784

Sheskin, D.J. (2011). Handbook of parametric and nonparametric statistical procedures. 5th ed. Boca Raton: Chapman & Hall /CRC.

Smolders, S.; Maximova, T.; Vanlede, J.; Plancke, Y.; Verwaest, T.; Mostaert, F. (2016). Integraal Plan Bovenzeeschelde: Subreport 1 – SCALDIS: a 3D Hydrodynamic Model for the Scheldt Estuary. Version 5.0. WL Rapporten, 13_131. Flanders Hydraulics Research: Antwerp, Belgium.

Van de Kreeke, J.; Robaczewska, K. (1993). Tide-induced residual transport of coarse sediment; application to the Ems Estuary. Netherlands J. Sea Res. 31(3): 209–220.

van Straaten LMJU, Kuenen PH. 1957. Accumulation of fine grained sediments in the Dutch Wadden Sea. *Neth. J. Geosci.* 19:329—54.

Van Straaten, L., and P. Kuenen (1958), Tidal action as a cause of clay accumulation, J. Sediment. Petrol., 28, 406–413.

Wang, Z. B., Jeuken, C., & De Vriend, H. J. (1999). Tidal asymmetry and residual sediment transport in estuaries. Deltares (WL).

J.C. Winterwerp (2001). “Stratification effects by cohesive and non-cohesive sediment”, Journal of Geophysical Research, Vol 106, No C10, pp 22559-22574

Winterwerp JC (2011) Fine sediment transport by tidal asymmetry in the high-concentrated Ems River: indications for a regime shift in response to channel deepening. Ocean Dyn 61:203–215.

DEPARTMENT **MOBILITY & PUBLIC WORKS**
Flanders hydraulics Research

Berchemlei 115, 2140 Antwerp
T +32 (0)3 224 60 35
F +32 (0)3 224 60 36
waterbouwkundiglabo@vlaanderen.be
www.flandershydraulicsresearch.be